Validation of a Three-Dimensional Culture System for the Differentiation of Multipotential Mesenchymal Stromal Cells by Uniaxial Strain

Lindsey C. Parker

MChem

Submitted in accordance with requirements for the degree of

Doctor of Philosophy

The University of Leeds

School of Mechanical Engineering

January 2017

The candidate confirms that the work submitted is her own and that appropriate credit has been given where reference has been made to the work of others.

This copy has been supplied on the understanding that it is copyright material and that no quotation from the thesis may be published without proper acknowledgement.

The right of Lindsey C. Parker to be identified as Author of this work has been asserted by her in accordance with the Copyright, Designs and Patents Act 1988.

<u>Acknowledgements</u>

First and foremost, I would like to thank my supervisory team: Dr Daniel Thomas, Professor Eileen Ingham and Professor John Fisher. I will be eternally grateful for the patience afforded to me by my supervisors, especially by Dan, who made himself available to assist me whenever required.

I am also particularly appreciative of the regular supervisory contact/meetings scheduled throughout my PhD, during which I could address any challenges in the project.

Special gratitude is extended to Dr Clare Brockett and Professor Joanne Tipper for their invaluable pastoral support. I acknowledge the very significant commitment of Joanne Tipper to the DTC TERM program – you have listened to us and done everything in your power to provide the PhD students in your charge with the most valuable experience possible. I am hugely grateful to the DTC TERM program and Eileen Ingham for granting permission and additional funding for my placement, which benefitted my development hugely.

I would like to thank the colleagues and dear friends that have supported me during my time in the Ingham lab. To my peers: having others to relate to and de-stress with has been invaluable in this process. The laboratory technicians of lab 7.63 have made an invaluable contribution to my experience; I sincerely thank you for your patience and considerable skill in maintaining an organised and well stocked lab, which facilitates all of our success. Many thanks also for the assistance of Lee Wetherill and Rhys Moore in re-engineering the Tencell bioreactor.

To my amazing friends Lauren, Amy, Rachael and Helen: thank you from the bottom of my heart for the many years of friendship without which I am certain my life would not be what it is now. You are the best friends anyone could hope for.

Also, much love to my neighbours Florence, Adrian and little Samuel – thank you for the many cups of tea and meals, and for your door always being open to support me.

Finally, special thanks to my brother, Lord Alexander Lynch, for submitting this thesis in person on my behalf without complaint.

<u>Abstract</u>

The differentiation potential of multipotential mesenchymal stromal cells is known to be affected by many aspects of the cellular microenvironment, including soluble factors, extracellular matrix composition, the Young's modulus of the substrate, cellular neighbours and externally applied forces. Despite this, reasonable understanding of harnessing soluble factors only exists. Few studies have investigated mechanotransduction in hMSC, and those published to date primarily employ unsuitable substrates, that do not facilitate the cellular adhesions known to be active in force transmission.

In this study, porcine pericardium was decellularised for use as a biologically-relevant, three-dimensional scaffold for the mechanostimulation of hMSC in a uniaxial strain bioreactor. Tissue stocks (n=67) were successfully decellularised and confirm biocompatible, sterile and free of contaminating genomic DNA. Histoarchitecture comparable to that of native tissue was also maintained. Tencell-specific seeding rings were found to release cytotoxic residue, and an alternative, nontoxic seeding approach was developed.

The Tencell bioreactor was initially unable to maintain cell viability as a culture system, and was validated with respect to chamber humidity, culture temperature and arm displacement. Temperature maintenance was inadequate prior to re-engineering of the heating apparatus and was rectified through the use of an autotunable module. Losses of cell viability were still observed following validation as a result of medium pH changes. A Tencell culture regime utilising the HEPES buffer was successfully developed for the culture of hMSC.

No significant differences in gene expression between strained and unstrained samples were found, and the greatest effects were observed between unseeded and other sample types. Additionally, seeded hMSC did not penetrate the scaffold.

Overall, this study investigated the differentiation potential of hMSC cultured in a three-dimensional scaffold. The Tencell bioreactor was fully validated for use as a uniaxial strain mechanostimulation device, and could be used in future studies to investigate the effect of different frequencies and magnitudes of cyclic strain.

<u>Contents</u>

List of Tables

List of Figures

<u>Abbreviations</u>

ANOVA	Analysis of variance
BHK	Baby hamster kidney [cells]
BLAST®	Basic local alignment search tool
BMP	Bone morphogenic protein
Cbfa1	Core-binding factor α1
C$_T$	Threshold cycle [in qPCR]
DMEM	Dulbecco's modified eagles medium
DMSO	Dimethyl sulfoxide
DNA	Deoxyribonucleic acid
cDNA	Complementary deoxyribonucleic acid
DP	Decellularised pericardium
EDTA	Ethylenediaminetetraacetic acid
EPC	Endothelial progenitor cells
ESC	Embryonic stem cell
FAK	Focal adhesion kinase
FBA	Fresh blood agar
FBS	Fetal bovine serum
FEGSEM	Field emission gun environmental scanning electron microscope
GAG	Glycosaminoglycan
GSK3*β*	Glycogen synthase kinase
HEPES	4-(2-hydroxyethyl)-1-piperazineethanesulfonic acid
HPRT1	hypoxanthine phosphoribosyltransferase 1

HUVEC	Human umbilical vein endothelial cells
MEF	Murine embryonic fibroblasts
hMSC	Human multipotential mesenchymal stromal cells
pMSC	Porcine multipotential mesenchymal stromal cells
MTT	(3-(4,5-Dimethylthiazol-2-yl)-2,5-Diphenyltetrazolium Bromide)
NA	Nutrient agar
NB	Nutrient broth
NBF	Neutral buffered Formalin
NCBI	National Center for Biotechnology Information
dNTP	deoxynucleotide mix
OGP	Octy-glucopyranoside
PAA	Peracetic acid
PDMS	Polydimethylsiloxane
PCR	Polymerase chain reaction
qPCR	Quantitative polymerase chain reaction
PLA	Polylactic acid
PPIA	Peptidylprolyl isomerase A
R^2	Coefficient of determination
RNA	Ribonucleic acid
RT	Room temperature
RUNX2	Runt related transcription factor 2
Rxn	Reaction
SCNT	Somatic cell nuclear transfer
SDS	Sodium dodecyl sulfate

SEM	Scanning electron microscopy
SM-22α	Smooth muscle 22α
SM α-actin	Smooth muscle α-actin
SMC	Smooth muscle cell
SM-MHC	Smooth muscle myosin heavy chain
TAE buffer	Tris-acetate-EDTA buffer
TBP	TATA box binding protein
TBS	Tris buffered saline
TGFβ1	Transforming growth factor-β1
T_a	Annealing temperature
T_m	Annealing temperature [of primer pairs in PCR assays

Chapter 1:   Introduction

1.1 Background

The term mechanotransduction is used to describe the conversion of physical forces into biochemical responses in cells, and whilst other signalling mechanisms such as hormones are now fairly well understood, the mechanobiological processes key to tissue development and homeostasis are still being unravelled. Key aspects of cellular behaviour have now been linked to mechanical force, including proliferation, migration and crucially to this project, gene expression and differentiation (Orr *et al.*, 2006; Chen, 2008; Hoffman *et al.*, 2011). Mesenchymal stem cells (MSC) offer advantages in the field of tissue engineering owing to their multipotency, comparatively fewer ethical caveats and relative safety as compared to other stem cells, and could be induced to differentiate to achieve tissue repair. Tissue engineering can be defined as the application of scientific principles to the construction, growth and maintenance of living tissues that may be used to replace or restore function in the body (Yang, 2012b). MSC are widely differentiated using soluble factors, but physical stimuli are not widely utilised. However, there is growing evidence that mechanical stimulation plays a central role in the differentiation of MSC, although this is little-studied. There are currently no reports of mechanostimulated MSC differentiation towards a smooth muscle lineage using a three-dimensional scaffold, and scarce investigation regarding the mechanism of mechanotransduction in MSC. During this project, the strain-mediated differentiation of MSC towards key lineages of interest, including smooth muscle, will be investigated using an acellular pericardial scaffold. It is hoped that a greater understanding of mechanotransduction in MSC, and hence more optimal use of mechanical stimuli, will allow MSC to be utilised more effectively in tissue engineered therapies.

1.2   Stem Cells

Stem cells can be defined as unspecialized cells that can self-renew indefinitely, whilst retaining a capacity to differentiate into more mature cells with specialized functions (Brown, 2004). Their ability to commit to cell lineages in response to physical, environmental and soluble stimuli makes them of great interest in tissue engineering and regenerative medicine, and they have been considered for use in the regeneration of a huge range of tissues (Deasy *et al.*, 2004; Chen *et al.*, 2006; Tae *et al.*, 2006; Wu *et al.*, 2006; Rada *et al.*, 2009). This literature review summarises the state of knowledge thus far regarding mechanotransduction and MSC.

1.2.1   Major Developments in Stem Cell Research

Since the late 19th century it has been known that certain cells retain the ability to differentiate into a variety of lineages. The term 'stem cell' was proposed for scientific use in 1909 by the Russian histologist Alexander Maksimov as a result of his studies of lymphocytes and hematopoeisis (Maksimov, 2009). However, stem cells were not the subject of major discovery until the 1960s when their involvement in adult neurogenesis was revealed (Altman and Das, 1965; Altman, 1966; Altman and Das, 1967; Altman, 1969a; Altman, 1969b) and self-renewing cells in mouse bone marrow were found (Siminovitch *et al.*, 1963). These developments resulted in the first stem cell therapy in 1968: a bone marrow transplant between two siblings for the treatment of severe combined immunodeficiency disease (Yang, 2012a). This was followed by the discovery of hematopoetic stem cells (1978) and the simultaneous discovery of ESCs (1981) (Evans and Kaufman, 1981; Martin, 1981).

MSC were first isolated by Friedenstein as an adherent fibroblast-like cell population from human bone marrow (Friedenstein *et al.*, 1974) following the earlier derivation of 'colony-forming fibroblasts' from guinea pig marrow capable of undergoing osteogenesis (Friedenstein *et al.*, 1966). MSCs were later described as adherent (Friedenstein *et al.*, 1970), non-phagocytic, fibroblastic and clonogenic cells isolated from bone marrow (Friedenstein *et al.*, 1987).

In recent decades controversy surrounding the creation and use of ESCs has piqued interest in somatic cell nuclear transfer (SCNT) and induced pluripotent stem (iPS) cells. SCNT gave rise to the well-publicized birth of lambs from enucleated eggs transplanted with adult somatic

nuclei (1997) (Wilmut *et al.*, 1997). Induced pluripotent stem cells were first generated from differentiated rat fibroblasts in 2006, and have since been derived from several other differentiated cell types (Takahashi and Yamanaka, 2006) including human fibroblasts (Wernig *et al.*, 2007), spermatological cells (Stimpfel *et al.*, 2012), and keratinocytes (Aasen *et al.*, 2008). Knowledge of stem cell biology is constantly advancing, particularly concerning adult stem cells and their expansion within scalable bioreactor systems for clinical applications (Mack *et al.*, 2013; Rafiq *et al.*, 2013; Huang *et al.*, 2015; Heathman *et al.*, 2016; Schmidt and Tranquillo, 2016; Zhao *et al.*, 2016; Eaker *et al.*, 2017; Simmons *et al.*, 2017; Sonnaert *et al.*, 2017).

1.2.2 Stem Cell Potency

Stem cells have now been found in a wide range of tissues and with different differentiation potentials. Classified according to their ability to differentiate into different cell types, stem cells are described as totipotent, pluripotent, multipotent or unipotent. Examples of each type are given in Table 1.1.

Table 1.1: The differentiation capacities of different stem cell types

Stem cell type	Definition	Examples
Totipotent	Capable of division into all cell types required to generate a complete organism, including extra-embryonic tissues	Cells from very early (1-3 days) embryos, or up to and including the 8-cell stage
Pluripotent	Differentiates to all tissues present in an adult organism, but cannot form extra-embryonic tissues	ESCs, as isolated from the inner cell mass (ICM) of a blastocyst (5-14 days post-coitus)
Multipotent	Stem cells able to differentiate towards multiple different linages (≥4)	Stem cells derived from fetal tissue, cord blood, peripheral blood, bone marrow and fat
Oligopotent	Progenitor cells able to differentiate towards 2-3 lineages within a tissue	Lymphoid & myeloid stem cells
Unipotent	Cells give rise to just one cell type. Sometimes described as precursor cells	Hepatocytes, keratinocytes

Adapted from (Choumerianou et al., 2008).

1.2.3 Decellularised substrates in Tissue Engineering

The goal of any decellularisation protocol is to remove all cellular and nuclear material from source tissue, maintaining the functional characteristics of the ECM (Gilbert *et al.*, 2006; Crapo *et al.*, 2011). Both allogeneic and xenogeneic tissue sources are decellularised, providing an almost limitless supply of scaffolds for potential clinical use. Although host immune targeting of any non-self cellular antigens transplanted can induce serious adverse effects in the clinic, such as graft versus host disease, ECM proteins are generally conserved amongst higher species and are well tolerated (Gilbert *et al.*, 2006). Additionally, natural matrices contain binding sites that facilitate cellular adhesion, as found *in vivo*, and provide cues that maintain cell phenotype.

The majority of decellularisation protocols utilise chemical reagents, enzymes and physical methods to remove cellular material (Crapo *et al.*, 2011). Cells are usually lysed using ionic reagents or physical methods, cellular components digested with enzymes and membrane structures disrupted with detergents (Table 1.2). Tissue washes, often comprising phosphate buffered saline (PBS), are performed between application of each active reagent and at the end of protocols, to remove reagents that may induce an adverse host tissue response or cytotoxicity. Physical methods used to facilitate decellularisation include agitation, suction (Butler *et al.*, 2017), freezing, sonication, and, where the target tissue is not characterised by densely organised ECM, application of direct pressure (Gilbert *et al.*, 2006; Badylak *et al.*, 2011; Crapo *et al.*, 2011).

Table 1.2: The mode of action of common reagents used in decellularisation protocols. Reagents may be applied as supercritical fluids, by perfusion, with a pressure gradient across tissue or with agitation (Crapo et al., 2011).

Reagent	Mode of action	References
Phosphate buffered saline (PBS)	*Rinsing of debris and reagents from tissue*	*(Booth et al., 2002)*
Aprotinin	*Protease inhibition*	*(Booth et al., 2002; Gilbert et al., 2006)*
EDTA	*Inhibition of metalloproteinases*	*(Booth et al., 2002; Gilbert et al., 2006; Crapo et al., 2011)*
DNase	*Catalyse hydrolysis of DNA*	*(Booth et al., 2002; Gilbert et al., 2006; Gilbert et al., 2009; Crapo et al., 2011; Butler et al., 2017; Lange et al., 2017)*

Reagent	Mode of action	References
RNase	Catalyse hydrolysis of RNA	(Booth et al., 2002; Gilbert et al., 2006; Crapo et al., 2011; Butler et al., 2017; Lange et al., 2017)
Hypertonic solution	Cell lysis by osmotic shock	(Booth et al., 2002; Gilbert et al., 2006; Crapo et al., 2011; Butler et al., 2017)
Hypotonic solution	Cell lysis by osmotic shock	(Booth et al., 2002; Gilbert et al., 2006; Crapo et al., 2011)
Detergents (e.g. SDS, Triton-X, CHAPS, Tween 20, sodium deoxycholate)	Solubilisation of cytoplasmic and nuclear membranes, removing nuclear remnants and cytoplasmic proteins	(Booth et al., 2002; Gilbert et al., 2006; Baptista et al., 2011; Crapo et al., 2011; Baiguera et al., 2012; Butler et al., 2017; Lange et al., 2017)
Peracetic acid	Terminal sterilisation	(Crapo et al., 2011)

Since the successful decellularisation of porcine small intestine submucosa by Badylak and coworkers (Badylak *et al.*, 1995; Badylak *et al.*, 1998), acellular ECM matrices have been prepared from a plethora of tissue sources. These include whole organs (Ott *et al.*, 2008; Uygun *et al.*, 2010; Badylak *et al.*, 2011; Baptista *et al.*, 2011), trachea (Seguin *et al.*, 2009; Remlinger *et al.*, 2010; Baiguera *et al.*, 2012; Zang *et al.*, 2012; Butler *et al.*, 2017; Lange *et al.*, 2017), cartilage (Elder *et al.*, 2009; Vindas Bolanos *et al.*, 2017), heart valves (Booth *et al.*, 2002; Rieder *et al.*, 2004; Ye *et al.*, 2009; Morticelli, 2013), tendon (Deeken *et al.*, 2011; Yin *et al.*, 2013; Xu *et al.*, 2017), pericardium (Mirsadraee *et al.*, 2006a; Mirsadraee *et al.*, 2007; Mendoza-Novelo *et al.*, 2011; Dong *et al.*, 2013; Vashi *et al.*, 2015), dermis (Barret *et al.*, 1999; Hoganson *et al.*, 2010a; Hogg *et al.*, 2015), urinary bladder (Brown *et al.*, 2006; Rosario *et al.*, 2008), mesothelium (Hoganson *et al.*, 2010b), small intestine (Crowley *et al.*, 2017) and veins (Schaner *et al.*, 2004). Numerous products have made use of decellularised xeno- and allogeneic matrices as bioactive materials for indications ranging from sports-related trauma, bone defects, maxilliofacial and reconstructive surgery and cardiovascular disease (Table 1.3), and medical innovation in the field is ongoing (Parmaksiz *et al.*, 2016).

Table 1.3: A selection of products derived from decellularised tissues for clinical applications

Product	Tissue source	Application(s)	Reference(s)
GraftJacket® (Wright Medical, USA)	*Allogeneic dermis*	*Rotator cuff trauma, Achilles tendon repair*	*(Lee, 2004; Furukawa et al., 2007; Snyder and Bond, 2007; Barber et al., 2008; Bond et al., 2008; Liden and Simmons, 2009; Snyder et al., 2009)*
DermaMatrix® (Synthes Corporation, USA)	*Allogeneic dermis*	*Breast reconstruction, oral cavity repair, bone regeneration, root coverage, gingival and soft tissue ridge augmentation*	*(Becker et al., 2009; Lee et al., 2010; Athavale et al., 2012; Brooke et al., 2012; Parmaksiz et al., 2016)*
Osteofil® (RTI surgical, USA)	*Demineralized allogeneic bone, also lacking organic compounds*	*Repair of bone defects*	*(Takikawa et al., 2003; Lee et al., 2005; Wang et al., 2007)*
Oasis® wound matrix (Smith and Nephew, USA)	*Porcine small intestine submucosa*	*Citical-sized skin defects, such as ulcers*	*(Mostow et al., 2005; Yeh et al., 2017)*
AlloMax™	*Allogeneic dermal collagen*	*Ventral hernia repair*	*(Chauviere et al., 2014; Roth et al., 2015)*
Surgisis® (Cook Biotech. Inc., USA)	*Porcine small intestine submucosa*	*Vaginal wall prolapse, fistula repair, sport's hernias*	*(Edelman and Selesnick, 2006; Ansaloni et al., 2007)*
CardioCel® (Admedus, Australia)	*Bovine pericardium*	*Congenital cardiac abnormalities*	*(Neethling et al., 2013; Strange et al., 2015; Sobieraj et al., 2016)*

1.2.4 Multipotential mesenchymal stromal cells

Following embryonic development orchestrated by ESCs, which form the hundreds of different cell types found in an adult organism, the majority of tissues of the body are believed to be supported by populations of adult stem cells that facilitate growth and repair. These 'adult stem cells' may be multi-, oligo- or unipotent, and can be defined as continuously self-renewing cells that retain the ability to produce differentiated progeny (Islam and Alison, 2009). Niches, the specific tissue locations in which stem cells are believed to reside, may

regulate the stem cell response by integrating various signal types, including physical forces. Adult stem cells with multi- or oligopotency have been discovered in most organs and tissues including peripheral blood, blood vessels, skeletal muscle, skin, dental pulp, gut, liver, placenta, umbilical cord and heart (Godara *et al.*, 2008). Whilst the focus of this thesis is concentrated on MSCs, the use of other multipotent stem cells, including adipose-derived, neural and dental pulp stem cells in tissue engineering is acknowledged.

By definition, MSC differentiate towards the osteogenic, adipogenic and chondrogenic lineages, and have great potential for the development of tissue engineered therapies (Islam and Alison, 2009). MSC have also been shown to differentiate into hepatocytes (Petersen *et al.*, 1999) and towards neuronal phenotypes (Deng *et al.*, 2001; Zheng *et al.*, 2013) Crucially, there are also indications of mechanosensitive behaviour. Knowledge of the mechanoresponsiveness of MSC could inform the design of culture conditions/device manufacture for the application of MSC in tissue engineering.

1.2.5 The Isolation of Multipotent Mesenchymal Stromal Cells

Bone marrow derived human multipotential mesenchymal stromal cells (hMSC) are typically isolated from aspirates harvested from the superior iliac crest of the pelvis (Tae *et al.*, 2006) but may also be isolated from tibial or femoral marrow compartments during surgery (Murphy *et al.*, 2002), or the cadaveric thoracic and lumbar spine (D'Ippolito *et al.*, 1999). However, multipotent stem cells have now been found in other tissues, some of which are capable of being harvested with minimally invasive techniques. These include periosteum (Hui *et al.*, 2005), deciduous and supernumerary teeth (Hara *et al.*, 2011; Gutenberg, 2012), synovium (De Bari *et al.*, 2001), adipose tissue (Zuk *et al.*, 2002; Dhanasekaran *et al.*, 2012) umbilical cord blood and tissue (Erices *et al.*, 2000; Dalous *et al.*, 2012), brain, liver, spleen, kidney, lung, thymus, pancreas, dermis (Godara *et al.*, 2008) and peripheral blood (Roufosse *et al.*, 2004).

Although MSC constitute a very low fraction of cells extracted from bone marrow (0.001-0.01%) methods for isolation and *ex vivo* expansion are efficient. Bone marrow aspirates are first subjected to fractionation on a density gradient solution, such as Percoll, and the light-density cells seeded (10^4-10^6 cells/cm^2). Basal medium containing fetal bovine serum is used in primary culture, lasting 12-16 days, during which nonadherent haematopoetic cells fail to persist in culture; since MSC are the only adherent cells present in this fraction, the property of plastic adherence in itself is adequate for their isolation (Deans and Moseley, 2000; Barry

and Murphy, 2004; Tae *et al.*, 2006). Extracted MSC are not immortalized and exhibit a finite lifetime (Deans and Moseley, 2000; Zimmermann *et al.*, 2003).

1.2.6 Ethics and safety of MSCs in tissue engineering

Ethical and safety considerations that render MSC a preferred choice for tissue engineered solutions include their relative lack of tumorogenicity and immunogenicity. Whilst ESC and iPSC offer advantages on account of their pluripotency, the issue of teratoma formation must be addressed before therapies enter the clinic (Miura *et al.*, 2009; Okano *et al.*, 2013); MSC have a lower degree of plasticity (it should be noted, however, that the list of possible MSC progeny is constantly increasing) but crucially, do not induce teratoma formation *in vivo* (Shi *et al.*, 2012). Additionally, culture conditions of therapeutic stem cells must not necessitate the use of allo- or xenogeneic products . The majority of basic research studies involving MSC are conducted in serum-containing media on account of cost, but where cultured cells may be expected to be clinically applied serum- and xeno-free systems can be employed (Mizukami *et al.*, 2016; Wu *et al.*, 2016). In contrast successful *in vitro* culture of ESC has only been reported with the use of murine embryonic fibroblast (MEF) feeder layers, or using adsorbed ECM proteins to achieve attachment. Xenogeneic feeder layers may transfer xenopathogens or confer hyperimmunogenicity to cultured ESC, and ECM substrate coatings comprising a single protein do not replicate the heterogeneous three-dimensional *in vivo* environment (Soteriou *et al.*, 2013; Laperle *et al.*, 2015).

Additionally, MSC research does not require the donation, destruction or creation of embryos. MSC may be sourced from a range of adult tissues after obtaining donor consent, presenting far fewer ethical concerns regarding their sourcing as compared to ESC (Tuan *et al.*, 2003).

1.3 Current differentiation of MSC in Tissue Engineering

The defining function of MSC is their multilineage differentiation potential. In the body the MSC population is believed to be both maintained in a quiescent state, and induced to differentiate by the local microenvironment, termed the MSC niche. *In vitro* this differentiation capacity has been exploited to generate cells of the required lineage using specific culture conditions. Current strategies to achieve MSC differentiation in tissue engineering mostly disregard the role of mechanical stimuli, and rely on soluble factors.

Although MSC may be induced to differentiate towards neurogenic, myogenic and skeletal muscle lineages, the ability to differentiate towards mesenchymal lineages is considered their defining quality (Dominici *et al.*, 2006). Hence, this discussion is restricted to the differentiation of MSC towards the mesenchymal and smooth muscle lineage, as relevant to this project.

1.3.1 Chondrogenic induction

Cartilage is a connective tissue that, amongst other functions, covers the articulating surfaces of bones in joints (Chen *et al.*, 2006). Articular cartilage is vital to the maintenance of normal joint motion, and joint pain is a major cause of disability. Cartilage damage may occur as a result of trauma or degenerative joint diseases such as primary osteoarthritis. The tissue is composed of a single cell type, chondrocytes, sparsely distributed in a highly specialized extracellular matrix and is relatively avascular and aneural, severely limiting natural regeneration (Chen *et al.*, 2006). Studies investigating MSC for cartilage tissue engineering have included combining MSC with soluble and/or injectable scaffolds (Quintavalla *et al.*, 2002; Murphy *et al.*, 2003; Csaki *et al.*, 2008), implantation of MSC after *in vitro* differentiation to chondrocytes, and loading MSC onto three-dimensional scaffolds *in vitro* (Csaki *et al.*, 2008). Chondrogenic differentiation of MSC is induced *in vitro* through three-dimensional culture, often in the form of a cell pellet, with serum-free medium containing a stimulus from the transforming growth factor beta (TGF-β) superfamily (Mucsi *et al.*, 1996; Barry and Murphy, 2004; Alberts *et al.*, 2008; Csaki *et al.*, 2008).

1.3.2 Osteogenic induction

Bone is formed of osteocytes embedded in a highly mineralized matrix that endows the tissue with the mechanical properties necessary for its structural purpose. There is demand for tissue-engineered bone in a wide range of fields including orthopaedic, neuro- and craniofacial surgery, periodontics and dentistry (Nassif and El Sabban, 2011). MSC have been used to engineer bone to treat site-specific bone defects, such as non-union fractures (Shang *et al.*, 2000), and degenerative conditions such as ostegenesis imperfecta and osteoporosis (Mauney *et al.*, 2005). Research into defect repair and healing has utilised hydroxyapatite, tricalcium phosphates (Wang *et al.*, 2005), synthetic and natural polymers (Yoshimoto *et al.*, 2003) and demineralized bone as scaffolds for MSC (Louis-Ugboo *et al.*, 2004; Meinel *et al.*,

2004; Nassif and El Sabban, 2011). Osteogenic differentiation in MSC requires the use of the glucocorticosteroid dexamethasone, organic phosphates such as β-glycerophosphate and fetal bovine serum. Bone morphogenic protein (BMP) family growth factors and other supplements such as 1,25-dihydroxyvitamin D_3 are also commonly used in osteogenic induction (Tuan *et al.*, 2003; Tae *et al.*, 2006). These soluble factors have been shown to encourage osteogenesis from experimental findings that show an increased expression of the osteogenic markers octeocalcin, osteopontin and alkaline phosphatase in MSC as a consequence of their use (Hanada *et al.*, 1997; Liu *et al.*, 1999; Fujita *et al.*, 2001; Lodish *et al.*, 2008). For example phosphates, such as the β-glycerophosphate used *in vitro* to induce osteogenic differentiation, are known to induce the mRNA and protein expression of these markers. Phosphate is transported into osteoblasts via the sodium-dependent type III phosphate transporter, and once in the cell, is thought to affect the production and nuclear export of core binding factor alpha 1 (Cbfa1) (Fujita *et al.*, 2001; Tuan *et al.*, 2003). Cbfa1 binds to the *cis-a*cting element OSE2, which in turn activates the osteocalcin promoter. OSE2 has since been found in the promoter regions of all major genes expressed by osteoblasts, so Cbfa1 may play an even greater role in ostegenic differentiation of MSC (Ducy *et al.*, 1997; Ducy, 2000).

1.3.3 Adipogenic induction

Adipose tissue is a loose connective tissue composed of adipocytes and characterized by its role in lipid storage and impact absorption. Fat also secretes a wide variety of hormones and proteins, including leptin, oestrogen, resistin, adiponectin, visfatin, omentin and cartonectin, and as such is recognized as an endocrine organ (Schäffler and Schölmerich, 2010). Adipogenic tissue engineering generally aims to restore the aesthetic function of soft tissue. Hence, such research finds applications in reconstructive, cosmetic and correctional treatments that may be necessary following tumour resection, carcinoma removal, trauma and to correct congenital abnormalities (Godara *et al.*, 2008). Attempts at adipose tissue engineering have typically used soft scaffold materials such as fragmented omentum, polyester based absorbables, hyaluronic acid, collagen, polyethylene glycol (PEG) and chemically modified alginate in a scaffold only or 'scaffold plus cells' approach (Gomillion and Burg, 2006). Although preadipocytes and adipose-derived stem cells have been commonly used (Flynn *et al.*, 2007), mesenchymal stem cells can be induced to undergo adipogenic differentiation by treatment with supplements such as dexamethasone, 3-isobutyl-1-methylxanthine and indomethacin in monolayer culture (Pittenger *et al.*, 1999; Tuan *et al.*,

2003; Tae *et al.*, 2006). The use of specific markers to assess the efficacy of adipogenic differentiation is not necessary; the presence of large lipid vacuoles in the differentiated cells is a suitable lineage determinant, and may be detected by oil red O staining. The supplements used to differentiate MSC towards an adipogenic lineage interact with transcription factors such as proliferator-activated receptor gamma (PPAR-γ), C/EBP-α and C/EBP-β (Lehmann *et al.*, 1997). Wnt signalling pathways, known to maintain preadipocytes in a naïve state by inhibiting C/EBP-α and PPAR-γ, can also be suppressed to enable adipogenic differentiation (Tuan *et al.*, 2003).

1.3.4 Smooth muscle induction of MSC

Smooth muscle is involuntary, non-striated muscle and is found in blood and lymphatic vessels, the urinary bladder, uterus, the reproductive, respiratory and gastrointestinal tracts and the iris. Smooth muscle engineering is of clinical interest for the regeneration/repair of the cardiovascular system. The high and increasing prevalence of cardiovascular disease means that demand for tissue-engineered therapies is high, and current treatments, such as the replacement of diseased arteries with autologous veins, are dependent on healthy donor sites (Gong *et al.*, 2009). However, there is a relative lack of research into MSC differentiation towards the smooth muscle lineage, so accepted protocols are yet to be established. Approaches used to induce and quantify differentiation towards a smooth muscle lineage are described in

Table *1.4*. Crucially, one such approach used to differentiate MSC towards a smooth muscle lineage is the application of strain. As summarised in

Table *1.4*, Park *et al* investigated the impact of biaxial and uniaxial strain, applied at a frequency of 1 Hz, on the expression of smooth muscle cell (SMC) markers in cultured MSC. Interestingly, this work noted a differential effect between uniaxial and biaxial strain; uniaxial strain induced upregulation of the markers studied, whereas biaxial promoted their downregulation(Park *et al.*, 2004). This may reflect the fact that uniaxial strain, applied in the circumferential direction, is the primary physical stimulus experienced by SMC *in vivo.* The signalling pathways that mediate smooth muscle differentiation of MSC are poorly understood; however the mitogen-activated protein kinase/extracellular signal-regulated protein kinase pathway (MAPK/ERK) pathway activity has been implicated in studies using inhibitors such as PD98059 and PD98059 (Tamama *et al.*, 2008; Goerke *et al.*, 2012). That

very little is understood regarding the differentiation of MSC to SMC provides scope for studies of the role of physical stimuli in smooth muscle tissue engineering (Park *et al.*, 2004).

Table 1.4: Summary of approaches to MSC differentiation towards a smooth muscle lineage in selected publications

Differentiation approach	Primary outcome(s)	Findings	Reference
Examination of the impact of different medium FBS concentrations, and transforming growth factor-β1 (TGFβ1)on the differentiation of MSC towards SMC	*Calponin, smooth muscle α-actin and smooth muscle 22α expression, detected by immunohistochemistry*	*No change in differentiation potential of MSC by [FBS] in the range 2-10%* *Promotion of smooth muscle lineage specification by TGFβ1*	*(Gong et al., 2009)*
Co-culture of MSC with endothelial progenitor cells (EPC) or human umbilical vein endothelial cells (HUVEC)	*Expression of smooth muscle myosin, smooth muscle 22α and calponin, detected by immunohistochemistry and relative quantitative polymerase chain reactions (qPCR)*	*Smooth muscle lineage specification of MSC cultured with EPC, in a time, cell-contact and of mitogen-activated protein kinase/extracellular signal-regulated kinase (MAPK/ERK) pathway-dependent manner*	*(Goerke et al., 2012)*
Measurement of the impact of biaxial and uniaxial strain on the regulation of SMC markers by MSC cultured on elastin- or collagen coated substrates	*Smooth muscle α-actin and smooth muscle 22α expression by qPCR, immunohistochemistry* *Protein expression by immunoblotting*	*Downregulation of smooth muscle α-actin by 40-50 % following application of biaxial strain* *Downregulation of smooth muscle 22α by ~25% following application of biaxial strain* *Transient increase in smooth muscle 22α and smooth muscle α-actin following application of uniaxial strain*	*(Park et al., 2004)*

		Alignment of MSC perpendicular to strain direction following application of uniaxial strain	
Measurement of the impact of angiotensin II treatment on the differentiation of MSC towards SMC	*Expression of smooth muscle α-actin, calponin, l-caldesmon, h-caldesmon and smooth muscle myosin heavy chain (SM-MHC) by immunoblotting and immunohistochemistry*	*Increased expression of smooth muscle markers in response to angiotensin II treatment* *Increased contractility in differentiated cells in response to membrane depolarisation*	*(Kim et al., 2008)*
Overexpression of micro RNA 145 for the production of mature SMC	*Expression of smooth muscle α-actin, calponin, caldesmon and SM-MHC, detected by qPCR* *Protein expression of the above, detected by immunohistochemistry*	*Upregulation of SMC markers in MSC and increased marker protein expression following the introduction of micro RNA 145* *Contractility in response to vasoactive agents in treated MSC* *Production of fully differentiated MSC-derived SMC using approach tested*	*(Pajoohesh et al., 2016)*
Inhibition MAPK/ERK pathway through inhibition of mitogen-activated protein kinase kinase (MEK). The MAPK/ERK pathway exerts anti-myogenic signals in SMC	*Expression of smooth muscle α-actin, h-caldesmon, SM-MHC and myocardin, detected by qPCR* *Protein expression of the above, detected by immunohistochemistry and immunoblotting*	*Upregulation of SMC markers and increased marker protein expression following MEK inhibition in MSC* *Adoption of SMC-like phenotype by treated MSC, including ligand-induced contractility*	*(Tamama et al., 2008)*

1.3.5 The MSC niche

There is evidence that the role of MSC in the body is regulated by a local microenvironment termed the niche. The stem cell niche is a three-dimensional environment composed of cells, soluble factors and ECM (Fuchs *et al.*, 2004; Sun *et al.*, 2012a). The purpose of MSC in the body is to act as a reserve for the maintenance and repair of the mesenchymal tissues, some non-mesenchymal lineages, and to support hematopoiesis (Bianco, 2011; Gotts and Matthay, 2012). Many studies have now suggested a perivascular location for the MSC niche in almost all tissues in which they are found (Kolf *et al.*, 2007; Kuhn and Tuan, 2010), as evidenced by the expression of α-smooth muscle actin in extracted MSC (da Silva Meirelles, 2006). A perivascular location for the niche appears logical as it may explain how MSC gain access to a wide variety of tissues. Cell types thought to interact with MSC in the bone marrow niche include hematopoietic progenitors and their progeny, fibroblasts, endothelial cells, osteoblasts, osteoclasts, adipocytes and cells of the immune system (Yin and Li, 2006). Cadherins, transmembrane glycoproteins that form cell-cell adhesions between MSC and these supporter cells, have been shown to influence migration, differentiation and polarity in MSC through their interaction with the Wnt pathway (section 1.8.4.1.1)(Alberts *et al.*, 2008; Kuhn and Tuan, 2010). As well as exerting influence through direct physical contact, these supporting cells have been reported to influence MSC fate through the secretion of soluble factors such as FGF-2, which maintains MSC growth and differentiation potential *in vitro*, and interleukin-6 (IL6), which acts as an autocrine signalling factor (Kuhn and Tuan, 2010). Additionally, hypoxic conditions, comparable to the *in vivo* bone marrow microenvironment, appear to enhance both the proliferative capacity and plasticity of MSC as compared to normoxic conditions (Grayson *et al.*, 2006). No specific ECM components have been identified that maintain MSC in a naïve state, but changes in the physical properties of the microenvironment can modulate cell shape and signalling events, affecting MSC specification. It is widely postulated that physical cues, soluble and cellular factors present in the niche all mediate MSC quiescence and fate; mechanotransduction studies are vital to understand the potential for MSC differentiation in tissue engineering.

1.4 Application of mechanical strain in Tissue Engineering

Physical cues present *in vivo* include compressive, uniaxial and biaxial strains, and may present in both static and cyclic fashion. Strategies for tissue engineering of many lineages now incorporate various stimuli, dependent on the tissue of interest, in biomimetic approaches. For example, researchers investigating tenogenic differentiation of MSC frequently apply uniaxial strain to seeded substrates (Butler *et al.*, 2008; Chen *et al.*, 2008; Morita *et al.*, 2014), and the histoarchitecture of cartilage engineered in the presence of compressive or hydrodynamic forces is more comparable to native tissue than constructs cultured in their absence (Heath, 2000; Marsano *et al.*, 2006; Huang *et al.*, 2010; Kelly and Jacobs, 2010). Additionally, Park *at al* have previously reported findings, of particular relevance to this study, that indicate that the application of uniaxial strain to MSC seeded on a flexible substrate promotes differentiation towards a smooth muscle lineage. In this work, hMSC were seeded on collagen- or gelatin-coated silicone membranes and strained in a custom bioreactor. The expression of genes indicative of lineage specification was measured using DNA microarrays; after one day, expression of the smooth muscle α-actin and smooth muscle 22α genes was selectively upregulated compared to markers of other lineages, with the return of gene expression to basal levels coincident with cell alignment changes (Park *et al.*, 2004). This work, amongst the plethora of other reports highlighting the role of mechanical stimuli in MSC differentiation, lends credence to the strategy of mimicking *in vivo* biomechanics in tissue engineering application.

Development of bioreactor systems that mimic the mechanical stimuli that help to guide tissue development and homeostasis *in vivo* is extensive (Zhao *et al.*, 2016), and the remit of this thesis is limited to the discussion of uniaxial strain apparatus only. Bioreactors are developed both commercially and in-house in academic institutions, and may be single or multi use. Single use designs may be preferable since they may mitigate sterility concerns, but commercially-produced, single-use apparatus are currently limited to stirred tank, rocking and perfusion systems (Bose, 2017; GE, 2017). In contrast, uniaxial strain bioreactors, relevant to the work presented in this thesis, are normally custom-built multiple use apparatus, with no consensus on design as yet established. However, these apparatus invariably involve clamping a seeded substrate to a stationary and motile each, and distending as required (Altman *et al.*, 2002b; Saber *et al.*, 2010; Salazar *et al.*, 2015; Schmidt and Tranquillo, 2016). Validation and wide adoption of an effective design style for uniaxial strain bioreactors to be used in mechanostimulation investigations is likely to enhance the insight provided by such work.

1.5 Evidence of MSC mechanosensitivity

As described in section 1.3, most differentiation of MSC *in vitro* has utilised soluble, chemical or cellular factors, and has not considered the physical environment. Despite this, there is increasing evidence that mechanical stimuli affect the differentiation of MSC. However, very little is understood regarding the mode in which physical stimuli elicit biochemical signalling, and many studies have failed to replicate the *in vivo* environment of MSC satisfactorily in the laboratory. The state of current research regarding mechanostimulation during the differentiation of MSC is presented here.

1.5.1 Physical stimulation during osteogenic differentiation of MSC

Mechanical stimuli are required for healthy bone formation and metabolism, and the osteogenic differentiation of MSC has been investigated under compression and strain. MSC seeded on non-natural scaffolds and subjected to compression have shown increased osteogenic differentiation as compared to controls. For example, Park *et al* observed increased production of osteogenic matrix components (bone sialoprotein, osteopontin and type I collagen), integrin expression and alkaline phosphatase staining when MSC cultured on microscale chips were placed under dynamic hydraulic compression (Park *et al.*, 2012b). Integrins are heterodimeric receptors that span the cell membrane, forming a link between extracellular matrix components to cytoskeletal, adaptor and signalling molecules in the cytoplasm (Alberts *et al.*, 2008).

Additionally, physical stimuli have shown similar efficacy in the osteogenic induction of MSC as commonly used soluble factors. MSC cultured on polyurethane foam and compressed at 5% global strain cyclically (1Hz) showed no difference in matrix production as compared to non-loaded MSC treated with the osteogenic inductor dexamethasone. This suggested that dynamic loading could stimulate the osteogenic induction of MSC in the absence of soluble factors, or may contribute additively towards more effective differentiation (Sittichokechaiwut *et al.*, 2010). Cyclic strain has also been found to direct MSC towards an osteoblastic lineage, but data reported has highlighted the importance of MSC culture on an appropriate matrix (Friedl *et al.*, 2007; Huang and Ogawa, 2010; Ngiam *et al.*, 2010). Huang *et al* grew MSC on substrates coated with various ECM proteins. Whilst mechanical stimulation (3% elongation at 0.1Hz) increased alkaline phosphatase activity and mineralized matrix

deposition in all cases, it appeared that cues from the substrate also drove differentiation. In this case, physical stimulus increased phosphorylation of focal adhesion kinase (FAK), which interacts with the MAP kinase signalling module to phosphorylate Cbfa 1. As mentioned previously, Cbfa 1 binds promoters of osteoblast-related genes, regulating differentiation (Huang *et al.*, 2009). Significantly, in another study investigators testing the effect of cyclic strain (1% at 1Hz) on MSC differentiation with a variety of substrates concluded that the effect of the stimulus was dependent on substrate-cell adhesion after obtaining mixed results (Ngiam *et al.*, 2010). This is logical, as adhesion molecules are thought to be responsible for mechanotransduction in many cell types, and highlights the needs for substrates that facilitate normal MSC adhesions.

1.5.2 Physical stimulation and adipogenic differentiation in MSC

In contrast to the other work described in this review, there is evidence that physical stimulation retards adipogenic differentiation of MSC. Although very little literature exists regarding mechanical stimulation during adipogenesis, separate investigators have reported that mechanical stimulation maintains levels of the gene regulatory protein β-catenin and even induces nuclear translocation (Sen *et al.*, 2008; Khayat *et al.*, 2012). In both cases, mechanical strain inhibited PPARγ and adiponectin expression and biased differentiation towards an osteogenic lineage. In adipogenesis, β-catenin is normally targeted for degradation by the molecule GSK3β, which is inactivated by strain through phosphorylation (see section 1.8.4.1.1). Whilst the effect on adipogenesis in MSC is one of retardation, it is a strong suggestion that mechanotransduction plays a significant role in these cells as adipogenesis of MSC was retarded by physical stimuli even after treatment with adipogenic inducers (Sen *et al.*, 2008).

1.5.3 Physical stimuli and tenogenic differentiation in MSC

Tendon is an obvious target for tissue engineering using physical forces owing to its mechanical function, and strain is known to be a crucial factor in tendon and ligament remodelling (Kim *et al.*, 2002). Studies investigating tendon and ligament differentiation in MSC typically examine the expression of marker genes, including type I collagen, type III collagen, scleraxis, tenascin-C and the mRNA expression of matrix metalloproteinase-3 (MMP-3), which contributes to matrix remodelling. Interestingly, whilst mechanical strain has

generally been found to increase differentiation of MSC towards a tendon/ligament lineage, there is evidence that substrate choice greatly affects the impact of the physical stimulus on MSC. In one study, cyclic strain of MSC on a collagen gel matrix led to tenogenic and osteogenic differentiation depending on the level of strain applied. Higher levels of strain (10%) contributed to tenogenic differentiation and lower (3%) to osteogenic differentiation, reflecting the higher strain experienced by tendon naturally (Chen *et al.*, 2008). Another study, measuring the marker molecule scleraxis and signalling and ECM molecules (collagens, Wnts, and MMP) of MSC undergoing cyclic stretch in a collagen gel also reported increased tenogenic differentiation, and found that Wnt signalling was involved. However, investigations of tenogenic differentiation of MSC at a comparable cyclic stretch, but on a poly(L-lactide) (PLA) scaffold, found that the stimulus had no effect on MSC differentiation (Kreja *et al.*, 2012). Whilst collagen gels present certain caveats in mechanotransduction studies (discussed in more detail in section 1.6), collagen I is the major component of tendon extracellular matrix and may offer an environment more comparable to natural tissue than PLA. Hence, stretch applied on the macroscale may be more appropriately transduced to the cellular level.

1.5.4 Substrate stiffness and mechanotransduction in MSC

Both externally and internally generated mechanical stimuli can initiate mechanotransduction. Mechanotransduction arising from internal forces has been investigated using gels of different stiffness, and has been found to influence MSC differentiation. Stiffer substrates promote MSC differentiation towards cell types found in stiff tissues *in vivo*, such as bone, and conversely softer substrates promote differentiation towards cell types normally located in softer tissues, such as neurons (Discher, 2005). This was confirmed by work in which matrix-induced lineage specification could not be reprogrammed with soluble induction factors after one week of culture on matrices of various elasticities (Engler *et al.*, 2006). Other workers found that in cultures treated with TGF-β, which can stimulate differentiation towards both smooth muscle and chondrogenic lineages, matrix elasticity determined cell fate. It also rendered traditional inducers of differentiation more effective (Park *et al.*, 2011a). The cytoskeleton has been strongly implicated as a facilitator of these mechanotransduction events, with the use of blebbistain, a myosin II inhibitor, blocking elasticity-induced differentiation. Actin structures are linked to focal adhesions, which provide a pathway for force transmission between the cytoskeleton and ECM, and are associated with signalling complexes such as protein kinases. In one of the few studies to date investigating the

signalling pathways in mechanotransduction, Shih *et al* found that inhibition of focal adhesion kinase (FAK) and Rho kinase (ROCK) eliminated the osteogenic effect of stiff matrices. This led investigators to conclude that cytoskeletally-generated forces from the cell interior sense substrate stiffness through integrins, and subsequently ROCK, FAK and finally the MAPK ERK ½ are activated. Erk is able to enter the nucleus and phosphorylate gene regulatory complexes, giving rise to gene expression patterns corresponding to differentiation towards specific lineages (Shih *et al.*, 2011).

1.6   Limitations of current approaches to mechanostimulation in MSC

Despite increasing evidence that MSC are mechanosensitive, there are several caveats associated with previous attempts at mechanostimulation of MSC. These are related to experimental design, substrate/scaffold choices and the relative lack of investigation into the force-mediated differentiation of MSC specifically towards a smooth muscle lineage.

1.6.1   The substrates used in current MSC mechanotransduction studies are inadequate

The substrates used in previous investigations of mechanotransduction in MSC do not adequately represent the natural environment. *In vivo* all cells, including MSC, exist in a three-dimensional environment of ECM proteins and cellular neighbours, to which they are attached through integrins and cadherins (Alberts *et al.*, 2008). These cellular adhesions are likely to be involved in transducing physical cues. If cell-substrate attachments cannot be made in three dimensions mechanical stimuli are not effectively transmitted to any associated mechanosensitive signalling pathways (see section 1.8.4). Adhesions cannot be made on substrates made from non-natural (non-ECM) materials that do not contain the appropriate sequences for binding, such as the RGD peptide integrin binding site. Even when more appropriate biomaterials are used, many pre-prepared scaffolds are not readily penetrated by cells. When applied to such a scaffold cells adhere to the surface only, and hence experience applied force in a two-dimensional environment. At the time of writing this review, there are few reports of the use of a three-dimensional scaffold for the mechanical stimulation of MSC (Chang *et al.*, 2007), and many materials reported are unlikely to encourage cellular adhesion. Of the ECM proteins used to coat substrates, collagen I gels are overwhelmingly employed (Park *et al.*, 2004; Ku *et al.*, 2006; Chen, 2008; Sen *et al.*, 2008; Huang *et al.*, 2009; Park *et al.*,

2011b; Shih *et al.*, 2011; Khayat *et al.*, 2012; Zhou and Niklason, 2012), and a fibronectin coating has also been tested (Friedl *et al.*, 2007). Non-ECM substrates used include polyacrylamide (Engler *et al.*, 2006), microchips (Park *et al.*, 2012b; Zhou and Niklason, 2012), polyurethane (Sittichokechaiwut *et al.*, 2010), PLA (Kreja *et al.*, 2012) and silicon (Huang *et al.*, 2012). The requirement for three-dimensional substrates for mechanostimulation of MSC that facilitate normal cellular adhesions highlights the importance of natural ECM scaffolds in this field.

1.6.2 Varying the mode and frequency of force application may optimise mechanostimulation of MSC

In current literature regarding the mechanostimulation of MSC the effect of the magnitude of applied forces has formed the primary focus, and varying the frequency and mode of force application has been largely neglected. It is now becoming increasingly clear that forces of equal magnitude may elicit distinct cellular responses, depending on whether they are applied in a static or cyclic fashion, and that the frequency of application of cyclic forces may also be important.

Mechanotranduction occurs as a result of protein conformational changes that are subsequently converted into biochemical signalling. This may occur directly, as in the case of membrane channels, or indirectly, through the subsequent binding of signalling proteins. According to the dynamic model of mechanotransduction, any frequency-dependent effect can be related to the bond lifetimes within the proteins involved in detecting the force (Hoffman *et al.*, 2011). For example, cellular adhesions may be dynamic (nascent) or stable (mature) depending on the rate of adhesion turnover. Nascent adhesions have a faster turnover because the weaker bonds integral to them have shorter lifetimes, and mature adhesions vice versa. It has been theorised that the rate of adhesion turnover may be related to the likelihood of mechanotransduction occurring. For example, cyclic force application may not stimulate the stronger mature adhesions, but conformational change is more likely in nascent adhesions as their weaker linkages yield, leading to transduction of the force to downstream signalling pathways. Conversely, nascent adhesions may readily adapt under the influence of static stretch, averaging the effect of the stimulus and resulting in no long-term signalling. Mature adhesions may be unable to adapt in this way and their conformation, and hence signalling, may be changed.

Additionally, the frequency of cyclic force application may impact the response generated. A mathematical model has suggested that cells may adopt a parallel or perpendicular alignment in response to force according to the relationship between remodelling rates of load bearing structures, such as focal adhesions, and the frequency of stimulus application. According to this theory, if the frequency of force application is faster than typical remodelling rates of the structures involved, cells may align perpendicularly to the direction of the force to minimize stretching on mechanically sensitive elements. This would be expected to reduce the impact of the applied stimulus and reduce or abolish mechanotransduction. However, if the rate of force application is lower than that of remodelling, these load bearing structures may be strengthened and cells may align parallel to the stimulus. It has been suggested that cells aligned in parallel to mechanical cues experience maximum force and hence are more sensitive to applied stimuli (Hoffman *et al.*, 2011). Hence, the mode and frequency of mechanical stimuli should be optimised as rigorously as the magnitude as the force itself if mechanotransductive effects are to be properly understood. Such experiments may also shed light on the stability and turnover rates of the subcellular structures involved.

1.6.3 There is little literature regarding mechanotransduction and the differentiation of MSC towards smooth muscle

Differentiation of MSC towards a smooth muscle lineage is little-studied in the field of mechanotransduction, despite arterial disease being a major cause of mortality worldwide. In one key study, Park *et al* showed that MSC are able to differentiate towards a smooth muscle lineage, but the experimental design suffered from the caveats described previously as only one duration and frequency of stimulus was investigated (10% strain, 1 Hz) (Park *et al.*, 2004). Interestingly, this work reported that smooth muscle markers (α-actin and SM-22a) were transiently upregulated but returned to basal levels after 1 day of stimulation, at which point the MSC had aligned perpendicular to the strain direction. This suggests that the way in which force is applied may affect alignment responses, and that perpendicular alignment of cells reduces downstream biochemical consequences as theorised by Hoffman *et al* (2011).

1.7   The Basis of Mechanotransduction

1.7.1   The stages of mechanotransduction

All mechanotransduction is caused by the impingement of force on proteins with conformations, and hence biochemical activity, that alter as a consequence of physical stimulation. Applied forces must first be delivered to a force sensitive protein, which may be distant from the stimulus, in a process termed mechanotransmission. On encountering a mechanically-gated protein the transmitted force induces conformational change, or mechanosensing. Conformational changes may alter the chemical activities of proteins, which in turn impacts upon cellular processes. The way in which mechanotransduction events ultimately influence the cell is termed mechanoresponse, and may involve changes in the cell cycle leading to proliferation, protein manufacture and cell alignment (Bao 2010; Hoffman et al. 2011). Crucially, gene expression and differentiation may also be induced as a form of mechanoreponse. The following section focuses on the process of mechanosensing, and provides a description of protein structure, conformation and conformational change.

1.7.2   Protein Structure, Conformation and Force

Proteins are polymers of amino acids that undergo self-assembly to form perhaps the most functionally sophisticated molecules known (Lodish et al. 2008; Alberts et al. 2008; Atkins & De Paula 2010). Whilst the functional properties of most molecules is determined by their configuration (the direct connectivity of atoms through chemical bonding), the biochemical activity of proteins is chiefly governed by their conformation (Atkins & De Paula 2010). Protein conformation, or the spatial arrangement of component residues, is determined by non-covalent interactions. The spatial arrangement of residues also determines the specificity and chemical activity of proteins. Thus, it is necessary to discuss protein structure and biophysics in order to appreciate the subcellular basis of mechanotransduction.

1.7.2.1   Levels of protein structure

Proteins are hierarchical and are described in terms of primary, secondary and tertiary structure. The primary structure of a protein is the polypeptide chain: the linear sequence of amino acids connected by covalent bonds, as coded for by DNA. Residues within this

polypeptide chain interact with each other to induce bond rotations, altering the spatial arrangement of residues and giving rise to secondary structure. Secondary structures are maintained by hydrogen bonding between the amine, carbonyl and R- groups of amino acids and principally comprise beta (β) sheets and alpha (α) helices (Fig. *1.1*).

'Tertiary structure' is used to describe the overall three-dimensional arrangement of all amino acid residues in a polypeptide. Some proteins also form quaternary structures through the aggregation of different polypeptide subunits. Whilst only hydrogen bonding is involved in the folding of secondary structures, additional driving forces, such as hydrophobic interactions and disulphide bonding, contribute to tertiary and quaternary structures. These driving forces, and how they combine to engineer the lowest energy conformation of a polypeptide in a given environment, will be discussed in section 1.7.2.2 (Lodish et al. 2008; Alberts et al. 2008).

| **A** | **B** | **C** |
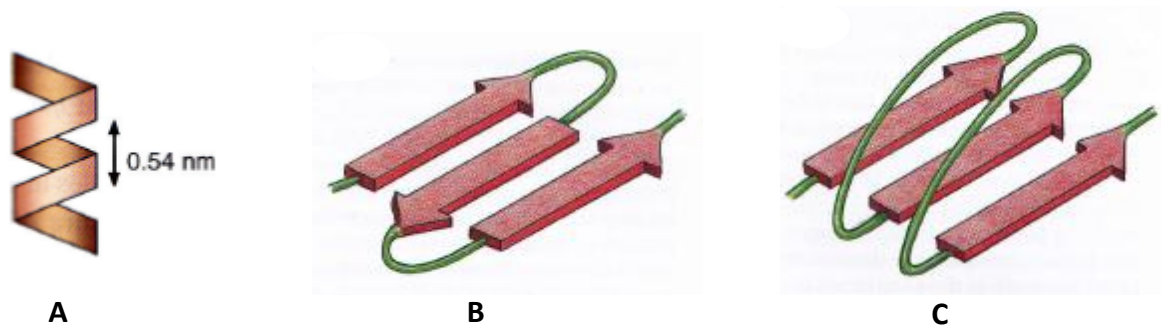
Fig. 1.1: The most common secondary structures formed by hydrogen bonding within polypeptide chains. *α-helices (A) form from interactions between amino acids within the same polypeptide, to give a helical structure, whereas β-sheets can arise from bonding between β strands originating from the same or a different polypepetide, giving rise to lateral packing (B & C). β-sheets can be antiparallel (B) or parallel (C), depending on the directionality of β strands. Diagram adapted from Alberts et al. 2008.*

1.7.2.2   Protein folding and conformation

A polypeptide chain folds to the conformation, or three-dimensional spatial arrangement, that has the lowest energy for its environmental conditions. Folding occurs as chemical attractions and repulsions are satisfied through weak intramolecular bonding that is changeable according to the chemical and physical environment. This typically includes hydrogen bonding, Van der Waals forces and the hydrophobic effect. Satisfying the chemical requirements of a

polypeptide by making favourable interactions reduces the free energy of a protein, and gives rise to the three-dimensional structures that determine function.

Despite the relationship between shape and function, there are in fact a number of conformations a polypeptide may adopt, and the favourability of each one is determined by the immediate environment. This is well recognised through the knowledge that changes in factors such as pH and temperature can cause denaturation – or the loss of biological function of a protein as a result of conformational change (Atkins & De Paula 2010; Boal 2012).

Mechanotransduction and denaturation in fact occur for strikingly similar reasons: changes in the protein environment initiate conformational changes that in turn affect functionality. Applied forces may break the intramolecular interactions responsible for protein structure, and any conformations that require these broken interactions for stabilisation will be more energetically disfavoured (Fig. 1.2).

Proteins that undergo mechanically-gated conformational changes may behave as mechanosensors, which impact upon downstream biochemical signalling to influence cellular behaviour, as described in section 1.8.4. This may occur directly, as in the case of ion channels, or indirectly through interactions with other proteins and biomolecules, as described by Fig. 1.3.
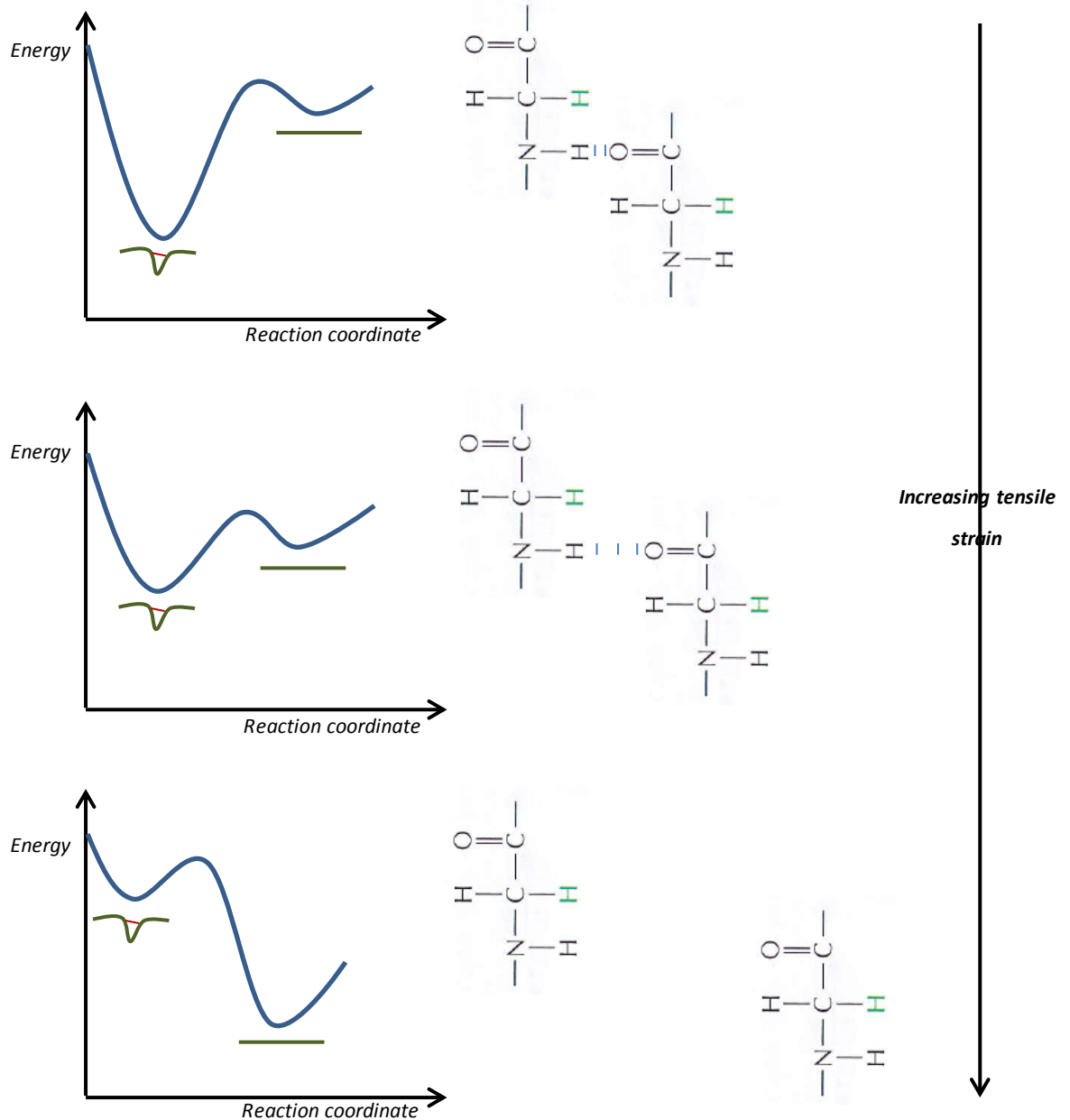
Fig. 1.2: Simplistic example of conformational change in a theoretical protein that may adopt a 'kinked'
or open conformation, depending on the state of hydrogen bonding between two glycine residues. *In*
the absence of mechanical strain the hydrogen bond is maintained, making the 'kinked' conformation
lower energy than the open (top). When moderate tensile strain is applied the hydrogen bond is
lengthened and weakened, making the kinked conformation increasingly difficult to maintain and
increasing the free energy for this conformation (middle). However, the protein most likely retains this
kinked conformation as it is still more energetically favourable than the open conformation. However,
higher tensile strains lead to a loss of hydrogen bonding between the glycine residues. This interaction is
crucial to maintaining the kinked conformation, which is now energetically disfavoured compared to the
open conformation. Conformational change is now likely to occur. Mechanotransduction may occur if this
conformational change leads to a change in downstream signalling. Partially adapted from Alberts et al.
2008.
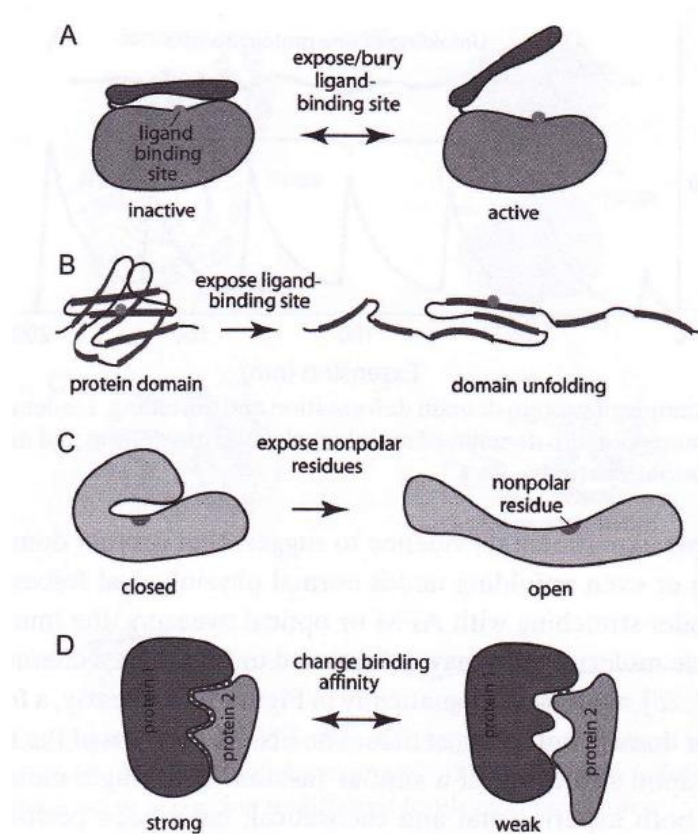
Fig. 1.3: Examples of conformational changes that initiate biochemical signalling in an indirect manner (i.e. through interactions with other species). *Ligand binding sites could be exposed or hidden in proteins with 'lids' as a result of force (A), or exposed by force-induced unravelling (B). Non-polar residues may be exposed in mechanically-gated proteins which may then interact non-specifically with other biomolecules (C). Finally, force-induced conformational change may alter the binding affinity of a mechanosensor protein with its substrate (D). Adapted from Bao 2010.*

1.7.3 Biophysical theories

Although mechanotransduction is not currently well understood, theories have been developed to explain the relationship between mechanotransmission, mechanosensing and mechanoresponse. Switch-like models suggest an entirely separate, serial progression through these stages. In this view, the frequency of force application does not impact the likelihood of mechanotransduction, and only forces strong enough to break the intramolecular bonds of mechanically-gated (mechanosensor) proteins elicit a response. Additionally, switch-like theories assume that the cellular response to mechanotransduction, or mechanoresponse, does not feed back to modify the proteins involved. This, however, is not supported by experimental data: many tissues show clear frequency-dependent tissue remodelling, and force-mediated signalling has been reported to modify structures

responsible for transmission and sensing (Balaban et al. 2001). To account for this, dynamic models have been devised that consider mechanotransduction as a fine balance of biophysical equilibria (Hoffman et al. 2011).

Unlike switch-like models, dynamic models do not consider proteins as indefinitely stable, fixed entities. Transmission of force to mechanosensor proteins can only occur through intact structures; these structures are often composed of subunits held together by linkages in dynamic equilibrium that may dissociate under applied force. Dynamic models suggest that the relationship between the time taken for the dissociation of mechanotransmitters and the frequency of applied force may be important in determining whether physical stimuli are actually delivered to mechanosensors, and that the process is not solely reliant on the magnitude of force applied (Hoffman et al. 2011). Subunit dissociation occurs at characteristic rates: if force is applied at a higher frequency than this rate mechanotransmitters cannot disintegrate before successful transmission occurs, regardless of the strength of binding. In simpler terms, subunits interchanging between a connected and dissociated state cannot fluidize, and hence dissipate an applied force, even if it exceeds the strength of bonding within the structure, if it is applied faster than the time taken for these bonds to break.

Finally, unlike switch-like models, dynamic models do not consider the stages of mechanotransduction to be separate. It is recognised that mechanoresponses can feed back to subcellular structures and affect how forces are transmitted and sensed. Examples include the regulation of cytoskeletal genes and ECM deposition, and the strengthening of binding between adhesions and the cytoskeleton in response to force application (see Fig. 3.4).
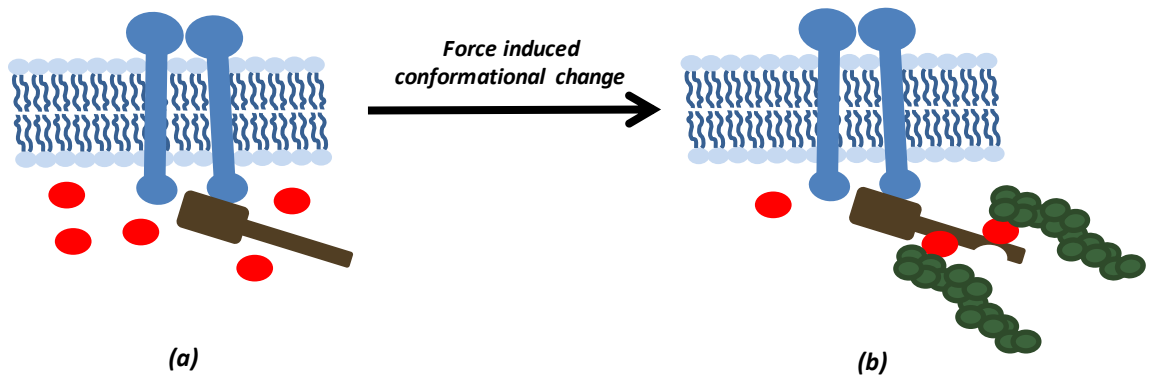
Fig. 1.4: Strengthening of the actin (green) and integrin (blue) linkage by strain-induced conformational change of the protein talin (brown). *In the absence of tension, vinculin (red) binding sites on talin are inaccessible, preventing talin-vinculin adhesion strengthening (a), but physical stimuli may expose these cryptic sites allowing vinculin to form a linkage between in and the actin cytoskeleton, (b) (Geiger et al. 2009; Hoffman et al. 2011).*

1.8 The Subcellular Processes: Key Players

Various structures may contribute to the force-mediated differentiation of MSC through participation in the processes of mechanotransmission, mechanosensing and mechanoresponse. Many more proteins than can be reasonably covered in this review are likely to be involved, but a discussion of the possible roles of proteins identified in mechanotransduction in the literature is here presented. Since there is virtually no work regarding the mechanism of mechanotransduction in MSC, the potential involvement of proteins is largely inferred from work carried out in other cell types and in theoretical studies. Although each protein type is discussed separately in this review, it is likely that mechanotransduction initiates feedback that modifies the structures involved, and that these are inherently coupled.

1.8.1 Holding it all Together: The role of the Cytoskeleton in mechanotranduction

The cell cytoskeleton operates on a subcellular level to perform many of the same functions as our skeletons on the macroscale: it maintains and modifies cell shape, resists physical forces and allows whole-cell movement (Saxen et al. 2008). It also participates in organelle trafficking. Additionally, the cytoskeleton is believed to have a significant role in mechanotransduction, related to its ability to both transmit and generate force.

1.8.1.1   The structure and function of cytoskeletal filaments

The cytoskeleton is composed of microtubules, actin and intermediate filaments that span large distances and connect the intra- and extracellular environment via discrete adhesions with the ECM. It maintains and modifies cell shape, resists physical forces and facilitates organelle trafficking (Saxen et al. 2008). Additionally, cytoplasmic signalling proteins, such as glycolytic enzymes, protein and lipid kinases and GTPases can localise to the cytoskeleton (Janmey 1998).

Actin filaments (F-actin) are nucleated at the plasma membrane, aided by focal adhesions, and are helical structures composed of globular actin (G-actin) monomers. Constant polymerisation and dissociation creates flexible, dynamic structures that are stable on a timescale of minutes to hours. Actin filaments are associated with many accessory proteins, including myosin II isoforms, which associate with actin filaments to generate the inherent contractility observed in all adherent cells. Mechanically, actin filaments have high tensile strengths in order to maintain contractility; strengths of 600 pN have been reported for a single filament (Tsuda *et al.*, 1996; Chen and Ingber, 1999; Pollard and Earnshaw, 2002; Alberts *et al.*, 2008; Lodish *et al.*, 2008).

Microtubules are composed of α- and β-tubulin and are rigid, hollow cylinders that direct the intracellular transport of membrane bound organelles. They normally originate from a microtubule organising centre (MTOC). Microtubules orchestrate mitosis, and in bundled arrangements, make up cell surface structures such as cilia and flagella. The tube-like structure of these filaments increases their second moment of inertia and allows them to resist bending and twisting. As a result, they are able to withstand high compressive forces (Chen & Ingber 1999; Pollard & Earnshaw 2002; Lodish et al. 2008; Alberts et al. 2008). Interestingly, although many glycolytic proteins and normally colocalised on actin filaments

(Murata *et al.*, 1997), some enzymes, such as Phosphofructokinase may also be bound and inhibited by microtubules (Vértessy *et al.*, 1997). This highlights the significance of microtubules in cellular metabolic processes in addition to their structural function.

Intermediate filaments are a biochemically heterogeneous protein family organised into rope-like fibres, with considerably flexibility and resistance to tensile stresses. Types of intermediate filaments include keratins, found in epithelial cells, neurofilaments, involved in axon organisation and lamins, which comprise the nuclear lamina. Whilst subunit exchange does occur, intermediate filaments are much more stable than F-actin and microfilaments (Pollard & Earnshaw 2002; Alberts et al. 2008; Lodish et al. 2008).

1.8.1.2   *The role of the cytoskeleton in mechanotranduction*

Applied mechanical forces are known to initiate biochemical signalling at distinct points in cells on millisecond timescales (Na *et al.*, 2008). This is suggestive that stimuli are not transmitted through the cell cytosol via diffusion-limited signalling, but are conducted through a solid structure. There is convincing evidence that the cell cytoskeleton is responsible for transducing force throughout cells, and also that it does itself generate force through actomyosin contractility. The cytoskeleton is therefore important in the process of mechanotransmission, whereby physical stimuli are delivered to sites where they can stimulate biochemical signalling.

It has been suggested (Alberts et al. 2008) that cellular metabolic and signal transduction proteins function in the solid state whilst immobilized on the cytoskeletal scaffolds, including those that envelop the nucleus (the nuclear lamina). It is possible that biochemical signalling is induced when enzyme and substrate species are brought into close proximity by force-mediated cytoskeletal rearrangement, initiating biochemical signalling. However, it is thought that force-mediated conformational change is the more likely explanation for the conversion of physical stimuli to cellular signalling (Chen & Ingber 1999). Hence, applied forces may travel along cytoskeletal elements until they impinge on force-sensitive proteins.

In addition to this 'outside in' mode of force application, cytoskeletal actomyosin filaments generate internal traction forces against the ECM. This has been termed 'inside-outside-in' mechanotransduction. In this mode, tension is generated by actomyosin filaments against focal adhesions, which mediate cellular adhesion with the microenvironment. Focal adhesions then pull against the cell substrate and dictate cytoskeletal tension according to the stiffness, and hence deformability, of the cellular substrate. Wrinkling of soft matrices as a result of

these traction forces is well documented (Ingber 1994; Even-Ram et al. 2006; Engler et al. 2006; Ingber 2010; Hoffman et al. 2011). The importance of traction forces in MSC mechanotransduction has been highlighted by Engler *et al* in work in which the lineage specifity of naïve cells was dictated by substrate stiffness, and hence the magnitude of traction forces, in a highly sensitive manner. In this work hydrogels of various elasticities (0.1 – 40kPa) comparable to the environment found in brain, muscle and bone tissue were found to direct MSC towards these lineages, and inhibition of nonmuscle myosin II proteins prevented lineage specification (Engler et al. 2006; Shih et al. 2011). Since internally generated forces are sufficient to initiate mechanotransduction in MSC, studies of mechanically-stimulated MSC must include a thorough analysis of static controls before biochemical effects can be attributed to the applied stimulus and not inherent contractility. Additionally, the cell substrates used must have consistent mechanical properties to ensure consistent cytoskeletal traction forces within cultured MSC.

1.8.1.3 Cytoskeletal dynamics

The behaviour of the cytoskeleton lends credence to dynamic theories of mechanotransduction. Switch-like theories, described in section 1.7.3, consider the stages of mechanotransmission, mechanosensing and mechanoresponse to occur sequentially, and describe mechanotransduction as a function of force magnitude only (Hoffman et al. 2011).

In reality, the viscoelastic nature of the cytoskeleton may mean that the mode of force application is equally important in determining the likelihood of mechanotransduction events. The cytoskeleton has been described as a viscoelastic material because depending on the mode of application, mechanical stimuli can result in either reinforcement (for example, by mechanisms such as that described in Fig. 3.4) or disruption of its structure. Viscoelastic behaviour is characterized by stress relaxation, which on the molecular level is caused by the dissociation of weak protein-protein interactions. If a force is great enough to break these linkages, but is applied at times shorter than the dissociation time, stress relaxation cannot occur and the assembly behaves as a force-transmitting elastic solid (Screen et al. 2005; Hoffman et al. 2011). Additionally the cytoskeleton, responsible for force generation and transmission, and focal adhesions, involved in mechanosensing, are co-dependent in their development. Focal adhesions, necessary for force transfer to the cytoskeleton in mechanotransduction, are transient at the onset of their formation and require actomyosin contractility to mature into permanent contacts (Geiger et al. 2009). Conversely, actin filaments, necessary for mechanotransmission, are nucleated at focal adhesions. Thus, the

relationship between focal adhesions and the cytoskeleton suggests that the processes of mechanotransmission and mechanosensing are mutually influential, as described by dynamic, but not switch-like theories.

1.8.1.4 The cytoskeleton as a tensegrity structure

The concept of tensegrity describes constructs that self-stabilize through the balancing action of opposing tension and compression elements that comprise their structure. In a tensegrity structure these elements are perfectly balanced by creating an internal pre-stress, and stability is provided by tensional integrity, not compressional continuity as utilised in most non-natural 'brick upon brick' structures (Ingber et al. 1994). The simplest examples of tensegrity force balances can be found in sculptures constructed of a tensed network of metal cables interconnected with compression struts (Fig. 1.5) (Snelson & Heartney 2013). Some investigators have suggested that rather than having entirely separate functions, cytoskeletal structures operate in concert as a tensegrity structure. In this hypothesis, internal pre-stress is generated by actomyosin contraction, and tensional forces are supported by the actin and intermediate filament networks. The tensional forces are counterbalanced by microtubules, which are able to withstand compressive forces (Hoffman & Crocker 2009). If shown to be correct, this theory explains the fact that applied physical stimuli often generate mechanotransduction events at disparate locations within milliseconds. Evidence to support a cytoskeletal tensegrity structure includes findings showing that microtubules in epithelial cells often have a buckled appearance, suggesting that they are in compression (Brangwynne et al. 2006), that severed actin filaments recoil, as expected of a chord in tension (Kumar et al. 2006), and that cell stiffness increases linearly with prestress, as is characteristic of tensegrity structures. The possibility of the cell cytoskeleton existing as a tensegrity structure may pose challenges for investigators of mechanotransduction in MSC hoping to decouple the individual roles of filament types. Whilst there are exceedingly few studies regarding the role of the cytoskeleton in mechanotransduction in MSC, those that exist, and those involving other cell types, utilise chemicals that disrupt a specific type of cytoskeletal filament (Engler et al. 2006; Sarraf et al. 2011; Park et al. 2012; Wang et al. 2013). This work is conducted on the assumption that since the agents used target only one of the three types of filament, any changes observed following their use must indicate the role of the target filament in mechanotransduction. In the case of a tensegrity structure, in which all structural elements are mutually dependent upon each other for stabilisation, the severing of just one element would be expected to cause a gross alteration in the position and mechanical properties of

other components. Thus, this may mean that drugs specific to the disruption of, for example, actin filaments, may cause the movement or distortion of organelles/proteins attached to microtubules. Recent work found that the impact of the disruption of intermediate filaments and microtubules on cell stiffness (a measure of cytoskeletal integrity) was approximately equal and not additive, suggesting disruption of one filament type affected the mechanical contribution of the other. However, the use of actin disrupting drugs in conjunction with either of those targeting the other filament types was additive. This may suggest that the actin cytoskeleton was less affected by the disruption of other filaments (Wang et al. 2013). A possible explanation for this is the fact that in most cells the actin cytoskeleton is the only filament type to form stabilising connections, via focal adhesions, to the ECM. Hence, it may be possible for the actin cytoskeleton to maintain some degree of integrity after the disruption of other filament types through anchorage points. That the entire cytoskeleton may be interconnected in a tensegrity structure may also explain why cytochalasin D, specific for the disruption of actin filaments, has been observed to disrupt the nuclear lamina, which is composed of intermediate filaments and attached to the cell cytoskeleton. Possible future experiments involving the chemical disruption of particular filament types, and observation of the knock-on impact on other cytoskeletal structures using immunofluorescence (such as the

Fig. 1.5: Tensegrity sculpture entitled 'study for able Charlie,' by Kenneth Snelson. Stability is achieved in this work through a balance between opposing tension elements (steel wires) and compression elements (aluminium struts). It has been postulated that the cell cytoskeleton may behave similarly, with tensional forces supported by the actin and intermediate filament network and compressive forces by microtubules. Adapted from Snelson & Heartney, 2013.

degree of microtubule buckling) could be conducted to qualitatively assess cytoskeletal tensegrity (Table 1.5).

Table 1.5: Drugs used for the disruption of cytoskeletal filaments

Chemical	Cytoskeletal protein disrupted	References
Cytochalasin D	Actin	(Cooper 1987; Wang et al. 2013)
Nocodazole	Microtubules	(Jordan et al. 1992; Wang et al. 2013)
Acrylamide	Intermediate filaments	(Oboeuf & Forest 1994; Wang et al. 2013)
Colchicine	Microtubules	(Lodish et al. 2008; Hastie 1991)
Blebbistain	Myosin II	(Friedland et al. 2009)
ML-7	Myosin light-chain kinase	(Friedland et al. 2009)
2,3-butanediome monoxime	Myosin II	(Friedland et al. 2009)
Latrunculin A	Actin	(Friedland et al. 2009)

1.8.2 Focal adhesions

1.8.2.1 Structure and function of focal adhesions

The primary function of focal adhesions is to provide cellular anchorage, and hence connect the cell interior, via the cytoskeleton, to the ECM (Fig. 1.6). The major transmembrane receptors in these sites belong to the integrin family. Integrins comprise two subunits (α & β) and have a large extracellular domain responsible for ligand binding, a transmembrane domain, and a cytoplasmic domain associated with a variety of other proteins (Zamir & Geiger 2001; Alberts et al. 2008). These proteins can be organised into three broad classes: adaptor proteins that mediate actin links to integrins, such as talin and vinculin (Fig. 3.4), actin regulators that regulate the organisation of the attached cytoskeleton and signalling proteins, such as kinases, phosphatases, G-proteins and modulators of small GTPases (Zamir & Geiger 2001; Bershadsky et al. 2006; Geiger et al. 2009). Kinases catalyse the addition of phosphate groups to other proteins, with phosphatases reversing their action. G-proteins are associated

with membrane receptors and serve to couple them to cytosolic signalling enzymes and ion channels (Mcallister et al. 1994; Alberts et al. 2008).
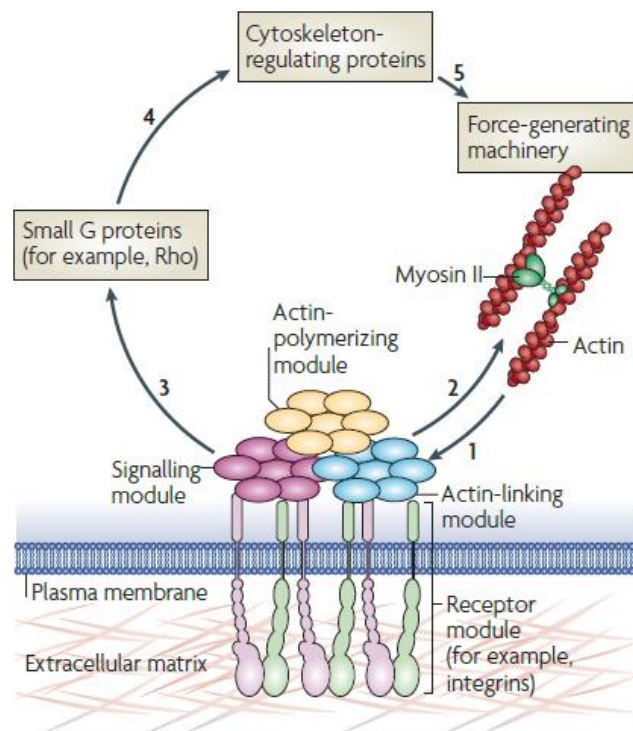
Fig. 1.6: Simplistic diagram of a focal adhesion showing interplay with, and regulation of, cytoskeletal proteins. *Cell-ECM adhesion is provided by integrins, which span the plasma membrane and associate with actin-linking, actin-regulating and signalling proteins. Forces generated externally, or internally from actin polymerisation and myosin II contractility, may impinge on mechanosensitive proteins (1). Actomyosin contractility is determined by the stiffness of the ECM, as detected via focal adhesions (2). Following mechanosensing by signalling proteins, the activity of small G-proteins is modulated, which modifies actin polymerisation and contractility through cytoskeleton-regulating proteins (3-5). Hence, the resulting mechanoresponse feeds back to modify force-generating and mechanotransmission proteins. Mechanosensing events in signalling proteins may also initiate biochemical signalling that regulates other cell processes, such as differentiation. Adapted from (Geiger et al., 2009).*

1.8.2.2   Focal adhesions: force transmitters and sensors

Focal adhesions are force sensitive even at the onset of their development, where their maturation from integrin clusters to stable, mature adhesions is highly dependent on cytoskeletal contractility (Geiger et al. 2009). Indeed, when internally generated tensional forces are abrogated these initial contacts are transient and do not persist (Aspenstro 1999; Butler et al. 2006). Whilst integrins connect the actin cytoskeleton to the ECM, and they must therefore transfer forces for cytoskeletal mechanotransmission, focal adhesions themselves

are composed of force-modulated signalling proteins. Therefore, focal adhesions may be participants in both mechanotransmission and mechanosensing. It is here postulated that focal adhesions contribute to mechanotransduction in three broad ways: by simply transferring externally applied forces to actin filaments, where they can be conducted to a variety of distal points within a cell for subsequent mechanosensing, mechanosensing of internally applied forces, and mechanosensing of externally applied forces. Externally applied forces are transmitted to focal adhesions by the ECM. It also possible that focal adhesions, being composed of multiple proteins, participate in different mechanotransduction events simultaneously. For example, it is theoretically possible that external forces may be transferred to actin via attached integrins, and be sensed elsewhere, whilst co-localised signalling molecules undergo force-mediated conformational changes that modulate their activity.

The molecular complexity of focal adhesions and their inherent coupling with the cytoskeleton presents challenges for their study, and violates switch-like theories, which do not account for feed back to structures involved in mechanotransduction. The intracellular signalling molecules found in focal adhesions, such as src, Cas and vinculin, experience force-mediated conformational changes that affect kinase activity, the availability of phosphorylation sites and intracellular localisation (Friedland et al. 2009). Kinases, such as focal adhesion kinase (FAK), catalyse the addition of phosphate groups to other molecules (Alberts et al. 2008). The role of phosphorylation in mechanotransduction events could be investigated by inhibiting the action of kinase proteins, or by chemically blocking cryptic phosphorylation sites exposed by mechanical force. However, there are many proteins that exhibit this behaviour that may be involved in mechanotransduction, and it would be necessary to establish the specificity of the agents used. The role of internally generated tension in mechanotransduction events is often assessed using myosin II inhibitors (Friedland et al. 2009) (Table *1.5*) , but a lack of tension in the actin cytoskeleton is known to lead to the demise of focal adhesions. Finally, the role of integrins in mechanotransductive processes has been probed by altering the configuration of one of their most common binding sequences (Doyle & Yamada 2010). Integrins often bind to ECM proteins via the tripeptide alanine-glycine-aspartate (RGD in single letter nomenclature), and a single amino acid substitution of glutamate in place of aspartate prohibits integrin binding. Matrix binding initiates integrin activation, which in turn aids the development of focal adhesions. As discussed previously, focal adhesions are the site of actin nucleation and regulation; any method that abrogates focal adhesion formation may also impact on the cell cytoskeleton, which may have a significant role in mechanotransduction. Hence, careful

experimental design is necessary to target adhesion proteins of interest, whilst also excluding the possibility that observed effects derive from interactions with other cellular structures.

Current work regarding the role of focal adhesions in mechanotransduction is scant, and at the time of writing, only two studies could be found that analyse the role of focal adhesions in the differentiation of MSC. These studies implicated focal adhesions in the anti-adipogenic (Sen et al. 2011) and tenogenic (Xu et al. 2012) differentiation of MSC under cyclic strain. Sen *et al* investigated the impact of focal adhesion formation, instigated by the application of biaxial strain to collagen I coated culture substrates, on the amplification of signalling pathways that restrict adipogenesis (Sen *et al.*, 2011). Supression of adipogenesis is dependent on β-catenin activity, which is inactivated by the inhibitor glycogen synthase kinase 3β (GSK3β). This inhibitor is in itself inactivated through serine phosphorylation (Sen *et al.*, 2009). Whether the restriction in MSC adipogenesis observed with mechanostimulation is mediated by GSK3β inactivation or β-catenin activation was determined using immunoblotting and immunofluorescence for species indicative of focal adhesion formation, markers of adipogenesis, phosphorylated GSK3β, and the GSK3β kinase Akt. In one of the few studies to date to determine the mechanism involved in a physically mediated effect, the investigators reported that focal adhesion maturation, leading to an increase in cell contractility and protein recruitment at integrins. One recruited protein, Akt, phosphorylates GSK3β, maintaining β-catenin activity and preventing adipogenesis of MSC.

Investigations conducted by Xu *et al* concerned the role of strain and focal adhesions in the tenogenic differentiation of MSC reported that these structures operate in concert with focal adhesion kinase (FAK), the G-protein RhoA and the cytoskeleton (Xu *et al.*, 2012). In this study, through the use of the inhibitors specific for each of these elements, the investigators demonstrated that the expression of tenogenic markers was increased only when the function of all was not impeded.

Work in cells other than MSC has focussed on the development of an *in silico* model to study the mechanism of focal adhesion mediated mechanotransduction (Cells et al. 2013), and a method of manipulating the forces applied to individual focal adhesions using coated beads and optical tweezers. Used in conjunction with fluorescent imaging, the latter method was used to visualise the localisation of signalling proteins at focal adhesions following force application (Honarmandi et al. 2011).

1.8.3 Opening the Floodgates: The Role of Mechanosensitive Ion Channels in Mechanotransduction

1.8.3.1 Ca^{2+} channels and cellular signalling

Calcium channels are transmembrane proteins that are specific for, and facilitate the transport of Ca2+ ions. This transport may be passive, and depend on concentration gradients and the shape of the channel pore, or active, and achieve transport by expending energy. There are numerous types of mechanosensitive (MS) channels involved in diverse processes, including the regulation of gene expression. For example calmodulin, a multipurpose intracellular Ca^{2+} receptor, undergoes conformational change when bound to Ca2+ that allows it to bind and modulate the activity of target proteins, although it may also exist as a permanent regulatory enzyme subunit. These include calmodulin-dependent kinases, which amongst other functions, phosphorylate gene regulatory proteins and regulate actomyosin contractility as part of their signalling cascades (Bootman et al. 2001; Alberts et al. 2008; Doyle & Yamada 2010). Although there is a lack of literature regarding mechanotransduction of MSC via MS channels, ion channels have been implicated in the differentiation of MSC towards neuronal (Yu et al. 2011) and osteogenic (Barradas et al. 2012) lineages. The only study to date examining the impact of strain mediated ion channels in MSC sought to determine their role in influencing the production of GAGs (McMahon et al. 2008); GAG production was increased following the application of cyclic tensile strain for a period of 7 days, and the dependence of this process on stretch-activated ion channels tested using inhibitors. Interestingly, although treatment with the strain-activated channel inhibitor GdCl3 attenuated GAG production significantly, it was not completely ablated, indicating an additive effect of other mechanotransduction pathways. Hence, it has been demonstrated that ion channel permeability impacts the differentiation potential of MSC, and that strain-activated ion channels mediate other processes within these cells. Research into any link between the strain-induced permeability of strain-activated ion channels and the differentiation of MSC should be conducted to elucidate their role in mechanotransduction.

1.8.3.2 Mechanosensitive ion channels in mechanotransduction

MS channels operate within mechanotransduction as mechanosensors, and form perhaps the most direct route between force impingement on proteins and biochemical signalling. Unlike most mechanosensors, the force-mediated conformational changes of MS channels do not initiate signalling by altering their binding to other protein mediators, but by directly altering

membrane permeability to a signalling ion. Two main mechanisms have been proposed to explain MS channel activation: activation through tension development in the lipid bilayer, and activation through pulling by cytoskeletal tethers (Arnadóttir & Chalfie 2010). Force transmission to the channels occurs via the lipid bilayer or cytoskeleton respectively, and there is evidence for the existence of both types of channel gating. Studies have shown that MS channels in cytoskeleton-free liposomes can be mechanically activated, providing strong evidence for force transmission solely through the bilayer (Ingber 2006). Alternatively, the 'tethered' model suggests that direct connections between the channel and cytoskeleton displace the channel gate, and hence alter membrane permeability, in response to force (Martinac 2004; Hayakawa et al. 2007). It could be argued that cytoskeletal structures may transmit forces more effectively than the fluid-like lipid bilayer (Hamill & Martinac 2001; Byfield et al. 2004). Additionally, an example of an MS channel that loses mechanosensitivity in the absence of a cytoskeleton has been found (Zhang et al. 2000). Finally, it is possible that MS channel conformational changes that alter membrane permeability may occur indirectly

as a res ult of interactions with another, mechanosensitive receptor. In this case, the channewould not in fact be a mechanosensor itself, but a participant in biochemical signalling with a mechanosensor that has undergone force-mediated conformational change that allows it to alter channel permeability. Such a force-sensitive channel mediator has been reported in bovine aortic endothelial cells, which has kinase activity that determines channel permeability (Davies 1995). Development of the patch-clamp technique, which allows the measurement of individual channel currents, has enabled the discovery of two types of response to force application (Hamill et al. 1981; Morris & Sigurdson 1989). MS channels may be stretch inactivated (SI) or stretch activated (SA), which adapt to restrict access to ions, or allow greater ease of passage under force respectively. A simple elastic transduction model, shown in Fig. 1.7, relates the regime adopted by an MS channel to its shape, membrane tension and the membrane-planar area of the open and closed conformations (Morris & Sigurdson 1989).

(a)   *(b)*
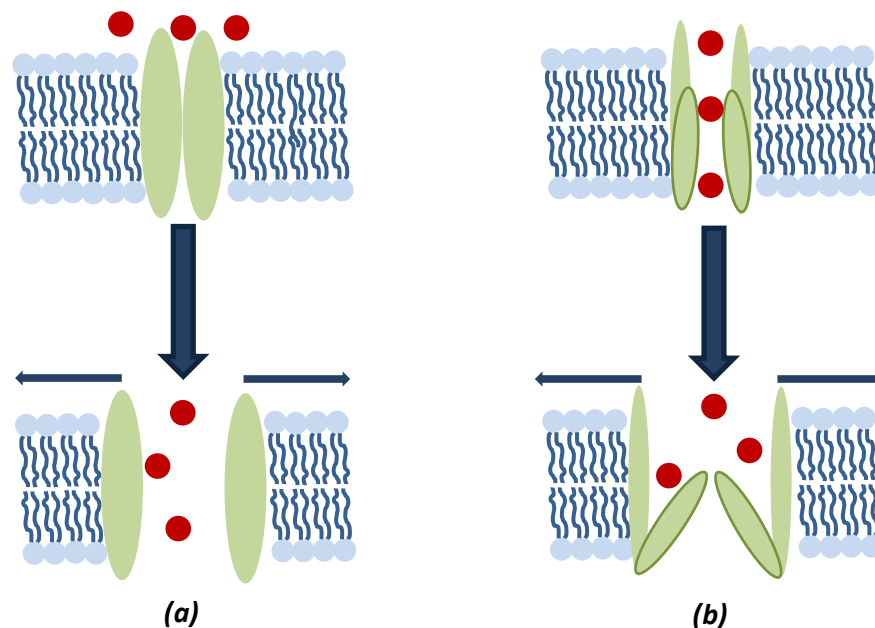
Fig. 1.7*: **Suggested mechanism of operation of SA (a) and SI (b) ion channels.** A simplistic lipid bilayer (blue) ion channel (green) for the transport of Ca^{2+} (red) is shown. It has been postulated that SA channels lack a suitable pore in the absence of tension. Upon force application, the channel is pulled apart, allowing the passage of ions. SI channels MAY have folded domains which sit compactly inside the channel pore in the absence of membrane tension. However, application of force may increase the available membrane-planar area and these domains unfold, obstructing the pore (Morris & Sigurdson 1989).*

1.8.4 Mechanical stimuli and gene expression

Mechanoresponses can take many forms, but altered gene expression, associated with differentiation processes, will form the focus of this section. Gene expression is thought to be influenced either by biochemical signalling initiated in the cytosol by mechanosensing, or by direct force transmission to the nuclear structures. It is not possible to discuss all the signalling pathways in MSC, so those that have been implicated in mechanotransduction-related gene expression in MSC have been selected.

1.8.4.1 Biochemical signalling and gene expression after mechanostimulation of MSC

1.8.4.1.1 Wnt signalling

Wnts are a family of cysteine-rich glycosylated ligands that bind to membrane receptors and induce signalling down at least three different pathways (Fig. 1.8). The most common of these is the canonical Wnt pathway, which controls gene expression through the translocation of the protein β-catenin to the nucleus. In the absence of Wnt signalling, β-catenin is sequestered by a degradation complex and degraded in proteasomes. However, when a Wnt binds to its corresponding receptor proteins, LDL-receptor-related protein (LRP) and Frizzled, the protein dishevelled is recruited, which recruits and inhibits the degradation complex. Inhibition of the degradation complex leads to an increase in unphosphorylated, active β-catenin which migrates to the nucleus and displaces Groucho, a co-repressor protein that binds to a gene-regulatory protein of the Wnt responsive gene in question (Alberts et al. 2008). Wnt signalling is well recognised for its role in the differentiation of MSC (Kuo & Tuan 2008) and investigators have reported a role in gene-regulatory signalling following mechanically-stimulated differentiation. As discussed previously (section 1.5.2), mechanical strain halts adipogenesis of MSC cultured in adipogenic media. A decrease in active and total β-catenin levels is normally observed during adipogenic differentiation; this appears to be reversed by mechanical strain, which also encourages translocation of the protein to the nucleus (Sen et al. 2008). Thus, the suppression of Wnt-regulated gene expression may be key to adipogenesis in MSC. Additionally, Wnt regulation is reported to be involved in both the initiation and retardation of tenogenesis in cyclically strained MSC, through the ligands Wnt4 and Wnt5a respectively (Kuo & Tuan 2008). The mechanism of upregulated Wnt ligand production, or enhanced binding between the ligand and MSC in response to physical stimuli is not yet clear.

Although there is little literature regarding biochemical signalling in MSC following mechanical stimulation, these reports suggest that Wnt signalling in mechanically strained MSC may merit further investigation.
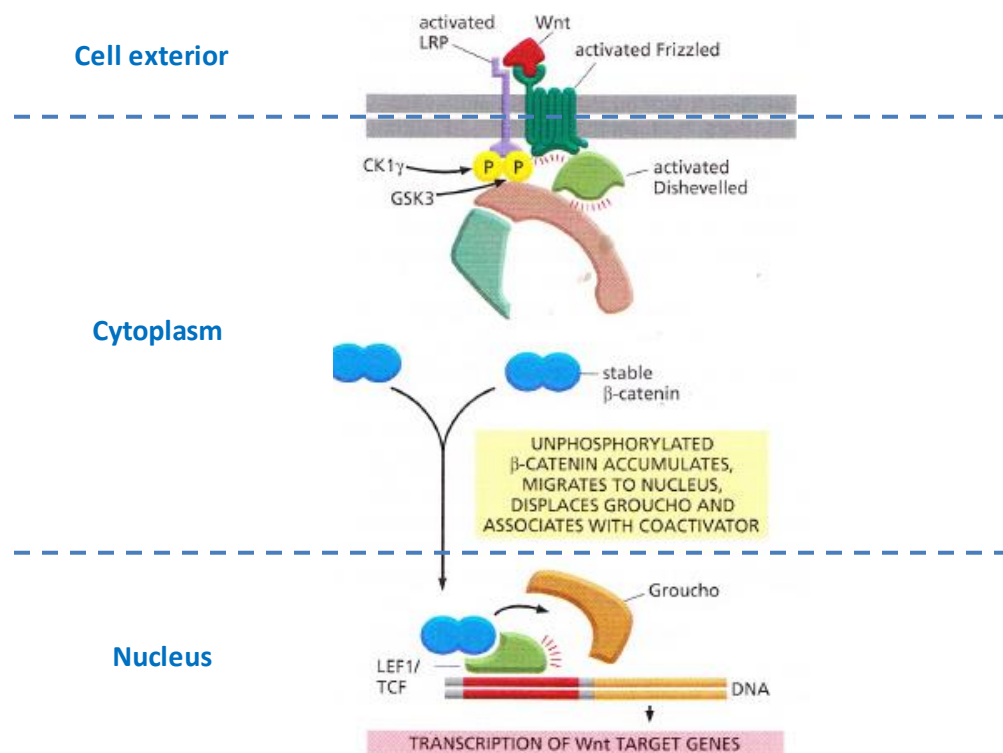
Fig. 1.8: Gene-regulatory biochemical signalling initiated by binding of Wnt ligands via the β-catenin pathway. *Wnt signalling influences gene expression through β-catenin. In the absence of Wnt ligand binding, β-catenin is phosphorylated (yellow circles) and sequestered in a degradation complex (GSK3β). However, the binding of Wnt ligands to their corresponding receptors (LRP and Frizzled, pictured) results in the recruitment of the protein dishevelled (labelled) and the degradation complex (green and brown horseshoe). This inactivates the degradation complex and leads to an increase of active, unphosphorylated β-catenin in the cytosol that is able to translocate the nucleus. Once in the nucleus, β-catenin displaces the co-repressor protein groucho and interacts with the regulatory protein of the Wnt responsive gene in question (LEF1 or TCF) to influence gene expression. Adapted from Alberts et al (2008).*

1.8.4.1.2   Mitogen-activated protein kinases

MAPK modules, or ERKs, are a class of three-protein signalling pathways that operate through a tiered sequential phosphorylation cascade. Receptor tyrosine kinases, membrane proteins induced to phosphorylate themselves following the binding of an extracellular ligand, activate proteins from the Ras superfamily of GTPases. This signalling is normally short-lived, and Ras proteins must interact with the MAPK module to convert the stimulus to long-lived signals able to alter the pattern of gene expression. Ras proteins recruit MEK kinase (MEKK for

simplicity) enzymes to the plasma membrane and activate them by phosphorylation. The MEKK protein in turn phosphorylates, and hence activates, MAP/ERK kinase (MEK), which itself phosphorylates MAP kinase. MAP kinase proteins relay the signal further downstream by phosphorylating other proteins, including gene regulatory proteins and other protein kinases (Robinson and Cobb, 1997). MAPK proteins are divided into four main subfamilies according to their sequence similarity, upstream regulation and interaction with different MEKs. Erk MAP kinase, for example, is reported to enter the nucleus and phosphorylate one or more components of gene regulatory complexes. This has been implicated in the osteogenic differentiation of MSC (Jaiswal 2000; Rhee et al. 2006; Huang et al. 2009; Shih et al. 2011). Some reports (Huang et al. 2009; Shih et al. 2011) regarding biochemical signalling in mechanostimulated MSC indicate that MAPK module signalling was initiated by FAK, suggesting that MAPK signalling may occur downstream of mechanosensing at focal adhesions (discussed section 1.8.2). In one study, the inhibition of Erk MAP kinase signalling initiated by strain abrogated osteogenic differentiation, and instead caused MSC to progress down an adipogenic lineage. Another MAP kinase pathway, JNK, was reported to be activated following mechanical stretch, although it participates at longer time points and appears to regulate ECM synthesis (Jaiswal 2000). Interestingly, MAP kinase module families frequently use the same kinases whilst eliciting distinct cellular responses. Cross-talk between pathways is prevented through physical adhesion to scaffold proteins. Since the cytoskeleton is believed to play an important role in force transmission, this raises the possibility that MAPK module signalling may be stimulated not only as downstream biochemical signalling from other, force sensitive mechanosensors, but that cytoskeletal attachment may mediate changes in the chemical activity of the kinases through direct force transfer (Alberts et al. 2008). Although force-mediated conformational changes that expose phosphorylation sites or affect kinase activity have been established in other proteins it is, however, not known whether MAPK signalling molecules are able to perform as mechanosensors.
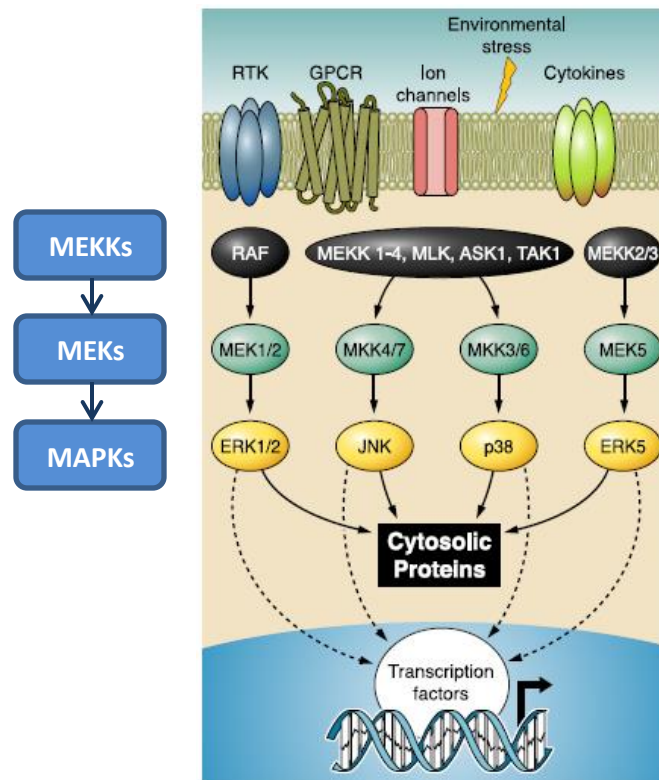
Fig. 1.9: The activation of MAP kinases following sequential phosphorylation of MEKKs and MEKs.
The four main subfamilies of this pathway are shown (right), with their component MEKKs, MEK and
MAP kinases. External stimuli induce tyrosine kinases at the plasma membrane to phosphorylate
themselves, activating GTPases. These GTPases recruit MEKK proteins (black), such as MEK1/2, MKK4/7,
MKK3/6 and MEK5, which in turn phosphorylate MEK proteins (green). MEK proteins then
phosphorylate MAP kinase proteins, which phosphorylate other proteins to relay the signal downstream

1.8.4.2   Direct force transmission to the nucleoplasm

It has also been suggested that changes in gene expression may be caused by direct force transfer to the nuclear structures. In such a mechanism, the cell cytoskeleton acts as a mechanotransmitter and the nucleus senses the delivered forces. Evidence for a physical connection between the cytoskeleton and the nucleus is abundant; as whole cells elongate in response to shear stress, their nuclei do also, in a process dependent on mediators of cytoskeletal organisation (Flaherty et al. 1972; Lee et al. 2005; Deguchi & Sato 2010). Additionally, investigators have reported nuclear remodelling following force application such that shape and stiffness is permanently altered (Deguchi et al. 2005).

Hypothetical models have been developed that describe how the mode of DNA packing, and hence gene expression, may be influenced by force (Gieni and Hendzel, 2008). In the nucleus, DNA is densely stored in the form of chromatin, along with protein complexes that mediate packing. The packing state of chromatin affects the transcriptional availability of its constituent DNA: chromatin in a less condensed state, termed euchromatin, is associated with DNA that is transcribed, whereas DNA packaged in denser heterochromatin is normally transcriptionally inactive (Meyer 2011). Physical continuity between the cytoskeleton and genetic material is provided by nuclear envelope-lamina spanning complexes (NELSCs) and LINCs (*li*nks the *n*ucleoskeleton and *c*ytoskeleton). The nuclear envelope consists of an outer membrane that is continuous with the rough endoplasmic reticulum, and an inner membrane attached to the nuclear lamina, connected by nuclear pore complexes. One possible mode of nuclear mechanosensing is that cytoskeletal rearrangement caused by force application to the cell distends the nucleus through cytoskeletal attachments, altering nuclear pore permeability (Deguchi and Sato, 2010). Regulatory proteins may then gain access to chromatin and alter gene expression. However, force transmission through the nuclear lamina to chromatin itself, which may attach to the membrane in one of two ways, is another suggested mechanism (Brown *et al.*, 1997).

One model suggests that mechanical stimulus is transmitted to the genome via attachment between the LINC and NELSC proteins and a hypothetical nuclear cytoskeleton termed a karyoskeleton. This karyoskeleton would bind chromatin at discrete sites that would be mechanosensitive. An alternative model theorises that, in the absence of a karyoskeleton, force may be transmitted directly through chromatin. Force would be sensed at the chromatin regions attached to the lamina. The likely result of chromatin mechanosensing would be decondensation of chromatin at attachment sites, and transcriptional availability of the exposed DNA (Gieni and Hendzel, 2008). The two scenarios described are shown in Fig. 1.10.
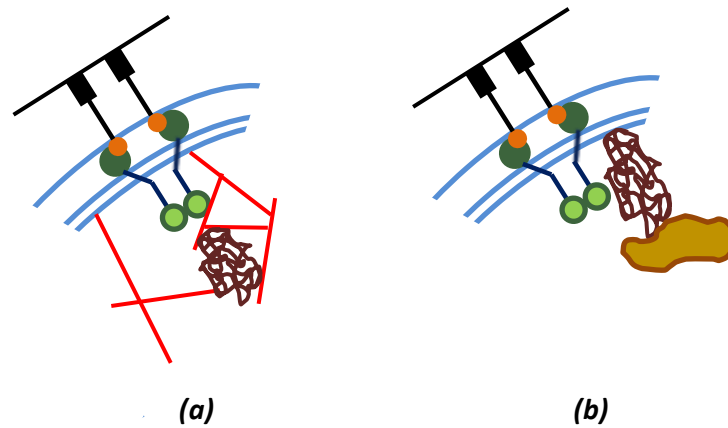
Fig. 1.10: *Possible modes of attachment of chromatin to the nuclear lamina.* *The LINC complex comprises a pair of Nespirin proteins (orange) interacting with a pair of SUN proteins (green), connecting the outer and inner nuclear membrane. Chromatin (brown) may be connected to the nuclear lamina via a karyoskeleton, (shown in red, a). In this case, force application may distort the chromatin from the points of attachment. Alternatively, chromatin may be fixed in the nuclear envelope by binding the nuclear lamina (blue) directly and a splicing factor compartment, (b). In this model, force transmission still occurs through the LINC complex but does not involve a karyoskeleton. In both scenarios mechanical stimuli are sensed via chromatin decondensation. Adapted from Gieni & Hendzel 2008.*

1.9   Concluding remarks

Mesenchymal stem cells, a promising cell source for tissue engineered therapies, are overwhelmingly differentiated using soluble factors. There is, however, evidence that physical stimuli play a role in differentiation, as reported in the differentiation of MSC towards osteogenic (Shih et al. 2011) and adipogenic lineages (Sen et al. 2008), and in MSC cultured on substrates of varying stiffness (Engler et al. 2006). There are scant reports regarding the mode of mechanotransduction of MSC and the mechanically-gated differentiation of MSC towards a smooth muscle lineage. Studies that do exist frequently present caveats such as poor substrate choice and a lack of consideration of the mode of mechanical stimulation.

Studies of mechanotransduction in other cell types, and the few existing reports in MSC, suggest the involvement of the cytoskeleton, focal adhesions, ion channels and biochemical signalling pathways, and that these structures may participate in mechanotransduction in three main ways. Structures may transmit, sense or facilitate a response to force. Physical

signals are ultimately translated to biochemical responses by instigating conformational changes in sensitive proteins that alter their chemical activity.

In summary, there is a need to understand the force-mediated differentiation of MSC in order to inform the manufacture of tissue-engineered MSC therapies. This project attempts to address these deficiencies, by assessing the impact of different magnitudes of strain on the differentiation potential of hMSC cultured in a three-dimensional, pericardial substrate.

1.10 Rationale for the study

Multipotential mesenchymal stromal cells (MSC) were chosen as the subject for this study owing to their potential for use in tissue engineered therapies, growing evidence of MSC mechanosensitivity and the lack of study of mechanotransduction in MSC. The differentiation of hMSC towards the critical lineages of bone, fat, cartilage, tendon and smooth muscle were investigated. Although this project did not involve the production of a clinical product, it is hoped that a greater understanding of mechanotransduction in MSC may contribute to such research.

Porcine pericardial tissue was used owing to its ready availability, suitability as a scaffold for MSC and the relative ease of decellularisation of this tissue. Decellularised pericardium comprises a collagenous sheet of ECM containing appropriate cellular binding sites. Hence, MSC can make cellular adhesions comparable to those found *in vivo,* which may mediate force transduction. Furthermore, MSC seeded on pericardium are able to penetrate throughout the tissue, providing cells with a three-dimensional environment (Morticelli, 2013). Additionally, porcine pericardium offers advantages in this study owing to its sheet-like morphology, which facilitates its use as a scaffold within bioreactors applying both tensile and biaxial mechanical strain.

1.10.1 Hypothesis

It is hypothesised that optimal bioreactor culture conditions, and a validated culture protocol, for the mechanostimulation MSC by uniaxial strain will enable future elucidation of the role of physical stimuli in the lineage specification of MSC.

1.10.2 Project Aim

The aim of the project is to validate a three-dimensional uniaxial strain culture system (termed Tencell) and qPCR assays for gene expression analyses of mechanostimulated MSC.

1.10.3 Objectives

The overall project objectives are as follows:

1. To decellularise and validate a stock of three-dimensional pericardial matrix for use as a biologically-relevant substrate
2. To devise and validate a seeding regime for the application of hMSC to pericardial matrices
3. To re-engineer and validate the Tencell uniaxial strain bioreactor with respect to cell viability and arm displacement
4. To validate a set of primer pairs for genes of interest with respect to their specificity and efficiency for qPCR applications
5. To measure any strain-induced differences in gene expression, and hence hMSC differentiation potential, following culture in the Tencell bioreactor at strains of 5, 10 and 20%

Chapter 2:   Materials and Methods

2.1 Materials

2.1.1 Microbial species

*Staphylococcus epidermidis, Clostridium perfringen*s and *Candida albicans* were used in this project as positive controls during tests for the presence of aerobic and anaerobic bacteria and yeast respectively. Microbial aliquots were kindly prepared by Dr Kirsty Owen, and originally sourced from the national collection of tissue cultures (NCTC) and the national collection of pathogenic fungi (NCPF), although NCTC numbers unfortunately were not provided or recorded.

2.1.2 Cells

Table 2.1: The origin of all cell types cultured in this project

Cell type	Origin
Human MSC (p0)	*StemCell Technologies (Canada)*
Porcine MSC (p0)	*Isolated from fresh legs from Leeds University farm (UK)*
Human chondrocytes (P2)	*PromoCell (Germany)*
Human fetal osteoblasts (p1)	*Supplier not indicated by previous investigator*
Human tenocytes (p6)	*Supplier not indicated by previous investigator*
Human smooth muscle cells (p1)	*Supplier not indicated by previous investigator*
Baby hamster kidney cells (resurrected at various passages)	*Supplier not indicated by previous investigator*
3T3 cells (resurrected at various passages)	*Supplier not indicated by previous investigator*

2.1.3 Nucleic acids

Table 2.2: The origin of nucleic acids used in this project

Nucleic acid	Origin
Tenocyte RNA	Existing human tenocyte stocks (Table 2.1)
SMC RNA	Existing human SMC stocks (Table 2.1)
Osteoblast RNA	Existing human osteoblast stocks (Table 2.1)
Fat-derived RNA	Human knee tissue
Cartilage-derived RNA	Human cartilage tissue

2.1.4 Tissues

Table 2.3: The origin of tissues used in this project

Tissue	Origin
Porcine leg	M & C meats (Leeds)
Human knee	Leeds General Infirmary

2.1.5 Reagents

Table 2.4: Suppliers of reagents used in this project

Reagent	Supplier
α-amylase	Sigma-Aldrich (UK)
Absolute ethanol (for molecular biology)	Thermo Fisher scientific (UK)
Acetone	Genta Medical (UK)
Agarose	Sigma-Aldrich (UK)
Alcian blue 1% (w/v)	Biostain Ready Reagents (UK)
Alizarin red S	Sigma-Aldrich (UK)
Ammonium hydroxide	Sigma-Aldrich (UK)
Anaerogen oxygen exclusion sachets	Thermo Fisher scientific (UK)

Reagent	Supplier
Ammonium hydroxide	Sigma-Aldrich (UK)
Aprotinin	Nordic pharma (UK)
L-ascorbic acid	Sigma-Aldrich (UK)
ATPlite™ luminescence assay system kit	PerkinElmer (UK)
B-2-glycerophosphate	Acros organics (Belgium)
Calibration buffer, pH 4.01	Hanna Instruments (UK)
Calibration buffer, pH 7.01	Hanna Instruments (UK)
Calibration buffer, pH 10.01	Hanna Instruments (UK)
Chondrocyte growth medium	PromoCell (Germany)
Cyanoacrylate contact adhesive	Tesco (UK)
DABCO	Sigma-Aldrich (UK)
Dexamethasone	Sigma-Aldrich (UK)
Dimethyl sulfoxide (DMSO)	Sigma-Aldrich (UK)
Disodium hydrogen orthophosphate	Sigma-Aldrich (UK)
DNAse	Sigma-Aldrich (UK)
DNeasy blood and tissue kit	Qiagen (UK)
DPX mountant	VWR international (UK)
Dulbecco's modified eagle's medium (DMEM)	Sigma-Aldrich (UK)
Low-glucose DMEM	Sigma-Aldrich (UK)
Dulbecco's phosphate buffered saline (Oxoid)	Thermo Fisher scientific (UK)
EDTA	Thermo Fisher Scientific (UK)
Eosin	Thermo Fisher scientific (UK)
Ethanol, 200 proof (for molecular biology)	Thermo Fisher Scientific (UK)

Reagent	Supplier
Ethylenediaminetetraacetic acid (EDTA)	Fisher scientific (UK)
Foetal bovine serum	Seralab (UK)
Gel loading dye (6×; 25 bp)	New England Biolabs (USA)
Gentamyacin sulfate	Biochrom AG (Germany)
Giemsa stain	Sigma-Aldrich (UK)
Glasgow's minimal essential medium (GMEM)	Sigma-Aldrich (UK)
Glutaraldehyde	
L-glutamine	Thermo Fisher Scientific (UK)
Glycerol	Thermo Fisher Scientific (UK)
Growth medium (Chondrocyte)	PromoCell (Germany)
Haematoxylin	Thermo Fisher Scientific (UK)
Haematoxylin (for alcian blue protocol)	Sigma-Aldrich (UK)
HEPES	Melford (UK)
Hydrochloric acid	VWR international (UK)
Hydrocortisone	Acros organics (USA)
Indomethacin	Sigma-Aldrich (UK)
Isobutylmethylxantine	Sigma-Aldrich (UK)
Isopropanol	Bios Europe (UK)
Live/dead staining kit (contains calcein AM and ethidium homodimer-1)	Invitrogen (USA)
Loading dye (5×)	Bioline (UK)
Magnesium chloride hexahydrate	VWR international (UK)
Magnesium sulfate anhydrous	Sigma-Aldrich (UK)
Methanol	Sigma-Aldrich (UK)

Reagent	Supplier
Methylated spirits	Atom scientific (UK)
Neutral buffered formalin (10% v/v)	Biostain Ready Reagents (UK)
Oil red O	Sigma-Aldrich (UK)
Osmium tetroxide	
Penicillin/streptomycin	Thermo Fisher Scientific (UK)
Peracetic acid (40-44%)	Sigma-Aldrich (UK)
Percoll	Sigma-Aldrich (UK)
Periodic acid	Thermo scientific (UK)
Phosphate buffered saline	Oxoid (UK)
Phosphate buffered saline (without calcium and magnesium)	Lonza (UK)
Polymyxin B	Fluka analytical (Germany)
Primers (various sequences; see chapter 5)	Sigma-Aldrich (UK)
Proteinase K	Qiagen (UK)
QuantiTect SYBR® Green one-step RT-PCR kit	Qiagen (UK)
RNAse	Sigma-Aldrich (UK)
RNase-free DNase set	Qiagen (UK)
RNeasy Mini Kit	Qiagen (UK)
Schiff's reagent	Sigma-Aldrich (UK)
Scott's tap water	Atom Scientific (UK)
Sodium chloride	Fisher scientific (UK)
Sodium dihydrogen orthophosphate	BDH chemicals (USA)
Sodium dodecyl sulphate	Sigma-Aldrich (UK)
Sodium hydroxide	Fisher scientific (UK)

Reagent	Supplier
Sodium pyruvate	Sigma-Aldrich (UK)
SYBR™ green one-step RT-PCR kit	Qiagen (UK)
SYBR™ safe	Thermo Fisher Scientific (UK)
TAE buffer (10×)	Fisher scientific (UK)
Thioglycolate broth	Fluka analytical (Germany)
Tris buffered saline	Sigma-Aldrich (UK)
Trizma base	Sigma-Aldrich (UK)
Trypan blue	Sigma-Aldrich (UK)
Tyrode's solution	Sigma-Aldrich (UK)
Vancomyacin hydrochloride	Sigma-Aldrich (UK)
Virkon	VWR international (UK)
Water (DNase- and RNase-free)	Qiagen (UK)
Wax (Paraffin; for histology)	Raymond A Lamb (UK)
Xylene	Atom scientific (UK)

2.2 Methods

2.2.1 Statistical analyses

Statistical analyses were performed using Minitab 17 statistical software, at p =0.05. Tests for differences between more than two sample groups were performed by one-way analysis of variance. Where p < 0.05, Tukey's post-hoc tests were performed to find the sample groups between which significance was indicated. The one sample t-test was used to compare a measured mean value with a known 'true' mean. The null hypothesis that there is no difference between the measured mean and the true mean was tested. Where appropriate, linear regression analysis was performed using Microsoft Excel.

It is acknowledged that standard deviation (SD) or standard error of the mean (SEM) is often reported as measurement error in many of the types of analyses reported in this thesis. Experimental error, however, is reported as confidence intervals (CI) in this work.

Since error bars/measurement error are quoted to approximate the proximity of a sample mean (x) to the population, or true, mean (μ) standard deviation, which quantifies the dispersion of individual datapoints in a sample, is not appropriate (Dytham, 2011). The calculation of SEM does indeed provide an estimation of the accuracy of a calculated sample mean, but should not be used for data with sample sizes of n < 30. For data from samples that satisfy this criterion, ± 2SEM must be plotted to display the range in which the true or population mean would be expected to lie; if only ± SEM is plotted, the probability that the range displayed encompasses the true mean is reduced to 66%.

The author suggests that CI, most frequently used to display the range over which there is a 95% probability that the population mean lies, should be quoted as the uncertainty of a measured value over ±SEM, because the n value of the sample examined must be supplied for calculation of the region in which the true mean lies in the latter case. CI values plotted graphically also give a clear indication of whether p<0.05 or p>0.05 when subjected to the correct statistical test of difference (Eileen Ingham, personal communication).

2.2.2 Sterilisation

2.2.2.1 Moist heat sterilisation

Moderately heat resistant items (such as glassware) were autoclaved at 121°C for 20 minutes at a pressure of 15psi. Solutions were sterilised by loosening container lids prior to autoclaving to allow sterilisation of the contents. Small items were placed in an autoclavable bag prior to sterilisation.

2.2.2.2 Dry heat sterilisation

Metallic items to be sterilised, such as dissection equipment, were heated at 180 °C for 4 hours.

2.2.2.3 Filter sterilisation

Solutions not suitable for autoclaving were sterilised using a filter with a pore size of 0.2 μm. Filtering was carried out aseptically in a class II safety cabinet..

2.2.2.4 Flame sterilisation

Microbiological instruments, such as application loops, were sterilised between each use by heating with a naked flame.

2.2.3 Measurement of pH

The pH meter used to measure the pH of decellularisation solutions was calibrated using solutions of pH 4, 7 and 10. The solutions were gently stirred (120 rpm) during pH measurement. Should pH adjustment be required, hydrochloric acid or sodium hydroxide (1-12 M) was added drop-wise.

2.2.4 Solution preparation

2.2.4.1 Decellularisation

Phosphate buffered saline (PBS)

Five Oxoid Dulbecco's PBS tablets were dissolved in 500 mL distilled water and the pH adjusted to 7.2-7.4 using NaOH (6 M) and HCl (6 M).

Disinfection solution

Vancomyacin hydrochloride (50 mg), polymyxin B (200 mg) and gentamyacin sulfate (775 mg) were added to 100 mL of PBS and sterilised by filtration. The volume was made up to 500 mL with sterile PBS.

PBS with aprotinin (10 KIUmL^{-1})

Five Oxoid Dulbecco's PBS tablets were dissolved in 500 mL distilled water, and the pH adjusted to 7.2-7.4 using NaOH (6 M) and HCl (6 M) before autoclaving. Aprotinin (500 µL; 10,000 KIU.mL^{-1}) was added immediately prior to use.

PBS with EDTA (2.7 mM, 0.1 % w/v) and aprotinin (10 KIUmL^{-1})

Five Oxoid Dulbecco's PBS tablets and 0.5 g EDTA were dissolved in 500 mL distilled water, and the pH adjusted to 7.2-7.4 using NaOH (6 M) and HCl (6 M) before autoclaving. Aprotinin (500 µL; 10,000 KIU.mL^{-1}) was added immediately prior to use.

SDS solution (10% w/v)

Sodium dodecyl sulphate (10 g) was dissolved in 100 mL distilled water and sterilised by filtration. Aliquots (10 mL) were stored aseptically for a maximum of six months at room temperature.

Hypotonic buffer (10 mM tris, 2.7 mM EDTA) with aprotinin (10 KIUmL^{-1})

Trizma base (1.21 g) and EDTA (1.0 g) were dissolved in 900 mL distilled water and the pH adjusted to 8.0-8.2. The volume was made up to 1 L and the solution sterilised by autoclaving. Aprotinin (1 mL; 10,000 KIU.mL^{-1}) was added prior to use.

Hypotonic buffer with SDS (0.1% w/v)

SDS solution (5 mL; 10% w/v) was added aseptically to 495 mL sterile hypotonic buffer.

Nuclease solution

Trizma base (6.1 g) and magnesium chloride (2.0 g) were dissolved in 80 mL distilled water and the pH adjusted to 7.5-7.7. The volume was made up to a total of 990 mL using distilled water and the solution autoclaved. Immediately prior to use, RNAase stock (10 mL; 100 UmL^{-1}) and DNAase (5 mL; 10,000 UmL^{-1}) were added.

Hypertonic solution (50 mM tris, 1.5 M NaCl)

NaCl (87.66 g) and tris (6.06 g) were dissolved in 900 mL distilled water and the pH adjusted to 7.5-7.7. The volume was made up to a total volume of 1 L and the solution autoclaved.

Peracetic acid solution (0.1% v/v)

Peracetic acid (5.5 mL; 40-44% v/v) was added to 2 L of sterile PBS and used within one hour of preparation.

2.2.4.2 Histology

Diastase solution

0.2 g α-amylase was dissolved in 40 mL distilled water.

Oil red O (0.3% (w/v))

Oil red O (50 mg) was added to isopropanol (10 mL) and stored at room temperature to create a stock solution (0.5% (w/v)). Stock solution (3 parts) was added to dH$_2$O and filtered sequentially (filters of pore sizes 0.8 and 0.2 μm respectively) immediately prior to use.

Ammonium hydroxide (10% (v/v)

Ammonium hydroxide (30 mL; 28%) was added to dH$_2$O (60 mL).

Alizarin red (40 mM)

Add alizarin red (2.0 g) to dH$_2$O (100 mL). Adjust to pH 4.1 by dropwise addition of ammonium hydroxide (10% (v/v)).

2.2.4.3 Scanning electron microscopy sample preparation

Phosphate buffer (0.9 M sodium dihydrogen orthophosphate, 0.11 M disodium hydrogen orthophosphate)

Sodium dihydrogen orthophosphate (45 mL) and disodium hydrogen orthophosphate (55 mL) were added to 100 mL distilled water.

2.2.4.4 Microbiology

Thioglycolate broth

Thioglycolate broth (29 g) was dissolved in 1L distilled water, and the solution sterilised by autoclaving.

2.2.4.5 Cell culture

Complete DMEM culture medium

To 174 mL Dulbecco's modified Eagle's medium (DMEM) 2 mL L-glutamine (200mM), 4mL penicillin/streptomycin (10,000 UmL^{-1}) and 20 mL foetal bovine serum (FBS) was added.

BHK cell culture medium

To 164 mL Glasgow's minimal essential medium (GMEM) 2 mL L-glutamine (200mM), 4 mL penicillin/streptomycin (10,000 UmL^{-1}) and 10 mL FBS was added.

hMSC culture medium

To 174 mL low-glucose Dulbecco's modified Eagle's medium (DMEM) 2 mL L-glutamine (200mM), 4mL penicillin/streptomycin (10,000 UmL^{-1}) and 20 mL foetal bovine serum (FBS) was added.

hMSC medium supplemented with HEPES
HEPES (1.37 mL; 1 M) was added to hMSC culture medium (48.63 mL).

Positive control culture medium with DMSO (40 % (v/v))(for cytotoxicity testing)
Culture medium (BHK or complete DMEM;12 mL) was added to DMSO (8 mL).

Seeding ring conditioned medium (for seeding ring cytotoxicity testing)

Tencell seeding rings sterilised by dry heat (n = 5) were placed in BHK and complete DMEM culture medium (100 mL) and incubated (37 °C) with agitation (120 rpm) for 3 days. Tencell seeding rings were removed from conditioned medium aseptically.

Percoll gradient preparation

Percoll (22.05 mL) was added to NaCl (2.45 mL; 1.5 M) and Tyrode's solution (10.5 mL), centrifuged to mix (15 min; 20,000 × g) and stored at 4°C until use.

Isobutylmethylxantine (0.5 M)

Isobutylmethylxantine (200 mg) was added to DMSO (1.8 mL), filtered (0.22 μm pore size) and aliquoted (100 μL) for storage at − 20°C.

Indomethacin (0.6 M)

Indomethacin (100 mg) was added to DMSO (467 μL), sterilised by filtration (0.22 μm pore size) and aliquoted (10 μL) for storage at − 20°C.

Hydrocortisone (0.1 mM)

Hydrocortisone (4.85 mg) was added to PBS (100 mL), sterilised by filtration (0.22 μm pore size) and aliquoted (550 μL) for storage at − 20°C.

Ascorbic-2-phosphate (200 mM)

Ascorbic-2-phosphate (2.57 g) was added to dH_2O (50 mL), sterilised by filtration (pore size 0.22 μm) and aliquoted (of sizes 50 and 75 μL in equal numbers) for storage at − 20°C.

Sodium pyruvate (200 mM)

Sodium pyruvate (1.1 g) was added to dH_2O (100 mL), sterilised by filtration (pore size 0.22 μm) and aliquoted (1 mL) for storage at − 20°C.

Dexamethasone (500 μM)

Dexamethasone (25 mg) was added to absolute ethanol (1.28 mL; 100%), sterilised by filtration (pore size 0.22 μm) and aliquoted (10 μL) for storage at − 20°C. Single aliquots were defrosted, added to complete DMEM (1 mL) and refrozen (20 μL aliquots).

β-2-glycerophosphate (2 M)

β-2-glycerophosphate (10 g) was added to dH_2O (23 mL), sterilised by filtration (0.22 μm pore size) and aliquoted (550 μL) for storage at − 20°C

Adipogenic medium (isobutylmethylxantine (0.5 mM), indomethacin (60 µM), hydrocortisone (0.5 µM)

Isobutylmethylxantine (100 µL; 0.5M), indomethacin (10 µL; 0.6M) and hydrocortisone (500 µL; 0.1 mM) were added to complete DMEM (100 mL).

Chondrogenic medium (ascorbic-2-phosphate (0.15 mM), insulin-transferrin-selenium (0.1 ×), sodium pyruvate (20 mM)

Ascorbic-2-phosphate (75 µL; 200 mM), insulin-transferrin-selenium (100 µL; 100×) and sodium pyruvate (1 Ml; 200 mM) were added to complete DMEM (100 mL).

Osteogenic medium (dexamethasone (0.1 µM), ascorbic-2-phosphate (0.1 mM)

Dexamethasone (20 µL; 500 µM), ascorbic-2-phosphate (50 µL; 200 mM) and β-2-glycerophosphate (500 µL; 2M) were added to complete DMEM (100 mL).

ATPlite™ substrate solution

Lyophilized substrate (one vial) and substrate buffer solution were allowed to equilibrate to room temperature (~20 min), and the buffer (5 mL) added to the substrate.

Sodium chloride (3 M)

Sodium chloride (87.66 g) was dissolved in dH$_2$O and sterilised by moist heat (section 2.2.2.1).

Tris buffered saline (TBS; 2M)

Trizma base (2.42 g) was dissolved in dH$_2$O (500 mL), the pH adjusted to 7.6 by adding hydrochloric acid (6 M) or sodium hydroxide (6 M) dropwise, and the volume adjusted to 1 L with dH$_2$O. The solution was sterilised by moist heat.

Live/dead staining solution (calcein AM and ethidium homodimer-1; 1 µM)

Calcein (3.6 µL) and ethidium homodimer-1 (15 µL) were added to PBS (15 mL) immediately before use.

Glycerol with DABCO (1.25% (w/v))

DABCO (10 mL; 2.5% (w/v)) was added to glycerol (90 mL) and stored at 2-8 °C immediately prior to use.

2.2.4.6 General molecular biology

DNase I stock solution

RNase-free water (550 µL) was directly injected into the DNase I vial provided (1500 Kunitz units), mixed by inversion, and stored at − 20°C.

DNase I digestion solution

DNase I stock solution (10 µL) was added to buffer RDD (70 µL) immediately before use and mixed by inversion.

Proteinase K digestion solution (17 µg/mL)
Proteinase K (10 µL; 1 mg/mL) was added to RNase-free water (590 µL).

Agarose gel (4% (w/v))
Agarose (4 g) was added to TBS (100 mL; 1 ×) and heated in a microwave (30 s; 850 W). SYBR™ safe (10 µL) was added and the mixture stirred briefly. Gel (33 mL) was added to trays fitted with comb inserts.

Amplicon loading mix
Bioline loading dye (2 µL; 5 ×) was added to each PCR product (10 µL).

2.2.4.7 Quantitative polymerase chain reaction

Stock primer solution (100 µM)
Lyophilized primers, designed according to section 2.2.10.1, were diluted to 100 µM by adding the appropriate volume of RNAase- and DNase-free water (given by the supplier information sheet).

Working primer solution (10 µM)
Stock primer solution (10 µL) was added to water (90 µL).

Working primer solution (1 µM)
Working primer solution (10 µL; 10 µM) was added to water (90 µL).

Template RNA (for primer specificity testing; section 2.2.10.5)
The concentration and purity of RNA solutions isolated from differentiated cells was measured using a NanoDrop spectrophotometer as described previously (section 2.2.9.1), and diluted as appropriate to a concentration of $2ng.\mu L^{-1}$.

Template RNA (for primer efficiency testing; section 2.2.10.4.2)

Isolated RNA was serially diluted (1:4) to provide a range of concentrations for efficiency testing. The concentration and purity of RNA solutions extracted from differentiated cells was measured using a NanoDrop spectrophotometer as described previously (section 2.2.9.1). Briefly, isolated RNA (20 µL) was added to DNAse- and RNAse- free water (80 µL) and mixed thoroughly by pipetting. The resulting dilution (20 µL) was added to water (80 µL), and so forth using the same method until 7 dilutions were prepared. If required, extracted RNA was re-diluted (1:3; 20 µL: 60 µL RNA isolate:water).

Template RNA (for Tencell gene expression analyses; section 2.2.10.7)

RNA was isolated from Tencell-cultured pericardium and cell pellets as described previously (sections 2.2.9.4 and 0) and stored at − 80 °C until use.

Reverse transcriptase dilution (1:1; comprised of Ominiscript and Sensiscript recombinant reverse transcriptases)

Reverse transcription mix (25 µL) was diluted with water (25 µL).

Reverse transcriptase/mastermix mix

Reverse transcription mix (7.5 µL; 1:1) was added to mastermix (375 µL).

Assay mastermix (for primer efficiency testing; section 2.2.10.4.2)

Reverse transcriptase/mastermix mix (357 µL) was added to each primer (17.5 µL each; 10 µM) and RNAse- and DNAse- free water (238 µL).

Assay mastermix (for Tencell gene expression analyses; section 2.2.10.7)

Mastermix (1200 µL) was added to reverse transcription mix (24 µL), oligonucleotide primers (120 µL.primer^{-1}) and DNase- and RNase-free water (897.6 µL), and mixed thoroughly by vortexing (5s).

2.2.5 Preparation of an acellular cell culture substrate

2.2.5.1 Tissue retrieval

Attached porcine hearts and lungs were obtained from a local abattoir (M&C Meats, Leeds) within 4 hours of slaughter, and the anterior portion of the pericardium removed using scissors, avoiding large (> 1cm^2) fatty deposits. Excess fat was manually peeled from the excised pericardia and smaller deposits removed manually.

Pericardia were measured and cut to an asymmetric shape (Fig. 2.1), such that the mesothelial and fatty surfaces were distinguishable. Samples were then rinsed in PBS to remove excess blood, and stored at -20°C in contact with PBS moistened filter paper. Pots were labelled with sample size and the date of dissection.
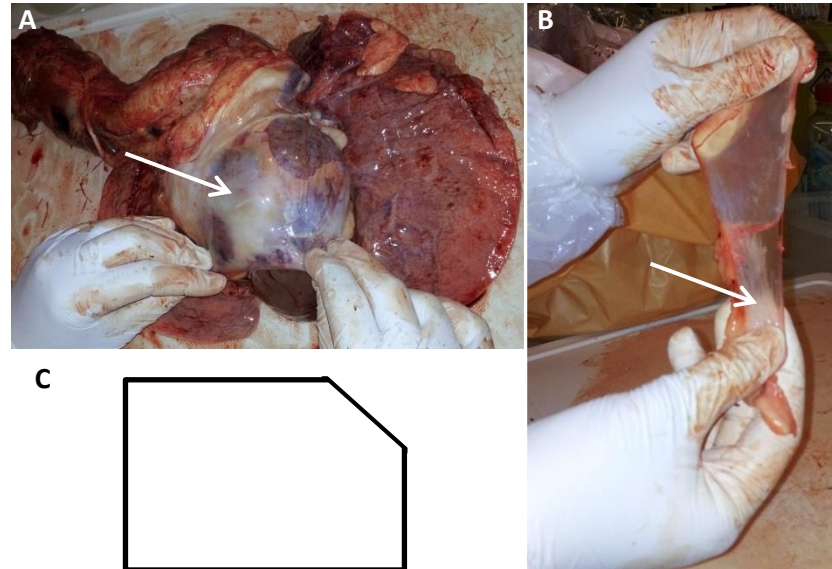
Fig. 2.1: Dissection of and fat removal from porcine pericardium. *The frontal portion of pericardium was removed from each heart (A, indicated by arrow) and the large fat deposits of the fatty layer removed (B, fat indicated by arrow). In order to distinguish between the fatty and mesothelial surfaces the samples were cut to an asymmetric shape such that the fatty layer was the upwards surface when the sample was arranged as shown (c).*

2.2.5.2   Preparation of acellular pericardium

Decellularisation was conducted in five batches (n= 7, 12, 12, 12 & 24 pericardia). Samples were processed simultaneously in individual vessels. The volume of solution required was dependent on sample size, as detailed below. The process was carried out under aseptic conditions. The conditions applied during each wash are given in Table 2.5.

Table 2.5: The conditions used during each wash of the decellularisation of porcine pericardium, unless stated otherwise. *Details of equipment used can be found in Appendix II.*

Wash reagent	Wash conditions			
	Volume required (mL/cm^2)	Temperature (°C)	Shaker speed (rpm)	Duration (hr)
PBS	4	22	100	0.5
PBS with EDTA	4	22	100	0.5
Disinfection solution	1	37	100	0.5
Hypotonic buffer	2	4	100	16
Hypotonic buffer with SDS	2	22	100	18-24
Nuclease solution	2	37	50	3
Hypertonic solution	2	37	100	18-24
Peracetic acid solution	2	22	150	3

Frozen pericardia were thawed in PBS (190 mL) at 37 °C and any remaining fat deposits removed. Samples were then incubated with disinfection solution and washed three times in PBS with EDTA. This was followed by treatment with hypotonic buffer and hypotonic buffer containing SDS. After rinsing the pericardia three times with PBS the samples were incubated in nuclease solution. The tissue was washed three times in PBS containing EDTA, and hypertonic solution was added to the tissue. Hypertonic solution was removed by washing in PBS three times and terminal sterilisation achieved using peracetic acid treatment. Finally, the tissue was rinsed with PBS four times, and stored in approximately 100 mL PBS at 4 °C.

2.2.6 Microbiology

2.2.6.1 Assessment of the sterility of acellular pericardium

Bacterial and yeast contamination of scaffolds was assessed by placing tissue and storage solution/culture medium samples in conditions ideal for microbial growth, and monitoring for the appearance of microbial colonies. Sterility of the scaffolds and storage solution/culture medium was examined both immediately post-decellularisation and post-culture in Tencell. Three replicates were tested per decellularisation and culture experiment.

2.2.6.1.1   Test for contamination by aerobic bacteria

The presence of any aerobic bacteria was tested using nutrient broth, fresh blood agar (FBA) and nutrient agar (NA) plates. Tissue samples (5 mm^2) were minced and placed in nutrient broth, using a broth containing the bacterium *Staphylococcus epidermidis* as a positive control. Additionally, 1 mL tissue storage PBS/well culture medium was removed and applied to both FBA and NA plates for each sample using standard techniques. *S. epidermidis* was introduced to both FBA and NA plates as a positive control, and all cultures incubated at 37 °C. Cultures were examined for bacterial growth after 3, 7 and 21 days.

2.2.6.1.2   Test for contamination by anaerobic bacteria

Tissue samples and storage solution/well culture medium were tested for contamination by anaerobic bacteria using thioglycolate broth, fresh blood agar (FBA) and nutrient agar (NA) plates incubated in oxygen-free conditions. Tissue samples (5 mm^2) were minced and placed in thioglycolate broth, using a broth containing the bacterium *Clostridium perfringens* as a positive control. Cultures were incubated at 37 °C for 72 hours, at which point 20 µL broth was removed and applied to both FBA and NA plates for each sample. Plates were placed in a sealed tub containing an oxygen exclusion sachet and incubated at 37°C. All cultures were examined for bacterial growth after 3, 7 and 21 days.

2.2.6.1.3   Test for contamination by yeast

Tissue storage solution/well culture medium was tested for the presence of yeast using Sabouraud dextrose agar plates. Liquid (20 µL) was removed using an application loop and applied to the plates aseptically. *Candida albicans* was cultured as a positive control. Plates were incubated at 30°C and examined for the presence of yeast colonies after 3, 7 and 21 days.

2.2.7 Histological techniques

2.2.7.1 Tissue processing

Pericardial samples were placed in histocassettes and fixed by immersion in 10% (v/v) neutral buffered formalin (NBF) for 90 minutes. Sequential dehydration of the tissue was performed

using an automated tissue processor. Details of the regimen used are given in Table 2.6. Cassettes were stored in molten wax prior to embedding.

Table 2.6: The dehydration and wax infiltration regimen applied to pericardial samples using a Leica TP1020 tissue processor

Wash number	Wash solution	Wash duration/hours
1	NBF (10 % v/v)	1
2	Ethanol (70 % v/v)	1
3	Methylated spirits (90 % v/v)	1
4	Methylated spirits (100 % v/v)	0.5
5	Methylated spirits (100 % v/v)	0.5
6	Methylated spirits (100 % v/v)	1
7	Methylated spirits (100 % v/v)	1
8	Xylene	1
9	Xylene	1
10	Xylene	1
11	Molten wax	1
12	Molten wax	1

2.2.7.2 Wax embedding

For comparison of the histoarchitecture of decellularised tissue, rectangular samples (of approx. size 2×1 cm) of each acellular (n=3 per decellularisation batch) and native (n=3) pericardium were dissected such that the long axis of each specimen was either parallel or perpendicular to the orientation of collagen fibres in the tissue. Collagen fibre orientation was visualised using a light box and polarized light filters. Molten wax was added and allowed to set for 12-16 hours. Excess wax was removed from the blocks manually following removal from the moulds.

For examination of the histoarchitecture of Tencell-cultured seeded substrates, scaffolds were removed from the bioreactor and cut in half with a scalpel. The long axis of one half was arranged perpendicular to the wax mould base. Molten wax was added and allowed to set for 12-16 hours. Excess wax was removed from the blocks manually following removal from the moulds.

2.2.7.3 Sectioning of wax embedded samples

Wax histology blocks were sectioned at a thickness of 10 µm using a microtome and floated on a water bath at 40°C to eliminate creases. Sections were transferred to SuperFrost™ plus microscope slides, and dried using a hot plate set to a temperature of 55 °C. A minimum of two slides for each sample and collagen orientation were produced.

2.2.7.4 Dewaxing of tissue sections

Sections to be stained were taken through washes of increasing hydrophilicity in order to remove wax. The slides were placed in pots of xylene twice for 10 minutes each, and immersed in 100% (v/v) ethanol for 3 minutes. This was followed by immersion in fresh 100% (v/v) ethanol for 2 minutes and 70% (v/v) ethanol for a further 2 minutes. Dewaxing was completed by rinsing the sections in running tap water for 3 minutes.

2.2.7.5 Dehydration and mounting of stained sections

Sections were dehydrated through treatment with solutions of increasing hydrophobicity. Slides were rinsed for 5 seconds with 70% (v/v) ethanol, followed by rinsing with methylated spirits three times for periods of 1, 2 and 3 minutes and immersion in xylene twice for 10 minutes each. Sections were mounted in DPX and covered with a cover slip.

2.2.7.6 Histological staining

2.2.7.6.1 Haematoxylin and eosin staining of tissue sections

Haematoxylin and eosin (H&E) staining is routinely used to visualise general tissue structure and was used to assess the cellularity of both fresh and decellularised tissue. Haematoxylin stains nuclei through the binding of its constituent Hemalum with DNA, aiding the identification of cells. Eosin imparts a pink/red colour to intra- or extracellular protein such as collagen, and allows visualisation of the structure of the ECM.

Sections on slides to be stained were placed in haematoxylin for 1 minute and rinsed in running tap water until all dye residues were removed. Slides were placed in the counterstain eosin for 3 minutes to visualise tissue structure. Excess eosin was removed by immersion in running tap water.

2.2.7.6.2 Alcian blue staining of tissue sections

Alcian blue stains acidic polysaccharides a blue/violet colour and allows visual assessment of the glycosaminoglycan (GAG) content of tissue. Alcian blue staining using the method described below was used to indicate the impact of decellularisation on the ECM composition of porcine pericardium.

Samples were immersed in 1% (w/v) Alcian blue for 15 minutes and rinsed in running tap water until all dye residues were removed. Diastase treatment was carried out by microwaving the slides in diastase solution for 20 seconds using the 'medium-high' setting of an 800 Watt microwave. Following diastase treatment, samples were immersed in periodic acid for 5 minutes and rinsed in distilled water 3 times. They were then immersed in Schiff's reagent for 15 minutes. Schiff's reagent was removed by rinsing the slides in running tap water for 5 minutes, and the slides were counterstained in haematoxylin for 90 seconds. Excess haematoxylin was removed by immersion in running tap water until all dye residues were removed.

2.2.7.6.3 Alcian blue staining of cultured cells

Alcian blue (500 μL; 1% (w/v)) was added to formalin fixed cells for 3 min, the dye aspirated and cells washed three times with H_2O (1 mL). Stained plates were dried in air overnight and viewed using an inverted microscope at 10 × magnification.

2.2.7.6.4 Oil red O staining of cultured cells

Cultured cells were stained with oil red o (500 µL; 0.3% (w/v)) for 10 min, the dye aspirated and cells rinsed three times with H_2O (1 mL). Stained plates were dried in air overnight and viewed using an inverted microscope at 10 × magnification.

2.2.7.7 Alizarin red staining of cultured cells

Alizarin red (500 µL; 40 mM) was added to formalin fixed cells for 20 min, and aspirated before rinsing the cells three times with dH_2O. Stained plates were dried in air overnight and viewed using an inverted microscope at 10 × magnification.

2.2.8 Cell culture techniques

2.2.8.1 Cell resurrection and maintenance

Cryovials containing frozen cells and medium containing 10% (v/v) dimethyl sulfoxide (DMSO) were warmed to room temperature and the contents transferred to a plastic universal. Working quickly to avoid cell shock, pre-warmed medium (10 mL) was added dropwise and the suspension centrifuged at 150 g for 10 min. The supernatant was discarded and the cell pellet resuspended in medium (10 mL) and seeded in a T75 tissue culture flask.

2.2.8.2 Cell counting and assessment of cell viability

Trypan blue was used to distinguish between dead and viable cells during counting. Trypan blue (20 µL) was added to cell suspension (20 µL) and the mixture carefully added underneath the cover slip of a hemocytometer. The viable cells in an engraved square of known volume were counted using a microscope and the cell count converted to the density of the cell suspension. The volume of the square was such that the cell count obtained was converted to a cell density of cells.mL^{-1} in the hemocytometer by multiplication by a factor of 10^4. The cell density of the original cell suspension was calculated by doubling this calculated density to account for dilution of the suspension with trypan blue solution.

2.2.8.3 Cell passaging

Cells in culture were passaged upon reaching approx. 80% confluency. Culture medium was removed and the cell layer washed with calcium and magnesium-free PBS (10 mL). Trypsin/EDTA (1.5 mL) was added and the flasks incubated at 37 °C for 5 min to detach the cells. Detachment was aided by tapping the flasks, and monitored using a microscope. After detachment culture medium (10 mL) was added and the suspension centrifuged (150 g, 10 min). The supernatant was discarded and fresh media added before seeding the cells at a 1:10 cell suspension:culture medium ratio.

2.2.8.4 Culture of differentiated cells

Differentiated cells were cultured because they were expected to express the genes of interest; RNA was extracted from these cultures for primer pair validation. Tenocyte RNA was used to validate pairs specific for scleraxis and collagen I and III, osteoblast RNA for RUNX2, smooth muscle cell RNA for calponin, smooth muscle 22α and smooth muscle α-actin and chondrocyte RNA for validation of SOX-9 primer pairs. Primer pairs specific for PPAR-ɣ and adiponectin were validated using RNA extracted from human knee adipose tissue, kindly supplied by Dr Stacy-Paul Wilshaw.

Cell culture was performed as described in sections 2.2.8.1, 2.2.8.2 and 2.2.8.3. Smooth muscle cells, osteoblasts and tenocytes were cultured with complete DMEM culture medium. Chondrocytes were cultured using chondrocyte growth medium purchased from PromoCell.

2.2.8.5 Assessment of the in vitro biocompatibility of acellular pericardium

The growth of baby hamster kidney (BHK) and 3T3 cells in the presence of acellular pericardium was compared with that in the presence of known cytotoxic (cyanoacrylate) and non-cytotoxic (collagen type I) materials.

Two samples (5 mm^2) were dissected from each control pericardium and temporarily stored in calcium and magnesium-free PBS (n=3 per decellularisation batch). One six well plate was used for each batch of decellularised pericardia and each cell type (total 10 plates). Collagen gel adhesive was kindly supplied by Dr. Ji Luo (prepared from rat tails using standard techniques). Collagen gel (15 µL) was applied to four wells of each plate. NaOH (7.5 µL; 0.1 % w/v) was added to neutralise the gel, and a tissue sample applied to three of the adhesive-

containing wells of each plate. No tissue was adhered in the fourth collagen-containing well per plate, which served as a negative control. Cyanocrylate contact adhesive (15 µL) was applied to one well per plate as a positive control, and the final well was left empty in order to compare results with cell growth on tissue culture plastic. Following drying of the collagen gel and cyanoacrylate adhesive the wells were washed three times with calcium and magnesium-free PBS (5 mL.well^{-1}). Each cell type was passaged, counted (sections 2.2.8.1, 2.2.8.2 and 2.2.8.3) and resuspended at densities of 2.5×10^5 cells.mL^{-1}. Cell suspension (2 mL) was added to each well and the plates incubated for 48 hours in 5 % (v/v) CO_2 in air at 37°C. BHK cells were cultured with BHK cell culture medium, and 3T3 cells complete DMEM culture medium. After incubation the plates were examined by microscopy, and stained to enable further visualisation. Prior to staining, culture medium was aspirated and the cell layer washed with PBS (5 mL.well^{-1}). The cells were fixed by adding NBF (2 mL; 10% v/v). NBF was aspirated after 10 min of incubation and Giemsa stain (2 mL) added to each well. After a further 10 min the stain was aspirated and the plates thoroughly washed with tap water. The plates were dried in air for approx. 16 hours and examined by bright field microscopy.

2.2.8.6 Isolation of Porcine multipotential mesenchymal stromal cells

Multipotential mesenchymal stromal cells were isolated from porcine femurs for use in preliminary seeding experiments with the Tencell seeding rings.

pMSC were isolated from bone marrow by Percoll density fractionation (Olofsson *et al.*, 1980; Rosca and Burlacu, 2010). Briefly, fresh (supplied within ~ 4 hr of slaughter) porcine femurs were bisected using a hacksaw under sterile conditions and the bone marrow (~ 5 mL) extracted using a sterile spatula. Marrow was added to complete medium (25 mL) and dispersed by drawing the mixture into a serological pipette. Excess adipose tissue was removed by discarding the supernatant following centrifugation (5 min; 600 × g). The bone marrow pellet was made up to a total volume of 4 mL and added dropwise onto a Percoll gradient (35 mL). The Percoll-bone marrow mixture was centrifuged (15 min; 460 × g) and the upper fraction (coloured pink) aspirated and added to culture medium (35 mL). Remaining Percoll solution in this fraction was removed by centrifugation (5 min; 600 × g), the cell pellet resuspended in complete culture medium (5 mL) and seeded in a T25 flask. Cells were passaged as described in section 2.2.8.3 upon reaching 80% confluency.

2.2.8.7 Trilineage differentiation of porcine multipotential mesenchymal stromal cells

Porcine MSC (passage 3) were passaged and counted as described previously (section 2.2.8.3) and seeded at densities of 3×10^3 and 4×10^4 cells.cm^{-2} in osteogenic and adipogenic medium (2 mL) respectively. The remaining cell suspension was centrifuged (150×g; 10 min), counted and resuspended at a concentration of 1×10^7 cells.mL^{-1} in chondrogenic medium and seeded in 10 µL droplets for 3 hr (Lavrentieva *et al.*, 2013). Additional culture medium (20 µL) was added to cell pellets in the event of visible drying. Pellet cultures were flooded with chondrogenic culture medium (2 mL) following seeding. To assess the extent of differentiation, pMSC were formalin fixed (2 mL; 10% (v/v)) for 10 minutes, rinsed with PBS (2 mL) twice and stained according to the alizarin red, alcian blue and oil red o protocols described in section 2.2.7.6 for cells differentiated towards the osteogenic, chondrogenic and adipogenic lineages respectively. Cells were stained on days 0, 3, 6, 14 and 21.

2.2.8.8 Seeding porcine MSC using the bespoke Tencell seeding rings

Tissue (of size ~ 2 × 4 cm) was resected from stock acellular porcine pericardium and conditioned in complete DMEM culture medium (~ 50 mL) (37 °C; 5% (v/v) CO_2 in air) overnight. Tissue conditioning is necessary to allow cell culture medium to penetrate the thickness of the tissue, to support three-dimensional cell culture. Porcine MSC (passage 5) were passaged and resuspended such that a total of 4.80×10^4 cells were applied per scaffold (seeding density 1.20×10^5 cells.cm^{-2}). Tencell seeding rings were placed on the mesothelial surface of the conditioned matrix and the cell suspension added to their reservoir. To contrast cell seeding with and without the use of the Tencell seeding rings, the same volume of cell suspension was applied directly to tissue, and small quantities (~50 µL) of culture medium added periodically throughout the seeding period to maintain moisture. Note that this direct seeding strategy was conducted for comparison purposes only; since the final seeding density of cells seeded in this manner cannot be controlled, and is unlikely to be even, it is not appropriate for cell seeding in this project. Cell-tissue substrates were placed in vented tissue culture tubs and incubated (37 °C; 5% (v/v) CO_2 in air). Seeding volumes of 150 and 80 µL were tested and cell attachment assessed by live/dead® staining after seeding periods of 2 and 4 hours (Section 2.2.8.10.1).

2.2.8.9   Seeding of human MSC using circular seeding rings

Cell viability of hMSC seeded for 2, 4 and ~ 18 hours on acellular porcine pericardium using the circular seeding rings was quantified using the ATPlite™ assay. Model pMSC were not used in these experiments as the efficacy of these rings with other tissue and cell types had been previously confirmed (Robert Guilliatt, personal communication) and loss of high value hMSC was deemed unlikely.

2.2.8.9.1   Preparation of a standard curve of the relationship between hMSC number and luminescence counts in the ATP assay

A standard curve, allowing estimation of the number of hMSC present from the ATPlite™ assay from the luminescence counts generated, was prepared.

Human multipotential mesenchymal stromal cells (passage 5) were passaged and resuspended at a concentration of 4.37×10^5 cells.mL^{-1} (sections 2.2.8.1, 2.2.8.2 and 2.2.8.3). Aliquots of 400, 320, 240 160, 80 and 40 µL of cell suspension were added to the appropriate volume of culture medium required to adjust the cell suspensions to 400 µL. Each cell suspension (100 µL) was added to mammalian cell lysis solution (50 µL) in an opaque 96-well plate, and shaken on an orbital shaker in the dark (5 min; 400 rpm). Substrate solution (50 µL) was then added to each test well and the mixture shaken on an orbital shaker in the dark (5 min; 400 rpm), before dark adapting the plate (10 min) and measuring the luminescence using a plate reader.

2.2.8.9.2   Seeding of hMSC on pericardial substrates using circular seeding rings

Tissue (of size ~ 1.5 × 1.5 cm) was resected from stock acellular porcine pericardium and conditioned in hMSC culture medium (~ 50 mL) (37 °C; 5% (v/v) CO_2 in air) overnight. Human MSC (passage 5) were passaged and resuspended at a concentration of 2.73×10^5 cells.mL^{-1} as previously described, and seeded in circular seeding rings (diameter = 1.1 cm) placed on the mesothelial surface of the matrix in 6 well plates (initial seeding volume 465 µL, as advised by previous investigator (Andrew Aldridge, personal communication); 1.2×10^5 cells.cm^{-2} applied). Cell seeding using circular seeding rings was examined both with and without a medium reservoir (3 mL) in the well plate around the exterior of the seeding ring. Samples were incubated (37 °C; 5% (v/v) CO_2 in air) and cell viability quantified by the ATPlite™ assay (Section 2.2.8.11) after seeding periods of 2, 4 and ~ 18 hours (overnight).

2.2.8.10 Assessment of cell viability in cell-seeded scaffolds

2.2.8.10.1 Live/dead® staining of cell-seeded acellular porcine pericardium

Cell survival in acellular scaffolds seeded using the bespoke Tencell seeding rings was assessed by live/dead staining.

The cell seeded surface was dissected from the matrix samples and washed in PBS (2 mL) twice in 6 well plates. Live/dead staining solution (2 mL) was added and the plates incubated in the dark (RT; 45 min). Live/dead staining solution was aspirated and stained samples washed with TBS (2 mL; 10 min) three times, before being wet mounted using glycerol with DABCO on a microscope slide with a glass coverslip. Live/dead staining was examined using a Zeiss microscope and photographed using an attached camera.

2.2.8.11 Measurement of luminescence counts of cell-seeded matrix

Cell survival in acellular scaffolds seeded with cells using the circular seeding rings was determined using the ATPlite™ assay, to provide quantitative data pertaining to cell viability.

The cell-seeded surface of the matrices was resected, cut approximately in half and minced in a 24 well plate. Approximately the same quantity of unseeded, medium conditioned tissue was similarly prepared as a negative control. Mammalian cell lysis solution (250 μL) was added and the plate agitated (400 rpm; 5 min). Technical replicates (50 μL) were added to an opaque 96 well plate and ATP substrate solution (50 μL) added. The cell lysate-ATP substrate mixture was agitated (400 rpm; 5 min) in the dark, dark adapted (10 min) and the luminescence counts measured using a plate reader.

2.2.8.12 Tencell culture of hMSC-seeded acellular pericardium scaffolds

Pericardial substrates seeded according to section 2.2.8.9 were cultured in HEPES-containing buffer according to section 2.2.12.6.1. Samples were subjected to strains of 5, 10 and 20% by selecting the arm displacement values shown in Table 2.7.

To optimise the duration of mechanostimulation, pericardium-seeded hMSC were strained for periods of 4 and 24 hours (total culture period 24 hours). Post-culture, each sample (n=6

for both static and strain samples) was bisected; three halves per sample type were analysed by histology and cell viability each, and six halves were analysed qPCR.

Table 2.7: The displacement selected using the amplifier knob of Tencell to achieve the desired strains for a strained region of length 1.0 cm

Strain (%)	Selected displacement (mm)
5	0.5
10	1.0
20	2.0

2.2.9 General molecular biology

2.2.9.1 Nucleic acid spectrometry using the NanoDrop apparatus

The measurement point of the instrument was wiped with a clean tissue and water (2 µL) applied to perform a blank measurement. The water was removed using a tissue and nucleic acid solution (2 µL) applied for measurement. The concentration and $A_{260/280}$ was recorded for each sample.

2.2.9.2 DNA removal from RNA solutions

Solutions of RNA were digested with DNase to ensure complete removal of residual DNA during the RNA extraction process.

RNeasy spin (supplied with RNeasy mini kit) columns were washed with buffer RW1 (350 µL) by centrifugation (15s; ≥ 8000 × g) and the eluent discarded. Residual DNA was digested by incubation (RT; 15 min) with DNase I digestion solution (80 µL). The digestion mix was removed by adding buffer RW1 (350 µL) and removing the eluent by centrifugation (15s; ≥ 8000 × g).

2.2.9.3 Extraction and measurement of RNA content of cell pellets

Extraction of RNA from cell pellets was performed to measure the amount and purity of RNA isolated from a sample of interest , or provide template material for qPCR.

The quantity of RNA isolated from cell pellets containing different numbers of cells was also measured.

A cell pellet was obtained by trypsinization/centrifugation as described by section 2.2.8.3. Pellets were lysed with buffer RLT (350 µL) and disrupted by flicking. The resulting lysate was homogenised by drawing it through a blunt needle 5 times (0.9 mm gauge). Ethanol (350 µL) was added to the lysate, mixed by repeat pipetting and transferred to an RNeasy spin column placed inside a collection tube (of volume 2 mL). The spin column was centrifuged (15s; ≥ 8000 × g) and the eluent discarded. Digestion of remaining DNA was conducted according to section 2.2.9.2.. Buffer RPE (500 µL) was added twice to the spin membrane, centrifuged after each addition (first addition: 15s; ≥ 8000 × g; second addition: 2 min; ≥ 8000 × g) and the eluents discarded. The column was dried by centrifugation in a fresh collection tube (1 min; 16000 × g) and RNA eluted in RNase-free water (50 µL) by centrifugation (1 min; 8000 × g). The concentration of nucleic acid species present and absorbance of the eluent at 260 and 280 nm was measured using a NanoDrop spectrophotometer. Where applicable, the total amount of RNA extracted was calculated by multiplying the concentration of eluted RNA by the eluent volume.

2.2.9.4 Comparison of methods of RNA extraction from seeded scaffolds

The amount of RNA extracted from seeded scaffolds using enzymatic digestion at a high temperature (55 °C) was compared with that extracted from undigested, macerated samples to determine the optimal method for RNA extraction from Tencell-cultured substrates. One half of each experimental replicate was processed by each method for direct comparison. All reagents, except proteinase K, described in this method were obtained from the RNeasy Mini Kit manufactured by Qiagen.

2.2.9.4.1 Enzymatic digestion method

Samples (of mass ≤ 30 mg) were finely macerated (to pieces approx. 1-2 mm^2) and lysed with buffer RLT (350 µL). Mixing was ensured by drawing the solution through a blunt needle (0.9 mm gauge) 5 times. Proteinase K digestion solution (600 µL) was added to the lysate and the mixture incubated (55 °C) for 10 min. Digested samples were centrifuged (3 min; 8000 × g) to

separate lysate and tissue and the supernatant added to absolute ethanol (450 µL) with repeat pipetting to aid mixing. A maximum volume of 700 µL of lysate mixture was applied per RNeasy spin column, centrifuged (15 s; 8000 × g) and the eluent discarded. This step was repeated with the same spin column where lysate volume was in excess of 700 µL/sample. On column DNase digestion was performed as previously described (section 2.2.9.2). Buffer RPE (500 µL) was then applied to the column twice and the eluent produced upon centrifugation (First wash: 15s; 8000 × g, second wash:1 min; 8000 × g) discarded. The spin column was dried by centrifugation in a fresh collection tube (1 min; 8000 × g) before RNA elution with RNase free water (50 µL) with centrifugation (1 min; 8000 × g). The concentration of RNA in the eluent was measured using a NanoDrop spectrophotometer as previously described.

2.2.9.4.2 Maceration-only method

RNA extraction was performed as described by section 5.2.1.3, with omission of the proteinase K digestion step.

2.2.9.5 Extraction of RNA from Tencell-cultured acellular pericardium scaffolds

Samples retrieved from Tencell were stored in RNAlater™ (2 mL) for a maximum of 48 hours prior to RNA extraction. Extraction was performed as described in section 2.2.9.4.2.

2.2.9.6 Extraction and measurement of the DNA content of pericardial tissue

DNA concentration of tissue extracts were measured by spectrophotometry after processing samples using a commercial kit (DNeasy, Quiagen).

Samples of each decellularised (250 mg) and fresh pericardium (50 mg) to be examined were macerated, placed in bijous and freeze-dried for 72 hours, or until the weight of the samples remained constant over 12 hours. The dry weights were measured using an accurate balance (sensitivity of 0.1 mg) and recorded. Dehydrated tissue was processed using sequential separation in miniaturised columns. Buffer ATL (180 µL) and proteinase K (20 µL) were added to each sample and mixed by vortexing. After incubation at 56°C for 3 hours, buffer AL (200 µL) and ethanol (200 µL) were added with vortexing after addition of each solution. The resulting mixture was added to a DNeasy mini spin column, centrifuged (1 min; 6000 × g) and

the eluent discarded. Buffer AW1 (500 µL) was applied to the column, followed by further centrifugation (1 min; 6000 × g). Finally, buffer AW2 was added and the column centrifuged (3 min; 20000 × g) to dry the DNeasy membrane. DNA was eluted by applying buffer AE (200 µL) and centrifuging the column (1 min; 6000 × g) twice for maximum DNA yield. The absorbance of the eluent at 260 and 280 nm was measured using a NanoDrop spectrophotometer to generate a ratio (termed $A_{260/280}$) diagnostic of the nucleic acid species present. DNA concentration readings were used to calculate the DNA content of dried tissue by volume.

2.2.9.7 *Gel electrophoresis of qPCR amplicons*

Combs were removed from fully set agarose gels. Gels were placed in an electrophoresis unit and submerged in TBS (1 cm depth above gel surface; 1 ×). A 25 bp DNA ladder (6 µL; leftmost well only) and amplicon loading mix (12 µL) for each PCR product was added to the loading wells created by the comb and the gel run (40 min; 1170 V). Product bands were visualised by UV.

2.2.10 Quantitative polymerase chain reaction

2.2.10.1 *Primer pair selection and design*

Primer pairs of genes of interest were selected for subsequent gene expression analyses of Tencell cultured hMSC. Sequences were obtained from published research articles where possible, and designed where no pairs meeting the primer design criteria were found.

2.2.10.2 *Selection of primer pairs from relevant literature*

A basic literature search was performed using web of science™ for research papers investigating gene expression towards the lineages of interest by qPCR. Papers describing qPCR assays involving the genes of interest were studied for primer pair sequences. Sequences targeting genes of interest to this study (Table 5.1) were examined for specificity using the BLAST tool provided by NCBI (NCBI, 2014). Briefly, individual primer sequences were inputted into the nucleotide BLAST tool and *homo sapiens* selected as the organism of interest. Search data indicated genes with which a significant degree of complementarity was predicted. Genes with which 100% complementarity was predicted were examined; if only the

gene of interest was targeted, the primer was further analysed *in silico* for use in qPCR assays, but if genes other than the target gene of interest were highly complimentary analysis of the primer was discontinued and literature searching resumed. Primers predicted to be specific were further examined using the OligoEvaluator™ tool provided by Sigma-Aldrich (Sigma-Aldrich, 2014). Sequences were inputted into the calculator tool and data concerning the T_m, percentage content of guanine and cytosine and likelihood of secondary structure and primer-dimer formation considered. Primer pairs having T_m values of 55 – 65 °C and within 5°C of each other, guanine and cytosine content of 50 – 60 %, low or moderate potential to form secondary structures and an enthalpy of primer-dimer formation ≤ 5 kJ.mol^{-1} were purchased from Sigma-Aldrich (UK) and taken forwards for experimental validation.

2.2.10.3 Design of primer pairs

Genes for which no primer pairs passing *in silico* validation were found were searched in the NCBI database (NCBI, 2014). Coding regions ≥ 500 bp were highlighted using the graphical tool and inputted into the primerBLAST primer pair generator. Search parameters were amended to generate primer pairs giving rise to amplicons 70 – 250 bp in length, with an optimum T_m of 60 °C and a minimum of 2 mismatches to unintended targets. Generated primer pairs were examined using the BLAST and OligoEvaluator tools according to the criteria described in section 2.2.10.2, and purchased from Sigma-Aldrich (UK) for experimental validation.

2.2.10.4 Examination of qPCR assay kinetics

The optimum primer concentration for each primer pair was determined to minimise the generation of unwanted amplicons, whilst giving C_T values for the amplicon of interest within the range suitable for relative quantification (12-30). The efficiency of qPCR assays using primer pairs of interest was measured to ensure that only pairs having efficiencies of approx. 100 %, and hence meeting the assumptions of the relative quantification method, were used in gene expression studies. Reaction efficiency investigations were also performed to find the working range for the primer pairs studied.

2.2.10.4.1 Optimisation of primer concentration in reaction mixtures

All manipulations of PCR reaction mixes, RNA or primer solutions were performed in a clean (nudeic acid contaminant-free) PCR UV cabinet. Individual assay mixes corresponding to final concentrations of 100, 250 and 500 nM, and control samples, were prepared using the QuantiTect one-step SYBR®Green RT-PCR kit according to Table 2.8 and Table 2.9. The mastermix of this kit contains many of the key components for PCR reactions, including HotStarTaq® DNA Polymerase, buffer, deoxynudeotide mix (dNTP), including dUTP, SYBR Green I DNA dye, ROX™ passive reference dye, MgCl2 (5 mM). Assays were subjected to the thermal cycle described in Table 2.10. All reaction mixtures underwent 30 cycles of amplification. If the reaction did not reach the plateau phase within 30 cycles, an additional 5 cycles were added. Fluorescence data was exported to Excel for analysis.

Table 2.8: Assay mixtures used to examine the reaction kinetics using the primer pairs of interest. Note that both forward and reverse primers were added to assays at the volumes indicated

Final reaction [Primer] (nM)	Reagent volume added (µL)					
	RT mix (1:1 dilution)	Mastermix	Primer (10 µM)	Primer (1 µM)	RNA solution (2 ng.µL^{-1})	H$_2$O
100	0.50	12.50	0.00	2.50	0.50	9.00
250	0.50	12.50	0.63	0.00	0.50	10.88
500	0.50	12.50	1.25	0.00	0.50	10.25

Table 2.9: Reaction mixtures of control samples used in qPCR assays. Note that both forward and reverse primers were added to assays at the volumes indicated

Control type	Reagent volume added (µL)					
	RT mix (1:1 dilution)	Mastermix	Primer (10 µM)	Primer (1 µM)	RNA solution (2 ng.µL^{-1})	H$_2$O
No template ([Primer] = 100 nM	0.50	12.5	0.00	2.50	0.00	9.50
No template ([Primer] = 250 nM)	0.50	12.5	0.63	0.00	0.00	11.37
No template ([Primer] = 500 nM)	0.50	12.5	1.25	0.00	0.00	10.75
No primer	0.50	12.5	0.00	0.00	0.50	11.50
No reverse transcription	0.00	12.5	1.25	0.00	0.50	10.75
Water only	0.00	0.00	0.00	0.00	0.00	25.00

Table 2.10: The thermal profile used in qPCR assays. *Underlined steps were repeated in the order in which they appear. The number of cycles used depended on the kinetics of individual reactions*

Step	Duration	Temperature (°C)
Reverse transcription	20 min	50
Polymerase activation	15 min	95
Denaturation	_15 s_	_94_
Annealing	_30 s_	_Specified annealing temperature (T_a) (Table 5.3)_
Extension	_5 s_	_72_
Melt curve activation	1 min	95
Melt curve analysis	~ 20 min	Through range 55-95

2.2.10.4.2 Measurement of reaction efficiency

All reagents described were purchased as part of the QuantiTect SYBR® Green RT one-step RT-PCR kit.

Each RNA dilution (10 μL) was added to assay mastermix (90 μL) and apportioned into technical replicates (n=4). Control samples were prepared according to *Table 2.9*, excluding the no template controls of [primer] = 100 and 250 nM for irrelevance. Reaction mixtures were cycled through the thermal profile detailed in Table 2.10, using the appropriate annealing temperature (Table 5.3). Mean C_T values were plotted against the quantity of RNA per rxn and the efficiency calculated using equation Eqn. 5.1. Data corresponding to the highest or lowest dilutions were excluded where results indicated abnormal reaction kinetics.

2.2.10.5 Examination of primer pair specificity

The specificity of primer pairs found/designed was assessed to ensure pairs producing a single amplicon only were used in relative quantification investigations, and that the amplicon is of the size predicted by the PrimerBLAST tool.

2.2.10.6 Examination of dissociation plots

Dissociation plots obtained during the melt curve analyses performed during primer concentration optimisation (section 2.2.10.4.1) were visually examined and the number of peaks, and the temperature at which they appeared, recorded. If multiple peaks were present, the annealing temperature was raised by 2°C to thermodynamically disfavour nonspecific molecular binding events.

2.2.10.7 Gene expression analyses of mechanostmulated hMSC

Gene expression investigations of strained (5, 10 and 20%), pericardium-seeded hMSC were performed and analysed using the comparative C_T method.

2.2.10.7.1 qPCR assay preparation

All reagents used in this method are supplied as part of the QuantiTect one-step SYBR® Green RT-PCR kit. One qPCR assay was performed per gene of interest, per strain condition.

For the 5 and 20% strain conditions, gene expression analyses were performed on unseeded, seeded (prior to sample transfer to the bioreactor), strained and unstrained samples. For the 10% strain condition, unseeded samples were erroneously omitted. Assay mastermix (98.4 µL) was aliquoted for each experimental replicate to be interrogated and the corresponding template RNA (1.6 µL) added. Mixtures were homogenised by vortexing (5s). Each mastermix aliquot, corresponding to an individual experimental replicate, was aliquoted into technical replicates (n=3) into qPCR tube strips. The thermal profile described in Table 2.10 was applied.

2.2.10.7.2 Data analysis

All gene expression data were analysed using the comparative C_T method. Many high quality descriptions of the application of this method have been published (Pongers-Willemse *et al.*, 1998; Huggett *et al.*, 2005; Wong and Medrano, 2005; Jain *et al.*, 2006; Schmittgen and Livak, 2008).

Mean threshold fluorescence cycle values for the housekeeping gene (28s ribosome) and genes of interest for each experimental replicate were calculated, and used to calculate corrected (or normalised) C_T values according to Eqn. 7.1. The value of $2^{-\Delta CT}$ was found for each normalised C_T data point and plotted, by sample type, with confidence limits (p=0.05).

2.2.11 Microscopy and image processing

2.2.11.1 Histological sections

Histological sections were examined by bright field microscopy, using an Olympus BX51 upright microscope. Images were captured at 10 or 20 × magnification using an Olympus U-CMAD3 camera, and processed using Olympus Cell^B image acquisition software.

2.2.11.2 Cultured cells

Cultured cells were examined by bright field or phase contrast microscopy at 10 × magnification using an Olympus IX71 inverted microscope, images captured using an Olympus U-CMAD3 camera and processed using Olympus Cell^B image acquisition software.

2.2.11.3 Examination of pericardium by scanning electron microscopy

Higher resolution images of fresh and acellular pericardium were captured using scanning electron microscopy (SEM). This allowed the visualization of collagen fibre crimping.

Selected samples (~ 1 cm^2) were dissected from acellular or native pericardial specimens, cut to shape to distinguish between the fatty and mesothelial surfaces as previously described (Fig. *2.1*) and fixed in glutaraldehyde for 2 hours (50 mL; 2.5% v/v). Pericardia were then washed in phosphate buffer (0.1 M) twice for 30 minutes each and post fixed in osmium tetroxide overnight (50 mL; 1% v/v). This was followed by dehydration using an ascending acetone series (50 mL; 20, 40, 60, 80, 100, 100% v/v) for 30 minutes per wash. To complete sample preparation, prepared tissue was critical point dried, mounted on standard (13 mm) pin stubs and sputter coated with platinum to a thickness of 5 nm. Specimens were imaged at 2000 and 20000 × magnification using an field emission gun environmental scanning electron microscope (FEGSEM). Selected specimens were also examined at higher magnifications (≥ 50000 ×) where possible.

2.2.12 Bioreactor culture validation

2.2.12.1 Measurement of medium depth in the bespoke Tencell seeding rings

A calibration curve showing the relationship between the volume of culture medium added to the Tencell seeding rings and the depth above the acellular porcine pericardium substrate was prepared to establish the volume of medium required to maintain an optimum depth of 3 mm.

Tissue samples (n = 3; approx. 2 × 3 cm) were placed underneath the Tencell seeding rings and the total seeding ring depth measured using callipers. Quantities of medium (50 − 200 µL) were added to the seeding ring and the medium depth calculated according to Eqn. 2.1. The distance of culture medium from the top of the well was measured by incrementally advancing the calliper probe towards the sample until the liquid meniscus was disturbed and medium was visibly in contact with the apparatus.

$$Medium\ depth = Seeding\ ring\ depth - meniscus\ distance\ from\ well\ top$$

Eqn. 2.1: The calculation to find the depth of culture medium above the seeded surface

2.2.12.2 Extract cytotoxicity of Tencell seeding rings

2.2.12.2.1 Extract cytotoxicity of the Tencell seeding rings with respect to 3T3 and BHK cells

Conditioned medium was tested for sterility as described in section 2.2.5. Baby hamster kidney (BHK) and 3T3 cells were passaged and resuspended to concentrations of 1.25×10^5 and 5.00×10^4 cells.mL^{-1} respectively. Cell suspension (200 µL) was seeded in an opaque 96 well plate (n = 4 per condition; conditioned, unconditioned and positive control medium conditions tested) in the corresponding unconditioned medium and cultured for 24 hours (37 °C; 5 % (v/v) CO_2 in air). Following initial culture, medium was aspirated and replaced (200 µL) by test medium as appropriate and incubated for 24 hr (37 °C; 5 % (v/v) CO_2 in air). Following extract culture, test culture medium was replaced with the appropriate unconditioned culture medium (50 µL) and measurement of the luminescence counts of cultured cells, as quantified by the ATPlite™ assay, performed as described in Section **Error! eference source not found.**. Statistical analyses were conducted using one way ANOVA and Tukey's post-hoc test.

2.2.12.2.2 Cytotoxicity of a concentrated Tencell seeding ring extract

Conditioned medium was tested for microbial contamination as described in section 2.2.5. Baby hamster kidney (BHK), 3T3 and pMSC were passaged and resuspended at cell densities of 1.25×10^5, 5.00×10^4 and 1.65×10^5 cells.mL^{-1} respectively. Cell suspension (200 μL) was seeded in an opaque 96 well plate (n = 4 per condition; conditioned, unconditioned and positive control media conditions tested) in the corresponding unconditioned medium and cultured for 24 hr (37 °C; 5 % (v/v) CO_2 in air). Following initial culture, medium was aspirated and replaced (200 μL) by test medium as appropriate and incubated for 24 hr (37 °C; 5 % (v/v) CO_2 in air). Test culture medium was replaced with the appropriate unconditioned culture medium (50 μL) and measurement of the luminescence counts of cultured cells, as quantified by the ATPlite™ assay, carried out as described by Section **Error! Reference source not found.**. tatistical analyses were carried out using one-way ANOVA and Tukey's post-hoc test.

2.2.12.3 Validation of temperature regulation of the Tencell bioreactor

Temperature regulation was validated to optimise cell culture in the Tencell bioreactor such that temperatures compatible with cell culture were maintained comparably and stably between different wells.

2.2.12.3.1 Engineering modifications of heating apparatus

Any initially apparent maintenance needs were addressed prior to conducting any validation. Engineering modifications were completed in two phases. In the first instance, the metallic clasps and sealant used to secure the perspex lid onto the heating base were replaced. Following initial temperature regulation validation (section 2.2.12.3.3), the original heating controller module (Tempatron dtc410) was replaced by a tunable EZ-zone PM heating controller. All engineering modifications of the Tencell bioreactor were performed by Lee Wetherill and Rhys Moore (Mechanical Engineering, University of Leeds).

2.2.12.3.2 Autotuning of the EZ-zone PM heating controller

The EZ-zone PM heating controller was autotuned to optimise the heating strategy employed by the apparatus for the conditions in use. In a class II biosafety cabinet, pre-warmed water (5.5 mL; appropriate volume found by experiment described in section 2.2.12.4.1) was added

to each Tencell well (Fig. 2.2), and the two heating controller thermocouples affixed in wells 1 and 9 such that the sensors were immersed in water, but not in contact with metallic parts. The Perspex lid was replaced, secured using clasps, and the heat lamp thermocouple secured on its surface by tape. The heat lamp was set to 60°C and lid warming commenced. The temperature controller was set to 36°C and the advance key (resembling the symbol commonly used to indicate that items are recyclable) was used to select the autotune function (displayed as 'AUT' on the device display). All components of the Tencell apparatus were individually switched off following completion of autotuning (~90 min).

2.2.12.3.3 Measurement of temperature regulation in the Tencell bioreactor

Water was incubated (1 hr; 37 °C) and added to the water bath (50 mL), Tencell well baths (wells 1, 8, 9, and 16; 5.5 mL.well^{-1}) and Tencell culture wells (5.5 mL.well^{-1}; appropriate volume found by experiment described in section 2.2.12.4.1) *in situ* in the bioreactor in a class II biosafety cabinet (Fig. 2.2). The heating controller thermocouples (n=2) were affixed in wells 1 and 9 such that the sensors were immersed in water, but not in contact with metallic parts. Thermocouples (n=4) connected to a handheld temperature probe were fixed in wells 3, 8, 11 and 14 using tape in a similar fashion. The wells selected reflected the spatial arrangement of heating elements inside the base, in order to cover them fully. The Perspex lid was secured and heated using a heat lamp as described in section 2.2.12.3.2. The temperature monitor was programmed to record the temperature of each probe every 5 minutes. The EZ-zone PM heating controller was set to 36 °C temperature regulation begun.

Recorded temperatures were printed on receipt roll and manually entered into, and plotted using, Microsoft Excel.
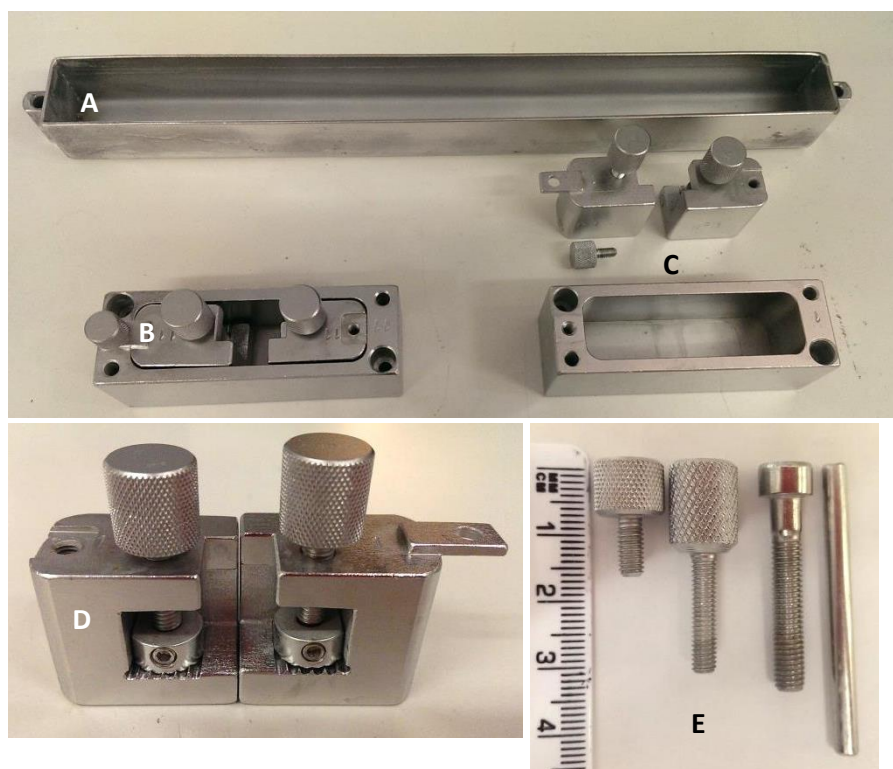
Fig. 2.2: Photographs of the removable parts of the Tencell bioreactor. A: The water bath, used to increase humidity in the cell culture chamber and disfavour evaporation from the culture wells; B: Tencell culture well with tissue clamps in situ. The stationary clamp is secured to the well using the short well screw (E; first screw); C: Dismantled cell culture well; D: Tissue clamps. Tissue is held in place by tightening the screws. The left-hand clamp is affixed to displacement arms in strained wells, using a long well screw (E; second left); E: Screws/posts used in conjunction with the Tencell wells. Far left: Short well screw used to secure tissue clamp (D; right-hand clamp) to Tencell wells; Second left: Long well screw, used to attach tissue clamp (D; left-hand clamp) to displacement arms; Second right: Long base screw, to secure Tencell wells to the heating base; First left: Steel post, used to secure Tencell wells to the heating base.

2.2.12.4 Reduction fluid loss in culture wells of the Tencell bioreactor

The degree of fluid loss was measured and minimised to maintain a medium osmolality conducive to maintaining cell viability during the culture of seeded scaffolds in the Tencell bioreactor.

2.2.12.4.1 Preparation of medium depth calibration graph

The relationship between medium depth and the volume of culture medium added was determined to ascertain the volume of medium that should be used for cell culture in Tencell.

The appropriate volume of culture medium should have a depth of 3 mm above the seeded surface, in common with conventional cell culture.

Acellular pericardium of dimensions approx. 1.1 × 3.3 cm was resected from tissue stocks using a Tencell cutting guide of the appropriate dimension, added to hMSC culture medium (~5 mL) and incubated (37 °C) overnight. Medium conditioned tissue (n=3) was fixed between clamps in Tencell culture wells and culture medium (in the range 3-7 mL) added incrementally (Fig. 2.2). Prior to medium addition, the tissue depth from the well top was measured using callipers. After each addition, the distance between the well top and the fluid level was measured by advancing the calliper probe until the liquid meniscus was disturbed. Measurements were taken in wells both attached and unattached [to the Tencell displacement arms] wells, and were recorded in triplicate.

The medium depth above the tissue surface was calculated using Eqn. 2.2 and plotted against the volume of medium added. The resulting straight line graph was interpreted to find the optimum medium volume for Tencell cell culture.

$$Depth\ above\ tissue\ surface = tissue\ depth\ from\ well\ top - fluid\ level\ from\ well\ top$$

Eqn. 2.2: The calculation performed to yield the medium depth above the seeded surface from the tissue depth from the well top and the level of added medium.

2.2.12.4.2 Measurement of culture well fluid loss

The Tencell apparatus was set up as described in section 2.2.12.3.3, excluding the use of the handheld temperature recorder, and the amount of water remaining in Tencell wells after a 24 hour mock culture period measured using serological pipettes. Fluid loss using this procedure was also tested following humidification at the beginning of the experiment. Tencell mock culture was prepared as previously described, and water (~ 30 mL) was added to a sealed flask and heated using a hotplate set to 300 °C. Once boiling, the flask was connected to taps on the Tencell culture chamber Perspex lid using tubing and the chamber humidified for 5 minutes (Fig. 6.1E). To more accurately replicate cell culture conditions, the chamber was gassed via the lid taps for an additional 5 minutes (5% (v/v) CO_2 in air; 40 mmHg). Fluid loss following Tencell mock culture with chamber humidification was also measured after an extended culture period of 72 hours. Water loss not significantly different from that lost due to the testing method was considered acceptable (section 2.2.12.4.3).

2.2.12.4.3 Measurement of fluid loss due to the testing method

The volume of water not recovered from Tencell wells due to liquid adherence to the metallic parts was measured for comparison with the volume lost during mock Tencell culture. Water (5.5 mL; appropriate volume found by experiment described in section 2.2.12.4.1) was added to Tencell wells (n=3) containing clamps, and the amount recovered following removal of the clamps measured using serological pipettes (Fig. 2.2). Each measurement was taken in triplicate and the mean fluid loss and confidence limit (p=0.05) calculated.

2.2.12.5 Validation of displacement of the arms of the Tencell bioreactor

The actual displacement of the Tencell displacement arms must be validated against that selected using the amplifier knob to ensure that the desired level of strain is being applied to seeded scaffolds, and to confirm that there are minimal differences in the strain applied between experimental replicates.

2.2.12.5.1 Engineering modifications of displacement arms

Initial examination by eye prior to displacement validation indicated fixation issues between the Tencell displacement arms and a displacement bar to which they were attached inside the device casing. Corroded nuts attaching these two items were replaced by Lee Wetherill and Rhys Moore (Mechanical Engineering, University of Leeds).

2.2.12.5.2 Measurement of arm displacement

Actual displacement of each Tencell arm in the range $0 - 33\%$ strain for a strain area of 1.1×1.0 cm ($0.0 - 3.0$ mm) was measured using a mounted dial gauge manufactured by Lee Wetherill (Mechanical Engineering, University of Leeds). The dial gauge was firmly secured to the heating base lightly in contact with the displacement arm under examination using double sided tape and the required displacement selected using the displacement module amplifier knob (Fig. 2.3). Movement of the dial gauge needle was recorded by video using a mobile phone. Video recordings were examined by frame using Windows Media Player 10 and the needle start and stop positions determined at the moments of inertia of the needle. Differences between needle positions, or the actual displacement of the arms, were calculated using Microsoft Excel and plotted against the theoretical arm displacement selected using the displacement module amplifier knob.
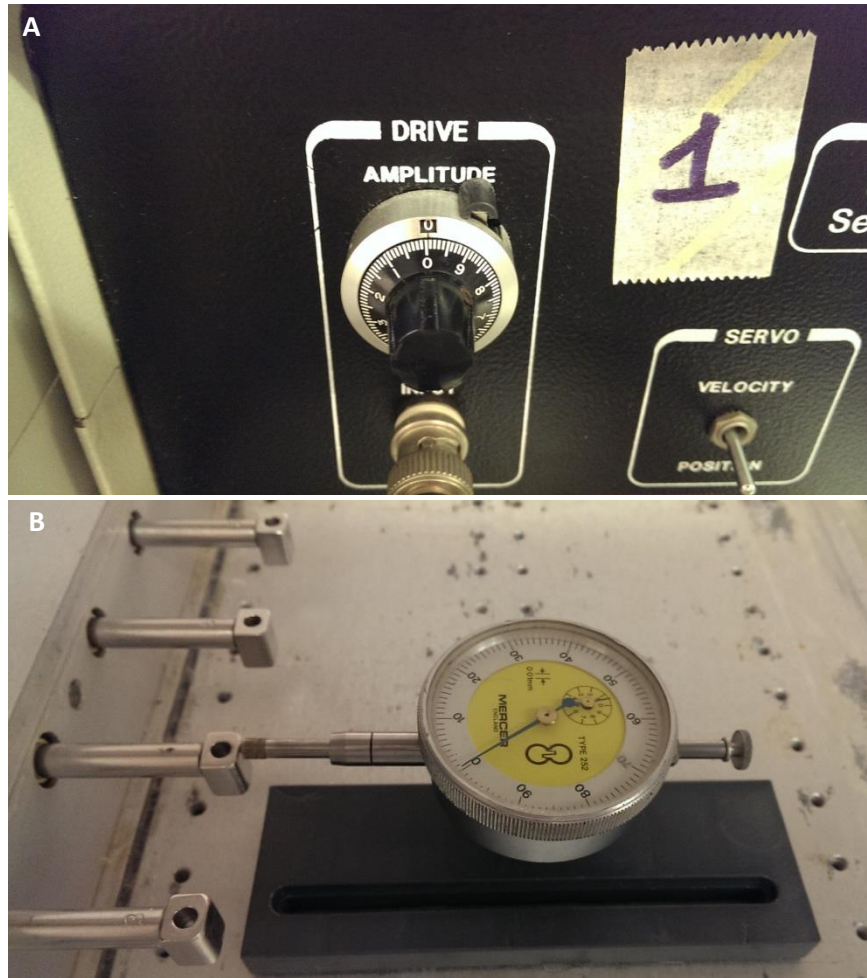
***Fig. 2.3: Images of the displacement module amplifier knob (A) and the experimental
setup, using a mounted dial gauge, used to measure the actual displacement of Tencell
arms (B)*** *. Major increments on the amplifier knob correspond to millimetres, and minor
increments tenths of millimetres. Selected set displacements in the range 0.1 − 3.0 mm
were measured. Video recordings of the dial gauge needle were analysed to calculate the
actual displacement measured for each set displacement. The number label on the
displacement module indicates the order in which various components of the Tencell
bioreactor should be switched on to minimise user errors.*

2.2.12.6 Validation of experimental protocol

The Tencell cell culture protocol devised according to theoretical criteria designed to accurately define optimal cell culture conditions was tested experimentally with hMSC to validate its use in subsequent investigations concerning bioreactor-cultured hMSC.

2.2.12.6.1 Culture of seeded substrates in the Tencell bioreactor

All manipulations of the bioreactor apparatus and cell seeded tissue were conducted aseptically using a class II biosafety cabinet, and using sterile implements. Metallic components/implements and tubing were sterilised by dry (section2.2.2.2) and moist heat (section 2.2.2.1) respectively. The Tencell heating base and lid were cleaned three times with ethanol (70% (v/v)). Seeded scaffolds were prepared as described previously (section 2.2.8.9.2) and transferred aseptically to the tissue clamps, keeping the cell seeded surface uppermost. Tissue clamps were placed in their corresponding wells and culture medium added (5.5 mL). Wells were incubated (37 °C; 5% (v/v) CO_2 in air) in vented culture pots prior to transfer to the Tencell bioreactor. Tencell culture wells were fitted to the heating base and displacement arms using screws and posts (Fig. 2.2) and bioreactor setup completed as described in section 2.2.12.4.2. To end Tencell culture (24 hours), the heating module was shut down approx. 30 minutes prior to the heat lamp, to prevent medium condensation on the Perspex lid. Cultured scaffolds were removed aseptically, placed in medium (~ 2 mL) and incubated (37 °C; 5% (v/v) CO_2 in air) immediately prior to analysis. Seeded substrates were cultured in the Tencell bioreactor using both normal complete hMSC medium, and that supplemented with HEPES.

2.2.12.6.2 Measurement of luminescence counts of Tencell cultured seeded substrates

Cultured pericardial substrates removed from the Tencell bioreactor as described in section 2.2.12.6.1 were assessed for cell viability using the ATPlite™ assay, according to the method described in section 2.2.8.11.

2.2.12.6.3 Extract cytotoxicity of Tencell culture wells

Extract cytotoxicity testing of the Tencell culture wells was performed according to the method described for the Tencell seeding rings (section 2.2.12.2.2), but conditioning one complete culture well per medium type in place of the seeding rings described previously.

Chapter 3: Dissection, decellularisation and characterisation of porcine pericardium

3.1 Introduction

3.1.1 Substrates for mechanostimulation of hMSC

This chapter describes the preparation of a stock of acellular porcine pericardia, used in this study as a substrate for three-dimensional mechanostimulation of hMSC. Although a general consensus as to the exact location of the hMSC niche *in vivo* is lacking, all cells exist in three-dimensional environments consisting of ECM components, cellular neighbours and physical stimuli. Despite this, research into the mechanostimulation of hMSC has frequently been conducted using artificial, two-dimensional substrates that do not themselves facilitate cell adhesion, such as polyurethane (Sittichokechaiwut *et al.*, 2010), polyacrylamide (Engler *et al.*, 2006; Byfield *et al.*, 2009), microchips (Park *et al.*, 2012b; Zhou and Niklason, 2012), polylactic acid (PLA) (Kreja *et al.*, 2012) and silicon (Huang *et al.*, 2012). Cell adhesion is often achieved using ECM proteins such as collagen I and fibronectin, but three-dimensional penetration of such scaffolds by hMSC is unlikely (Park *et al.*, 2004; Ku *et al.*, 2006; Friedl *et al.*, 2007; Chen *et al.*, 2008; Sen *et al.*, 2008; Huang *et al.*, 2009; Park *et al.*, 2011b; Shih *et al.*, 2011; Chopra *et al.*, 2012; Khayat *et al.*, 2012; Zhou and Niklason, 2012). Acellular xenogenic scaffolds avoid the caveats of artificial substrates by providing a three-dimensional environment to which cells can make appropriate adhesions. Furthermore, components of cell-ECM adhesions, especially integrins, are thought to be mechanosensitive. Force transmission through cytoskeletal elements is also strongly suspected; logically, the cytoskeleton of hMSC cultured in a three-dimensional substrate is distinct from that in monolayer culture, potentially eliciting distinct mechanoresponses. Although this work is concerned with attaining a fundamental understanding of the response of hMSC to strain, and not the manufacture of tissue-engineered therapies, the knowledge gained is intended to be relevant to such endeavours through the use of a biologically-relevant substrate.

Acellular porcine pericardium has been previously investigated for use as a three-dimensional, biologically-relevant scaffold for bone grafting and regeneration (Gardin *et al.*, 2015) and

cardiac diseases (Mirsadraee *et al.*, 2007; Mendoza-Novelo *et al.*, 2011; Morticelli, 2013; Vashi *et al.*, 2015). Pericardium forms a fluid-filled sac around the mammalian heart to limit its motion and prevent overexpansion during the cardiac cycle. A largely collagenous material, it is readily available from porcine sources, and has a sheet-like morphology when dissected that can be easily cut to shape. Of critical importance, acellular pericardium has also been shown to facilitate infiltration by hMSC (Morticelli, 2013).

3.1.2 Decellularisation of porcine pericardium

Decellularisation protocols should result in tissue that maintains native histoarchitecture, is devoid of cellular debris, non-cytotoxic, and sterile. In research concerning the development of tissue engineered therapies, removal of cellular material is essential for reducing the immunogenicity of the scaffold and biocompatibility. In the present study, efficacious decellularisation of the pericardial tissue, to be used as a substrate for studies of the response of hMSC to physical stimuli, was critical for ensuring the validity of qPCR data; since target cDNA sequences are amplified approximately 30 billion times during a typical PCR assay, any residual porcine DNA in the pericardial matrix could significantly confound gene expression analyses.

In this work, a patented protocol used in the development of a vascular patch, now marketed in Europe (Tissue Regenix Group plc), was used to decellularise porcine pericardia in 5 batches. This protocol utilised commonly used reagents for the decellularisation of a wide range of tissues (Booth *et al.*, 2002; Mirsadraee *et al.*, 2006a), but uniquely, aprotinin and EDTA were added to wash solutions to inhibit native protease activity, which can degrade ECM proteins. The purpose of each reagent in the decellularisation process is given in Table 1.2. In some decellularisation protocols, physical methods such as snap freezing, mechanical forces and mechanical agitation may also be used to achieve cell lysis and debris removal (Gilbert *et al.*, 2006; Crapo *et al.*, 2011); these were not necessary in this study, although fat deposits were manually removed during sample preparation. Adipose tissue sequesters sodium dodecyl sulfate (SDS) and hence may confound the decellularisation process if present (Booth *et al.*, 2002; Mirsadraee *et al.*, 2006a).

3.2 Aims and objectives

3.2.1 Aim:

The aim of the work presented in this chapter was to produce a stock of validated, acellular pericardium for future use as a substrate for hMSC. The specific objectives were as follows:

3.2.2 Objectives:

- To decellularise a stock of porcine pericardia according to an existing protocol developed for the manufacture of a vascular patch

- To validate the acellular pericardium stocks for future use as a substrate for hMSC via histological analysis and total DNA content analysis, and by biocompatibility and sterility testing

3.3 Experimental approach

During initial investigations, acellular porcine pericardia were prepared (n=67) according to an existing protocol, and validated to determine their suitability as cell scaffolds.

Decellularisation was carried out to remove porcine cells and cellular debris from the tissue, and the acellular stock validated using selected techniques. Histology was carried out in order to qualitatively assess the histoarchitecture of acellular samples. The efficacy of decellularisation was determined by extraction and quantification of DNA from native and acellular pericardial samples. Sterility testing was conducted to test the decellularised tissue for the presence of any microbes, since such contamination would preclude its use as a scaffold for tissue culture experiments with hMSC. Finally, contact cytotoxicity testing was performed to assess the biocompatibility of the acellular porcine pericardium prior to use with cells.

3.4 Results

A total of 67 fresh pericardia were decellularised in five batches (n=7, 12, 12, 12 & 24 respectively). Three control pericardia from each batch were analysed to confirm that the decellularisation process had been successful. The cellularity, ECM composition and structure, DNA content and *in vitro* biocompatibility of the three control acellular pericardia from each batch was determined. This was necessary to assess the suitability of the acellular pericardia as the scaffold material for future studies using MSC.

3.4.1 Histoarchitecture of fresh and acellular tissue

3.4.1.1 Haematoxylin and eosin stained tissue sections

Haematoxylin and eosin staining of tissue sections was performed to compare the cellularity and histoarchitecture of native and decellularised tissue. Native pericardium was found to be composed of layers of parallel crimped collagen fibres fully infiltrated by cells, as shown in Fig. *3.1*a. These layers were arranged orthogonal with respect to each other. Pericardia subjected to the decellularisation protocol do not retain cells and the collagenous structure of native tissue was largely maintained (Fig. *3.1*b-f). There was an increase in collagen fibre separation in the decellularised tissue from batch one (Fig. *3.1*b), but this was not observed in the decellularised samples from other batches (Fig. *3.1*c, d, e & f). In all batches, fibre directionality and crimping was maintained. The orthogonal layer structure of the collagen fibres was also maintained following decellularisation (Fig. *3.1*d; inset).

Collagen fibre layer parallel to cutting plane

Collagen fibre layer orthogonal to cutting plane
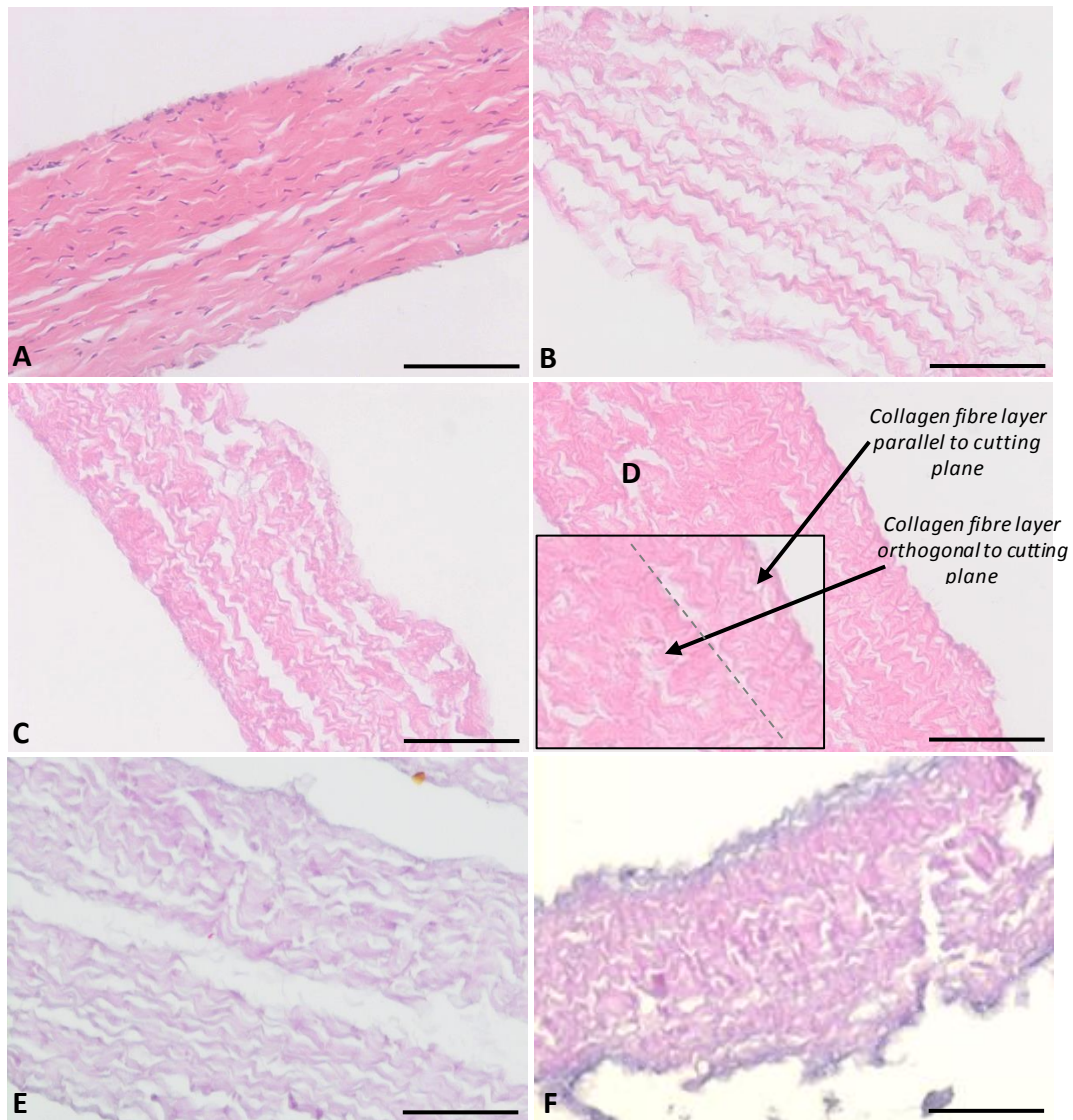
Fig. 3.1: Haematoxylin & eosin stained sections of native and decellularised pericardia. *Native pericardium (A) showed significant cellular content. No haematoxylin staining was observed in decellularised tissue, indicating complete removal of cells. B, C, D, E and F correspond to control samples taken from decellularisation batches 1, 2,3 4 and 5 respectively. Image D (inset) shows that the orthogonal layer structure of native pericardium was maintained following decellularisation. Parallel and orthogonal collagen layers are separated by a dashed line. Layers of collagen parallel to the plane of the microscopy slide can be identified through their visible collagen crimping, whereas layers orthogonal to the plane imaged have been bisected and their crimping therefore cannot be seen. Images were captured at 20 × magnification. Scale bars are 100 µm.*

3.4.1.2 Alcian blue stained tissue sections

Alcian blue staining of pericardial tissue sections was conducted to determine any changes in ECM composition of pericardium following decellularisation, with particular regard to GAGs. GAGs were found to be localized at the surfaces of native tissue (Fig. 3.2a). These surface GAGs were absent following decellularisation (Fig. 3.2b) in samples from all batches.

Observation of alcian blue stained sections revealed that the histoarchitecture of ECM collagen fibres was maintained following decellularisation, as also indicated in Fig. 3.1.
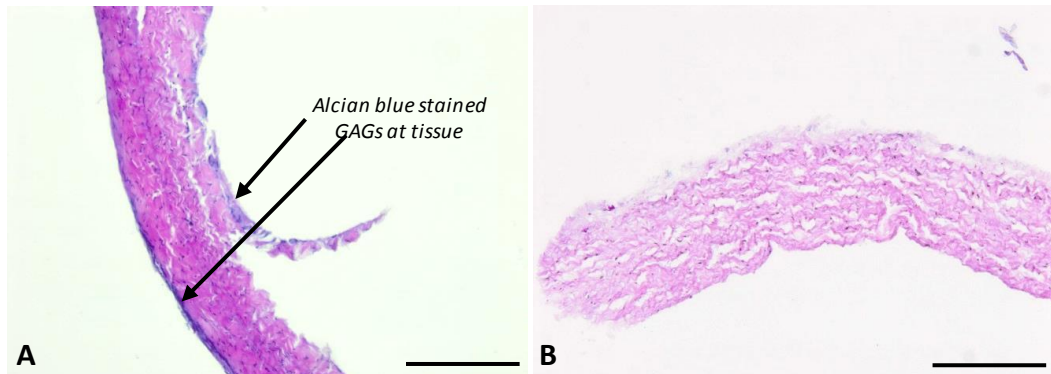
Fig. 3.2: ***The GAG content of porcine pericardium before (a) and after (b) decellularisation.*** *GAGs, normally found at the surfaces of native tissue, was absent following decellularisation for all batches. Images were captured at 10 × magnification. Scale bars are 200 µm*

3.4.2 Scanning electron microscope images of native and acellular pericardium

SEM imaging of native and decellularised pericardia was performed to examine the collagenous extracellular matrix in finer detail. Pericardial tissue retained tight collagen crimps following decellularisation, but individual collagen fibrils were more distinct than those of native tissue, indicting a loss of surface components (Fig. *3.3*). The subunit structure of collagen fibrils in acellular tissue was distinguished at high magnification (90,000 ×) (Fig. *3.4*).

2000 × *20,000 × magnification*
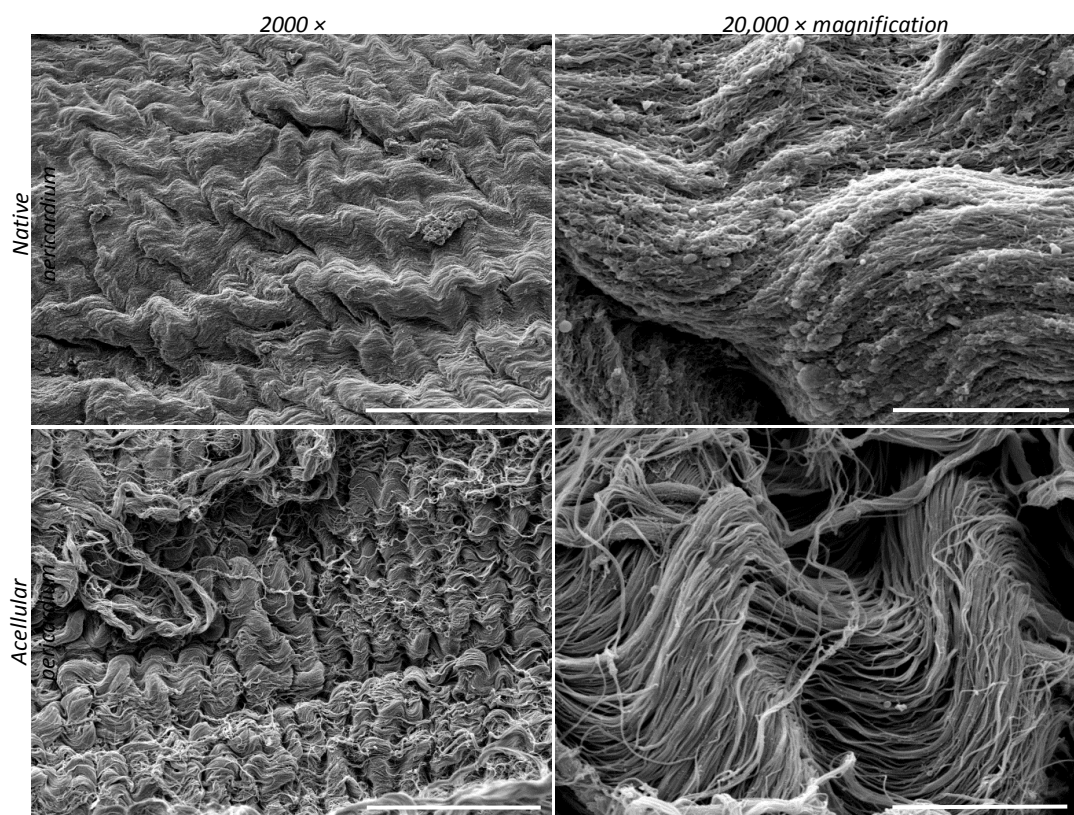
Fig. 3.3: SEM images of native and acellular pericardium at 2000 and 20,000 × magnification. *Scale bars are 50 μm and 5 μm respectively. The tight collagen crimping of native pericardium was maintained following decellularisation, but the surface of the tissue appeared smoother in the native tissue compared to the decellularised tissues, indicating a loss of surface elements.*
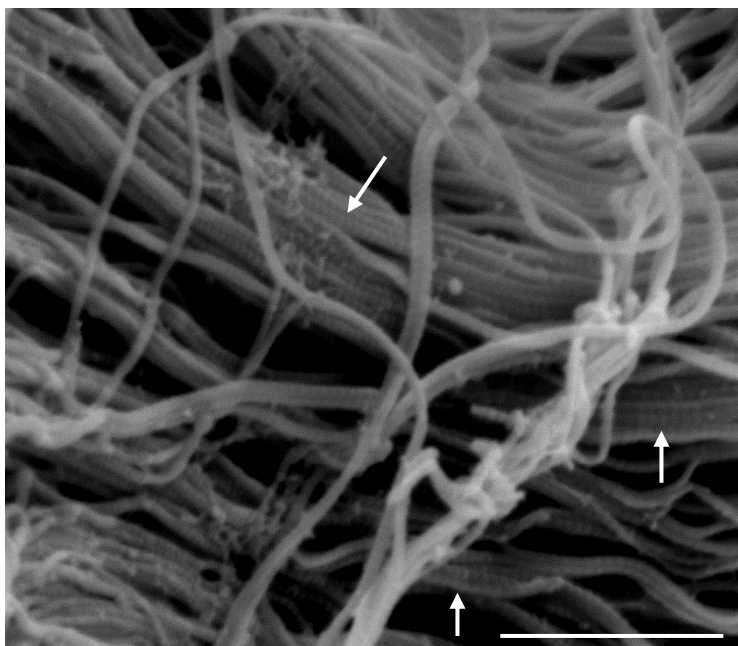
Fig. 3.4: SEM image of an acellular pericardium scaffold at very high magnification (90, 000 ×), showing the subunit structure of collagen fibrils (indicated by arrows). *Scare bar is 1 μm.*

3.4.3 Sterility of decellularised pericardia

Sterility testing was performed to test the acellular pericardia for the presence of bacterial and yeast contamination. No growth was observed in broths containing tissue samples, and positive controls were cloudy in appearance, indicating microbial growth. All fresh blood agar, nutrient agar and Sabouraud dextrose agar plates corresponding to the acellular samples were free of microbial colonies. Positive control plates and broths showed extensive microbial growth in all cases.

3.4.4 DNA content of native and acellular pericardia

The DNA content of native and acellular pericardia was determined following extraction of the DNA using the Quiagen DNeasy kit by spectrophotometry in order to quantify the extent of decellularisation. The mean DNA content of native and treated tissue was an average of 700.31 ng.mg^{-1} and 3.12 ng.mg^{-1} respectively, corresponding to a 99.56% reduction of the total DNA content (Fig. *3.5*). Statistical evaluation using one-way ANOVA and determination of the minimum significant difference using the T-method showed that the DNA levels in acellular pericardia were significantly less than the DNA levels in native pericardia ($p < 0.05$) for

all batches that had been decellularised. An isolated anomalous result was recorded: one acellular specimen was found to contain 72.00 ng.mg^{-1} DNA.
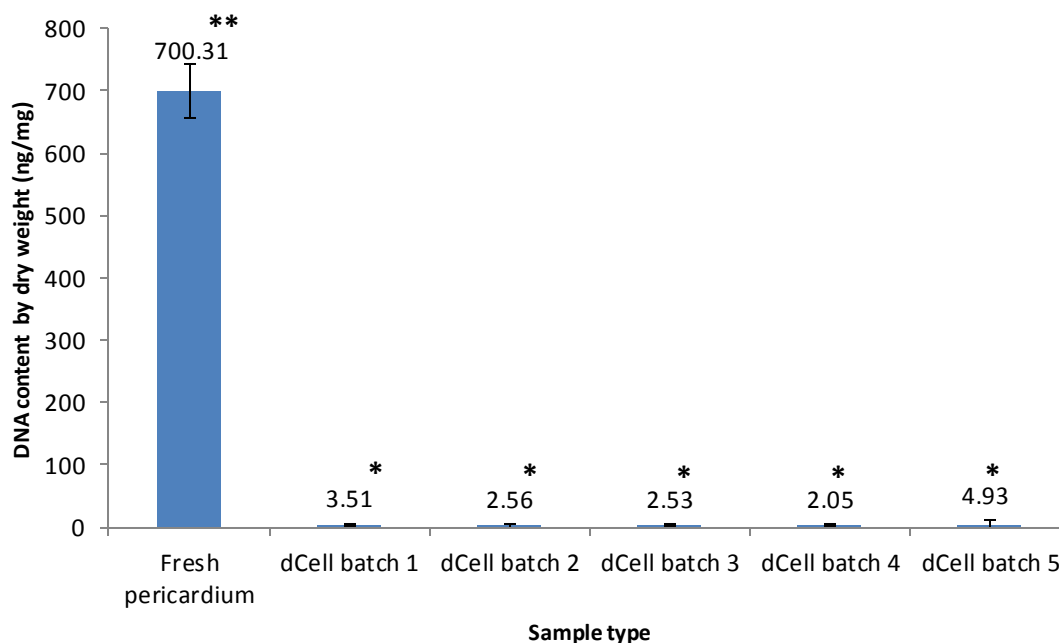
Fig. 3.5: DNA content of decellularised pericardia compared to native tissue pericardia. *Data shown as the mean (n=3) for each group ± 95% confidence limits. Analysis of these data by ANOVA (p=0.05) indicated that decellularised tissue from all batches contained significantly less DNA than native tissue. Groups not significantly different from each other are denoted by the same asterix symbol, and vice versa.*

3.4.5 Contact cytotoxicity testing of decellularised pericardial tissue

BHK and 3T3 cells were incubated with acellular pericardial tissue samples from each decellularisation batch, positive and negative controls, and on tissue culture plastic to assess the *in vitro* biocompatibility of decellularised pericardium. Contact cytotoxicity testing was performed following completion of decellularisation. Microscopy images from each condition are shown in Figures Fig. 3.6 and Fig. 3.7. Collagen, with its known ability to support cell growth, was used as a negative control with respect to cytotoxicity, and cyanoacrylate, known to be cytotoxic, was used as a positive control. Both cell types exhibited a normal morphology following culture with the acellular pericardial tissue and showed similar growth compared to those in the presence of collagen and on tissue culture plastic. Cells grew up to the edge of the test samples, but displayed a different morphology and growth pattern in wells in which

collagen gel seepage from underneath samples occurred (Fig. *3.6*a).   Wells containing cyanoacrylate contained no cells.
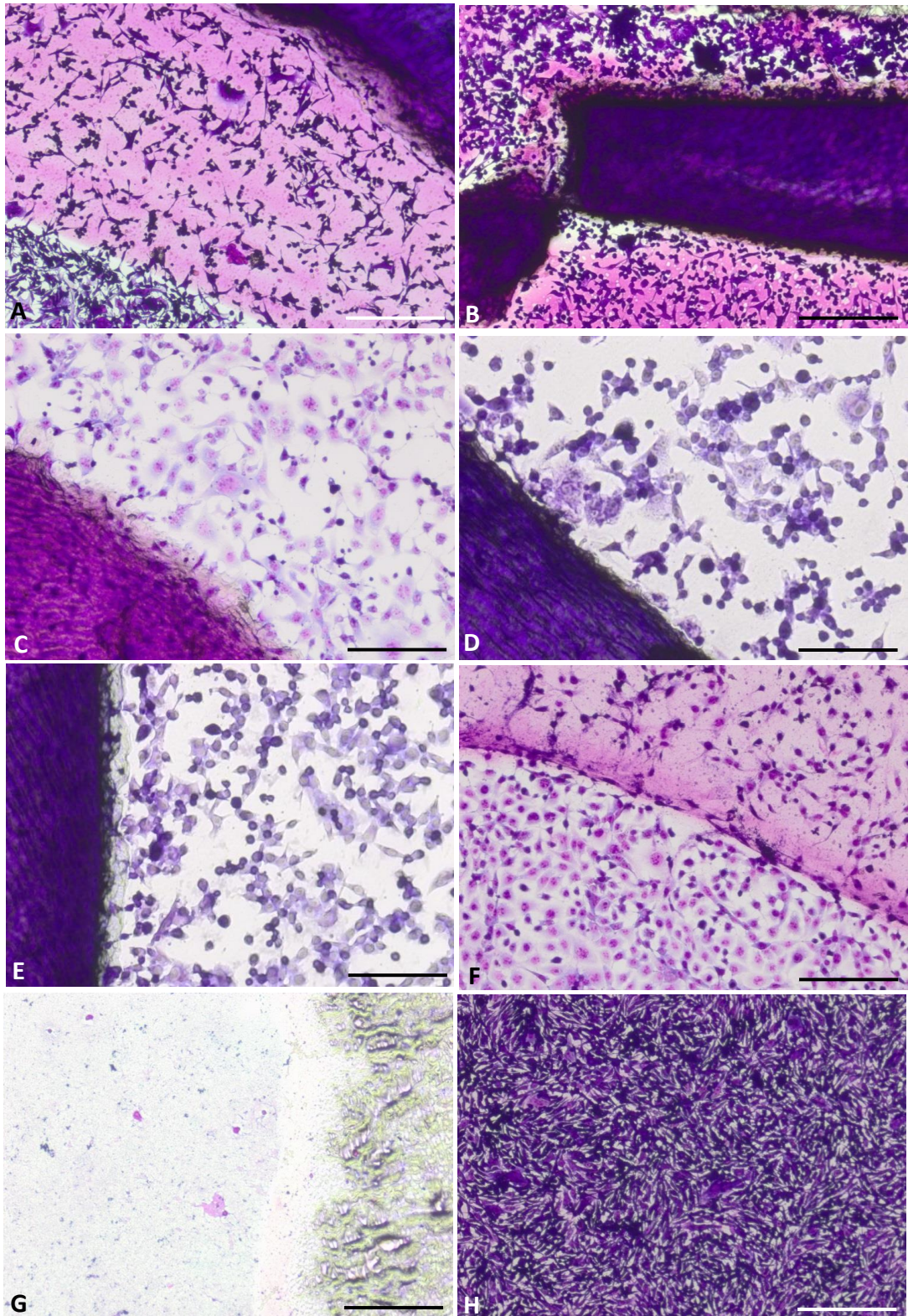
Fig. 3.6: The effect of decellularised pericardium on the growth of 3T3 cells as compared to known cytotoxic (cyanoacrylate adhesive) and non-cytotoxic (collagen I) materials. *The cytotoxicity of decellularised pericardium was assessed following completion of the decellularisation protocol. Images a-e show the growth of 3T3 cells in the presence of acellular pericardium from batches 1, 2, 3, 4 and 5 respectively. The cells grew normally in the presence of the tissue and made contact with its surface. Growth was also extensive in the presence of the collagen negative control (f), but was completely absent in the presence of the cyanoacrylate positive control (g). Dense growth was also observed on tissue culture plastic, included to represent standard cell culture conditions (h). In some cases, collagen seepage from underneath tissue was evident (a) leading to altered growth/behaviour in the immediate vicinity of the sample. Images were captured at 10 × magnification. Scale bars are 200 μm.*
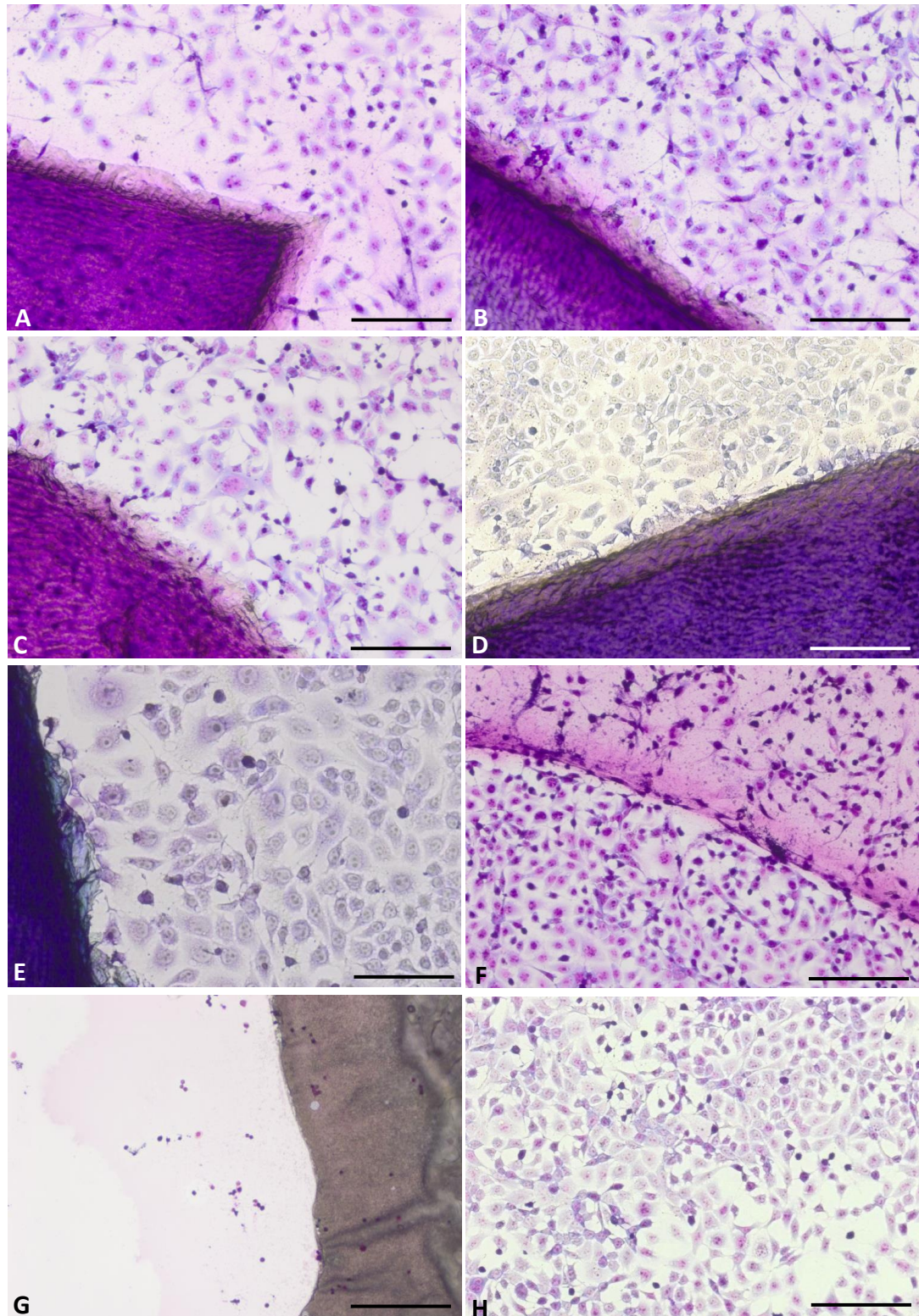
Fig. 3.7: The effect of decellularised pericardium on the growth of BHK cells as compared to known cytotoxic (cyanoacrylate adhesive) and non-cytotoxic (collagen I) materials. *The cytotoxicity of decellularised pericardium was assessed following completion of the decellularisation protocol. Images a-e show the growth of BHK cells in the presence of acellular pericardium from batches 1, 2, 3, 4 and 5 respectively. The cells grew normally in the presence of the tissue and made contact with its surface, although cells in image E were alrger and more granular. Growth was also extensive in the presence of the collagen negative control (f), but was absent in the presence of the cyanoacrylate positive control (g). Dense growth was also observed on tissue culture plastic, included to represent standard cell culture conditions (h). Images were captured at 10 × magnification. Scale bars are 200 µm.*

3.4.6 Summary of results

The results of all validation analyses must show that test acellular pericardia meet key inclusion criteria for corresponding stocks to be utilised as cell culture substrates. Table 3.1 provides a summary illustrating the suitability of each batch of native pericardium decellularised by method of validation. Batches 2-5 satisfy all inclusion criteria, but the histoarchitecture of acellular pericardium decellularised in batch 1 (section 3.4.1), as visualised by haematoxylin and eosin and alcian blue staining, was significantly altered from that of native tissue during processing, and hence is inadequate.

Table 3.1: Summary of validation results for each batch of decellularisation performed. Results that indicate suitability of acellular tissue for use as a cell culture scaffold are indicated by 'Y', and results indicating poor suitability 'N'. Results of all analyses should indicate suitability for a batch of acellular tissue to be used as a cell culture substrate.

	Suitability of acellular pericardium as a cell culture scaffold by analysis			
Batch number	*Histological staining*	*Contact cytotoxicity testing*	*Sterility testing*	*DNA content analysis*
1	*N*	*Y*	*Y*	*Y*
2	*Y*	*Y*	*Y*	*Y*
3	*Y*	*Y*	*Y*	*Y*
4	*Y*	*Y*	*Y*	*Y*
5	*Y*	*Y*	*Y*	*Y*

3.5 Discussion

Despite growing evidence of the importance of mechanotransduction in MSC differentiation, few studies have been conducted that examine the effect of different modes of strain on the smooth muscle differentiation of MSC. Additionally, many previous studies have utilised artificial substrates, which are lacking in cellular binding sites (Park *et al.*, 2004; Engler *et al.*, 2006; Park *et al.*, 2012a; Zhou and Niklason, 2012). Decellularised pericardium offers potential advantages in that it has been shown to encourage normal cellular adhesion and provide a three-dimensional environment for cell adhesion and proliferation (Mirsadraee *et al.*, 2006a; Mirsadraee *et al.*, 2007). Hence, physiologically-relevant stimulus may be applied to MSC cultured on an acellular pericardium scaffold. The goals of this project involved the physical stimulation of hMSC cultured in the acellular scaffold using a bioreactor, and subsequent examination of gene expression. During initial investigations, 67 pericardia were decellularised and validated for their suitability as scaffolds. Validation focussed on analysing the efficacy of decellularisation and the impact of decellularisation on tissue structure and the biocompatibility of the tissue.

Haematoxylin and eosin staining of tissue sections was used to assess the efficacy of decellularisation and to compare the histoarchitecture of native and acellular pericardia. This demonstrated a complete lack of cellular material in all of the samples of decellularised pericardia analysed and showed that the collagenous structure of the ECM remained intact for most samples. Pericardia decellularised in batch one showed tissue damage in the form of increased separation between collagen fibres, and in some cases, obvious and large-scale tearing of the tissue. This was attributed to poor dissection and fat removal technique at early stages of the learning curve; layers of collagen may have been removed or disrupted during handling. This was subsequently remedied during preparation of batches 2-5 through the use of a light box for greater ease of fat visualisation, and maintaining tissue moisture. The ECM of subsequent batches remained undamaged, with densely packed, crimped collagen fibres. Since structurally compromised ECM may not transfer applied forces appropriately, tissue batch one tissue was not used as a scaffold for studies described in the following chapters. It is recommended that tissue dissection is practiced a number of times by the relevant operative prior to the dissection of tissue to be used in cell culture investigations.

Examination of haematoxylin and eosin stained acellular pericardium also revealed that attempts to cut the tissue orthogonal or parallel to the collagen fibre direction had limited

success. Macroscopically, collagen fibres in pericardium have been observed in multiple directionalities and not uniformly as in tissues such as tendon (Lin *et al.*, 2004). This may be because pericardial ECM is arranged into layers in which the fibres are parallel to one another within a layer, but are orthogonal to those within neighbouring layers (Fig. 3.1). Hence, collagen fibre visualization using polarised light filters showed collagen from several layers with different directionalities. The layer structure of pericardium has been reported previously and was evident in images collected in these investigations (Ishihara *et al.*, 1980). Collagen fibres are highly anisotropic and have considerable resistance to tensile strain, but are much less resistant to strain applied across their long axis. Thus, in a tissue in which collagen fibres are uniformly arranged, it is important to apply mechanical strains consistently with regard to fibre direction. This may prove less important in future studies involving the stimulation of hMSC in acellular pericardium, as the orthogonal, multilayer structure of collagen is likely to cancel the anisotropic nature of individual layers.

DNA content in the acellular pericardia was measured and compared to that in native tissue to quantify the extent of decellularisation. A 99.56% reduction in DNA content was observed, with acellular samples containing an average of 3.12 ng.mg^{-1} DNA per dry weight. This compared favourably to the maximum dry weight DNA content of 50 ng.mg^{-1} commonly used to judge the efficacy of decellularisation (Crapo *et al.*, 2011). However, many commercially available decellularized products, such as Graftjacket™ (Wright medical technology, Inc), Zimmer™ collagen repair patch (Zimmer, Ltd.) and Acell™ (Acell, Inc) have been reported to contain lower levels of DNA (< 1.25 ng.mg^{-1}) (Gilbert *et al.*, 2009).

Despite this apparent disparity, the data reported in the literature were obtained using less sensitive techniques. In the experiments reported here a NanoDrop™ spectrophotometer was used to measure the absorbance of total DNA extracted from digested tissue at 260 nm. Such measurement is sensitive to all forms of nucleic acids. The widely accepted maximum DNA content of 50 ng.mg^{-1} refers to double-stranded DNA only, as measured by the PicoGreen™ assay (Invitrogen, USA). The PicoGreen™ assay was used to measure the DNA content of the commercially available products described previously and is not able to detect it in its single-stranded form. Treatment of acellular tissues with SDS alone has been shown to result in extremely low DNA content values as measured by the PicoGreen™ assay, despite 100% of the component nucleic acids remaining in the tissue without further treatment. Hence, it is highly likely that the content of DNA-derived molecular species of the decellularised pericardia produced here was lower than that of commercially available products (Andrew Aldridge, personal communication). In these investigations, the PicoGreen™ assay was not performed

because more accurate quantification of the presence of DNA remnants is achieved using the NanoDrop™ spectrophotometer. However, it is suggested that in future, similar investigations the PicroGreen™ assay be performed in parallel to allow direct comparison with commercially-available products and widely-accepted standards.

An anomalous result was recorded during DNA content analysis: an acellular sample was found to have a higher DNA content than $50 \, \text{ng.mg}^{-1}$ ($72 \, \text{ng.mg}^{-1}$), and DNA removal may have been hindered by fat remnants on the tissue.

Ribonucleic acid (RNA) content of acellular pericardial tissues was not measured, despite RNA being the intended template for downstream gene expression analyses. This was because RNA is not stable at temperatures above - 80°C, and thus the probability of any RNA surviving temperatures $\geq 4°C$, as used in the decellularisation protocol described, was extremely remote. Conversely, DNA will not degrade at room temperature for several months, and so poses a threat to the validity of qPCR data (Fabre *et al.*, 2014).

The lack of cellular material in the decellularised pericardial tissues, as confirmed by haematoxylin and eosin staining of tissue sections, and high reduction in DNA content demonstrated that decellularisation of the porcine pericardial stock was successful. Further histological analysis was carried out to investigate the impact of decellularisation on ECM composition. Observations of alcian blue stained tissue sections showed that GAGs, normally present at the surfaces of native pericardium, were lost following decellularisation. GAG loss following decellularisation has been well documented for a variety of tissues and investigators have suggested that acids, bases and SDS may be the cause (Gilbert *et al.*, 2006; Lovekamp *et al.*, 2006; Prasertsung *et al.*, 2008; Brown *et al.*, 2009; Reing *et al.*, 2010; Mendoza-Novelo *et al.*, 2011). Hence, GAG loss from the pericardia decellularised in these investigations most likely occurred during washing with SDS solution and/or during terminal sterilisation with PAA.

GAGs are charged, hydrophilic species responsible for maintaining water content within tissues. *In vivo*, pericardium forms a barrier between internal organs to prevent harmful friction, so GAGs on the pericardial surface may enhance fluid-film lubrication between this tissue and other organs. GAG loss in acellular tissues has been shown to affect mechanical properties. Although of huge significance in studies that aim to produce functional tissue replacements, in fundamental studies that do not involve comparisons between tissue engineered constructs and natural tissue it is of less importance. Acellular pericardium has already been demonstrated to support MSC adhesion and proliferation regardless of GAG loss

(Lucrezia Morticelli, personal communication). It is of note that reagents suggested as alternatives to SDS, such as octy-glucopyranoside (OGP) and Triton X-100, also deplete porcine pericardium of GAGs when used in decellularisation protocols (Dong *et al.*, 2013).

Biocompatibility testing conducted with BHK and 3T3 cells revealed that the acellular pericardium was not toxic to cells. Growth proximal to decellularised pericardium was similar to that in the presence of collagen gel and tissue culture plastic. In contrast, a complete absence of living cells was observed in culture wells containing toxic cyanoacrylate. Some images appeared to show a halo of lower cell density immediately around acellular pericardial samples, but this may explained by collagen gel seepage from underneath the specimens. As cells encountered the collagen they may have stopped proliferating and begun to remodel the collagen gel matrix. This may have given the false impression that the acellular tissue, also in close proximity, was reducing cell numbers. However, cells were observed to grow up to, and onto the surface of the acellular pericardium with normal cellular morphology. Thus, contact cytotoxicity data strongly suggested that the acellular tissue prepared in these investigations was suitable as a scaffold for MSC.

Sterility testing to detect any microbial contamination showed that processed tissue was sterile following decellularisation. The maintenance of sterility was essential in order to determine whether the scaffold could be used in cell culture experiments.

Scaffold consistency, both between and within decellularisation batches, presents a limitation to the use of acellular pericardium, and indeed other tissue-derived matrices, as a cell culture scaffold. In addition to operator error, which may be partially controllable, the tissue is inherently variable. On the macroscale, obvious differences between samples include tissue size and fat content. Differences in fat content and distribution within and between samples is significant since adipose tissue is known to sequester SDS, and so may impact the efficacy of decellularisation. The success of manual fat removal is highly dependent on investigator judgement and eyesight, and the process may benefit from inclusion of reagents to chemically remove this tissue, which to the author's knowledge, have not been investigated. Additionally, the extent to which the genetics of different individuals induces variability in ECM composition of pericardium is not known, and would present an uncontrollable variable.

Variation in tissue culture substrates, which may translate to non-uniform transmission of both chemical and physical cues to adhered cells, remains a concern in tissue engineering, where the production of consistent products for clinical application and research is paramount. One approach to solving this issue is to use artificial substrates (Byfield *et al.*,

2009; Sittichokechaiwut *et al.*, 2010; Huang *et al.*, 2012; Kreja *et al.*, 2012), or those comprised of a single ECM protein (Arnoczky *et al.*, 2004; Cao *et al.*, 2006; Hankemeier *et al.*, 2009; Charoenpanich, 2012). Neither substrate type satisfies all the requirements of this study, to enable three-dimensional culture of MSC; a substrate capable of facilitating normal cellular adhesions with a multiprotein composition comparable to *in vivo* microenvironments, in terms of chemical and physical properties, is needed. Hence, at the present time, decellularised natural tissues are most satisfactory for studies of MSC behaviour in three-dimensional culture, but developments in multiprotein, biomimetic manufactured matrices may resolve some associated caveats.

In conclusion, although inherently variable, acellular pericardium must meet key quality criteria with respect to tissue histoarchitecture, DNA content, contact cytotoxicity and sterility to be utilised as a cell culture scaffold. During these investigations sufficient acellular stock was produced for use as a cell culture substrate for future studies involving the mechanostimulation of hMSC.

Chapter 4:   Culture and Seeding of hMSC on an Acellular Pericardium Scaffold

4.1 Introduction

This chapter describes efforts to devise a method for seeding hMSC on acellular porcine pericardium. Previous work by others primarily studied mechanotransduction in cells adhered to two-dimensional, artificial substrates (Engler *et al.*, 2006; Sittichokechaiwut *et al.*, 2010; Huang *et al.*, 2012; Kreja *et al.*, 2012; Park *et al.*, 2012a; Zhou and Niklason, 2012), or encapsulated within hydrogels comprised of one extracellular matrix protein only (Park *et al.*, 2011b; Charoenpanich, 2012; Steward *et al.*, 2014; Ho *et al.*, 2015). Acellular pericardium provides a three-dimensional environment arguably more similar to an *in vivo* MSC niche, facilitating normal cell-substrate adhesions and providing exposure to a heterogeneous ECM (Chen, 2010). In addition, data presented in Chapter 3 indicated that the collagenous matrix, the major stress-bearing component of pericardial ECM, was retained following decellularisation, in agreement with previous reports (Mirsadraee *et al.*, 2006b). Porcine pericardium was also previously used to dynamically culture pMSC (Morticelli, 2013). Ease of use of the scaffold in the intended system was also a primary concern in its selection; on the macro scale, acellular pericardium is a sheet-like tissue, and is readily resected to a desired shape and size for bioreactor culture (Fig. 2.1).

Ultimately, the seeding approach developed in these investigations was required to facilitate mechanostimulation of the cell-seeded scaffolds in the Tencell bioreactor, and assessment of the differentiation potential of cultured hMSC by qPCR. It was decided to use seeding rings to seed the cells onto the scaffold. The seeding rings investigated had to cover an area approximately equal to the sample strain region in the Tencell bioreactor (1 cm × 1.3 cm). Further, sufficient cells had to be seeded on the scaffold to allow reliable measurement of the purity and concentration of isolated RNA, to ensure the integrity of relative gene expression data. The concentration and purity of nucleic acids can be quantified using UV-vis spectrophotometry; the concentration of a given species may be calculated according to the

Beer-Lambert Law given its absorbance at a particular wavelength and molar absorption coefficient, and purity judged by the ratio of the absorbance at 260 and 280 nm ($A_{260/280}$) (Braude *et al.*, 1950; Atkins and De Paula, 2010) (Eqn. 4.1). Solutions having RNA concentrations below the limit of detection of conventional nucleic acid spectrophotometers (~ 0.4 ng/μL) cannot be reproducibly analysed using this technique.

$$A = \varepsilon [J] L$$

Eqn. 4.1: The Beer-Lambert Law. *A is the absorbance at a given wavelength, ε a constant known as the molar absorption coefficient, [J] the concentration of the measured species and L the sample thickness.*

As calculated from the absorption spectrum of RNA, the value of $A_{260/280}$ of pure RNA is expected to be 2.0-2.2. In contrast, typical $A_{260/280}$ values of DNA are in the range 1.8-2.0. It is of critical importance that the DNA produced and detected in qPCR reactions is derived from copy DNA (cDNA) manufactured from isolated mRNA during reverse transcription, and not from other DNA present; DNA encoding the full genome of an organism is present in almost every cell of eukaryotes, regardless of its application in a given cell, but the presence of mRNA corresponding to a particular gene confirms its expression by that cell. Therefore, $A_{260/280}$ values, as measured using a spectrophotometer, should be used to validate the purity of RNA prior to its use in PCR, and RNA samples not meeting this minimum acceptance criterion are unlikely to generate accurate gene expression data (Glasel, 1995).

Experiments described in this chapter investigated the seeding of hMSC on an acellular pericardium substrate, with respect to the viability of seeded cells and the subsequent isolation of verifiable RNA extracts to be used as template material in qPCR assays.

4.2 Aims and objectives

4.2.1 Aim:

The aim of investigations presented herein was to find the optimum approach, examining the cell number, apparatus and incubation time used, for seeding hMSC on acellular pericardium for culture in the Tencell bioreactor.

4.2.2 Objectives:

- To find the minimum number of hMSC from which RNA purity and quantity can be reliably ascertained using nucleic acid spectrophotometry

- To isolate and characterise model pMSC by Percoll® fractionation and trilineage differentiation and cell morphology respectively

- To investigate, using live/dead staining and the ATPlite™ assay, viability of cells seeded using the Tencell seeding rings at different seeding times and medium volumes

- To investigate, using ATPlite™, viability of cells seeded using the circular seeding rings at different seeding times, and using different methodologies

4.3   Experimental approach

During these investigations, porcine and human MSC were seeded on acellular pericardium using different approaches (using both bespoke Tencell seeding rings and circular seeding rings) and the viability of the cells seeded onto the matrix was determined.

The quantity and purity of RNA extracted from cell pellets containing $0.5 - 2.0 \times 10^5$ hMSC was measured to determine the minimum total number of seeded cells from which sufficient quantities of validated RNA could be extracted. This range was examined because is corresponds to the range of cell seeding densities previously validated for use on acellular pericardium (Morticelli, 2013). Isolation and basic characterisation of pMSC from fresh porcine femurs was undertaken to provide a stock of model cells for initial seeding investigations. Since the Tencell seeding rings were previously untested for cell culture use, less precious pMSC were used to test the efficacy of this equipment, as opposed to more precious hMSC. Cell viability of pMSC seeded on acellular porcine pericardium using bespoke Tencell seeding rings was examined to ascertain their suitability for use as the seeding apparatus prior to Tencell culture. Medium depth in the Tencell seeding rings was measured and extract cytotoxicity testing conducted to determine the cause of loss of cell viability during the course of these experiments. Cell viability of hMSC seeded on acellular porcine pericardium using alternative circular seeding rings was quantified to determine a suitable seeding method for subsequent studies.

4.4 Results

4.4.1 RNA measurements by cell number

Cell pellets containing different numbers of hMSC were tested for purity and total RNA quantity to determine the minimum number of cells that could be lysed to produce verifiable RNA. The mean concentration of RNA in assay eluent was 2.6 ± 3.2, 16.7 ± 22.1 and 63.5 ± 21.6 ng.μL^{-1} for samples containing 0.5, 1.0 and 2.0 × 10^5 cells respectively, and the total mean amount of RNA extracted for all quantities was sufficient for extensive qPCR analyses ($\geq$ 100 ng; Fig. 4.1). Absorption ratios (A$_{260}$/A$_{280}$) of extracted RNA solutions were within the expected range of 2.0 – 2.2 for samples containing 1.0 and 2.0 × 10^5 cells (2.07 – 2.19 and 2.03 – 2.18 respectively) but did not correspond to typical values for solutions of RNA for samples containing 0.5 × 10^5 cells (-4.12 – 3.98). The large error bars may be accounted for by the fact that the amount of ATP produced by individual cells is variable. A standard curve of these data would not be expected to be linear as the concentration of the lowest total cell number may not have been determined accurately. Additionally, a minimum of five data points must be plotted to represent such data as a standard curve in a mathematically acceptable manner.

From these data, it was determined that a minimum total of 1.0 × 10^5 cells should be seeded onto the acellular pericardium matrix for subsequent qPCR analyses to enable reproducible quantity and purity measurement.
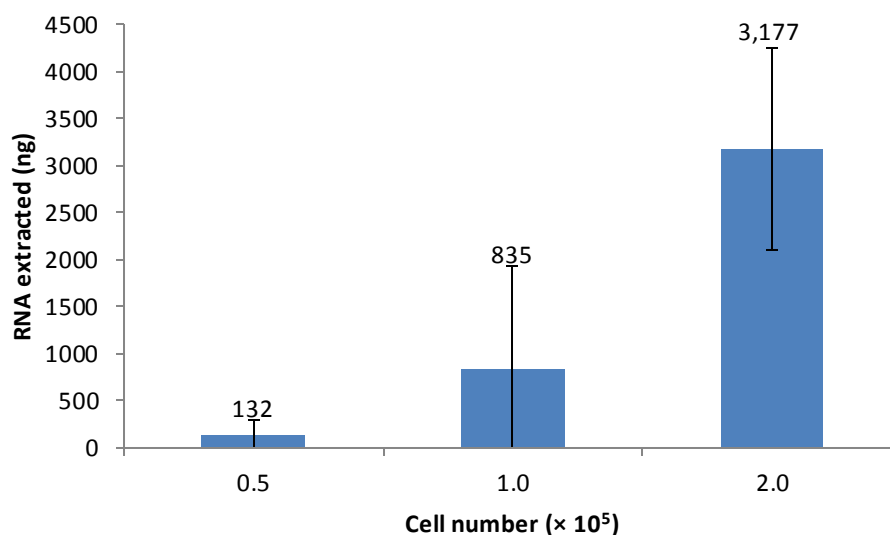
Fig. 4.1: Total RNA extracted from from hMSC by cell number. *Total RNA values correspond to mean concentrations of 2.6 ± 3.2, 16.7 ± 22.1 and 63.5 ± 21.6 ng.μL^{-1} in assay eluent for samples containing 0.5, 1.0 and 2.0 × 10^5 cells respectively. Absorption ratios (A$_{260}$/ A$_{280}$) were not within the expected range of 2.0 − 2.2 for samples containing the lowest number of cells, but were satisfactory for both larger samples. Data presented as means (n=3) ± 95% confidence intervals.*

4.4.2 Characterisation of isolated pMSC

Multipotential mesenchymal stromal cells were isolated from porcine femurs to provide a stock of 'model' cells for investigation of the seeding behaviour and sensitivity of hMSC to cytotoxic agents. Isolated cells were characterised with respect to cell morphology and differentiation towards the key mesenchymal lineages of fat, bone and cartilage. Isolated pMSC had a fibroblastic morphology (Fig. 4.2, day 0 images). Positive histological staining of cultured cells was apparent after culture periods of 20 (Fig. 4.2 & Fig. *4.4*) and 6 (Fig. 4.3) days in osteogenic, chondrogenic and adipogenic culture medium respectively.

Control medium	Differentiation medium	
		Day 0
		Day 6
		Day 20
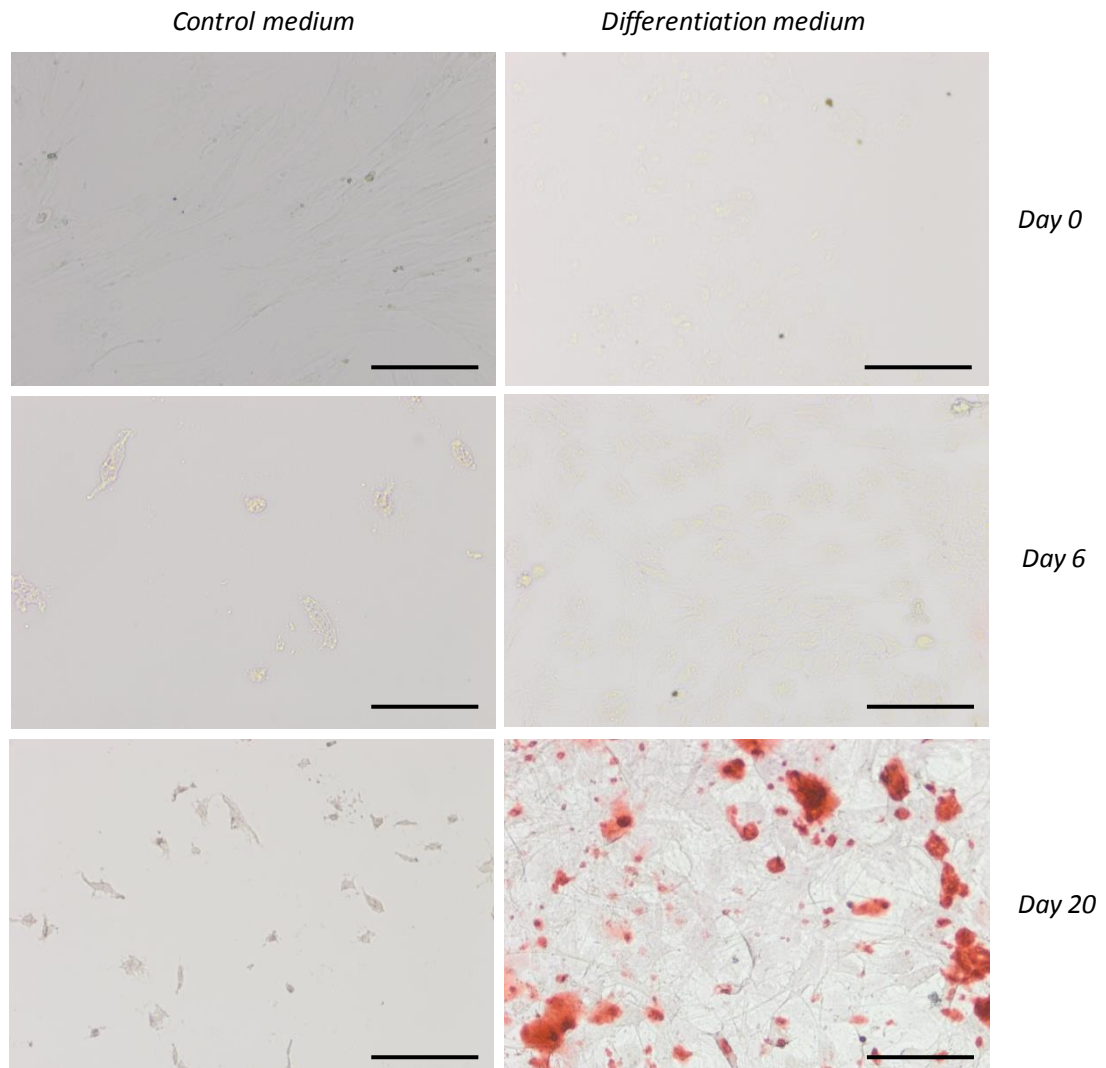
Fig. 4.2: Porcine MSC cultured in osteoinductive (right) and unsupplemented complete DMEM (left) media following alizarin red staining. *Staining was only present in cells grown in differentiation medium after 20 days, with control cultures remaining unstained throughout. Loss of cell viability/density in control plates analysed after 6 and 20 days was observed. This was probably caused by a drying event in the cell culture incubator in which they were cultured. Images were taken at 10 × magnification using an Olympus IX70 inverted microscope and processed using cell^B imaging software. Scale bars are 100 µm.*

Control medium	Differentiation medium	
		Day 0
		Day 6
		Day 20
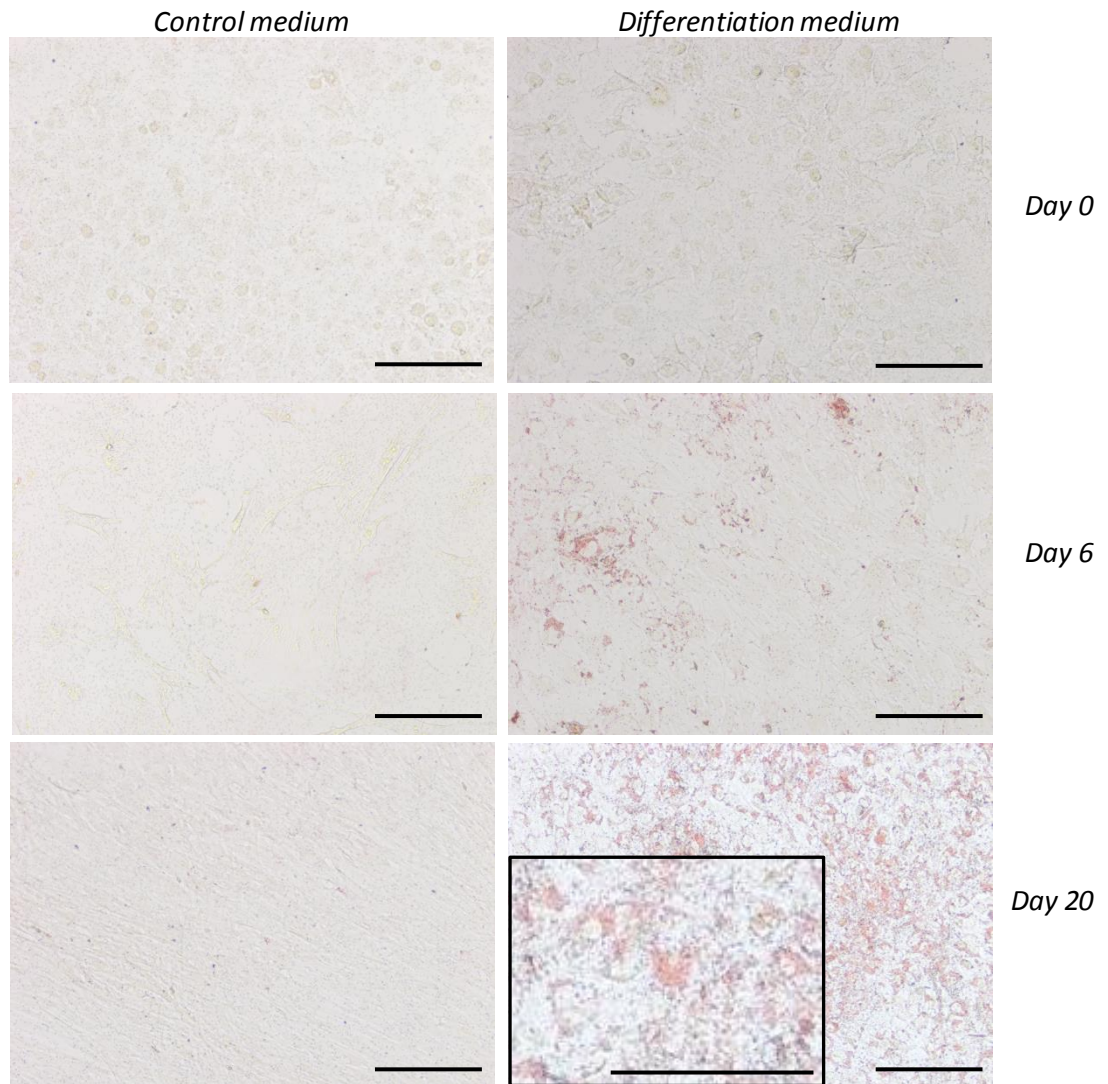
Fig. 4.3: Porcine MSC cultured in adipogenic (right) and unsupplemented complete DMEM media following oil red O red staining. *Staining was present in cells grown in differentiation medium after 6 days, with control cultures remaining unstained throughout. Images were taken at 10 × magnification using an Olympus IX70 inverted microscope and processed using cell^B imaging software. Scale bars are 100 μm.*

Control medium *Differentiation medium*

Day 0

Day 6

Day 20
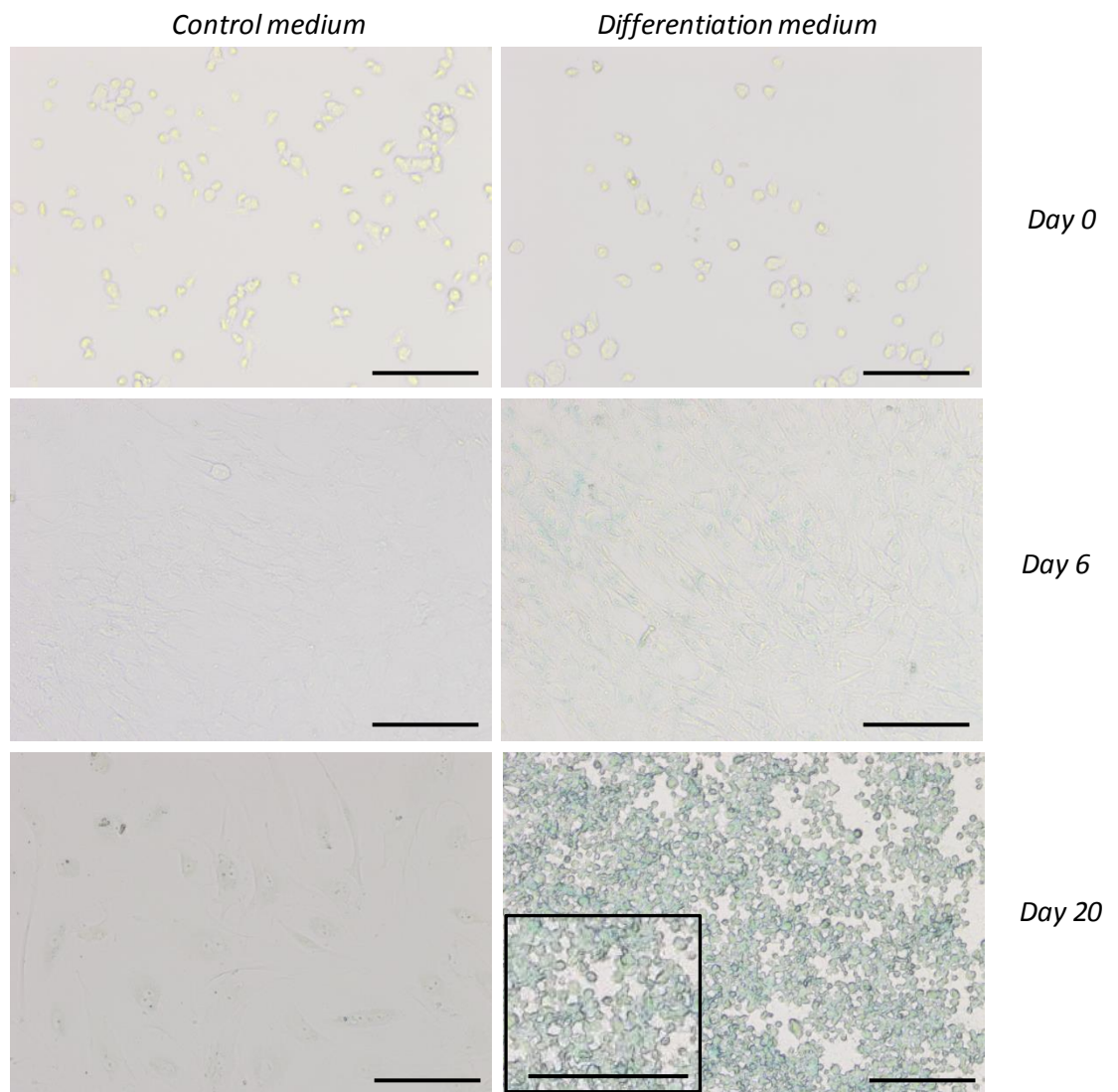
Fig. 4.4: Porcine MSC cultured in chondrogenic (right) and unsupplemented complete DMEM (left) culture media following Alcian blue staining. *Staining was present in cells grown in differentiation medium after 20 days, with control cultures remaining unstained throughout. Images were taken at 10 × magnification using an Olympus IX70 inverted microscope and processed using cell^B imaging software. Scale bars are 100 µM.*

4.4.3 Cell survival in bespoke Tencell seeding ring seeded scaffolds

The survival of porcine multipotential mesenchymal stromal cells following seeding in the Tencell seeding rings, as compared to direct seeding, was assessed to ascertain the suitability of these rings for use in Tencell culture experiments. Porcine cells were used to model the seeding behaviour of human MSC in the first instance to avoid loss of limited human cell stocks that may occur with unsuitable apparatus.

Seeded acellular pericardia were live/dead stained to assess pMSC survival following seeding with Tencell seeding rings and direct seeding. No live cells were observed on Tencell-seeding ring seeded scaffolds seeded in initial experiments for any seeding period, but abundant live cells were apparent in samples seeded by direct seeding (seeding volume 150 μL; Fig. 4.5).
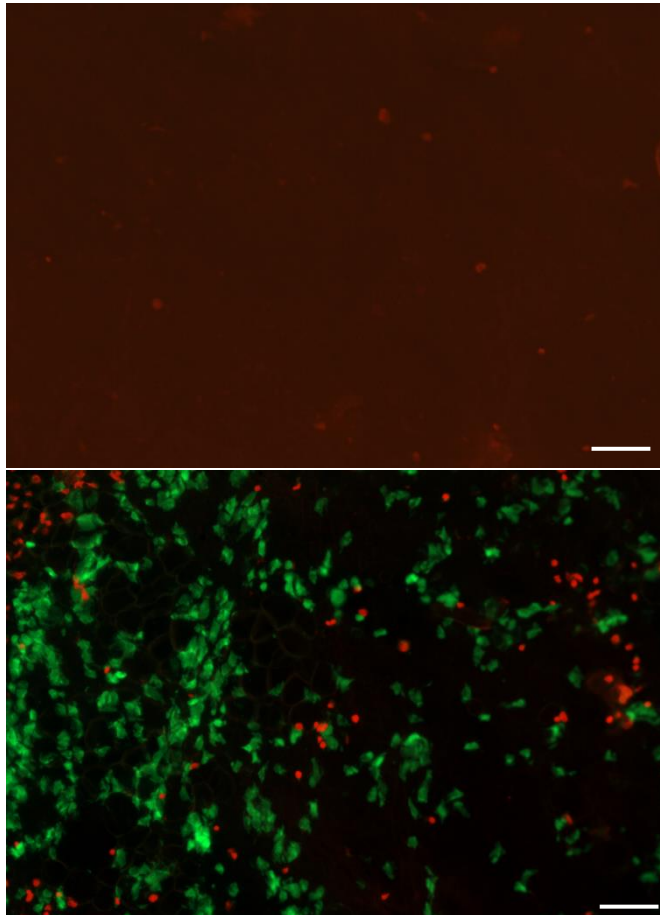
Fig. 4.5: Image of live/dead stained porcine pericardium following seeding of pMSC using the Tencell seeding rings (top) and by direct seeding (bottom) for 4 hr. Dead cells are stained red and live cells green. No live cells were observed in the Tencell seeding ring condition. Good cell viability was apparent in scaffold seeded by direct seeding. However, this seeding method is not appropriate for subsequent cell seeding as the final cell density is not controllable, and was included for comparison only. Image taken at 10 × magnification. Scale bars are 100 μm.

It was hypothesised that a medium depth greater than 3 mm above the cell culture surface, beyond which the partial pressure of oxygen (pO_2) may result in hypoxic conditions, may have caused loss of cell viability during seeding. Hence, the maximum seeding volume capable of maintaining appropriate oxygen diffusion throughout the seeding wells was investigated.

Medium depth above acellular pericardium substrates increased linearly with increasing seeding ring volume (Fig. 4.6), and data indicated that a medium depth of 3 mm may be achieved by seeding pMSC in a seeding cell suspension of volume 80 µL. However, despite seeding medium volume optimisation, no live pMSC were observed in Tencell-seeding ring seeded scaffolds following reduced volume seeding, as evidenced by a lack of cytoplasmic staining by calcein AM (green; Fig. 4.7). However, extensive live cells were apparent in directly seeded scaffolds. All Tencell seeding ring experiments were repeated to eliminate investigator error; images presented are representative of all repeats.
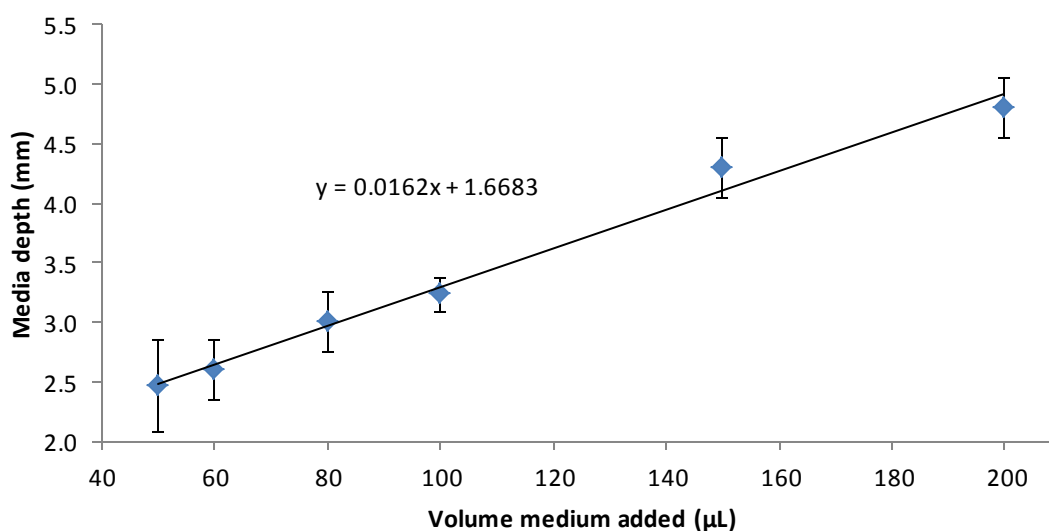
Fig. 4.6: Graph showing the relationship between the volume of cell culture medium added to the Tencell seeding rings and the depth of medium above the seeding surface. *A medium volume of 80 µL was found to give the optimum depth of 3 mm above the tissue surface. Data presented as the mean (n=3) ± 95% confidence limits.*
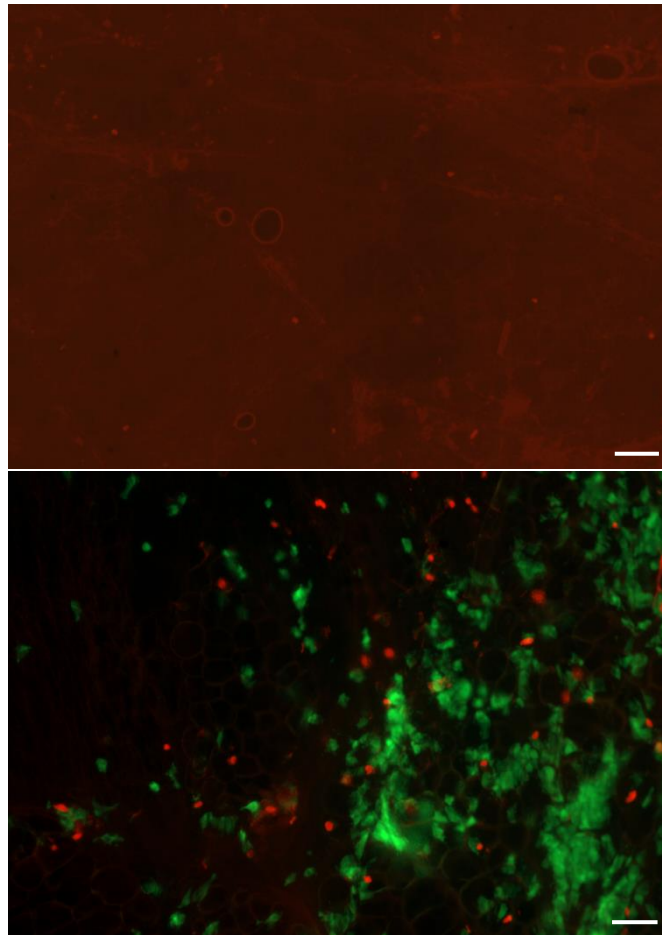
Fig. 4.7: Image of live/dead stained porcine pericardium following seeding of pMSC using the Tencell seeding rings (top), and by direct seeding (bottom) using the optimal volume of cell culture medium and conditioned tissue, for 4 hr. Dead cells are stained red and live cells green. No live cells were observed in the Tencell seeding ring condition. Good cell viability was apparent in scaffold seeded by direct seeding. However, this seeding method is not appropriate for subsequent cell seeding as the final cell density is not controllable, and was included for comparison only.. Image taken at 10 × magnification. Scale bars are 100 μm.

4.4.4 Cytotoxicity of the Tencell seeding rings

Cell survival during seeding with the Tencell seeding rings was not improved through the use of an optimal seeding volume of culture medium, so an alternative hypothesis, that cytotoxicity of the seeding apparatus was causing loss of cell viability, was investigated.

Extract cytotoxicity of materials is frequently tested using immortalized cell lines exposed to medium conditioned with the material of interest. Tencell seeding rings were conditioned in BHK and complete DMEM culture medium and the viability of BHK and 3T3 cells cultured in treated and untreated medium quantified.

During seeding ring conditioning of culture medium, particulates were visible to the naked eye. However, an initial extract cytotoxicity assay performed using 3T3 and BHK cells showed statistical significances in cell viability ($p < 0.001$), quantified using the ATPlite™ assay method, between cells grown in positive control medium and all other conditions only; there was no significant difference between cells grown in seeding ring conditioned and unconditioned medium (Fig 3.7) Using large volumes of culture medium during incubation of the seeding rings may result in a more weakly concentrated solution of extract species than would be encountered by cells cultured in the Tencell seeding rings, which have a high surface area to volume ratio. Hence, a more concentrated extract medium was tested for cytotoxicity. Additionally, the concentrated extract cytotoxicity assay was also performed using pMSC, included as a model cell type for hMSC, since it is not known whether the sensitivity of 3T3 and BHK cells to cytotoxic agents is comparable to that of hMSC. Freeze drying of the water-extract mixture obtained following incubation with Tencell seeding rings yielded an orange-brown residue (Fig. 4.9). Culture with concentrated Tencell seeding ring extract resulted in a loss of cell viability in 3T3 cells and pMSC ($p < 0.001$ for both cell types) as compared to cells in unconditioned medium (Fig. 4.10 and Fig. 4.11), but BHK cells were not affected by the presence of the seeding ring extract ($p < 0.001$; significant difference between luminescence counts of BHK cultured in positive control medium and other sample types only).

No microbial growth was observed on any culture plate or in any culture broth inoculated with test media, whereas extensive microbial growth was apparent in positive controls. Hence, the null hypothesis that loss of cell viability during Tencell seeding ring culture was not caused by cytotoxic effects was rejected and the use of the Tencell seeding rings discontinued.
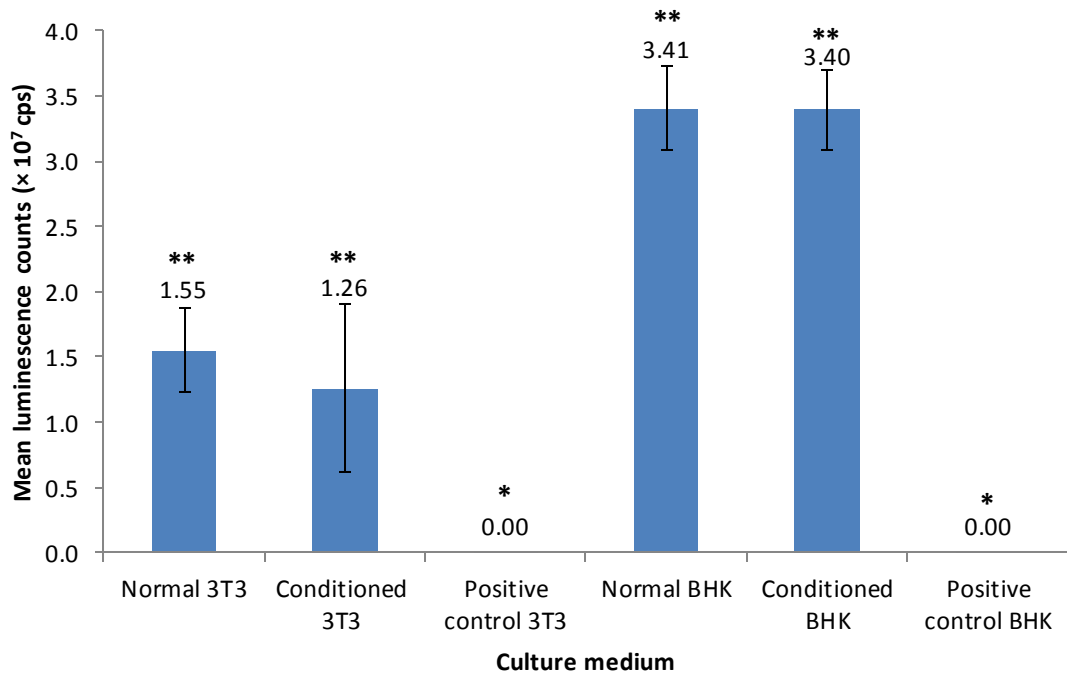
Fig. 4.8: Chart showing the luminescence counts of 3T3 and BHK cells grown in the appropriate unconditioned complete culture medium and those grown in Tencell seeding ring conditioned medium, as measured by the ATPlite™ assay. *Positive control medium contained DMSO (40% (v/v)). Luminescence counts of both 3T3 and BHK cells cultured in positive control medium were significantly lower than counts for all other culture conditions (p < 0.001 in both cases), as measured by ANOVA and Tukey's post hoc test. There were no significant differences in luminescence counts between cells grown in conditioned and unconditioned media within the same cell type. Significant differences between samples are indicated by different asterix symbols. Data presented as the mean (n=4) ± 95% confidence limits.*
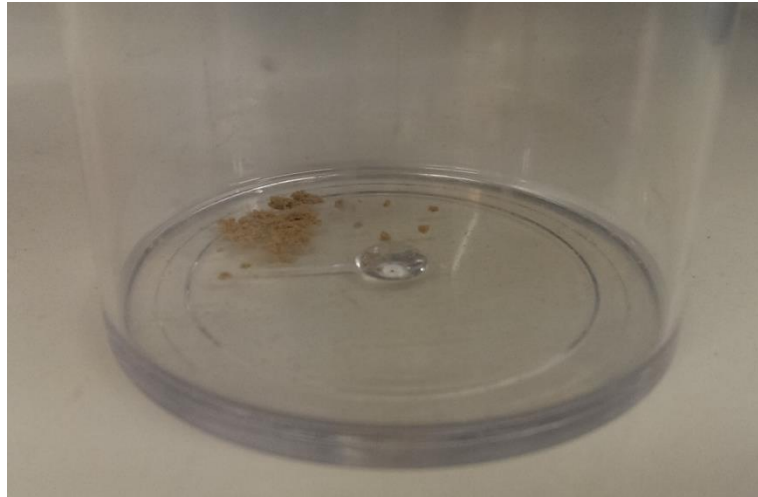
Fig. 4.9: Tencell seeding ring residue extracted from 6 seeding rings following incubation in deionised water for 6 days at 37 °C.
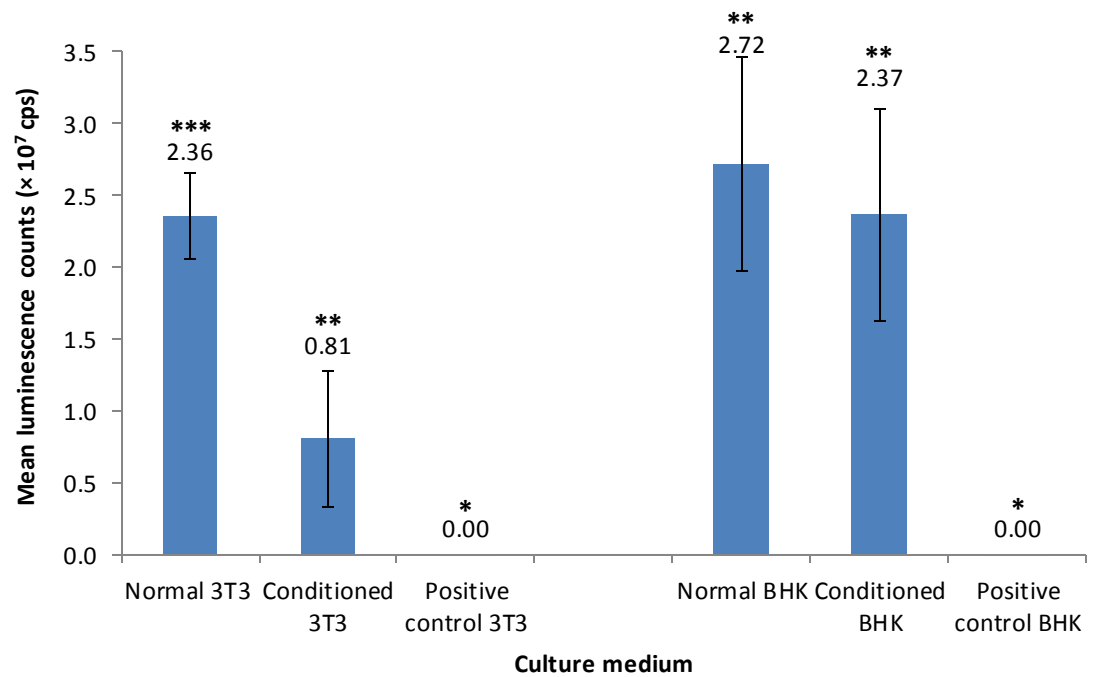
Fig. 4.10: Chart showing the luminescence counts of 3T3 and BHK cells grown in the appropriate unconditioned complete culture medium and those grown in concentrated Tencell seeding ring conditioned medium, as measured by the ATPlite™ assay. *Positive control media contained DMSO (40% (v/v)). Luminescence counts of BHK cells cultured in positive control media were significantly lower than counts for all other culture conditions (p < 0.001). Luminescence counts of 3T3 cells showed significant differences between all culture medium groups (p < 0.001). Significant differences between samples are indicated by different asterix symbols Statistical analysis done by ANOVA and Tukey's post-hoc test. Data presented as the mean (n=4) ± 95% confidence limits.*
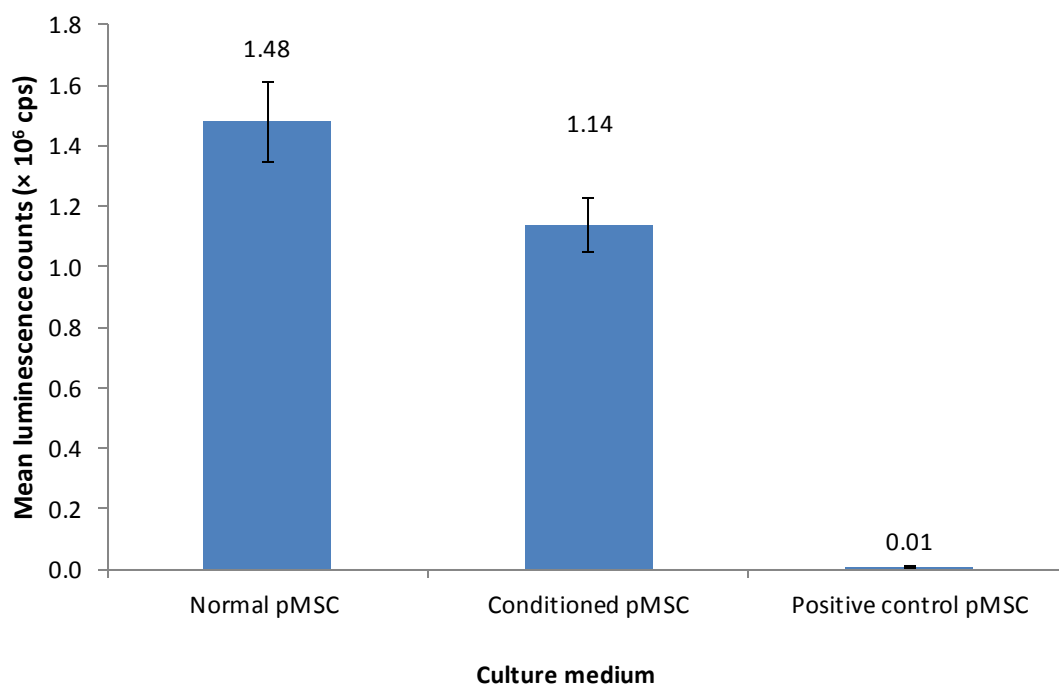
Fig. 4.11: Chart showing the luminescence counts of pMSC grown in unconditioned complete culture medium and those grown in concentrated Tencell seeding ring conditioned medium, as measured by the ATPlite™ assay. *Positive control medium contained DMSO (40% (v/v)). Luminescence counts were significantly different between all sample types (p < 0.001). Statistical testing carried out using one way ANOVA and Tukey's post hoc test. Data presented as the mean (n=4) ± 95% confidence limits.*

4.4.5 Cell survival in circular seeding ring seeded scaffolds

Since the Tencell seeding rings were shown to be incompatible with cell culture, cell survival in alternative seeding rings of circular shape (diameter = 1.1 cm) was investigated. These studies were performed using human MSC and not model pMSC, as other cell types were previously successfully cultured using this apparatus (Dr Robert Guilliatt, personal communication). Additionally, efficacy of seeding was measured quantitatively using the ATPlite™ assay, instead of live/dead® staining.

4.4.5.1 Standard curve of the relationship between luminescence counts and cell number

To estimate the number of hMSC present following seeding, a standard curve of the relationship between luminescence counts detected by the ATPlite™ assay and the number of cells assayed was prepared (Fig. 4.12). These data showed a linear relationship. At low cell
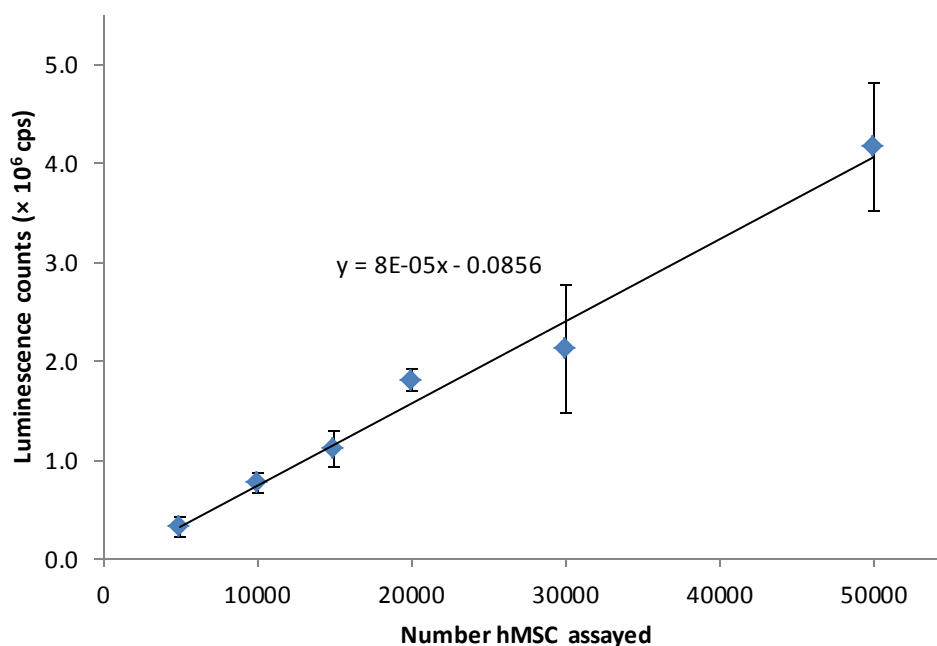
Fig. 4.12: Standard curve showing the relationship between luminescence counts, as detected by the ATPlite™ assay, and the number of human MSC assayed. *Data are presented as the mean (n=5) ± 95% confidence limits*

numbers (< 5000 cells/rxn) there was a very large degree of error between technical replicates, indicating the limit of detection of the assay in this system. Data points corresponding to cell numbers below this number were thus excluded from the calibration plot.

4.4.5.2   Survival of hMSC seeded using circular seeding rings

The viability of hMSC following seeding periods of 2, 4 and 18 hours in circular seeding rings was assessed to determine an optimal seeding time prior to culture in the Tencell bioreactor.

Cell survival decreased with increasing seeding time in initial investigations (estimated total cells seeded ~ 14820, 12320 and 3570 for scaffolds seeded for 2, 4 and 18 hours respectively). Scaffolds seeded for 18 hours yielded luminescence counts significantly lower than those seeded for 2 or 4 hours, and were comparable to counts of unseeded tissue (p = 0.026). There was no statistically significant difference between scaffolds seeded for 2 and 4 hours.

If cell culture is performed correctly and with compatible materials, the number of adherent cells on a scaffold should increase with seeding time. Additionally, previous work by co-workers, in which other cell types were successfully cultured, did not suggest the release of cytotoxic species by these seeding rings (Robert Guilliatt, personal communication). Hence, the seeding method used was interrogated further. In initial investigations using circular

seeding rings, the pericardial matrix outside of the centre of the seeding ring was not in contact with culture medium. If drying of the unseeded areas of the substrate had occurred, the seeded cell suspension may have diffused through the tissue and away from the intended seeding area. Lack of moisture in the well plates used to perform seeding may have also caused excessive evaporation, and hence concentration of the components of the culture medium.

Cells cultured with circular seeding rings with a reservoir of culture medium around the ring showed improved viability, (approximately 36070, 24820 and 44820 hMSC present in scaffolds seeded for 2, 4 and 18 hours respectively). Although there was an increase in the estimated number of total seeded cells with time, there were no significant differences in luminescence counts between seeding periods. Unseeded pericardial matrix gave significantly fewer luminescence counts than all of the cell-seeded sample types ($p = 0.031$).
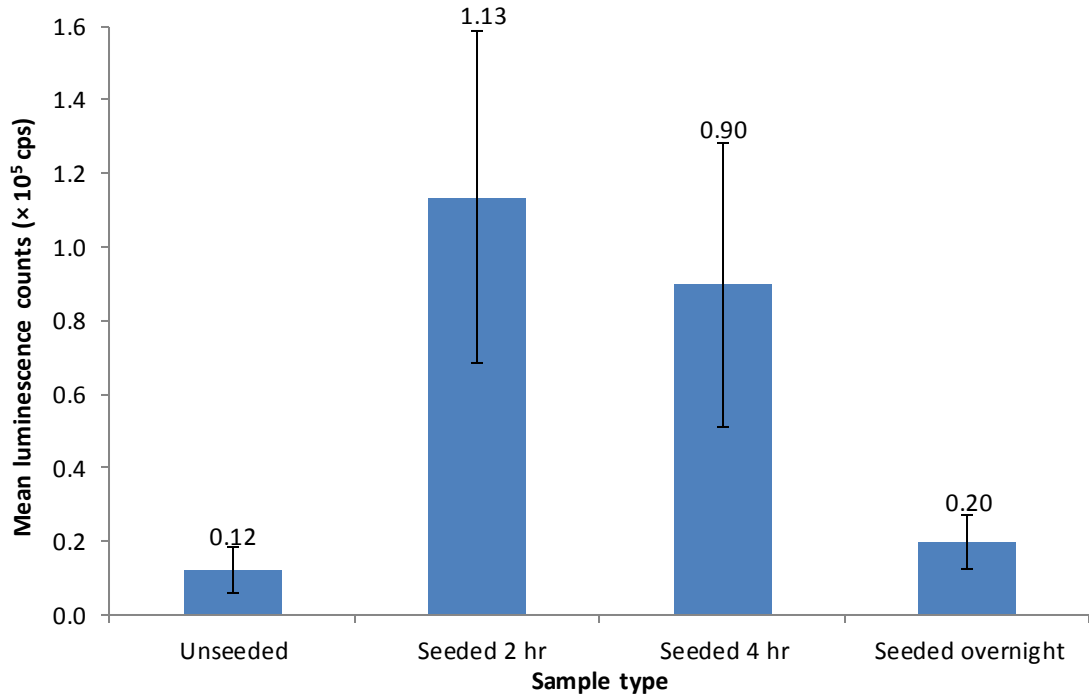
Fig. 4.13: Mean luminescence counts by sample type for cells seeded using circular seeding rings (d= 1.1 cm). *There was a significant difference between unseeded and overnight seeded samples and those seeded for 2 or 4 hours (p=0.026). Statistical analysis was done by ANOVA and Tukey's post-hoc test. Data presented as the mean (n=4) ± 95% confidence limits.*
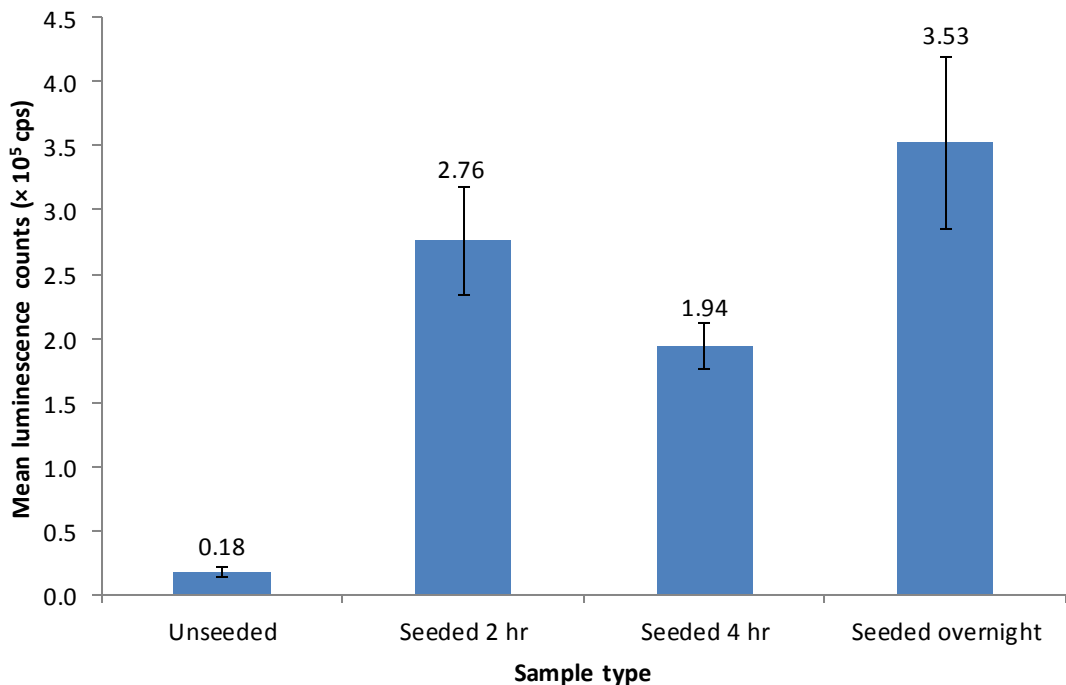
Fig. 4.14: Mean luminescence counts by sample type for cells seeded using circular seeding rings (d= 1.1 cm) using the reservoir seeding method. *There was a significant difference between unseeded and all other samples (p=0.031). Statistical analysis was done by ANOVA and Tukey's post-hoc test. Data presented as the mean (n=4) ± 95% confidence limits.*

4.5 Discussion

The investigations described in this chapter were performed to devise an optimal seeding method for hMSC on acellular porcine pericardium substrates. The seeding approach developed needed to be suitable for both bioreactor culture and subsequent gene expression analyses by qPCR.

The density at which hMSC are seeded is a significant factor in determining their differentiation potential (Hayflick, 1965; Sekiya *et al.*, 2002; Dominici *et al.*, 2006), and demand on cell stocks may influence whether a given approach is plausible. Sufficient RNA must be extracted from cell-seeded substrates to allow virtually limitless qPCR analyses and accurate assessment of its concentration and purity isolates. Additionally, the total number pf cells seeded must produce luminescence counts, by ATPlite™ assay, above the limit of detection for the assessment of cell viability. In these studies, the quantity of RNA extracted from cell suspensions containing a total of 0.5, 1.0 and 2.0×10^5 hMSC was measured using a NanoDrop spectrophotometer. Nucleic acid spectrophotometry measures the absorbance of the species in question at 260 and 280 nm to calculate its concentration and $A_{260/280}$. Absorbance ratio values for lowest number of cells examined (0.5×10^5 cells) were not reliably measured, and frequently did not fall within the expected range for RNA solutions (2.0-2.2). Hence, RNA extracted from this quantity of cells cannot be tested for purity reliably and a larger number of cells needed to be used. Polymerase chain reaction assays may be affected by contaminants and measurement of the purity of template material to be used is thus essential (Edwards *et al.*, 2004; Bustin *et al.*, 2009).

In contrast, the absorption ratios of cell suspensions containing 1.0 and 2.0×10^5 cells were characteristic of RNA solutions, and luminescence counts for these cell numbers are sufficient to allow viability assessment (Fig. 4.12). Additionally, previous work by co-workers (Morticelli, 2013) indicated that hMSC seeded on acellular pericardium at densities of 1.0 and 2.0×10^5 cells.cm^{-2} retained good cell viability, as assessed by live/dead staining. The lowest cell seeding density that satisfied cell viability and RNA quantity and quality requirements needed to be used to minimise cell stock demands; hMSC were therefore seeded on acellular pericardium at a density of approximately 1.2×10^5 cells.cm^{-2} in subsequent seeding investigations.

Porcine multipotential mesenchymal stromal cells extracted from freshly sacrificed animals were used as model cells during initial screening of seeding apparatus. To date, no significant

differences in morphology or functionality between porcine and human MSC have been identified, and pMSC are widely used in tissue engineering, recellularisation and mechanotransduction based investigations (Ringe *et al.*, 2002; Lee *et al.*, 2007; Proffen *et al.*, 2015; Chang *et al.*, 2016; Hu *et al.*, 2016)

Multipotential mesenchymal stromal cells are typically characterised according to minimal criteria proposed by the Mesenchymal and Tissue Stem Cell committee of the International Society for Cellular Therapy (Dominici *et al.*, 2006). Specifically, to be described as MSC, cells must exhibit plastic adherence and a fibroblastic morphology, differentiate *in vitro* towards adipocytes, chondrocytes and osteoblasts, express CD105, CD73 and CD90, and lack expression of CD45, CD34, CD14 or CD11b, HLA-DR and CD79α or CD19. In this project, MSC were either isolated from fresh porcine legs or purchased following commercial supplier validation. Porcine MSC (pMSC) were used in screening experiments as a model cell type for hMSC, and were extracted in a process well-described in the literature using Percoll gradient fractionation (Section 2.2.8.6) (Olofsson *et al.*, 1980; Ellis *et al.*, 1984; Rosca and Burlacu, 2010). In this method, pMSC is obtained passively; bone marrow, used for extraction, does not contain adherent cell types that persist in culture except MSC. Additionally, any such contaminating cells present in early culture are morphologically distinct from MSC, making their presence obvious by microscopy. Since experiments utilising pMSC in this study were designed to model subsequent investigations with hMSC, in which any discrepancies in behaviour between the species would be revealed, only basic characterisation was performed. Cell morphology, examined using bright field microscopy, and the results of a tri-lineage differentiation assay strongly indicated an MSC phenotype (Fig. 4.2, Fig. 4.3, Fig. 4.4).

Human MSC used in this project were purchased from a commercial supplier (STEMCELL™ Technologies inc.) and were validated according to ISCT criteria for designation as MSC prior to sale. Repeat validation may be deemed necessary for cells subjected to extended culture due to the limited proliferative capacity of MSC, but since all experiments described herein used cells at an early passage this was considered unnecessary (passage 6) (Turinetto *et al.*, 2016). In common with most normal somatic cells, hMSC are telomerase negative and senesce after prolonged culture (Hayflick, 1965; Zimmermann *et al.*, 2003). The average number of population doublings undergone by human MSC prior to senescence was found to be 38 ± 4, by Bruder *et al* (Bruder *et al.*, 1997).

Model cells were seeded using seeding rings of dimensions and shape compatible with culture in the Tencell bioreactor (available culture area ~ 1 cm^2) and that allowed a sufficient number of cells for subsequent qPCR analyses to be cultured. Since the poor viability of cells seeded

using the Tencell seeding rings was not improved through seeding volume optimisation, and a red-brown solid was obtained during incubation of the rings, it was concluded that the apparatus itself may be cytotoxic. Such cytotoxicity was confirmed by the loss of cell viability detected during extract cytotoxicity testing of the concentrated extract, although the lack of toxicity towards BHK cells in the presence of a significant impact on cell viability of 3T3 cells and pMSC contraindicated their use in such assays. It is therefore suggested that BHK cell may be less sensitive to some cytotoxic agents than MSC. Hence if practicable, possible cytotoxicity of apparatus/biomaterials should be tested using the cell type of interest.

Based on the chemistry of stainless steel, it is suggested that the red-brown substance obtained from the Tencell seeding rings during extract cytotoxicity testing, and the cause of loss of viability of seeded cells, was probably rust (iron oxide(s)). Self-repairing rust layers are known to form on stainless steel products, particularly in the presence of water and salts as may be found in cell culture medium, protecting the underlying metal from further corrosion (Tamura, 2008). However, the seeding rings were vigorously scrubbed prior to each use to remove adhered proteins, removing any protective layer and rendering the steel reactive in cell culture medium. The use of Raman spectroscopy to study iron oxides is well established, and could be used to confirm the identity of the extract species (Dünnwald and Otto, 1989). However, for the purposes of these studies it was sufficient to establish that the materials used were cytotoxic; detailed chemical analyses were beyond the remit of this work.

Seeding of MSC on acellular pericardium was continued using alternative, circular (d = 1.1 cm) seeding rings of similar seeding area as the strained region in Tencell wells (0.95 cm^2), and cell viability of seeded cells quantified using the ATPlite™ assay. Since these seeding rings were previously used successfully with other cell types, hMSC were used in these investigations.

Live/dead staining was discontinued for the measurement of cell viability owing to its semi-quantitative nature. Live/dead imaging can be rendered quantitative through cell counting, but this method assumes that all cells can be visualised. Pericardium is a three-dimensional scaffold, and previous work by co-workers indicated that MSC penetrate the tissue (Morticelli, 2013). Hence, seeded cells are found at different depths throughout pericardial substrates, and are not visualised in a single focal plane. Additionally, dead cells are not accurately recorded since they do not adhere to substrates.

The ATPlite™ calibration curve produced, showing the relationship between the cell number and luminescence counts of an individual assay, indicated a limit of detection of ~ 5000 cells/rxn. In previously published work, Grimsey *et al.* compared the sensitivity of several

methodologies for the quantification of leukocyte migration (Grimsey *et al.*, 2012). In this application, the ATPlite™ assay reliably detected 400 cells/rxn. These contrasting findings highlight the importance of generating ATPlite™ calibration curves for all applications in which it is to be used; ATP content differs by cell type and experimental conditions (Stanley, 1986), and hence the lowest number of cells detectable by ATPlite™ may vary. Calibration data should be used to inform assay method development to optimise the number of cells lysed per reaction with respect to the limit of detection.

It is essential to maintain a humid environment for successful *in vitro* cell culture (Ham and Puck, 1962). In order to attribute cellular changes such as differentiation to test conditions, and not environmental changes, investigators must also be sure that the composition of the culture medium remains constant during an experiment. Cell culture medium is designed with an osmolarity that renders it isotonic to cells; if concentrated by evaporation, increased salt concentration induces osmosis from the cytoplasm to the cell exterior (Waymouth, 1970). The cell viability of seeded cells in initial investigations with circular seeding rings decreased with increased seeding time, but was improved at longer seeding times through the use of a medium reservoir around the ring (Section 4.4.5.2). It is likely that in the absence of a reservoir around the seeding ring, unseeded areas of the tissue lose moisture by evaporation, causing diffusion of the seeding medium away from the seeding area and loss of cell viability. Wherever such issues can be mitigated, it is advantageous to use the maximum seeding time possible to maximise the proportion of applied cells successfully seeded. Additionally, for subsequent Tencell culture investigations, scaffolds were seeded overnight to satisfy time constraints.

Chapter 5: Quantitative polymerase chain reaction assay development

5.1 Introduction

This chapter describes qPCR assay development for genes suggestive of differentiation of hMSC towards the osteogenic, adipogenic, chondrogenic, tenogenic and smooth muscle lineages.

The polymerase chain reaction (PCR), first described by Mullis *et al* (Mullis *et al.*, 1986)*,* uses thermostable DNA polymerases and specific oligonucleotide primers to produce thousands of copies of a defined segment of DNA from a quantity of starting material at levels too low for direct detection (Murray *et al.*, 2009). This technique may be utilised in a qualitative fashion, where the product(s) of a PCR reaction are identified according to their size by gel electrophoresis, or less frequently, by sequencing (Newton *et al.*, 1988), and in quantitative investigations in which fluorescent dyes are used to trace the reaction profile in real time (Delidow *et al.*, 1989). Quantitative PCR is most commonly used in contemporary molecular biology due to the more detailed insight possible with this technique, and is the method employed in this chapter.

To quantify gene expression in cells of interest, mRNA is first extracted using standard purchased kits, and reverse transcribed to produce copy DNA (cDNA) of all the sequences present, upon which PCR may be performed (Bustin, 2000). In PCR, cDNA is denatured at high temperatures (typically 94 °C), separating the strands, and rapidly cooled to the annealing temperature, which is primer-pair dependent. During this annealing step, oligonucleotide primers hybridize the template at the target sequence; the original strands of cDNA are too long and complex to reanneal during this rapid cooling stage. DNA polymerase in the reaction mixture targets the template region defined by the primer and synthesises the area of interest at 72 °C (McPherson and Møller, 2006). Approximately 30-40 PCR cycles are conducted in a typical assay, and the polymerase used is exposed to very high temperatures during the

denaturation step; early attempts at PCR used an *E. coli* enzyme that was destroyed during a single cycle, but modern reactions utilise a heat-stable form from thermophilic bacteria, such as *T. aquaticus* (Murray *et al.*, 2009).

In quantitative PCR, reaction progress is monitored in real time by measuring a fluorescent signal generated as a result of amplicon synthesis. This may be achieved using fluorescent dyes, such as SYBR Green I, an asymmetric cyanine dye that undergoes a conformational change upon binding double stranded DNA, increasing its fluorescence, or by fluorescent resonance energy transfer (FRET). This method, used in the popular TaqMan® probes, relies on altering the spatial arrangement of photon donor and acceptor molecules, such that amplification of a specific DNA sequence causes an increase in fluorescence (Pongers-Willemse *et al.*, 1998; Edwards *et al.*, 2004). Following qPCR cycling, products are often analysed using a further melt curve analysis step; the reaction mixture is taken through a range of temperatures (typically 55 − 95 °C) and dissociation of amplicons indicated by changes in fluorescence at their dissociation temperatures. The number of amplicons produced in a given assay is equivalent to the number of peaks in the resulting dissociation plot.

The kinetics of a functional PCR assay pass through three different phases, and reaction profiles of qPCR assays should be examined to confirm normal behaviour. In the early stages of an assay, primer pairs search template DNA for their complementary sequences and produce small quantities of amplicon. The mid cycles are characterised by exponential amplification of the product fragment, and the late stages, or plateau, by suboptimal amplification. This reduction in amplicon manufacture is often caused by assay reagents reaching limiting concentrations or inhibition of the reaction by the presence of large quantities of DNA (McPherson and Møller, 2006). A threshold, the point at which sufficient amplicon has been generated to give a fluorescent signal significantly greater than the baseline, is set for each qPCR assay and the point at which amplification exceeds this value, the threshold cycle number (C_T), reported. This is normally defined as ten times the standard deviation of the baseline fluorescence (Wong and Medrano, 2005). The fluorescence of background reference dyes that do not bind DNA, such as ROX, is monitored by thermal cyclers to allow corrections for factors such as reagent evaporation during cycles. Threshold cycle numbers may be converted to actual gene copy numbers using calibration graphs, or related to both those of housekeeping genes within the same sample, and those of calibrator samples, to determine the relative expression of the gene in question (Schmittgen and Livak, 2008).

The expression of genes indicative of hMSC differentiation towards the tenogenic, smooth muscle, adipogenic, osteogenic and chondrogenic lineages was measured. Differentiation towards the latter three lineages is a defining characteristic of MSC, and their differentiation towards tendon and smooth muscle tissue has previously been reported (Galmiche *et al.*, 1993; Park *et al.*, 2004; Gong and Niklason, 2008; Gong *et al.*, 2009; Park *et al.*, 2011a; Williams *et al.*, 2012) The minimum panel of genes considered necessary and sufficient to identify differentiation potential was examined. The genes of interest studied are described in Table 5.1.

Table 5.1: Function and associated lineage(s) of the characteristic genes of interest

Lineage	Gene of interest	Function	Reference
Smooth muscle	SM-22α (a.k.a. transgelin) (TAGLN)	Codes for actin cross-linking/gelling protein found exclusively in fibroblasts and smooth muscle	(Park et al., 2004; van Tuyn et al., 2005; Kim et al., 2008; NCBI, 2016l)
	Calponin (CNN1)	Binds actin to promote and sustain polymerisation. Specific to differentiated smooth muscle cells	(Kim et al., 2008; NCBI, 2016c)
	Smooth muscle α-actin (ACTA2)	Structural component and major constituent of contractile apparatus. Indicator of myofribroblast formation	(Park et al., 2004; Kim et al., 2008; NCBI, 2016a)
Tenogenic	Scleraxis (SCXB)	Member of the basic helix-loop-helix superfamily of transcription factors	(Kuo and Tuan, 2008a; Peach et al., 2012; Yin et al., 2013; NCBI, 2016j)
	Collagen I (COL1A1)	Fibril-forming structural protein found in skin, bone and tendon tissue	(Omae et al., 2009; Lui et al., 2011; Muiznieks and Keeley, 2013; Yin et al., 2013; NCBI, 2016d)
	Collagen III (COL3A1)	Fibril-forming structural protein found in extensible connective tissues, often in association with collagen I, including bone, cartilage, tendon, dentin and bone marrow	(Omae et al., 2009; Lui et al., 2011; Yin et al., 2013; NCBI, 2016e)
Osteogenic	Runt related transcription factor 2	Member of RUNX family of transcription	(Muruganandan et al., 2009; Shi et al., 2011;

Lineage	Gene of interest	Function	Reference
	(RUNX2)	factors. Acts as scaffold for nucleic acids and regulatory factors involved in skeletal gene expression	NCBI, 2016i)
Adipongenic	Peroxisome proliferator receptor gamma (PPARG)	Nuclear receptor; regulator of adipocyte differentiation	(Lehmann et al., 1997; NCBI, 2016g)
	Adiponectin, C1Q and collagen domain containing (ADIPOQ)	Exclusively expressed in adipose tissue, the encoded protein circulates in plasma and is involved in metabolic and hormonal processes	(Degawa-Yanauchi et al., 2005; Sen et al., 2008; NCBI, 2016b)
Chondrogenic	SRY-box 9 (SOX9)	Transcription factor that recognises the sequence CCTTGAG. Acts exclusively during chondrocyte differentiation	(Murphy et al., 2002; Grad et al., 2011; NCBI, 2016k)
Housekeeping (not lineage specific)	Glyceraldehyde-3-phosphate dehydrogenase	Glycolytic enzyme that catalyses the reversible oxidative phosphorylation of glyceraldehyde-3-phosphate in carbohydrate metabolism	(Schmittgen and Zakrajsek, 2000; Kim et al., 2002; Huggett et al., 2005; NCBI, 2016f)
	β-actin (ACTB)	Encodes cytoskeletal proteins that form a major component of the contractile apparatus	(Schmittgen and Zakrajsek, 2000; Huggett et al., 2005; NCBI, 2016m)
	S28 ribosomal protein (RPS28)	Encodes a protein component of the 40S ribosome subunit	(Xue et al., 2010; NCBI, 2016h)

Quantitative PCR data can either be reported using absolute or relative expression approaches. In absolute gene quantification, the exact copy number of a gene of interest is quoted following transformation of the data with a standard curve. This method is utilised when finding the precise quantity of amplicon is critical, such as calculation of viral load, but where gene copy numbers are not required it is not favoured due to the increased workload associated with this method: standard curves must be generated to transform C_T values to gene copy numbers (Schmittgen and Livak, 2008). Relative gene expression analyses report

fold change or normalised C_T values of to illustrate the impact of a given treatment on gene expression. In the comparative threshold method, also known as the $2^{-\Delta\Delta ct}$ method, discrepancies in reverse transcription efficiencies and input RNA are corrected through normalisation of target gene C_T values with a gene expected to be unaffected by the treatment in question (known as housekeeping genes). Corrected C_T values corresponding to treated and untreated samples may then be compared to discern changes in gene expression as a result of the treatment (McPherson and Møller, 2006). In this study, the comparative threshold method was used, as it is sufficient to identify changes between gene expression of strained and unstrained samples, and no additional insight from gene copy number was anticipated.

To ensure accurate gene expression data, the primer pairs used must anneal only to the target sequence, and produce a single amplicon. There are many online tools for primer design that incorporate criteria designed to minimise these issues, although further laboratory validation is always required (NCBI, 2014; Sigma-Aldrich, 2014). In fact, guidelines published in the literature advise reviewers of manuscripts concerning gene expression to seek assurances that all primers were validated by both *in silico* methods and efficiency and specificity assays (Bustin *et al.*, 2009). The comparative threshold method depends on the assumption that the efficiency of all primer pair assays is approximately 100%, meaning that the amount of amplicon present in reactions doubles with each thermal cycle. Hence, primer assays for each gene of interest must be validated according to their specificity and efficiency, and the identity of the amplicon produced confirmed.

Primer specificity can be confirmed definitively using melt curve analysis of PCR products. The double stranded DNA of PCR products is denatured at a specific temperatures according to the amount of energy required to break the hydrogen bonding between strands. Once strands separate, the fluorescence of the SYBR Green I reporter dye is altered, producing a peak in a fluorescence vs temperature plot (McPherson and Møller, 2006). Although dissociation curves can be readily interpreted to find the number of amplicons present, they do not confirm amplicon identity. Amplicon identity can only be proven by sequencing, but less expensive techniques such as gel electrophoresis are routinely used to validate products beyond reasonable doubt. Electropheresis separates molecules by their speed of migration through a porous medium when subjected to a strong electric field. Migration speed is related to molecular size, and through comparison to a molecular ladder, a mixture of nucleic acids of known sizes, the size of test species can be estimated and compared to that predicted by *in silico* methods (Alberts *et al.*, 2008; NCBI, 2014).

Primer assay efficiency is found by performing serial dilutions of input material and plotting C_T values against the log of their corresponding amounts of RNA. The assay efficiency may be found from the gradient of this plot according to Eqn. 5.1. The assumption that the amount of amplicon in the assay mixture doubles with each cycle of PCR can be considered met if the efficiency of the assay in question is found to be 90-110 % (McPherson and Møller, 2006). Additionally, the coefficient of determination, or R^2, obtained from linear regression of efficiency data should have a value $\geq$ 0.98, indicating that $\geq$ 98 % of the change in C_T values in response to changes in the value of log(mass RNA) is explained by the line of best fit calculated (Edwards *et al.*, 2004; Dytham, 2011).

$$Assay\ efficiency = \left(10^{\left(-\frac{1}{m}\right)}\right) - 1$$

Eqn. 5.1: Calculation of primer assay efficiency from the gradient (m) of a C_T vs log(mass RNA) plot.

The inclusion of controls is essential in all PCR assays to exclude, or highlight, the possibility that fluorescence data may be confounded by the presence of contamination and unwanted amplicons. A description of the utility and indications afforded by each type of control is provided in Table *5.2*.

Table 5.2: Recommended controls to be included in qPCR assays

Control type	Indication(s) if amplification present
No reverse transcriptase	*Presence of genomic contaminating DNA from environment/investigator or cells of interest*
No template	*Presence of genomic contaminating DNA or amplification of primer-dimer/primer secondary structure amplicons*
No primer	*Presence of genomic contaminating DNA from environment/investigator or cells of interest, or faulty/spoiled reagent(s)*
Water only	*Apparatus malfunction(s), contamination of ultrapure water supply, contamination of equipment/consumables used*

5.2   Aims and objectives

5.2.1   Aim:

The aim of the investigations described in this chapter was to validate primer pairs for the genes of interest (Table 5.1) with respect to their specificity and efficiency, as determined by dissociation plots, gel electrophoresis, reaction profiles and efficiency plots.

5.2.2   Objectives:

- To design and pre-validate primer pairs for the genes of interest using an *in silico* approach

- To perform specificity validation of primer pairs using melt curve analyses and gel electrophoresis

- To examine the reaction kinetics of primer pair assays through efficiency testing and amplification plots

- To determine the optimum primer concentration for use in gene expression analyses

5.3 Experimental approach

During qPCR assay validation, primer pairs were either designed using an *in silico* approach or sourced from literature, and validated with respect to their specificity and reaction kinetics.

The purity and quantity of RNA extracted using enzymatic and maceration-only methods was compared to validate an approach for the isolation of sufficient high-quality RNA from Tencell-cultured substrates for use in gene expression analyses. Primer pairs were designed using the primerBLAST tool provided by the NCBI or taken from literature in which the expression of gene of interest was investigated. All primer pairs were screened *in silico* with respect to predicted annealing temperatures, primer-dimer or secondary structure forming potential, and specificity using the OligoEvaluator™ and BLAST tools to reduce the number of laboratory experiments required. Primer pairs were validated with respect to their efficiency to ensure that only assays having normal PCR reaction profiles and meeting the assumptions of the comparative C_T method were used for gene expression analyses. Assay specificity was validated using melt curve analysis to examine the number of amplicons produced, and by gel electrophoresis to ensure that the amplicon(s) produced were of the size predicted by *in silico* methods. The primer concentration used in assay mixtures was optimised to reduce the probability of primer-dimer and secondary structure formation and hence the amplification of unwanted products. The reaction profiles of assays containing different primer concentrations were examined to ensure that only primer concentrations giving C_T values in template-containing reactions significantly lower than any amplification in controls from environmental contamination were used.

5.4   Results

5.4.1   RNA extracted from seeded scaffolds by different techniques

The extraction of RNA from seeded acellular pericardium (performed using the method described in section 2.2.8.9.2, using a seeding volume of 80 µL as validated during chapter 4) using enzymatic and enzyme-free methods was investigated. Proteinase K digestion is recommended for RNA extraction from tissue, but requires a high temperature incubation (55 °C, 10 min). Additionally, acellular pericardium is relatively thin (~ 200 − 500 µM) and hence may be more readily penetrated by extraction reagents without prior digestion. The null hypothesis that there was no statistically significant difference between the amount of RNA extracted from tissue treated with both enzyme and enzyme-free protocols was tested by direct comparison of RNA extracted by each approach.

There was no statistically significant difference between the amount of RNA extracted by each method (p=0.151). Although the mean quantity of RNA extracted from tissue that did not undergo enzymatic digestion was far greater, the associated confidence limit (p=0.05) was very large. Hence, the null hypothesis that there was no significant difference in the amount of RNA extracted by each method was accepted and the enzyme-free approach adopted for RNA extraction from seeded acellular pericardium for its simplicity.
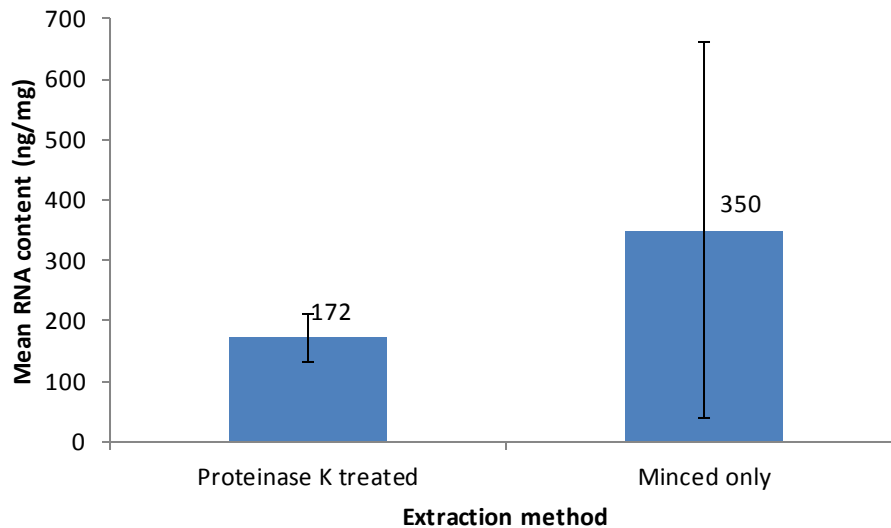
Fig. 5.1: Total RNA extracted from hMSC-seeded acellular pericardium treated with two different RNA extraction methods. *There was no significant difference between the amount of RNA extracted from tissue digested by the proteinase K protocol (55 °C, 3 hr) and the enzyme-free protocol (p=0.151). Data presented as means ± 95% confidence limits. Statistical analysis done by paired t-test.*

5.4.2 qPCR primer validation

In order to quantify relative gene expression by the comparative C_T method, underlying model assumptions must be met, and qPCR assays must be performed under optimal conditions (McPherson and Møller, 2006). In common with all PCR techniques, the primer pairs used must be specific; only the desired amplicon should be generated by the PCR assay. Additionally, and unique to quantitative PCR, reaction efficiencies must be approximately equal and in the range 90-110% for accurate expression data (Edwards *et al.*, 2004). Validation of any given pair was discontinued upon failing any of these critical quality attributes.

5.4.2.1 Generated primer sequences

Primer pair sequences for genes indicative of the lineages of interest were found either from relevant literature or by using the Primer-BLAST online tool provided by the National Center for Biotechnology Information (NCBI). Details of the primer sequences generated are in Table *5.3*. All primers were confirmed specific for their corresponding genes of interest *in silico* using the basic local alignment tool (BLAST) prior to laboratory validation.

Table 5.3: Base pair sequences, annealing temperature and expected amplicon size for primer pairs obtained from a review of relevant literature and the primerBLAST and BLAST design tools.

Associated lineage	Gene of interest	Primer name	Forward sequence	Reverse sequence	T_a (°C)	Predicted amplicon size (bp)	Reference
Housekeeping	28s ribosomal protein	h28A	ACCTCTACCCTGCCCTAACC	CGGGGCCAGAATACAGATCG	58	120	Designed by author
	28s ribosomal protein	h28SB	TTGAAAATCCGGGGGAGAG	ACATTGTTCCAACATGCCAG	58	100	(Ku et al., 2006)
	β-actin	β-actinA	CAGCACAATGAAGATCAAGATCATT	GGACAGCGAGGCCAGGAT	54	112	Designed by author
	β-actin	β-actinB	CATGTACGTTGCTATCCAGGC	CTCCTTAATGTCACGCACGAT	60	250	(Yu et al., 2010)
	GAPDH	hGAPDHA	CTCCAAACAGCCTTGCTTGC	AAGTAGTGGTGCCAGCTTCC	55	84	Designed by author
	GAPDH	hGAPDHB	GAGCCGCACCTTGTCATGTA	GTCTCACCTTGACACAAGCC	55	120	Designed by author
	GAPDH	hGAPDHC	TCCATGACAACTTTGGTATCG	TGTAGCCAAATTCGTTGTCA	54	226	(Kim et al., 2009)
	GAPDH	hGAPDHD	AACATCATCCCTGCCTCTACTG	CTCCGACGCCTGCTTCAC	59	189	(Kuo and Tuan, 2008b)
Adipogenic	PPAR-γ	hPPAR-γA	GCCGAGAAGGAGAAGCTGTT	CTCGCCTTTGCTTTGGTCAG	60	140	Designed by author
	Adiponectin	hAdiponA	AAGGAGATCCAGGTCTTATTGG	ACCTTCAGCCCCGGGTAC	57	68	(Degawa-Yanauchi et al., 2005)
Chondrogenic	SOX-9	hSOX-9B	CCCATGTGGAAGGCAGATG	GAAGGTTAACTGCTGGTGTTCTGA	60	69	(Miyanishi et al., 2006)
Osteogenic	RUNX2	hRUNX2A	CAGCGTCAACACCATCATTC	CAGACCAGCAGCACTCCATA	59	178	(Hsu and Huang, 2013)
Smooth muscle	Calponin	hCalponinA	GCATGTCCTCTGCTCACTTCAA	GGGCCAGCTTGTTCTTAACCT	60	72	(Kurpinski et al., 2006)

Associated lineage	Gene of interest	Primer name	Forward sequence	Reverse sequence	T_a (°C)	Predicted amplicon size (bp)	Reference
	SM-22α	hSM-22αA	TGAAGAAAGCGCAGGAGCATA	GCCAATGACATGCTTTCC	58	71	Designed by author
	Smooth muscle α-actin	hSM α--actin A	TGACTCTTGGGATGGGGGTA	GCCTATGTCACGACTGCGTT	55	101	Designed by author
	Smooth muscle α-actin	hSM α--actin B	ACCCTGCTCACGGAGGC	GTCTCAAACATAATTTGAGTCATTTTCTC	59	71	(Park et al., 2004)
Tenogenic	Collagen III	hColIIIA	GATGTGCAGCTGGCATTCC	CCACTGGCCTGATCCATGTAT	61	101	(Peach et al., 2012)
	Scleraxis	hScleraxisA	CAGCGGCACACGGCGAAC	CGTTGCCCAGGTGCGAGATG	60	163	(Kuo and Tuan, 2008a)
	Scleraxis	hSB	GAGAAAACGGGGTGGTGGGT	GGAGGAACTGGGAGGTCGC	60	104	Designed by author
	Scleraxis	hSC	CGCACCAACAGCGTGAAC	GCGTCTCAATCTTGGAGAGCTT	61	91	(Peach et al., 2012)
	Collagen I	hCol1A	GGTTAGCGTCCGCTCATGC	GTTCCTCCCTGCTCTCCATCAG	56	132	Designed by author
	Collagen I	hCol1B	GCCAAGACGAAGACATCCCA	CACACGTCTCGGTCATGG	62	70	Designed by author
	Collagen I	hCol1C	TGGTGCAGCTGGTCTTCCA	CACGGACGCCATCTTTGC	63	92	(Peach et al., 2012)

5.4.2.2 Suitability of primer pairs for relative gene expression analyses

Primer pairs described in section 5.4.2.1 were used in qPCR analyses with RNA extracted from cell types in which the gene of interest was expected to be expressed, and the reaction profile and specificity of an assay with a given pair assessed. Efficiency plots, showing the relationship between the amount of template added to a PCR reaction and corresponding C_T values, were prepared to calculate reaction efficiency, or the relative amount of amplicon produced per cycle, of assays using the primer pairs tested. Optimal reaction conditions and summarized validation data for primer pairs satisfying all critical quality attributes are summarised in Table 5.4.

5.4.2.2.1 Reaction kinetics

Amplification plots of assays with each primer pair were generated at three primer concentrations (100, 250 and 500 nM) and the reaction profile and C_T values for each concentration examined. In a functional qPCR assay the rate of production of amplicon passes through lag, exponential, linear and plateau phases (*Fig. 5.2*A), and C_T values fall within a optimum range (C_T ~ 12-30). All primer pairs, except β-actinA (Fig. 5.2B), which did not have an exponential amplification phase, had normal reaction profiles (Fig. 5.2A), and assays with primer concentrations of 500 nM had optimal C_T values (C_T = 12 - 30). Amplification in no template controls, indicating environmental contamination, was frequently present, but at very late C_T values easily distinguishable from those of template-containing test reactions ($\geq$ 31).

Fig. 5.2: Example amplification plots of primers suitable (A; hCol1C) and unsuitable (B; β-actinA) for relative gene expression analyses by qPCR. *Amplification plots of functional primer pairs show lag, exponential, linear and plateau phases and C_T values within a reliable range (~12-30). Additionally, controls should not show amplification, or if present, should have statistically significantly greater C_T values than test samples. Assays of the hCol1C primer pair with tenocyte RNA generated amplicon in the manner described (A), but the β-actinA primer pair assays did not show an exponential amplification phase during the experiment (B). See Table 5.3 for annealing temperatures used in each assay.*

Efficiency plots, prepared by measuring C_T values of assays of a primer pair with different quantities of template, were obtained to measure the rate of amplicon production. In a functional qPCR assay, the amount of amplicon generated during the exponential phase approximately doubles per cycle, and the reaction efficiency falls in the range 90-110% (Eqn. 5.1). Additionally, the goodness of fit of efficiency plots should be very high ($R^2 \geq 0.98$).

Efficiency testing was performed only on primer pairs that had normal amplification plots, indicating normal reaction kinetics. However, all primer pairs have a working range that is dependent on the copy number of a given gene and the amount of template added to the reaction. Hence, some primer pairs found to be inefficient initially showed good efficiencies and high R^2 values when tested in more appropriate ranges (Fig. 5.3A), and the ranges tested were thus adjusted accordingly, by adjusting the concentration of RNA in the strongest dilution or the dilution ratio. The minimum working range spanned by all primers was 1-70 ng/rxn. Excessively high amounts of RNA/rxn for a primer pair's working range were indicated by low C_T values compared to those that would be extrapolated by the line of best fit, whereas excessively low quantities gave rise to late/absent C_T values and/or significant background noise in dissociation plots (similar in appearance to Fig. 5.4B).
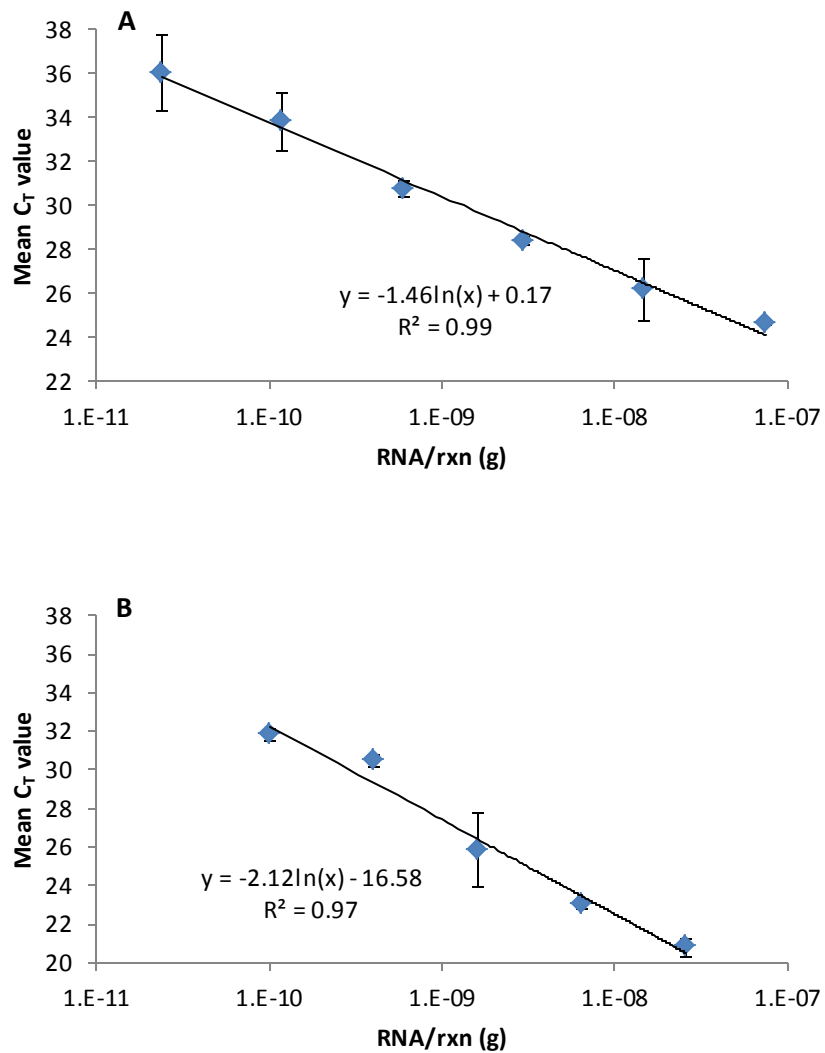
Fig. 5.3: Example efficiency plots of primer pair assays suitable (A; hCol1C) and unsuitable (B; PPAR-γA , tested with low copy number RNA) for relative gene expression analyses by qPCR. Efficiency plots of primer pairs that are efficient, and result in the doubling of amplicon with each PCR cycle, have assay efficiencies in the range 90-110%, as calculated from the gradient of the efficiency plot (Eqn. 5.1). Additionally, the goodness of fit of the efficiency plot, assessed by the value of the coefficient of determination, R_2, must be very high ($R^2 \geq 0.98$). The hCol1C primer pair shows good reaction efficiency (101.5%) and a high coefficient of determination ($R^2 = 0.985$) when assayed with tenocyte RNA in the range 0.1 − 75 ng/rxn (A), whereas the PPAR- γA primer pair shows poor reaction efficiency (59.8%) and a low coefficient of determination ($R_2 = 0.975$) when assayed with human knee fat in the range 0.01- 19 ng/rxn. Data presented as means(n=3) with 95 % confidence limits and line of best fit calculated by linear regression.

5.4.2.2.2   Primer specificity

In order to accurately quantify relative expression of genes of interest, primer pairs must amplify the target amplicon only. Dissociation plots, indicating amplicon melting temperatures, were obtained following each qPCR validation assay to assess the specificity of primer pairs. The number of amplicons produced in a PCR assay may also be deduced by electrophoresis of PCR products, but the sensitivity of this method is lower than that of fluorescence-based techniques. However, gel electrophoresis may also be used to estimate the size of amplicons generated for comparison with the amplicon sizes predicted by the primer-BLAST tool.

Primer pairs that gave rise to one amplicon showed one peak in dissociation plots at temperatures $\geq 77\ °C$ (Fig. 5.4A), whereas those undergoing nonspecific binding, and hence the production of multiple amplicons, had dissociation plots containing multiple peaks (Fig. 5.4B). All tested primer pairs that were not successfully validated for qPCR, with the exception of the β-actinA pair, were excluded due to nonspecific binding apparent in dissociation plots. Frequently, dissociation plots of pairs failing to meet specificity criteria showed a broad, low intensity peak in the range 72-76 °C. This peak was often present in no template controls showing amplification. Raising the annealing temperature did not reduce the number of amplicons produced in any case.
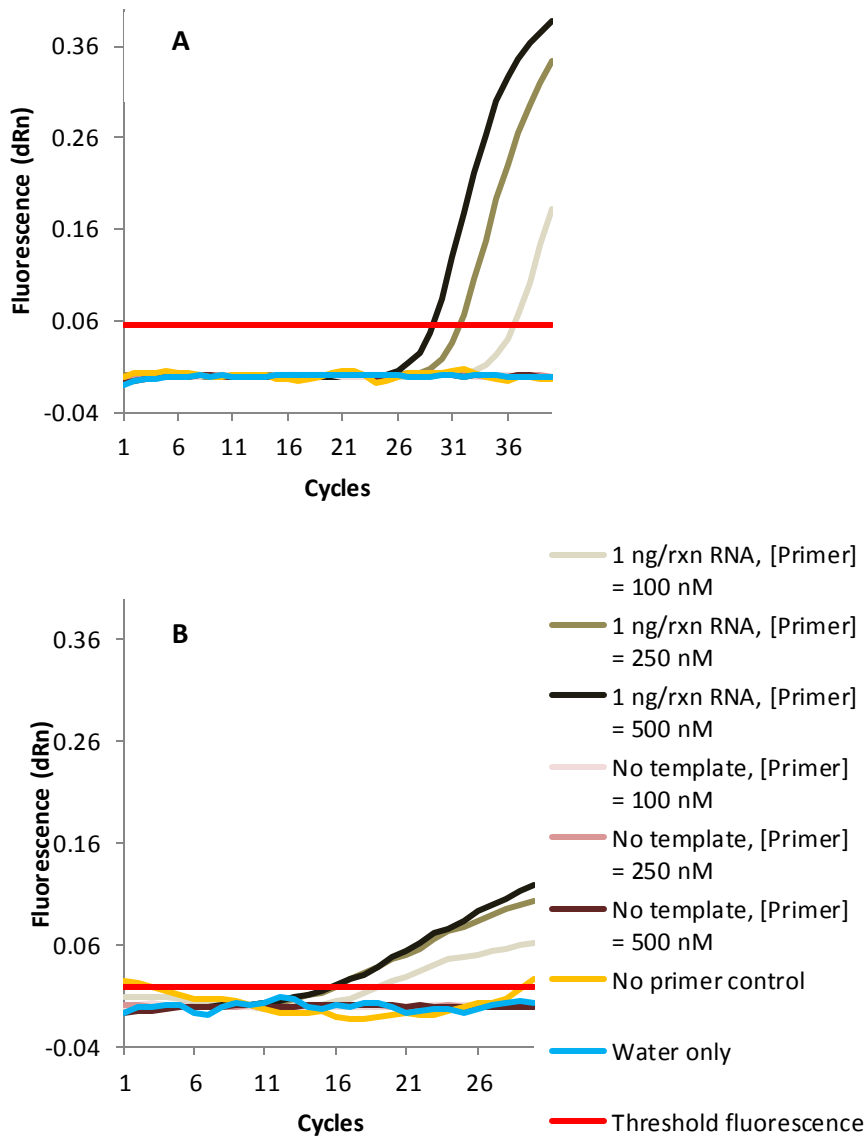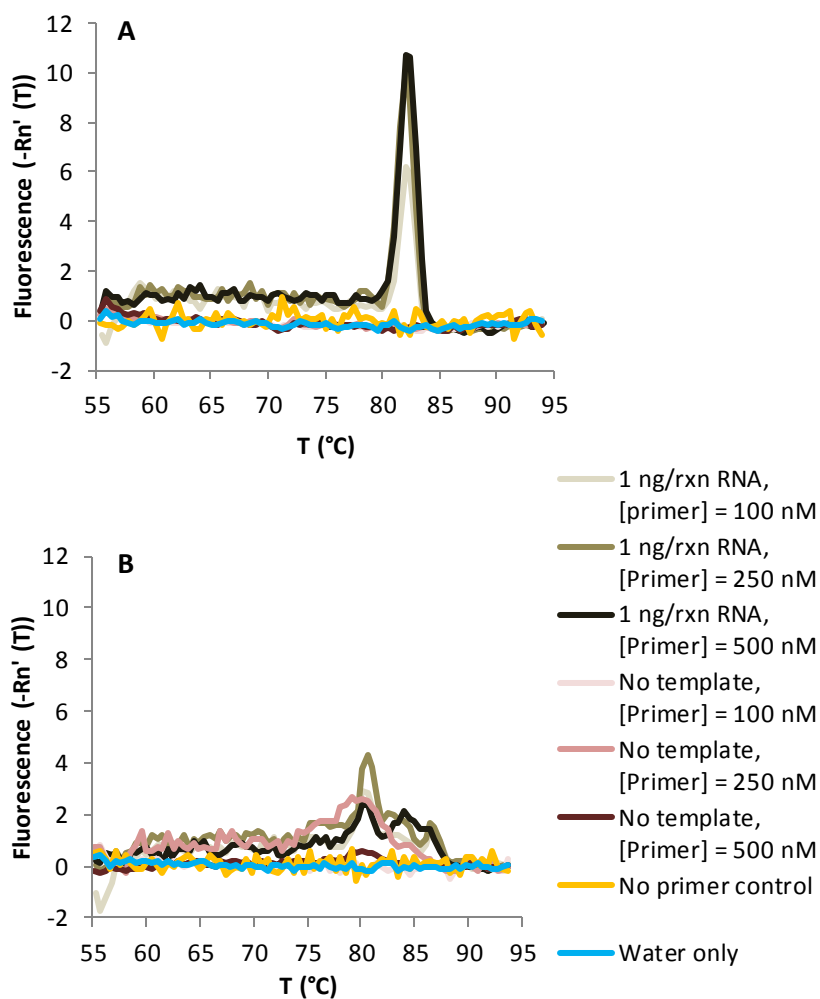
Fig. 5.4: Example dissociation plots of primer pairs suitable (A; hCol1C) and unsuitable (B; hSB) for relative gene expression analyses by qPCR. *Dissociation plots of specific (generating the intended amplicon only) primer pairs show one sharp peak at the melting temperature (T_m) of the target amplicon. Control samples should not give rise to any product peaks. Assays of the hCol1C primer pair with tenocyte RNA showed one sharp peak in assay dissociation plots at 82 °C, but hSB assays showed many peaks in corresponding dissociation plots, indicating the presence of many amplicons (B).*

Gel electrophoresis of primer pairs showing acceptable reaction kinetics and the production of one amplicon was performed to estimate amplicon size (for predicted sizes see Table 5.3). Amplicons of all validated primer pairs were of the size predicted by the primerBLAST design and analysis tool, and no other bands indicating the presence of other products were present (Fig. 5.5, Table 5.3).
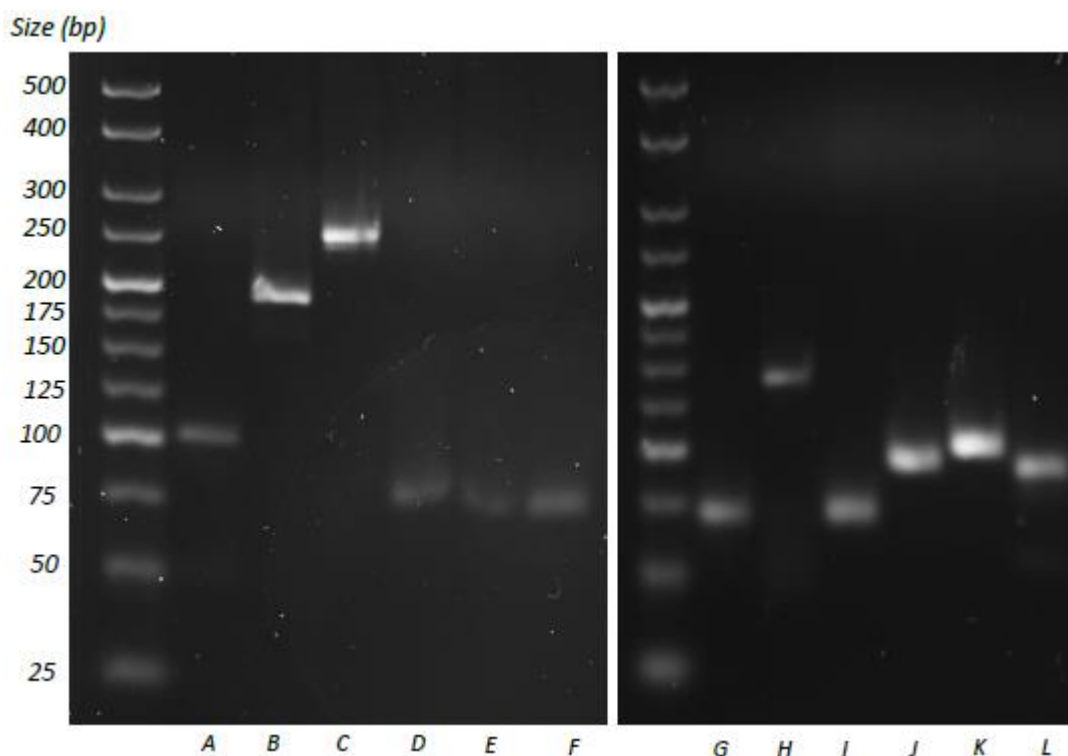
Fig. 5.5: Gel electrophoresis of the amplicons generated by the primer pairs used in relative gene expression analyses. *All primer pairs assayed generated one amplicon of the expected size. A: H28SB; B: hGAPDHD; C: hβ-actinB; D: hCalponinA; E: hSM-22αA; F: hSM α-actinB; G: hSOX-9B; H: hPPAR-γA; I: hAdiponA; J: hCol1C; K: hColIIIA; L: hSC. Bioline 25bp ladder applied in the far left lane of each gel. Gels were run for 40 min at 110 V.*

5.4.2.2.3   Summary of primer validation

Primer pair assays with favourable reaction profiles, specific binding behaviour and optimal reaction efficiencies were validated for relative gene expression analyses of Tencell cultured scaffolds. Primer pairs satisfying validation criteria are listed in Table *5.4*. Primer pairs included in Table *5.3* but excluded from Table *5.4* were found to be unsuitable for qPCR assays with respect to the tests described previously. Unsuitable primers, with the exception of β-actinA, were excluded from use in gene expression studies because multiple peaks were present in dissociation curves present due to nonspecific binding events.

Table 5.4: Summary of validated primer pairs suitable for use in relative gene expression analyses. *Primer pairs detailed in Table 5.3 but absent in this list of validated primers were excluded due to nonspecific binding, and hence the production of multiple amplicons, with the exception of the β-actinA pair, which was excluded due to its abnormal reaction profile (**Error! Reference source not found.**). The optimal concentration of each primer in assays was 500 nM in all cases.*

Associated lineage	Gene of interest	Primer name	Forward sequence	Reverse sequence	T_a (°C)	Actual amplicon size (bp)	Amplicon T_m (°C)	Efficiency (%)	R^2 value	Working range (ng/rxn)	Reference
Housekeeping	28S ribosomal protein	h28SB	TTGAAAATCCGGGGGAGAG	ACATTGTTCCAACATGCCAG	58	100	82.5	91.5	0.997	0.024-15	(Ku et al., 2006)
	β-actin	hβ-actinB	CATGTACGTTGCTATCCAGGC	CTCCTTAATGTCACGCACGAT	60	250	86	101.9	0.996	0.0124-8	Yu et al, 2010
	GAPDH	hGAPDHD	AACATCATCCCTGCCTCTACTG	CTCCGACGCCTGCTTCAC	59	189	85	92.8	0.993	0.1-200	Kuo and Tuan 2008
Adipogenic	PPAR-γ	hPPAR-γA	GCCGAGAAGGAGAAGCTGTT	CTCGCCTTTGCTTTGGTCAG	60	140	82	99.8	0.997	0.01-19	Designed by author
	Adiponectin	hAdiponA	AAGGAGATCCAGGTCTTATTGG	ACCTTCAGCCCCGGGTAC	57	68	78	98.6	1.00	0.1-35	(Degawa-Yanauchi et al., 2005)
Chondrogenic	SOX-9	hSOX-9B	CCCATGTGGAAGGCAGATG	GAAGGTTAACTGCTGGTGTTCTGA	60	69	80	105.9	0.999	0.0124-39	Miyanishi et al, 2006
Osteogenic	RUNX2	hRUNX2A	CAGCGTCAACACCATCATTC	CAGACCAGCAGCACTCCATA	59	178	83	110.0	0.989	0.6-70	Hsu & Huang, 2013
Smooth muscle	Calponin	hCalponin A	GCATGTCCTCTGCTCACTTCAA	GGGCCAGCTTGTTCTTAACCT	60	72	83	92.7	0.998	0.02-55	(Kurpinski, Chu, Hashi, & Li, 2006)
	SM-22α	hSM-22αA	TGAAGAAAGCGCAGGAGCATA	GCCAATGACATGCTTTCC	58	71	79	104.2	0.994	0.09-55	(van Tuyn et al., 2005) and modified by LCP
	Smooth	hSM	ACCCTGCTCACGGAGGC	GTCTCAAACATAATTTGAGTCATTT	59	71	80	99.7	0.996	0.002-55	Park 2004

Associated lineage	Gene of interest	Primer name	Forward sequence	Reverse sequence	T_a (°C)	Actual amplicon size (bp)	Amplicon T_m (°C)	Efficiency (%)	R^2 value	Working range (ng/rxn)	Reference
	muscle α-actin	alpha-actin B		TCTC							
Tenogenic	Collagen III	hColIIIA	GATGTGCAGCTGGCATTCC	CCACTGGCCTGATCCATGTAT	61	101	80	97.5	0.996	0.08-50	Peach 2013
	Scleraxis	hSC	CGCACCAACAGCGTGAAC	GCGTCTCAATCTTGGAGAGCTT	61	91	85	106.4	0.995	1-100	Peach 2014
	Collagen I	hCol1C	TGGTGCAGCTGGTCTTCCA	CACGGACGCCATCTTTGC	63	92	82	101.5	0.980	0.1-75	Peach 2012

5.5 Discussion

The investigations described in this chapter were performed to devise validated qPCR assays for gene expression analyses of Tencell cultured hMSC. To enable accurate relative quantification, primer pairs must be specific to their intended target, approximately double the amount of amplicon present in the assay mixture with each cycle and give rise to C_T values in an appropriate range ($C_T = 12 - 30$).

Although primer sequences are routinely provided in published investigations (Kim *et al.*, 2009; Bai *et al.*, 2010; Kuo *et al.*, 2012; Krishnamurithy *et al.*, 2016) it is necessary to validate all primer pairs prior to use. Improper primer pair validation by previous investigators, or differing reagents/reaction conditions may mean published sequences are unsuitable for use in other studies. In spite of the previous publication of minimum standards of primer pair validation (Bustin *et al.*, 2009), there is little or no evidence available pertaining to the suitability of primer pairs used in the plethora of published relative gene expression studies (Jung *et al.*, 2016; Zhang *et al.*, 2016), and different reaction conditions used may affect assay kinetics. For example, the concentration of magnesium chlorides, which differ in different preparations, affects primer annealing, product specificity and enzyme activity (Karsai *et al.*, 2002). Nath *et al* found that increasing magnesium chloride concentration in an assay ablated the inhibitory effect caused by the inclusion of SYBR® Green I, but reduced reaction specificity (Nath *et al.*, 2000). Further highlighting the role of experimental conditions, two of the primer pairs obtained from literature searching were found to be unsuitable for use in gene expression analyses using the reagents and protocols developed (Table 5.3, Table 5.4).

Primer pairs were validated using the QuantiTect® one-step RT-PCR assay kit. In single step PCR reactions, reverse transcription of mRNA and target amplification are performed sequentially in the same reaction mixture. In this approach, reaction preparation steps are reduced and there are fewer opportunities for environmental contamination to be introduced (Wong and Medrano, 2005). The reaction profiles of assays with different primer concentrations were analysed to ensure primer pairs giving rise to normal reaction kinetics, and hence satisfying the assumptions of the comparative C_T method of relative quantification, were validated for future use (Schmittgen and Livak, 2008). Only one primer pair, β-actin A, did not generate the expected exponential reaction profile; assays of this pair did not exhibit exponential amplification. This may be explained by the fact that, ironically, excessive quantities of DNA are known to inhibit PCR; β-actin is typically expressed in large quantities

and corresponding DNA may reach inhibitory levels at early cycles (McPherson and Møller, 2006).

Although both the quantity of template material present and the degree of expression of the gene of interest influence assay kinetics, C_T values at different primer concentrations were also examined. If too high a primer concentration is used the formation of primer-dimer or secondary structure amplicons may be increasingly favoured, potentially impacting the specificity of the reaction, and too low a concentration may not produce amplification that exceeds the threshold cycle value. For the majority of primer pairs, all primer concentrations tested gave rise to exponential amplification, but the highest concentration (500 nM) was most easily distinguished from amplification in no template controls caused by environmental contamination (McPherson and Møller, 2006; Bustin *et al.*, 2009). Additionally, C_T values of some validation assays with RNA from differentiated cells, in which genes of interest are more likely to be highly expressed than Tencell cultured hMSC were high; lower primer concentrations may render the gene of interest undetectable in mechanostimulation experiments. Validation testing yielded no evidence that lowering the primer concentrations used reduced nonspecific binding; all primer pairs giving rise to multiple peaks in dissociation plots did so consistently for all conditions tested. Therefore, primer concentrations of 500 nM were used in all subsequent gene expression analyses.

Efficiency testing of primer pairs for genes of interest must be conducted to ensure that the assumptions of the comparative C_T method, which require that the amount of amplicon produced approximately doubles with each cycle, are satisfied (Huggett *et al.*, 2005; Schmittgen and Livak, 2008). Any differences in normalised C_T values between experimental conditions must be caused by changes in gene expression, and not by variable reaction kinetics, to ensure validity of gene expression data.

Primer pair specificity and amplicon identity were validated by examining dissociation plots and gel electrophoresis respectively. Both techniques may be used to determine the number of amplicons produced in a qPCR assay, but fluorescence detection of products is considerably more sensitive than gel electrophoresis. Additionally, amplicons generated in low quantities or of small size, such as products arising as a result of nonspecific binding or primer-dimers, may not be detected by gel electrophoresis. Primer pairs should be fully complementary to only the target sequence, but may bind to other sequences of mRNA more weakly. Further, DNA polymerases are known to be active at low levels at annealing temperatures, and extend primers as soon as annealing occurs – even if primers are weakly hybridised to the incorrect sequence (McPherson and Møller, 2006). In theory, for primer pairs producing multiple

amplicons, raised annealing temperatures may disfavour this less complementary binding (Edwards *et al.*, 2004; McPherson and Møller, 2006). The fact that the number of amplicons generated, and hence the degree of nonspecific binding, was not reduced by raising the annealing temperature for any case of primer nonspecificity indicates that for inadequately designed primers, nonspecific binding is frequently thermodynamically favoured over annealing the target sequence. It is possible that the energetic barrier for such events is frequently smaller than the reduction in potential energy conferred by the more numerous/stronger hydrogen bonds formed upon binding a fully complementary sequence (Atkins and De Paula, 2010).

Despite its relative lack of sensitivity compared to fluorescence detection, analysis of assay products by gel electrophoresis was performed to validate the identity of amplicons generated. For this purpose electrophoresis was used to determine the size of the amplicons produced for comparison with those predicted *in silico* by BLAST. Although amplicon identity can be definitively proven only by sequencing (Adams *et al.*, 1991; Cernomaz *et al.*, 2016), the production of a different amplicon of the same size as the intended product is highly improbable and validation by gel electrophoresis was deemed sufficient for these purposes.

Several housekeeping genes, coding for GAPDH, β-actin and 28s ribosome, were successfully validated as efficient and specific. Only one housekeeping gene is absolutely necessary for normalisation of gene expression, although the inclusion of several is advantageous. By definition, housekeeping genes should display highly uniform expression throughout the cell cycle and under varying environmental conditions (Jain *et al.*, 2006). Other investigators have shown that β-actin and GAPDH expression is not stable with respect to culture conditions in every instance, and is altered by factors such as the serum concentration used, and critically, mechanical stimuli (Schmittgen and Zakrajsek, 2000; Rauh *et al.*, 2015). Hence, only the validated 28s ribosome primer pair was used as the internal control in all subsequent gene expression analyses.

The use of only one reference gene in these investigations must be acknowledged as a major limitation, and should be remedied in any future work. Ideally, a selection of housekeeping genes should be tested and the pair of genes found to alter the least between conditions used for normalisation. For this study, the C_T values of potential housekeeping genes from each sample type (strained, static, seeded-only and unseeded suspension cells) of each strain condition experiment could have been found and checked for variability. This may be analysed using software packages such as BestKeeper©, geNorm and NormFinder (Vandesompele *et al.*, 2002; Andersen *et al.*, 2004), or perhaps more simply, by calculating the coefficient of

variation for each candidate (Rauh *et al.*, 2015). Previous reports by Rauh *et al* and Li *et al* employed these methods to find normalisation genes for studies of MSC cultured on three-dimensional acellular matrices, and to compare foetal- and bone-marrow derived MSC respectively (Li *et al.*, 2015; Rauh *et al.*, 2015). Interestingly, both reported disagreement between the different software packages, but peptidylprolyl isomerase A (PPIA) was found to be one of the stablest normalisation candidates by both. Since the stability of 28S expression with respect to normalisation has, to the author's knowledge, never been tested, it is suggested that it be examined using the techniques described alongside PPIA and other genes reported as stable, such as hypoxanthine phosphoribosyltransferase 1 (HPRT1) and TATA box binding protein (TBP) (Li *et al.*, 2015; Rauh *et al.*, 2015). This enhanced rigour in the selection of housekeeping genes may remove bias from dependent gene expression data.

Chapter 6: Validation of the Tencell Apparatus for use as a Tensile Strain Bioreactor

6.1 Introduction

The work described in this chapter focussed on the re-engineering and validation of a uniaxial strain bioreactor. Bioreactors are widely used in contemporary tissue engineering for large-scale mammalian cell expansion, as required to deliver cell therapy products at industrial scales (Rafiq *et al.*, 2013; Heathman *et al.*, 2016; Zhao *et al.*, 2016), for the culture of tissue-engineered constructs or in fundamental studies examining the impact of applying specific stimuli (Zhao *et al.*, 2016). Bioreactors may also be used for other applications; the first report of bioreactor use concerned the microbial oxidation of hydrocarbons (Einsele and Fiechter, 1969).

In tissue engineering, bioreactors are frequently used to impart physical forces to cell-seeded substrates. In cartilage tissue engineering shear, perfusion, hydrostatic pressure and compression forces may be applied; vascular tissue such as stents, valves and bypass grafts may also be manufactured using bioreactors (Morticelli, 2013; Schmidt and Tranquillo, 2016); skin may be cultured using expanding bioreactors for skin grafts and rotating culture systems, and nerve conduits may be engineered (Zhao *et al.*, 2016). Crucially, bioreactors are also frequently used to apply uniaxial or biaxial strain (Morticelli, 2013; Lei and Ferdous, 2016). Since many tissues, including heart, heart valves, arteries, muscle, bone, tendon and ligament, experience strain as part of their *in vivo* function(s), it is logical that such bioreactors may be necessary to replicate the cellular niche in which these tissues develop and maintain homeostasis.

Bioreactor systems typically comprise an actuating, motion-transforming unit to apply the desired stimulus, monitoring and control systems, a sample culture chamber to provide the appropriate culture conditions and a nutrient exchange system (Lei and Ferdous, 2016). In common with standard cell culture incubators, bioreactors must maintain an appropriate

temperature (36- 37 °C), gaseous environment (5 % (v/v) CO_2 in air) and humidity to maintain cell viability (Ham and Puck, 1962; Hayflick, 1965).

The Tencell apparatus is a bespoke, uniaxial strain bioreactor with actuating units comprised of displacement arms that may be attached to the tissue clamps to apply strain to substrates. The displacement arms are fixed to a single moving bar inside the apparatus casing, which in turn is displaced by a piston. The culture chambers consist of open stainless steel culture wells affixed to a heating base and enclosed by the latter and a heated perspex lid (Fig. 6.1A, Fig. 2.2). The medium composition, heating base and corresponding controller, humidifying and gassing apparatus must maintain optimal culture conditions. There is no nutrient exchange system, so Tencell culture regimes must be carefully designed to avoid or facilitate manual medium changes. Note that some of the bioreactor components described in this introduction and Fig. 6.1 were modified/introduced as a result of the work package described in this chapter.
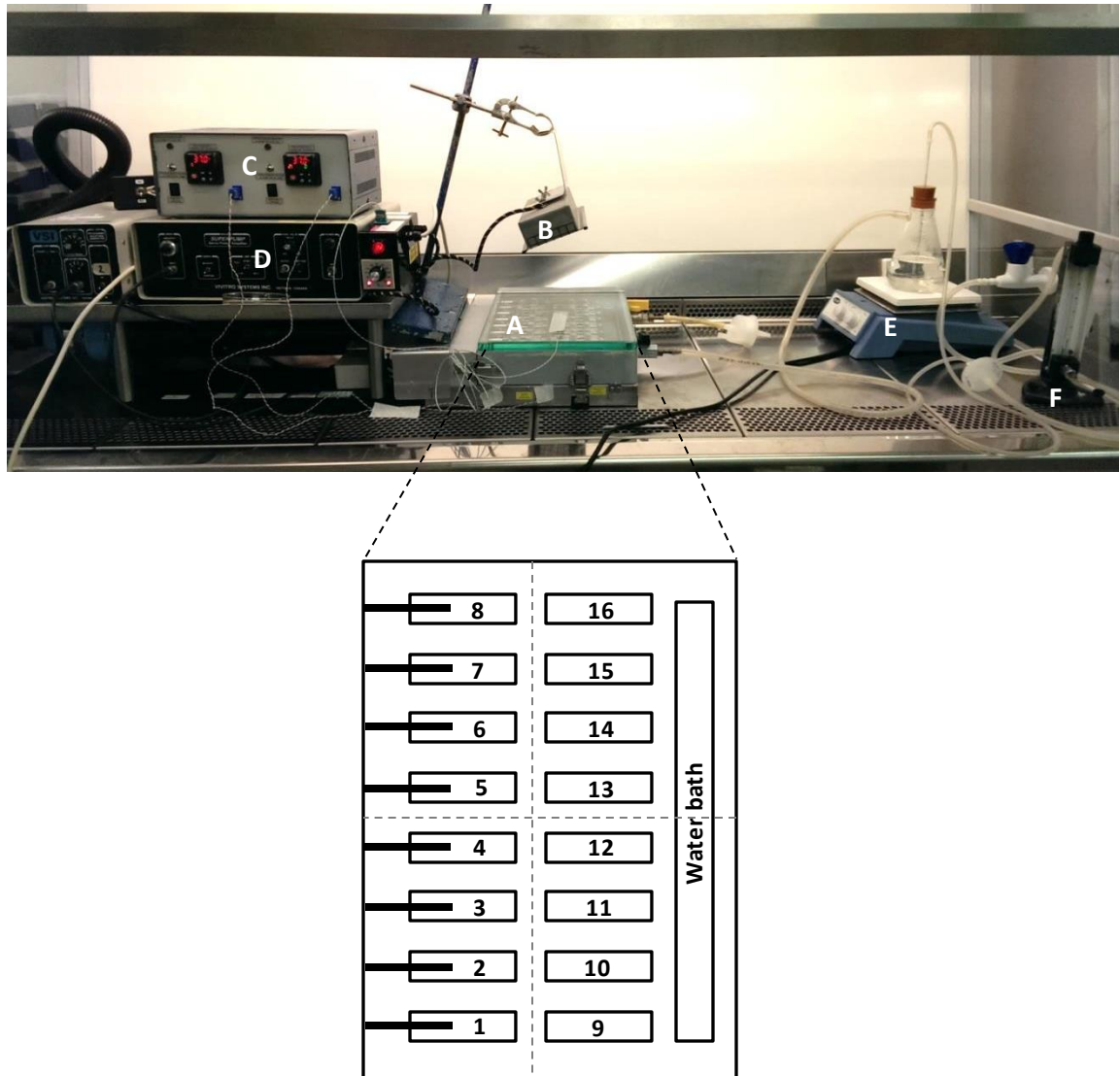
Fig. 6.1: Photograph of the Tencell bioreactor, and schematic of the culture chamber from above, of the Tencell apparatus following the validation works performed in this chapter. *Tencell consists of 16 cell culture wells affixed to a heated base (A, schematic). Both static controls (n=6) and strained samples (n=6) are cultured simultaneously. The water bath and wells 1, 8, 9 and 16 contain water during operation to maintain chamber humidity. A Perspex lid is clamped to the heating base during use and is heated during experiments by the heat lamp (B). Following temperature regulator replacement to the EZ-zone PM device, as described in this chapter, the heating base casing contained 4 ceramic heating elements controlled by the temperature regulation unit (C). The heating elements are located in each quadrant of the base, as indicated by dashed lines in the schematic. Displacement of the arms is controlled via the displacement module (D), on which the amplifier knob used to select the magnitude of displacement is located. Humidifying apparatus, consisting of a flask of sterile water heated by a hot plate and connected to Tencell by sterile tubing, was introduced during the works described in this chapter to solve the problem of culture medium evaporation (E). The bioreactor is gassed through taps on the perspex lid at the outset of culture only (F). Tencell is operated within a class II cabinet to ensure sterility of the culture environment.*

6.2 Aims and objectives

6.2.1 Aim:

The aim of the investigations described in this chapter was to re-engineer and validate the Tencell bioreactor for the culture and mechanostimulation of hMSC-seeded scaffolds, with particular regard to the maintenance of appropriate temperatures, medium osmolality and accurate arm displacement.

6.2.2 Objectives:

- To measure and optimise the temperature maintained in the Tencell culture wells

- To find the relationship between the actual displacement of the Tencell arms and that selected using the amplifier knob on the displacement module

- To measure and reduce fluid loss from the Tencell culture wells due to evaporation

- To validate the cell culture approach devised from the above testing packages with respect to cell viability following Tencell culture

6.3   Experimental approach

The Tencell bioreactor was validated with respect to temperature maintenance, arm displacement and fluid loss to render it suitable for the culture and mechanostimulation of hMSC-seeded acellular pericardia.

The temperature maintained in culture wells of the Tencell apparatus using both Tempatron dtc410 and EZ-zone PM heating controllers to establish a heating regime that equally maintains stable temperatures conducive to cell culture (36 – 37 °C) between all wells. The actual arm displacement by arm as compared to that selected using the displacement module was measured to assess the accuracy of the strains applied in subsequent mechanostimulation investigations, and the variation in strain applied, and hence error, between experimental replicates. The degree of fluid loss from Tencell wells was measured, both with and without evaporation reduction measures, to devise an experimental protocol for hMSC culture in Tencell that maintains the osmolality of cell culture medium. The experimental protocol designed according to the validation work packages previously described was tested by measuring the viability of pericardium-seeded hMSC after bioreactor culture to validate its suitability as a cell culture system, and make any adjustments found to be necessary.

6.4   Results

6.4.1   Temperature regulation in Tencell culture wells

Validation of temperature regulation in Tencell culture wells was performed to determine whether temperatures suitable for cell culture (36 – 38 °C) were maintained within the apparatus.

6.4.1.1   Temperature maintenance using the Tempatron dtc410 temperature controller

The temperature maintained in the Tencell apparatus using the Tempatron dtc410 regulator was measured as previous investigations by coworkers indicated that overheating of cell culture wells may occur (Dr Andrew Aldridge, personal communication).

The temperature of four cell culture wells, located in each quadrant of the heating base and thus heated by different heating elements, was measured overnight (Fig. 6.2, Fig. 6.1). Temperatures in cell culture wells did not equilibrate for the duration of the experiment and cycled in the range 34.5 – 39.5 °C. Each heating and cooling cycle lasted ~ 15 minutes. There was no apparent difference in temperature maintenance between the wells tested, and hence heating behaviour between different heating elements.
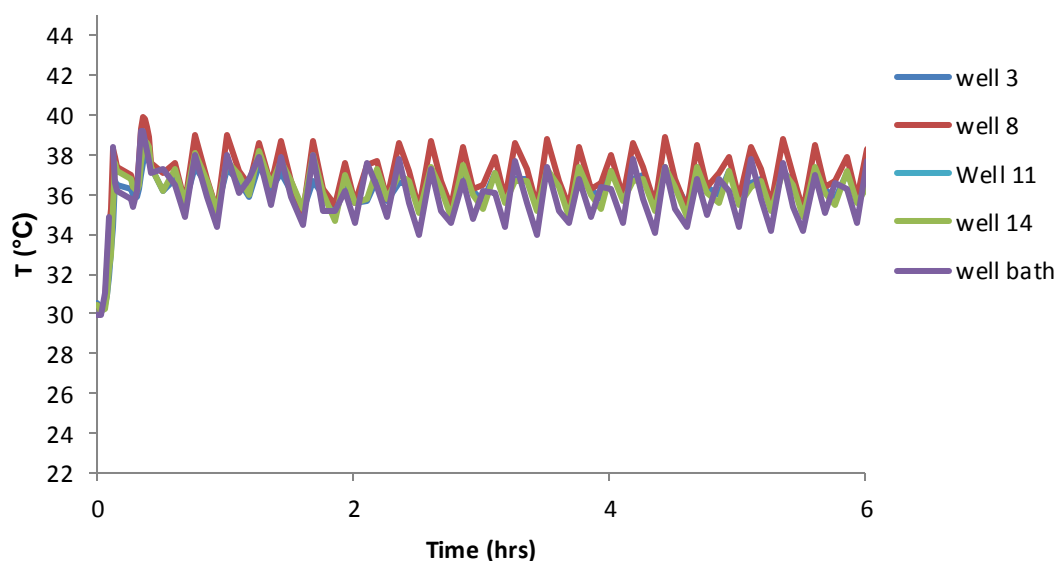
Fig. 6.2: Temperature control in the Tencell apparatus with the Tempatron dtc410 temperature controller. *A steady optimal temperature (36 − 38 °C) was not maintained. The temperature inside cell culture wells cycled between 34.5 and 39.5 °C for the duration of temperature control. Data shown as measured by each probe.*

6.4.1.2   Temperature maintenance using the EZ-zone PM temperature controller

The EZ-zone PM heating regulation system, operating with two heating elements housed in the heating base, was fitted to the Tencell bioreactor to improve temperature maintenance in the apparatus. The temperature maintained by this system was validated with respect to optimal cell culture temperatures (36 − 38 °C) before and after heating regime optimisation by instrument autotuning.

The temperature of culture wells regulated by the EZ-zone PM controller prior to autotuning was not steadily maintained in the optimal range; there was an initial spike of temperature, reaching a maximum of 44 °C, followed by inconsistent heating thereafter (Fig. 6.3). However, repetitive temperature cycling, as observed with the use of the Tempatron dtc410 controller, did not occur. Temperature regulation differed between different wells following the initial heating period, with a maximum variation in temperature of ~ 2 °C over the duration of the experiment within individual wells not monitored by the EZ-zone PM system (3, 11), but very little variation in individual wells fitted with thermocouples for reporting to the controller (8, 14).

The temperature maintained in culture wells following autotuning of the EZ-zone PM controller was satisfactorily maintained; there was an initial spike of temperature, but the maximum temperature reached was within limits conducive to cell culture (37.5 °C) (Fig. 6.4). Following initial heating, the temperature of individual wells was maintained consistently (T variation ≤ 1 °C with wells for the duration of monitoring) but differences between individual wells were apparent; wells 3 and 11 were maintained at approximately 34.5 − 35.0 °C, whereas well 14 and well 8 were maintained at approximately 36 and 37 °C respectively.
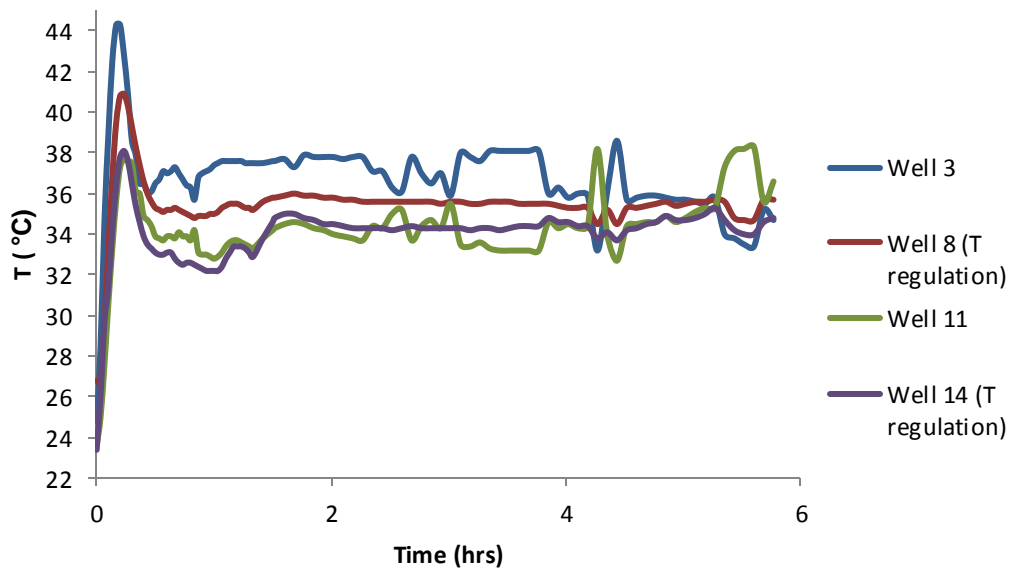
Fig. 6.3: *Temperature control in the Tencell apparatus with the autotunable EZ-zone PM temperature controller, but prior to heating regime optimisation.* *A constant optimal temperature was not maintained; there was an initial period of very excessive overheating, reaching a maximum temperature of ~ 44 °C, followed by inconsistent temperature maintenance thereafter. The temperature maintained within the apparatus did not cycle repetitively, as observed when the Tempatron dtc410 heating controller was used (Fig. 6.2).*
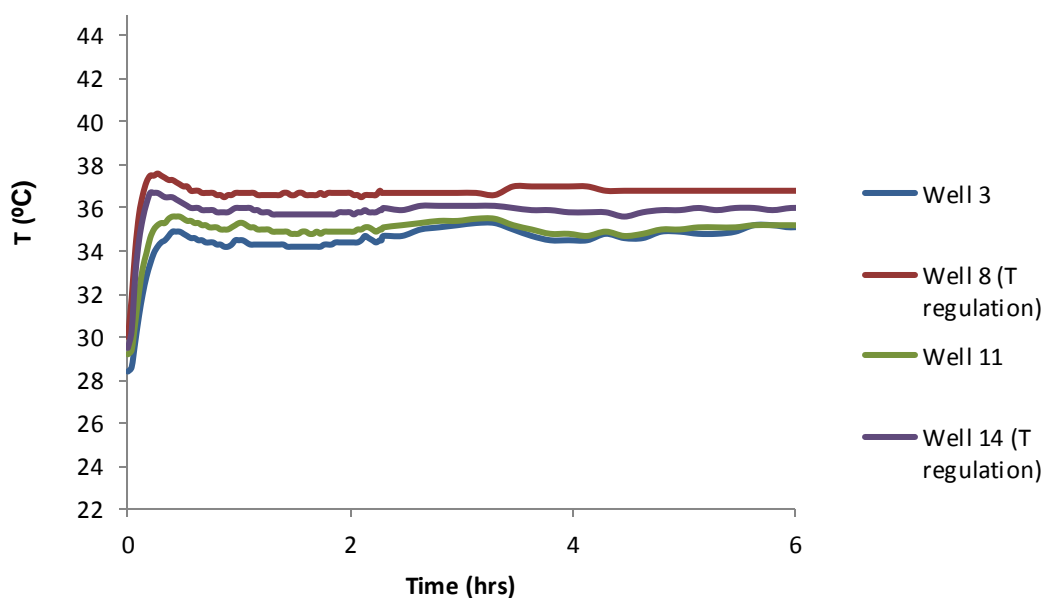
Fig. 6.4: Temperature control in the Tencell apparatus using the EZ-zone PM temperature controller after autotuning. *There was an initial period of higher, but not excessive (max. T ~ 37.5 °C), heating. The temperature maintained thereafter fluctuated within an acceptable range and remained within levels conducive to hMSC culture.*

6.4.2 Fluid loss in Tencell culture wells

Fluid loss in Tencell culture wells was measured to find the degree of evaporation over the culture period to be used in subsequent gene expression analyses. Fluid loss should be minimised to maintain medium osmolality.

A calibration curve of liquid depth above the tissue surface and the volume of medium added was prepared to find the amount of culture medium that should be added to Tencell wells (Fig. 6.5) to achieve a maximum depth of 3 mm above the seeded surface. Depth calibration was originally performed using wells that were not attached to the displacement arms of the bioreactor. However, lifting of the tissue clamps was apparent on attachment, meaning that original calibration data, indicating an optimal culture medium volume of 4.0 mL in the Tencell wells, was not relevant to cell culture conditions in Tencell (Fig. 6.5A). Additionally, the R^2 value of the linear regression fitted to these data was 0.97, below the value of 0.98 generally accepted to indicate adequate goodness of fit (Dytham, 2011). Calibration data obtained with culture wells fitted *in situ* indicated that a culture medium volume of 5.5 mL has the optimum depth of 3 mm above a seeded pericardial substrate (Fig. 6.5B), and the R^2 value of the line of best fit produced by linear regression analysis was acceptable (R^2=0.99).
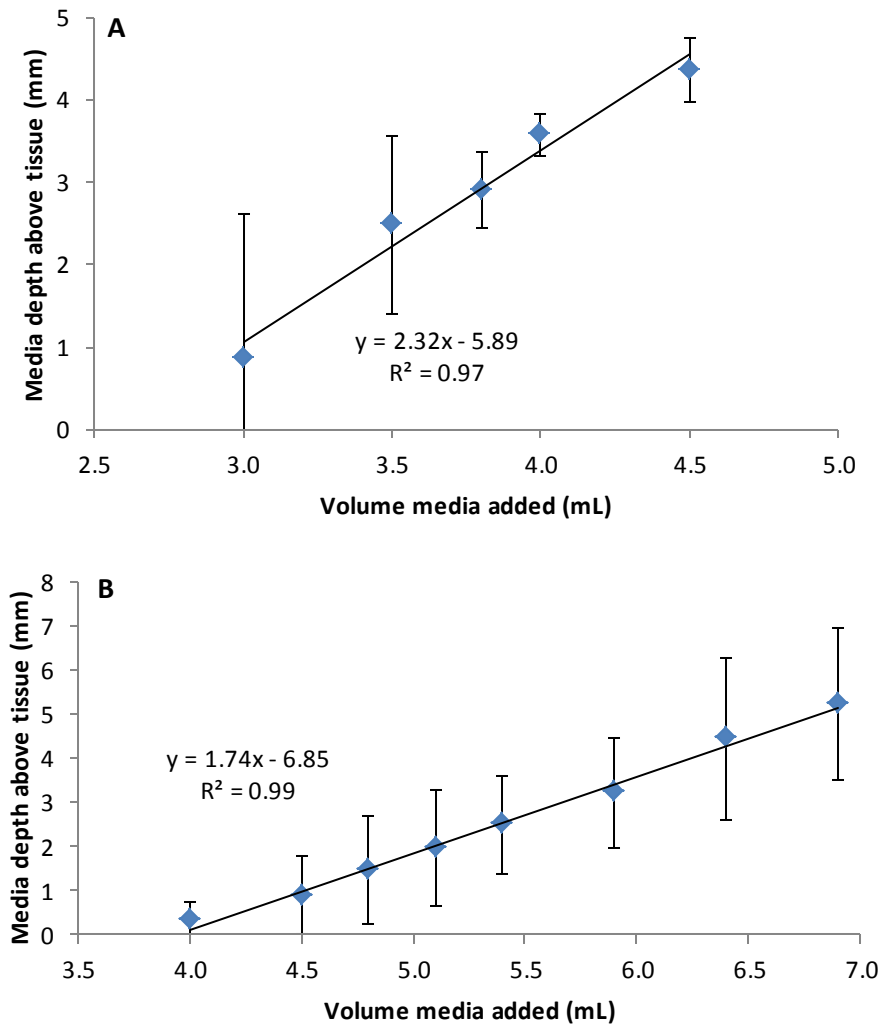
Fig. 6.5: Calibration graph of the relationship between culture medium depth above the empty clamp (A) tissue surfaces (B) and the volume of media added. *Testing was conducted both without (A) and with (B) mock tissue fitted into the Tencell culture wells, and absorption of the medium by the tissue was found to impact results. According to (B), which better represents conditions during Tencell culture of seeded substrates, approximately 5.5 mL media should be added to Tencell culture wells to achieve an optimal depth above the seeded surface of 3 mm.*

The total volume of culture medium retained in culture wells following mock Tencell cultures was measured to find the percentage fluid loss using the optimal volume of culture medium. In order to measure fluid loss, tissue clamps, and a small volume of adherent culture medium were removed from culture wells. The proportion of fluid lost due to this method of measurement was found to be 11 ± 1 %. Hence, any measured fluid loss from Tencell wells following culture ≤ 12% may be deemed negligible and not the result of medium evaporation.

In previous investigations with the Tencell bioreactor, coworkers added a larger volume of water (120 mL) to the water bath for chamber humidification. To increase the surface area to

volume ratio, and encourage evaporation of this reservoir in place of fluid loss from culture wells, this volume was decreased to 50 mL. Mean fluid loss from Tencell culture wells over 24 hours in the presence of this lesser volume (50 mL) only was 24 ± 4 %, but anecdotal reports suggest that the previous approach resulted in up to 90% culture well fluid loss.

Culture well fluid loss was further reduced to 12 ± 3 % through the use of humidifying apparatus (Fig. 6.1), but was 33 ± 1 %. following a longer culture period of 72 hours. Hence, culture medium evaporation was reduced to negligible levels by using the humidifying apparatus described in section 2.2.12.4.2 for cultures of 24 hours but was not sufficient to prevent a significantly greater ($p < 0.001$) fluid loss from the method of measurement alone for 72 hour cultures.

6.4.3 Displacement of Tencell arms

Actual displacement of uniaxial strain arms was validated with respect to the strain selected using the amplifier dial. Trendline equations for all arms were similar and suggest that the degree of strain applied to different experimental replicates does not differ significantly, but the mean gradient and intercept values of strain arms was significantly different from their expected true values of 1.0000 and 0.0000 respectively ($p < 0.001$) (Fig. 6.6).
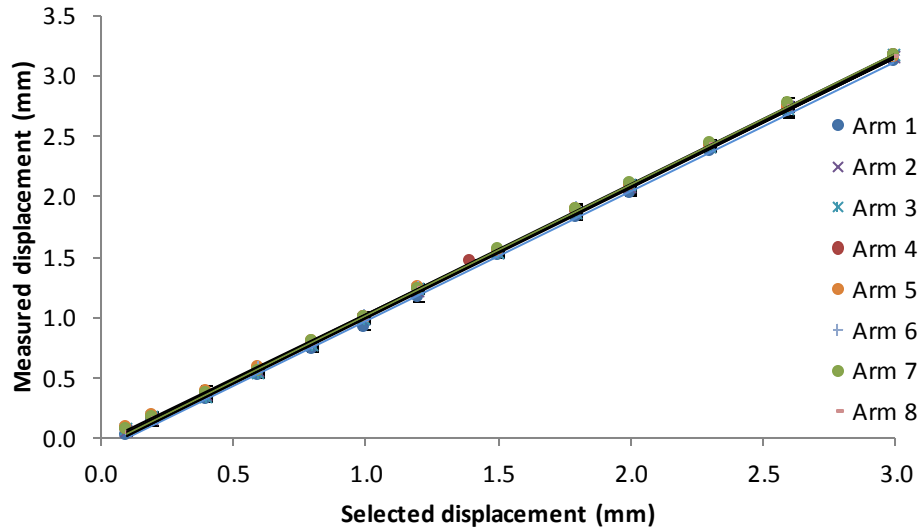
Displacement arm	Trendline equation
1	y = 1.0729x - 0.1116
2	y = 1.0764x - 0.0801
3	y = 1.0771x - 0.0787
4	y = 1.074x - 0.0622
5	y = 1.066x - 0.0436
6	y = 1.0773x - 0.0564
7	y = 1.0829x - 0.0655
8	y = 1.0802x - 0.0841

Fig. 6.6: Calibration graph and trendline equations (table) showing the measured displacement of Tencell arms compared to the displacement selected using the amplifier dial. Trendline equations were similar between different arms, but the mean gradient and intercept value were significantly different from the true values of 1.0000 and 0.0000 respectively ($p < 0.001$ for both). Statistical analysis done by one sample Student's t test.

6.4.4 Viability of Tencell cultured human multipotential mesenchymal stromal cells

The viability of Tencell cultured hMSC was examined to develop an optimal protocol for cell culture using this apparatus. During initial investigations, seeded substrates were cultured for 24 hours with hMSC culture medium following initial humidification and gassing of the culture chamber (CO_2 in air; 5 % (v/v)). There was a significant loss of cell viability of hMSC cultured in the apparatus compared to seeded tissue ($p < 0.001$) (Fig. 6.7).

Loss of cell viability during culture may be caused by issues regarding the cells and/or materials used or unsuitable environmental conditions. Tencell parts (clamps and culture wells) were tested for cytotoxicity since temperature maintenance, evaporation and cell viability of hMSC stocks were previously confirmed acceptable.
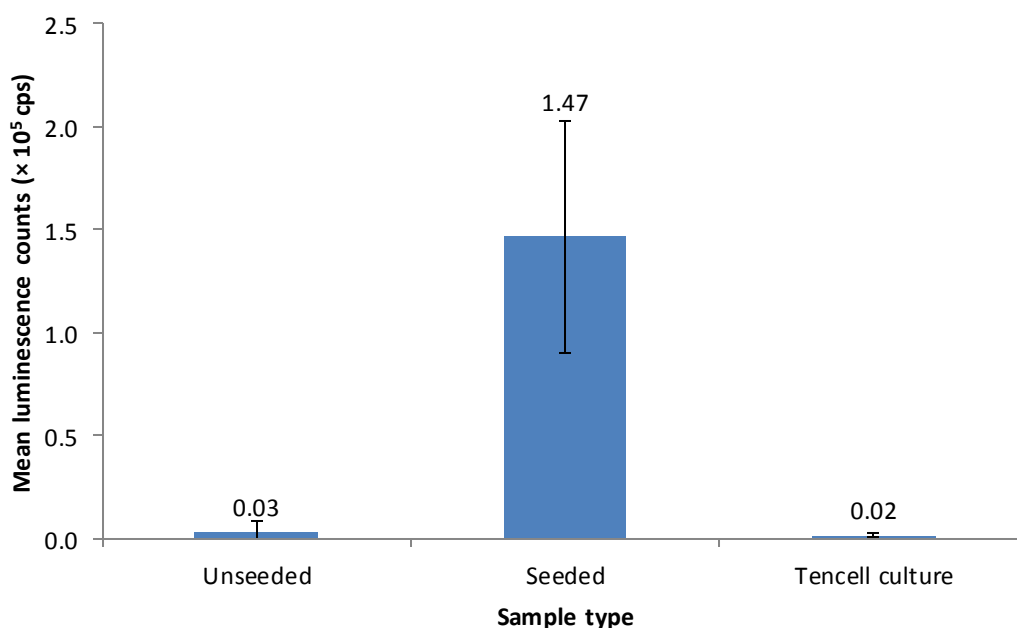
Fig. 6.7: Mean luminescence counts, as detected by the ATPlite™ assay, by sample type comparing the survival of Tencell cultured hMSC with those seeded and cultured in a standard cell culture incubator. *There was a statistically significant difference between the luminescence counts of seeded scaffolds and other sample types, but there was no statistically significant difference between unseeded and Tencell scaffolds (p < 0.001). Statistical analysis done by ANOVA and Tukey's post-hoc test. Data presented as means with 95% confidence limits.*
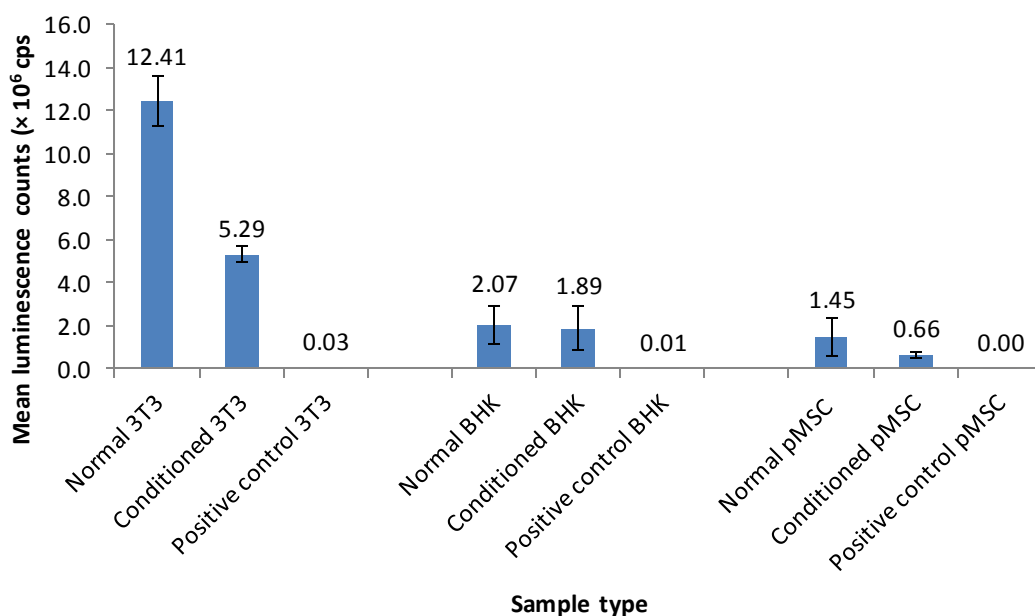
Fig. 6.8: Chart showing the luminescence counts of 3T3, BHK and porcine multipotential mesenchymal stromal cells grown in the appropriate unconditioned complete culture medium and those grown in Tencell seeding ring conditioned medium, as measured by the ATPlite™ assay. *Positive control medium contained DMSO (40% (v/v)).There was a statistically significant difference between luminescence counts of all 3T3 sample types (p < 0.001), but only between positive controls and other sample types for BHK and pMSC cultures (p < 0.001 and = 0.010 respectively). Data presented as means with 95% confidence limits.*

There was a statistically significant difference between luminescence counts of all sample types for 3T3 cells but between positive controls and other sample types for BHK cells and pMSC only. Hence, although a reduction in cell viability could be discerned, there was no statistically significant difference between pMSC cultured in Tencell conditioned and normal culture medium. There were no visible particulates following conditioning of Tencell components. No microbial growth was observed on any culture plate or in any culture broth inoculated with test media, whereas extensive microbial growth was apparent in positive controls.

In addition to evaporation, the pH of culture medium may be affected by the gaseous environment of a bioreactor. The effect of the inclusion of HEPES (25 mM), which is more robust to changes in atmospheric composition than sodium bicarbonate (Good *et al.*, 1966), in culture medium on cell viability was investigated. Cell viability of seeded substrates cultured in the Tencell bioreactor, which was gassed only during apparatus setup, and of substrates cultured in a standard cell culture incubator were compared. There was no significant difference in the luminescence counts of samples cultured in either environment,

but luminescence counts of unseeded tissue were lower that that of all other sample types (p = 0.002).
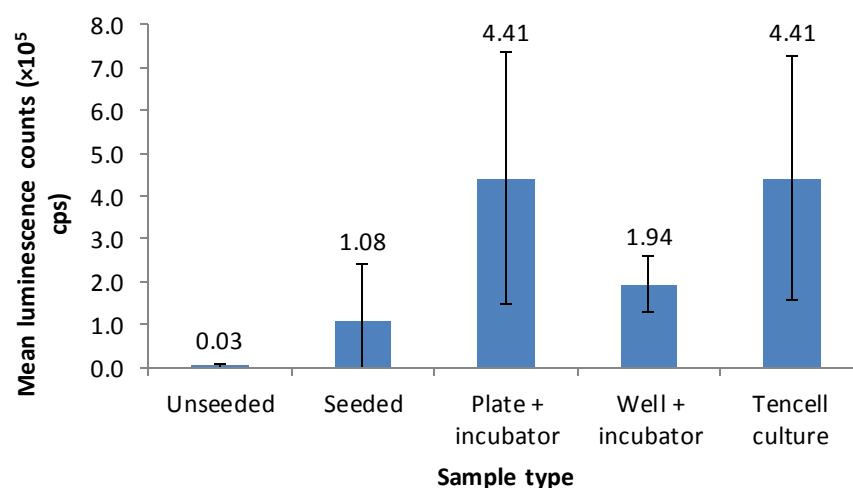
Fig. 6.9: Mean luminescence counts of hMSC cultured in the Tencell apparatus as compared to counts of unseeded and seeded tissue, and seeded scaffolds cultured in a 6 well plate and Tencell wells in a cell culture incubator. *Cell culture medium was buffered with HEPES (25 mM). There was no statistically significant difference between scaffolds cultured in the Tencell apparatus and those cultured in 6 well plates and Tencell wells in a cell culture incubator, but luminescence counts of unseeded scaffolds were significantly lower than other sample types(p = 0.002), indicating that the high luminescence counts recorded can be attributed to the presence of live cells on all other sample types, and not interfering reactivity of the scaffold. The lack of significant difference in luminescence counts between cells cultured in the Tencell bioreactor and those cultured in Tencell wells inside a standard cell culture incubator indicates that environmental conditions (temperature, pH, pCO_2) inside the bioreactor were adequate to maintain cell viability. A lack of significant difference between viability of samples cultured in Tencell wells and 6-well plates inside a standard cell culture incubator indicates that the Tencell culture well was not cytotoxic to the constructs.*

6.5 Discussion

The investigations conducted in this chapter were concerned with re-engineering and optimising the Tencell bioreactor to achieve optimal physico-chemical conditions for cell culture, and to validate the displacement applied to tissue substrates by the Tencell arms.

In common with early efforts in *in vitro* cell culture (Ham and Puck, 1962; Good *et al.*, 1966), the temperature, culture medium pH and gaseous environment maintained during operation of the Tencell bioreactor must be carefully validated. The cell culture environment must support good cell viability and avoid influencing cell functionality, especially gene expression.

It was found that the Tencell bioreactor did not stably maintain an appropriate (36 − 37 °C) temperature in cell culture wells prior to replacement and autotuning of the heating controller. The Tempatron dtc410 temperature regulator maintains culture well temperature in an on/off fashion − it is only able to activate and deactivate the associated heating elements, unlike the EZ-zone PM device, which adjusts the heating regime used to regulate temperature as required. If cell cultures are exposed to unsuitable temperatures, both cell viability and differentiation potential of hMSC may be affected. Previous investigators have reported significant losses of hMSC viability at raised temperatures (Bronzini *et al.*, 2012; Reisiss *et al.*, 2013). Although Reisiss *et al* reported that MSC survived temperatures of 48 °C for up to 150 seconds, temperatures significantly higher than 37 °C are extremely unlikely to be tolerated for extended periods of time as employed in this project (Reisiss *et al.*, 2013). Moreover, the full effects of suboptimal temperatures on hMSC viability are not completely understood and are frequently studied in the context of transplantation; hMSC tested are often in parenteral substances, and are most often examined at temperatures lower than 37 °C only, so such studies may not accurately model the impact of temperature changes in the cell culture environment (Pal *et al.*, 2008).

It has been widely reported that the differentiation potential of hMSC may be affected by a multitude of factors, in addition to physical stimuli. Crucially to this project, culture of hMSC at different temperatures impacts their differentiation potential, particularly with respect to the osteogenic lineage (Chen, 2009; Hee-Hoon, 2015). Additionally, the equilibrium position of the weak buffers used in culture media may be altered by temperature changes, in turn changing the pH of the culture medium, which must be maintained in the range 7.2-7.4 (Eagle, 1971).

In order to attribute cellular changes such as differentiation to applied strains and exclude the influence of other factors, investigators must also be sure that the composition of the culture medium remains constant for the duration of an experiment in a bioreactor system. Cell culture medium is designed with an osmolarity that renders it an isotonic solution with respect to cells; if concentrated by evaporation, increased salt molarity induces osmosis from the cytoplasm to the cell exterior (Waymouth, 1970). In fact, treatment with hypertonic solution is often a key stage of the decellularisation of fresh tissues as this process readily kills cells (Gilbert *et al.*, 2006; Mirsadraee *et al.*, 2006a). In addition, in the case of high levels of evaporation, the medium level in culture wells may fall below the level of the substrate clamps and result in drying of cell-seeded scaffolds. Hence, culture systems in which medium is not constantly replaced must be designed to prevent medium evaporation.

It is logical that a system comprising open culture wells may be prone to fluid loss from evaporation. However, using simple humidification apparatus was sufficient to reduce culture well evaporation to minimal levels. It is likely that the internal environment of the bioreactor becomes saturated with water vapour, and evaporation of culture medium is consequently disfavoured.

Despite confirming that temperature regulation and fluid loss were within acceptable bounds, and that the was no significant cytotoxic effect from the Tencell culture wells, there was a loss of cell viability of matrix-seeded hMSC cultured in Tencell. Since all other critical culture conditions had been satisfactorily validated the possibility of inadequate pH regulation was investigated. Sodium bicarbonate in culture media is able to buffer the pH within acceptable bounds only in the presence of sufficient CO_2, and is routinely used in cell culture incubators that have a constant supply of CO_2 (5 % (v/v) in air). In contrast, the Tencell bioreactor was gassed with this mixture at the outset of culture only, after which the partial pressure of CO_2 probably decreases significantly. In media buffered with sodium bicarbonate, as is the case in this study, a lack of CO_2 can raise the pH to approximately 8.0 by altering which of two possible buffer reactions of sodium bicarbonate dominates.

Where a constant supply of CO_2 is not feasible, other buffers, such as HEPES, may be used to lower the pH of bicarbonate-buffered cultures (pK_a = 7.55) (Good *et al.*, 1966; Eagle, 1971). In these studies, Tencell cultured scaffolds maintained cell viability comparable to that of matrices cultured in traditionally gassed incubators.

The measured displacement of Tencell arms was found to be in very good agreement with that selected using the amplifier knob. Whilst the values of the gradient and intercept of these

graphs differed significantly from their 'true' values of 1.000 and 0.000, it is unlikely that the measurement approach used is able to approach this degree of accuracy. For example, the amplifier knob (Fig. 2.3) has an analogue display and the accuracy of the displacement selected was reliant on human judgement. Perfect fixation of the dial gauge during measurement is also unlikely; it is possible that some of the kinetic energy imparted by the displacement arms was transferred into small movements of the dial gauge apparatus as a whole, and not wholly into movement of the measurement needle. Additionally, it was not possible to measure the displacement of different arms simultaneously, so apparent differences between arms may be the result of minor differences in experiment setup between arms. Overall, as compared to the comparatively high degree of variation in biological systems, differences between calibration data and true values were considered acceptable for the purposes of this project.

Chapter 7: Mechanostimulation and gene expression analyses of hMSC-seeded pericardial matrices

7.1 Introduction

The investigations described in this chapter aimed to devise a mechanostimulation regime for hMSC seeded on pericardium matrices that maintained cell viability, and to find any differences in gene expression between strained and unstrained samples cultured in the Tencell bioreactor.

Whilst ample evidence of mechanosensitivity of hMSC has been reported (Altman *et al.*, 2002a; Discher, 2005; Butler *et al.*, 2008; Chen, 2010; Park *et al.*, 2011b; MacQueen *et al.*, 2013; Haase and Pelling, 2015), no studies have examined the differentiation of hMSC in biologically-relevant acellular matrices to date (Friedl *et al.*, 2007; Ren *et al.*, 2008; Sen *et al.*, 2008), and very few studies have examined hMSC differentiation towards the smooth muscle lineage for any approach (Park *et al.*, 2004). Application of strain may affect cell viability if the regime is not validated prior to use (Reisiss *et al.*, 2013); cells must be maintained within optimal cell culture conditions to prevent changes in gene expression as a result of factors other than the treatment applied.

Gene expression may be quantitated as relative to internal or external standards in relative and absolute quantification respectively (Bustin, 2000; Edwards *et al.*, 2004; Huggett *et al.*, 2005; McPherson and Møller, 2006; Bustin *et al.*, 2009). Absolute quantification involves the generation of standards curves to elicit gene copy number information from C_T values, and is comparatively onerous for investigators. Where exact gene copy numbers are not the metric of interest, it is satisfactory to report the change in expression of genes between sample types.

The comparative C_T method of relative quantification of qPCR data relates C_T values for genes of interest to those of housekeeping genes, also known as internal controls, expected to remain constant regardless of culture conditions (Schmittgen and Zakrajsek, 2000; Wong and

Medrano, 2005; Schmittgen and Livak, 2008). This normalisation process corrects for differences in the overall rate of mRNA synthesis and the quantity of template material added to assays (Eqn. 7.1).

$$\Delta C_T = C_{T(gene\ of\ interest)} - C_{I(housekeeping\ gene)}$$

Eqn. 7.1: Calculation of corrected C_T values, or ΔC_T from gene of interest and housekeeping gene threshold fluorescence data.

Gene expression data for experimental replicates investigated during the same experiment can be plotted by sample type with confidence limits as $2^{-\Delta CT}$ data (Wong and Medrano, 2005; Schmittgen and Livak, 2008). To obtain fold change data, calculated as $2^{-\Delta\Delta CT}$ values, ΔC_T data from treated and untreated (or endogenous control) samples are compared mathematically as given by Eqn. 7.2.

$$\Delta\Delta C_T = \Delta C_{T\ (treated\ sample)} - \Delta C_{T(untreated\ sample)}$$

Eqn. 7.2: Mathematical comparison of corrected C_T values of treated and untreated samples to obtain fold change values

In the Tencell experimental setup, there is no scientifically valid justification for the pairing of any particular pair of strained and unstrained experimental replicates. Therefore, fold change data can be calculated from the mean of all strained and endogenous control samples within an experiment, to obtain a single value of $2^{-\Delta\Delta CT}$. Therefore, Tencell experiments must be performed in triplicate for each strain condition examined. This was not practicable in this project due to the time constraints and high workload associated with performing a total of nine bioreactor experiments, and fold change data is presented in this chapter for reference only.

7.2   Aims and objectives

7.2.1 Aim:

The aim of the experiments described in this chapter was to validate a suitable mechanostimulation regime for pericardium-seeded hMSC cultured in Tencell, and to determine whether their differentiation potential towards the adipogenic, osteogenic, chondrogenic, tenogenic and smooth muscle lineages is altered by the application of different magnitudes of strain.

7.2.2 Objectives:

- To quantify the viability of hMSC strained for time periods of 24 and 4 hours using the ATPlite™ assay, and select a strain duration that maintains good cell viability for mechanostimulation studies

- To quantify the viability of hMSC subjected to different magnitudes of strain (5, 10 and 20%) using the ATPlite™ assay

- To visualise the histoarchitecture of Tencell-cultured seeded pericardium

- To measure and compare the expression of lineage-specific genes in hMSC subjected to different magnitudes of strain

7.3 Experimental approach

During the experiments described in this chapter, an optimal straining regime of Tencell-cultured hMSC-seeded pericardia was devised, and the relative expression of genes indicative of differentiation towards the smooth muscle, tenogenic, osteogenic, adipogenic and chondrogenic lineages measured.

Sterility testing of all bioreactor culture runs was performed to validate that all cell viability and gene expression analyses were free of bias that may be caused by the presence of microbes. The viability of hMSC seeded on pericardial matrix and subjected to different magnitudes (5, 10 and 20%) and durations (4 and 24 hours) was measured to validate a uniaxial cyclic strain regime that maintained cell viability for the duration of Tencell culture. The magnitudes of strain examined were selected so as to encompass the most commonly examined magnitudes reported in literature (Kim *et al.*, 1999; Park *et al.*, 2004; Katsumi *et al.*, 2005; Friedl *et al.*, 2007; Maier *et al.*, 2008; Qi *et al.*, 2008; Huang *et al.*, 2012; Kreja *et al.*, 2012; Rathbone *et al.*, 2012). A seeding period of 24 hr was initially tested to investigate the viability of cells mechanostimulated for the duration of bioreactor culture, and reduced to 4 hr as per results to represent straining periods previously reported (Park *et al.*, 2004). The histoarchitecture of Tencell-cultured (strained and unstrained) and seeded-only pericardia was examined by haematoxylin and eosin staining to discern any differences in cell penetration and collagen structure of the tissue between conditions. The relative expression of genes of interest was measured to determine whether any of the strain regimes applied resulted in changes in lineage specification behaviour of hMSC.

7.4 Results

7.4.1 Sterility of Tencell-cultured samples

All microbiological plates and broths corresponding to test samples for all Tencell culture experiments were free of, and all positive control samples exhibited extensive, microbial growth.

7.4.2 Viability of mechanostimulated cells by duration of strain

Cell viability testing by the ATPlite™ assay at different durations of strain was conducted to establish an optimal straining regime for cell seeded substrates.

Although statistically significant differences in luminescence counts were only found between unseeded and seeded samples, there appeared to be a reduction in cell viability between strained and unstrained hMSC, when cyclic uniaxial strain (10%; 1 Hz) was applied for 24 hr (Fig. 7.1). A repeat of this experiment with BHK cells yielded similar results (Fig. 7.2). Luminescence counts of unseeded tissue in experiments with BHK cells were not measured and would be expected to be similar to that of unseeded tissue measured previously.
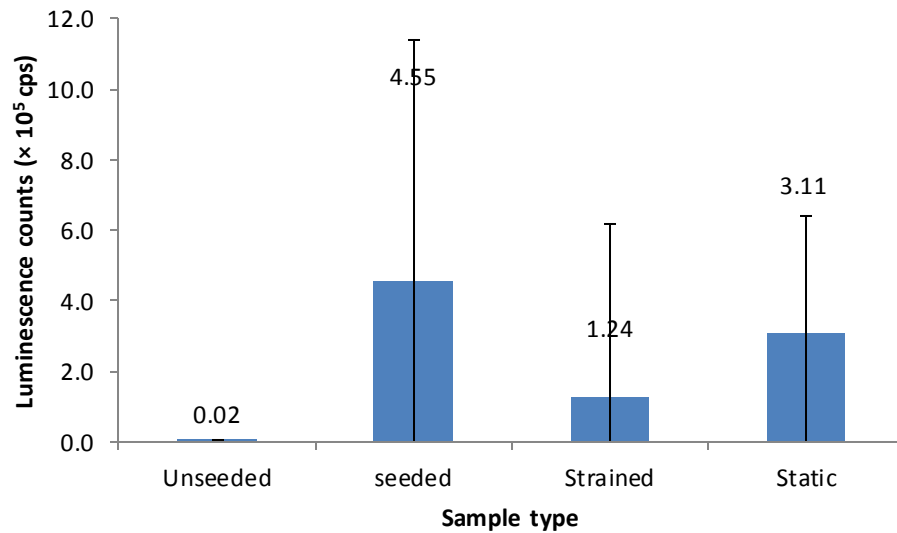
Fig. 7.1: Luminescence counts by sample type of hMSC cultured in Tencell, as measured by the ATPlite assay. *Seeded cells were seeded overnight. Stimulated scaffolds were seeded overnight and cultured in Tencell whilst subjected to cyclic uniaxial strain (10 Hz) for 24 hours. Static scaffolds were seeded overnight and cultured in Tencell for 24 hours in the absence of mechanostimulation. Luminescence counts of seeded and unseeded samples were significantly different (p=0.033), as measured by ANOVA and a Tukey test. Although there was no significant difference between luminescence counts of static and mechanostimulated scaffold, the data appear to indicate a loss of cell viability of strained hMSC. Data presented as means ± 95%*

To examine whether shorter durations of strain encourage maintenance of cell viability during Tencell culture, the cell viability of BHKs cultured with and without uniaxial strain (10%; 1 Hz) applied for 4 hrs was quantified by ATPlite™. There was no significant difference between cell viability of strained and unstrained cells for this shorter application of strain, but luminescence counts of cells cultured in scaffolds subjected to strain were greater than those of other samples (Fig. 7.3). Confidence limits (p=0.05) for all ATPlite™ assay-based cell viability experiments were large, indicating a high degree of variability between experimental replicates.
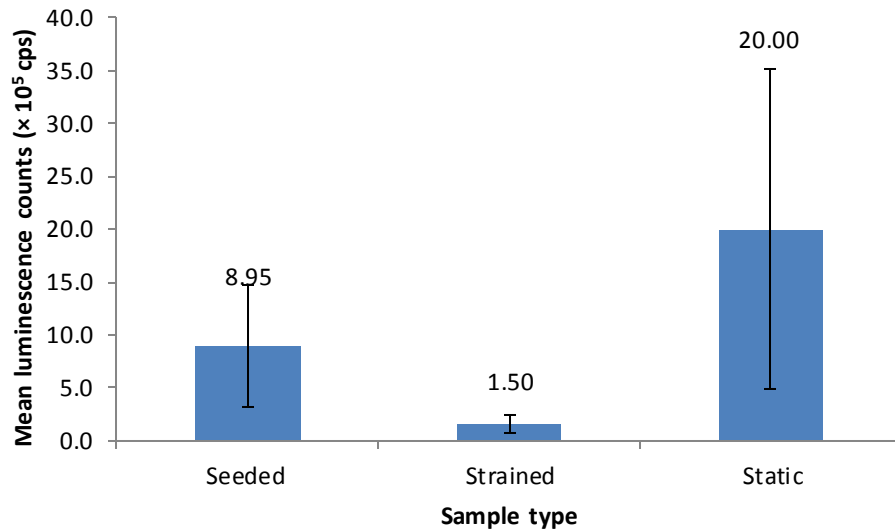
Fig. 7.2: Luminescence counts by sample type of BHK cells cultured in Tencell. Seeded cells were seeded overnight, as measured by the ATPlite assay. *Stimulated scaffolds were seeded overnight and cultured in Tencell whilst subjected to cyclic uniaxial strain (10%; 1 Hz) for 24 hours. Static scaffolds were seeded overnight and cultured in Tencell for 24 hours in the absence of mechanostimulation. Luminescence counts for static samples were significantly greater than other sample types (p=0.005), as measured by ANOVA and a Tukey test.*
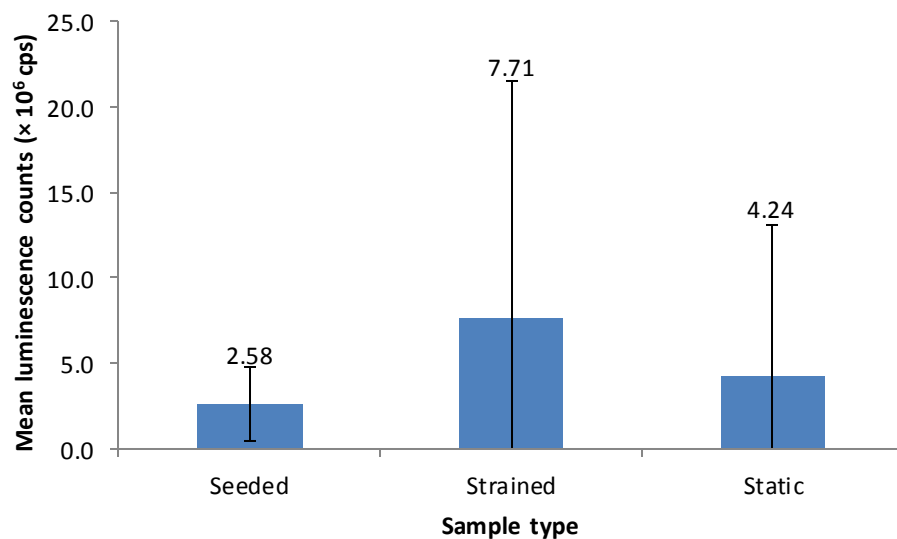
Fig. 7.3: **Luminescence counts by sample type of BHK cells cultured in Tencell, as measured by the ATPlite assay.** *Seeded cells were seeded overnight. Stimulated scaffolds were seeded overnight and cultured in Tencell whilst subjected to cyclic uniaxial strain 10%; (1 Hz) for 4 hours. Static scaffolds were seeded overnight and cultured in Tencell for 24 hours in the absence of mechanostimulation. There was no significant difference in luminescence counts between sample types (p=0.320), as measured by ANOVA.*

7.4.3 Viability of mechanostimulated hMSC by magnitude of strain

Since the relative expression of genes of interest (Table 5.3) was measured for hMSC cultured with different magnitudes of strain (5, 10 and 20%), the viability of cells under these magnitudes of strain was also measured. Any detected changes in relative gene expression for cells showing a loss of viability during an experiment cannot be attributed to applied mechanical stimuli, and may instead be the result of apoptosis or cell stress. For all magnitudes of strain, there was no significant difference in the luminescence counts of strained and unstrained samples (p = 0.002, 0.057 and 0.032 for strains of 5, 10 and 20% respectively), but samples cultured in the 5 and 20% experiments had luminescence counts that were significantly greater than unseeded tissue (Fig. 7.4 & Fig. 7.6).
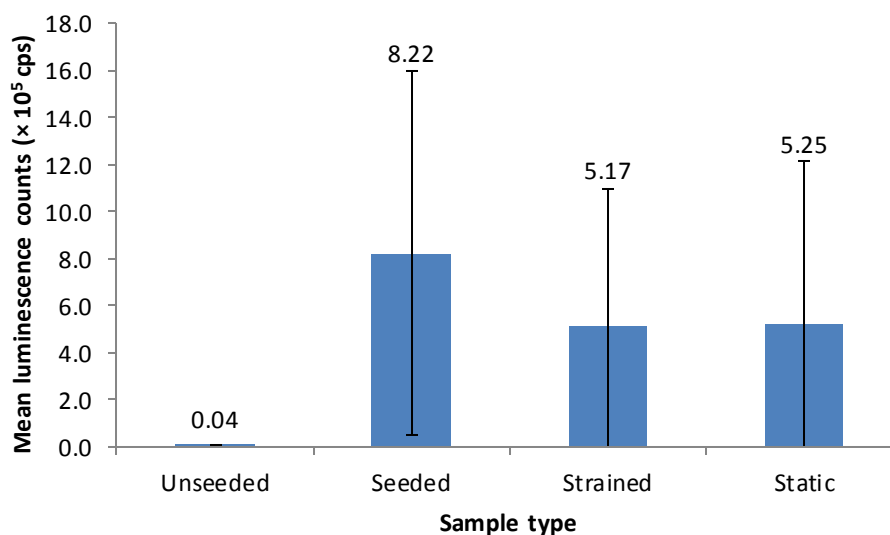
Fig. 7.4: Luminescence counts by sample type of hMSC cultured in Tencell for downstream relative gene expression analyses, as measured by the ATPlite assay. *Seeded cells were seeded overnight. Stimulated scaffolds were seeded overnight and cultured in Tencell whilst subjected to cyclic uniaxial strain (5%; 1 Hz) for 4 hours. Static scaffolds were seeded overnight and cultured in Tencell overnight in the absence of mechanostimulation. There was a significant difference in luminescence counts between unseeded and other sample types only (p=0.002), as measured by ANOVA and Tukey's post-hoc test.*
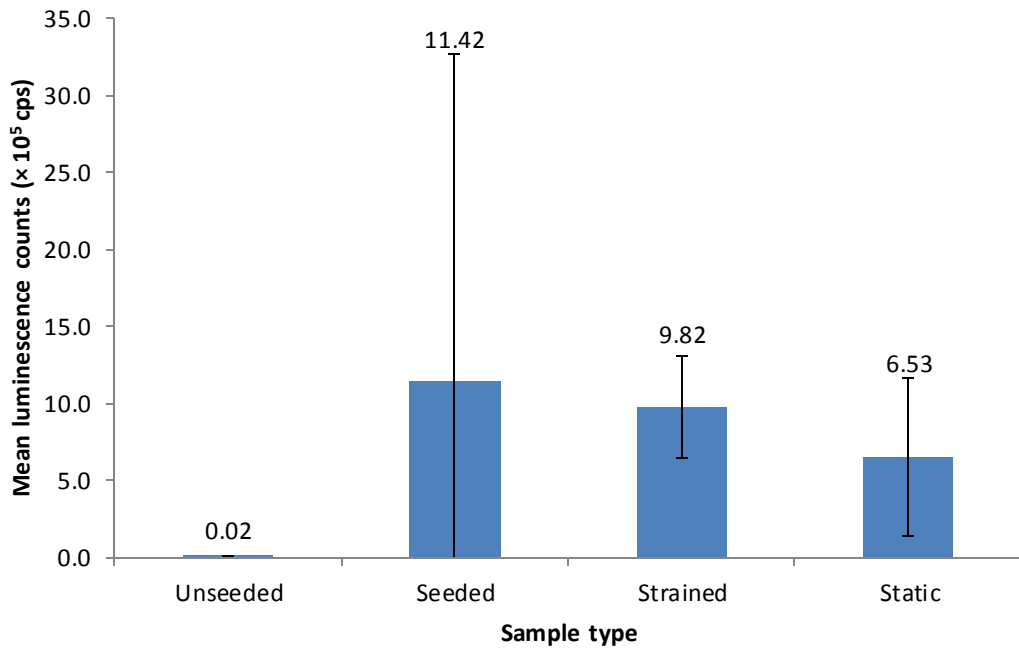
Fig. 7.6: Luminescence counts by sample type of hMSC cultured in Tencell for downstream relative gene expression analyses, as measured by the ATPlite assay. *Seeded scaffolds were seeded overnight. Stimulated scaffolds were seeded overnight and cultured in Tencell whilst subjected to cyclic uniaxial strain (10%; 1 Hz) for 4 hours. Static scaffolds were seeded overnight and cultured in Tencell overnight in the absence of mechanostimulation. There was no significant difference in luminescence counts between sample types (p=0.057), as measured by ANOVA and Tukey's post-hoc test.*
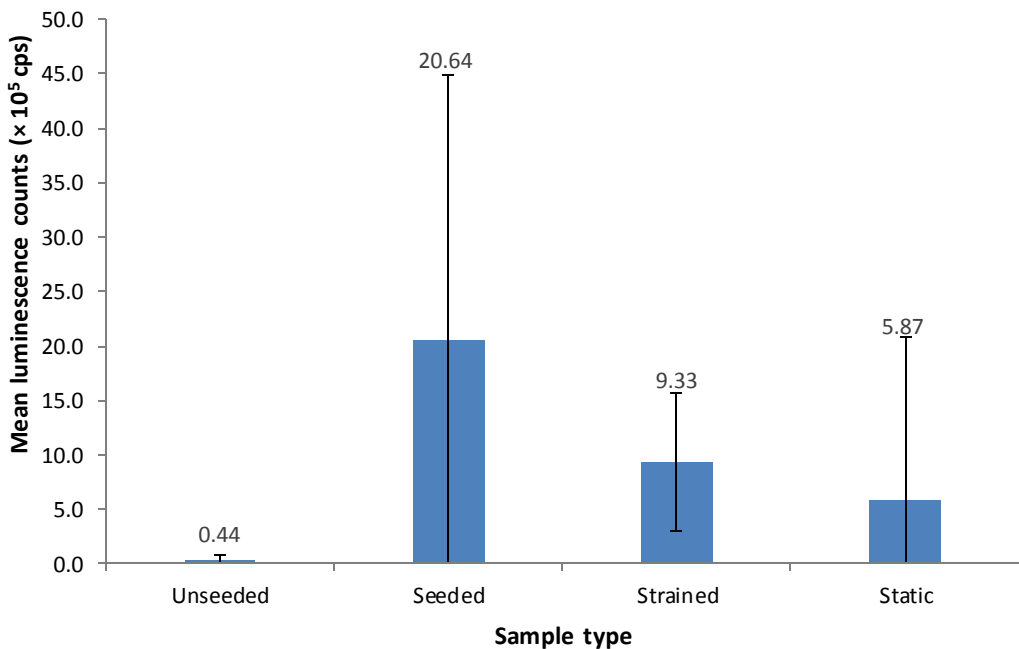
Stimulated scaffolds were seeded overnight and cultured in Tencell whilst subjected to cyclic uniaxial strain (20%; 1 Hz) for 4 hours. Static scaffolds were seeded overnight and cultured in Tencell overnight in the absence of mechanostimulation. There was no significant difference in luminescence counts between sample types (p=0.032), as measured by ANOVA and Tukey's post-hoc test.

7.4.4 Histoarchitecture of strained scaffolds

Haematoxylin and eosin staining of seeded-only, and statically and strained Tencell-cultured substrates was performed to assess the penetration of cells in the scaffold for each condition (Fig. 7.7 & Fig. 7.8). The histoarchitecture of Tencell cultured scaffolds was examined in experiments in which mechanostimulation was applied for four hours only, since there was a loss in cell viability in samples strained for 24 hours. Histology was performed following the full 24 hour culture time.

Seeded hMSC (Fig. 7.7) formed a monolayer on the mesothelial surface to which they were applied; penetration of cells into the scaffold was not observed for any sample. There was no apparent difference in hMSC attachment and penetration into tissue between statically and strained Tencell cultured substrates, and seeded cells remained a monolayer on the mesothelial surface. During mounting of sectioned tissue, separation of the tissue was apparent at higher water bath temperatures, and in some cases, the cell monolayer was removed intact from the bulk tissue (Fig. 7.8; 10% strained image). The crimping and orthogonal layer structure of the collagenous extracellular matrix, as described in chapter 3, was maintained for all sample types.
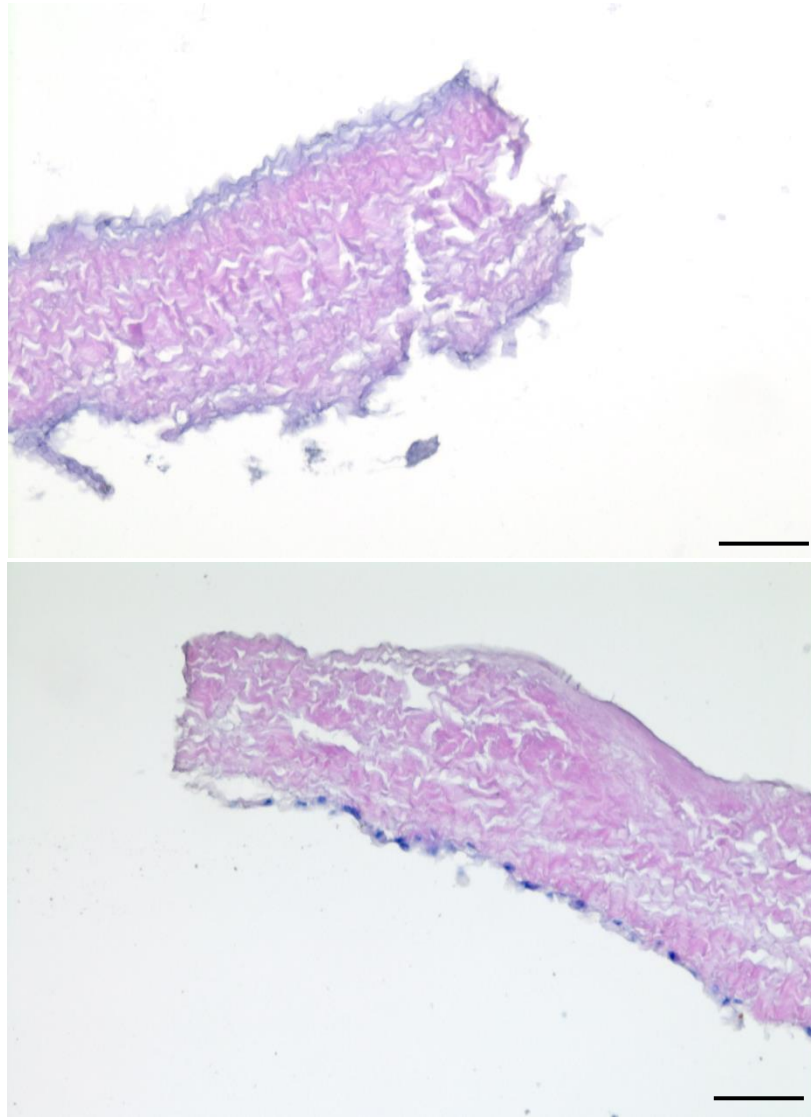
Fig. 7.7: Representative image of haematoxylin and eosin stained unseeded (top) and seeded (bottom) acellular pericardium specimen. Scale bars are 100 μm.
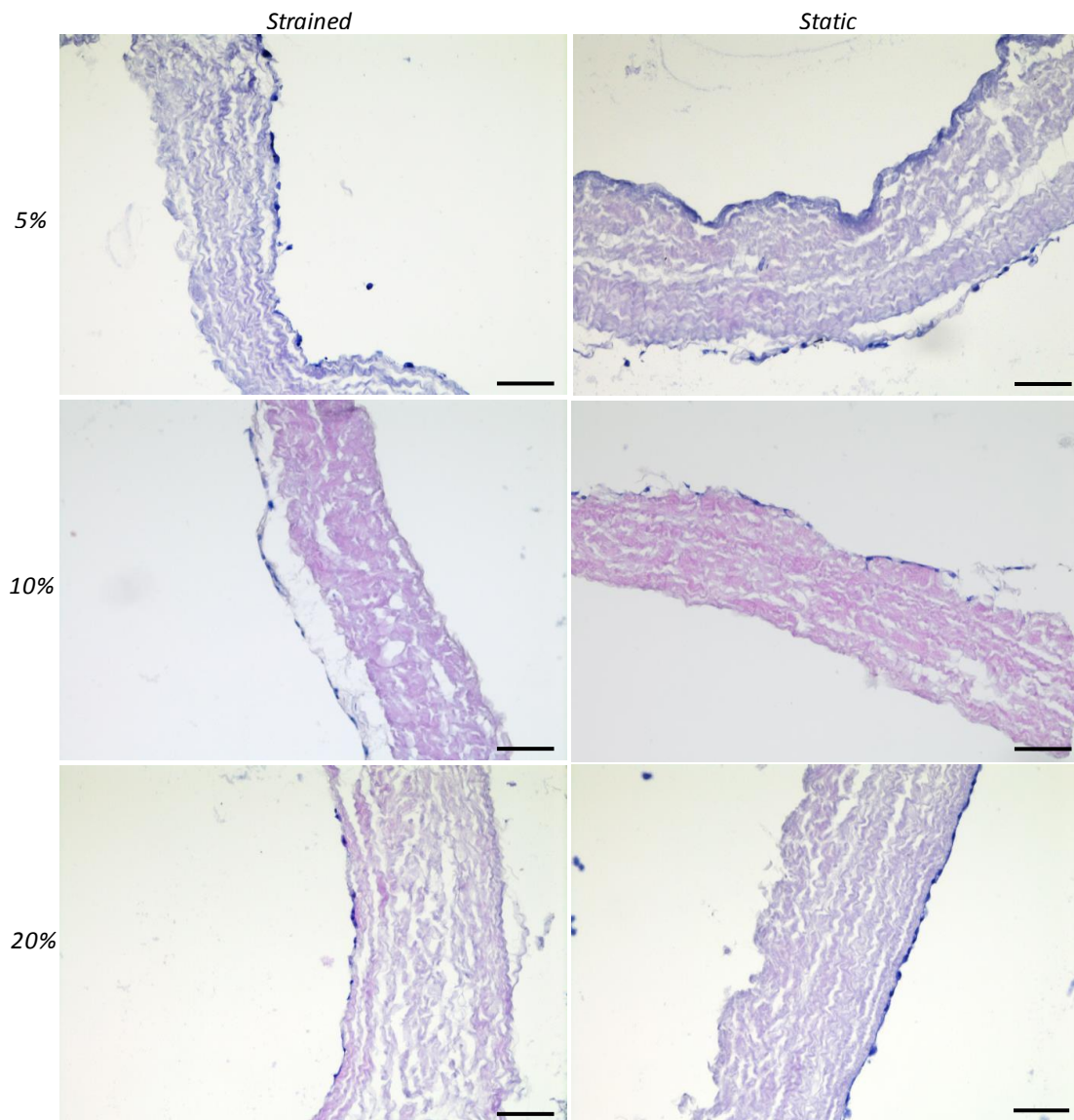
Fig. 7.8: Haematoxylin and eosin stained sections of Tencell-cultured seeded substrates. Cells (dark purple) remain as a monolayer on the mesothelial surfaces of cultured tissue for both strained and statically cultured samples. In some cases, the cell monolayer was prone to detachment from the bulk tissue. There were no obvious differences in histoarchitecture between sample types and magnitudes of strain. Images were captured at 10 × magnification. Scale bars are 100 μm.

7.4.5 Relative gene expression of strained MSC

Relative expression of genes indicative of differentiation towards the lineages of interest was measured by qPCR to determine whether different magnitudes of strain induce distinct lineage specification in hMSC using the validated Tencell bioreactor and protocol.

7.4.5.1 Tenogenic genes

Collagen I gene expression in seeded scaffolds subjected to uniaxial strain was downregulated as compared to static controls for the 5 and 20% strain magnitude conditions, but slightly upregulated for the 10% strain condition. Collagen III expression did not differ by sample type for the 10 and 20% strain conditions. Both collagen I and III were expressed significantly more in the suspension used to seed scaffolds (also described as 'unseeded' cells) than for all other sample types for the 5% strain conditions (p = 0.005 and 0.031 respectively) (Fig. 7.9Fig. 7.10). There were no statistically significant differences between scleraxis expression between sample types for all strain conditions, but strained cells cultured in the 10% strain experiment exhibited a larger downregulation than those of other strain conditions (Fig. 7.)..
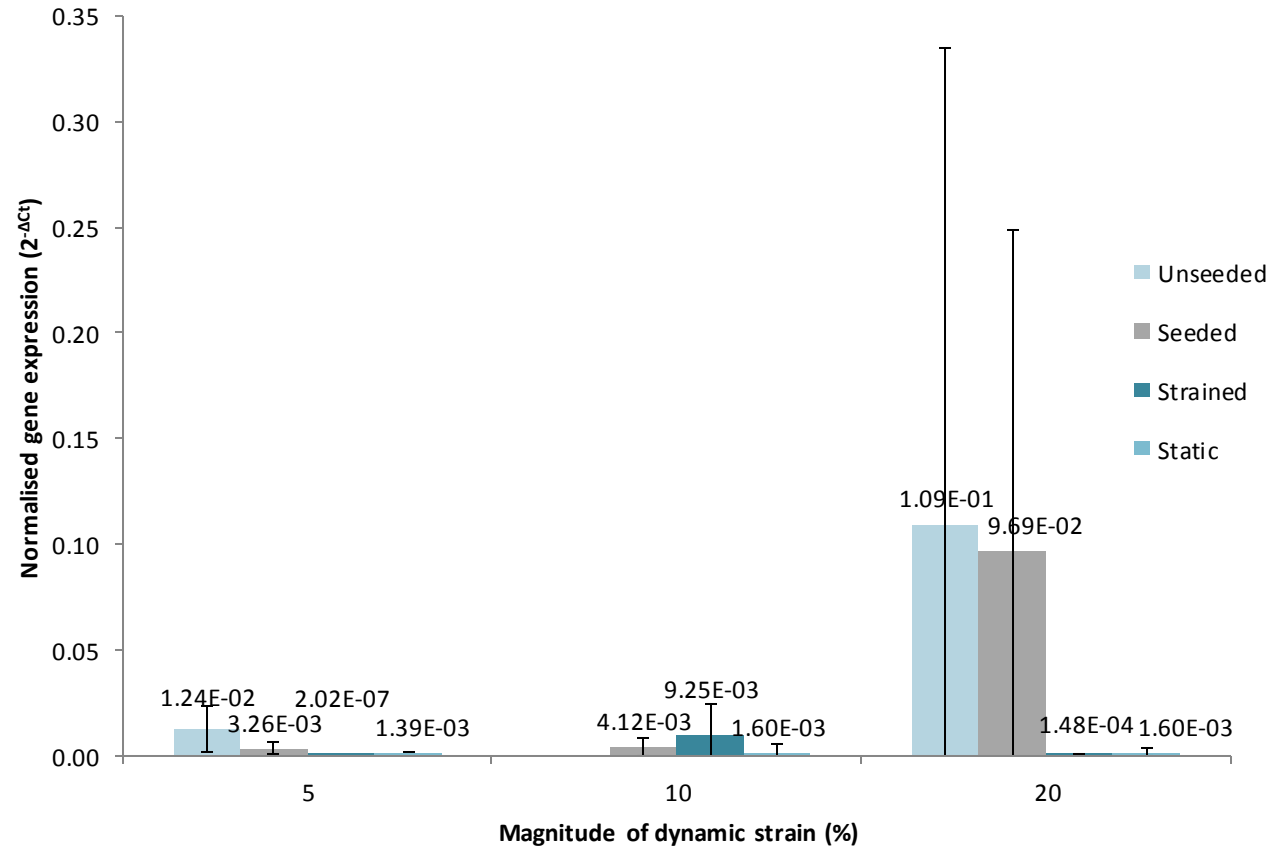
Fig. 7.9: Normalised collagen I expression of hMSC cultured in Tencell culture experiments. Strained samples were subjected to uniaxial strains of 5, 10 and 20%. There were no significant differences in gene expression between sample types cultured in the 10 and 20% strain experiments (p=0.422 and 0.176 respectively), but collagen I expression was significantly greater in seeding suspension cells (or unseeded) compared to other sample types in the 5% strain experiment (p=0.005), as calculated by ANOVA and Tukey's test. Data presented as means ± 95 % confidence limits.
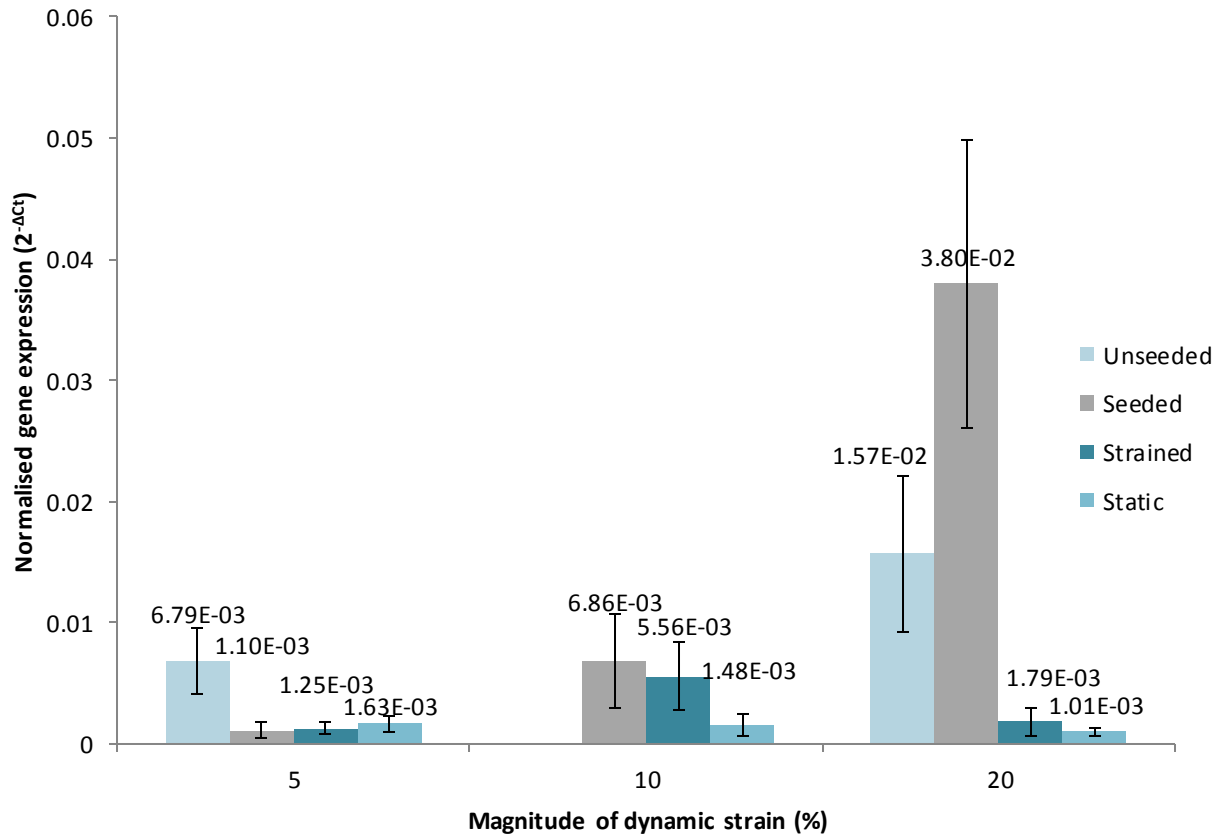
Fig. 7.10: Normalised collagen III expression of hMSC cultured in Tencell culture experiments. Strained samples were subjected to uniaxial strains of 5, 10 and 20%. There were no significant differences in gene expression between sample types cultured in the 10 % strain experiment (p=0.320). Collagen III expression was significantly greater in seeding suspension cells (or unseeded) compared to all other sample types in the 5% strain experiment (p=0.031). Expression in unseeded and seeded hMSC was significantly greater than other sample types in the 20% strain experiment (p=0.004). Statistical analysis done by ANOVA and Tukey's post-hoc test.
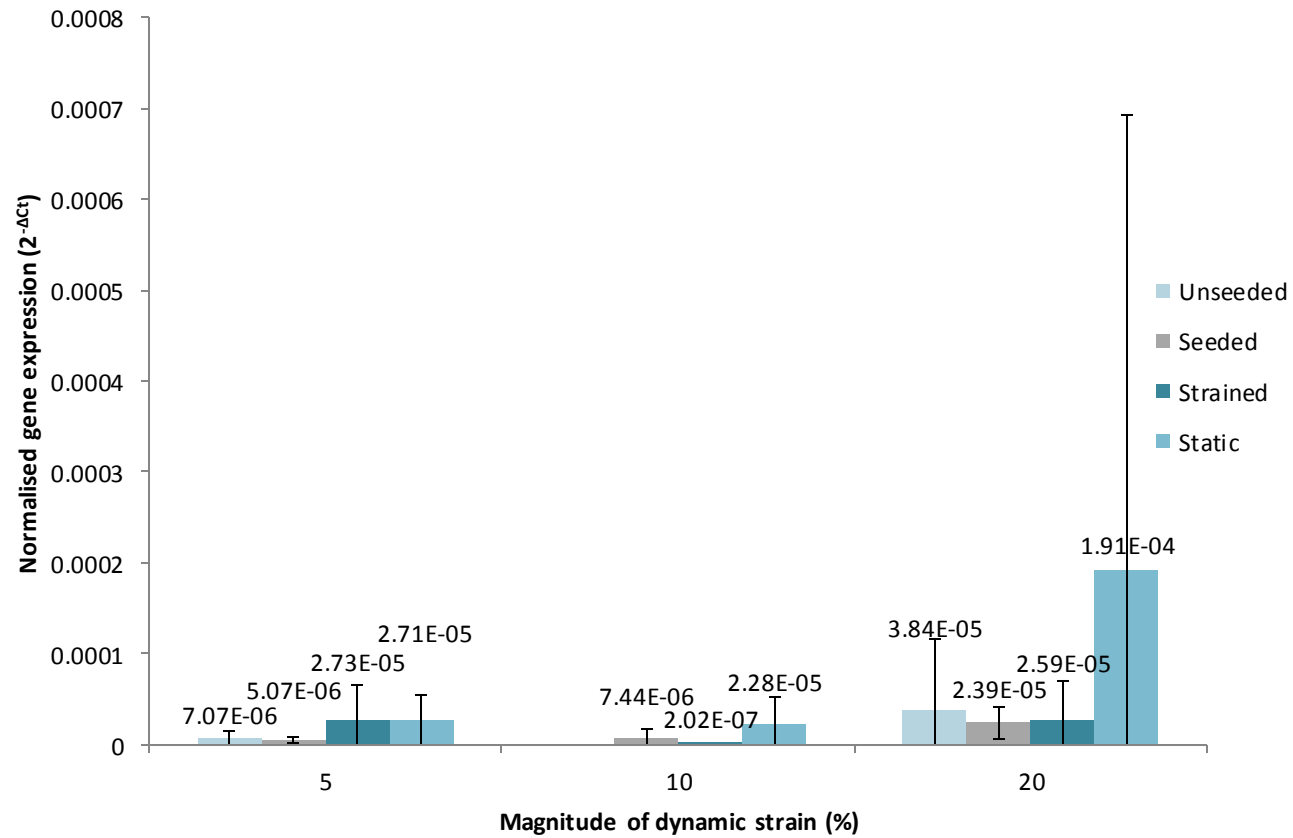
Fig. 7.11: Normalised scleraxis expression of hMSC cultured in Tencell culture experiments. Strained samples were subjected to uniaxial strains of 5, 10 and 20%. There were no significant differences in gene expression between groups in any experiment (p=0.368, 0.126 and 0.483 respectively). Statistical analysis was done by ANOVA.

7.4.5.2 Adipogenic genes

There were no statistically significant differences in adiponectin expression between sample types for all strain conditions examined, but it was upregulated in cells subjected to 10% strain as compared to static controls, in contrast to the 5 and 20% conditions (Fig. 7.12). There were no significant differences in PPAR-γ expression by sample type for the 10 and 20% strain experiments (Fig. 7.13). No PPAR-γ was detectable by qPCR in any sample cultured as part of the 5% strain condition experiment.
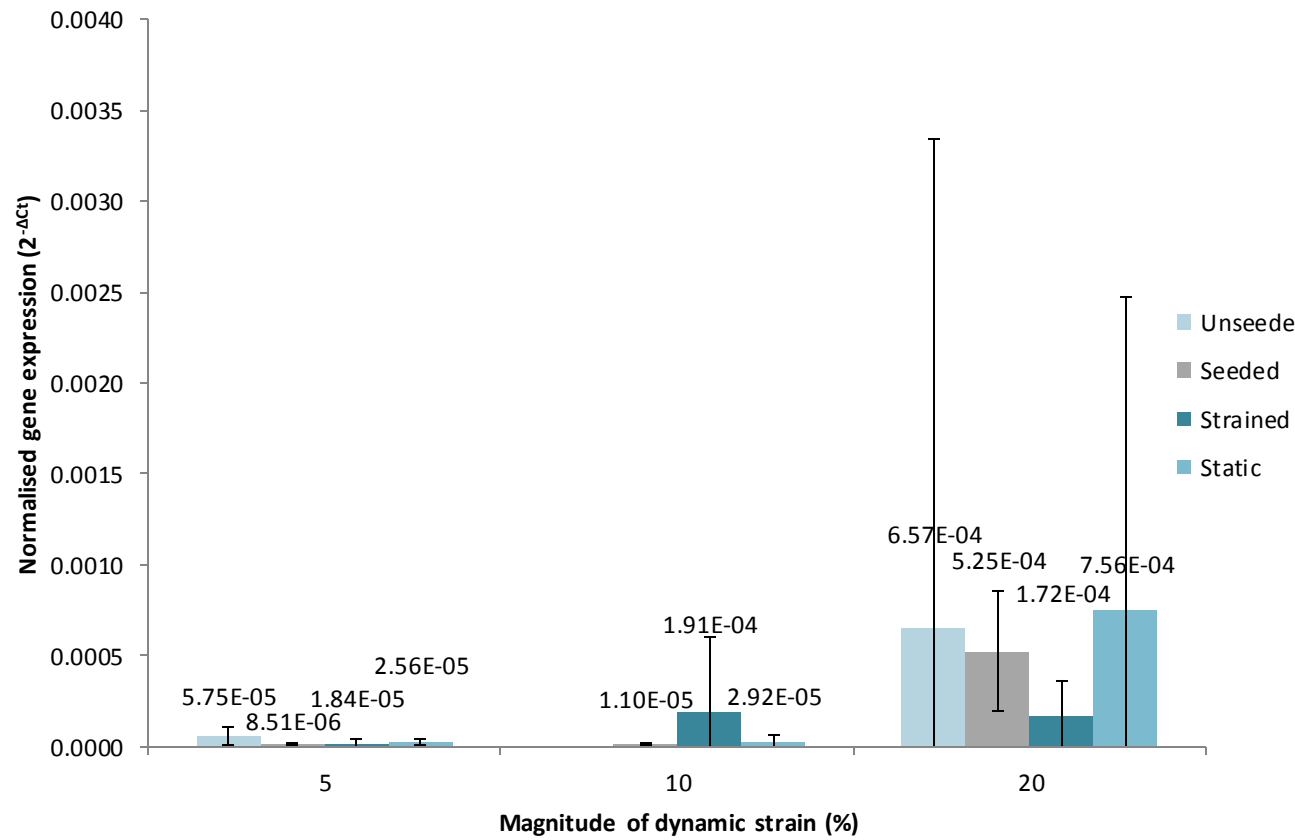
Fig. 7.12: Normalised adiponectin expression of hMSC cultured in Tencell culture experiments. Strained samples were subjected to uniaxial strains of 5, 10 and 20%. There were no significant differences in gene expression between groups in any experiment (p=0.073, 0.300 and 0.670 respectively). Statistical analysis was done by ANOVA.
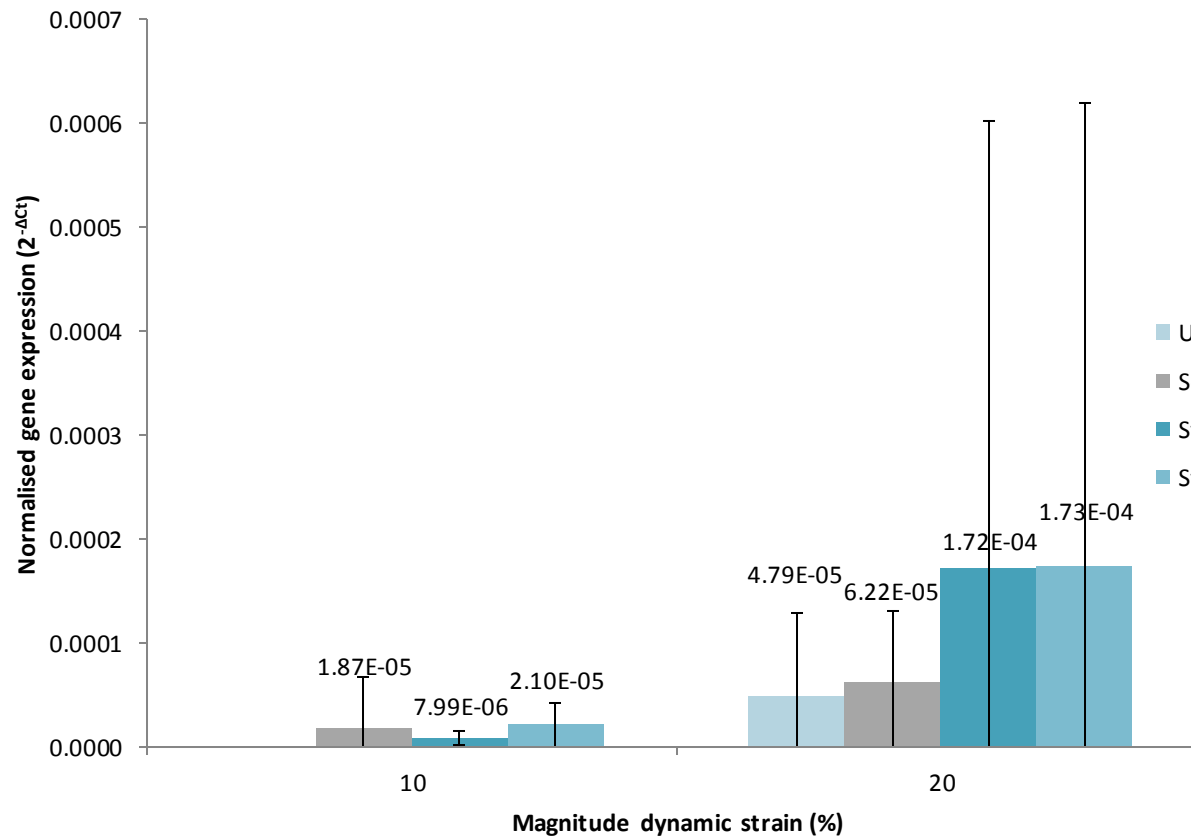
Fig. 7.13: Normalised PPAR-γ expression of hMSC cultured in Tencell culture experiments. Strained samples were subjected to uniaxial strains of 5, 10 and 20%. PPAR-γ expression was undetectable by qPCR in hMSC cultured in the 5% strain experiment. There were no significant differences in gene expression between groups in the 10 and 20% experiments (p=0.622 and 0.733 respectively). Statistical analysis was done by ANOVA.

7.4.5.3 SOX-9

There were no significant differences in SOX-9 expression between sample types for all strain

conditions examined (Fig. 7.14).
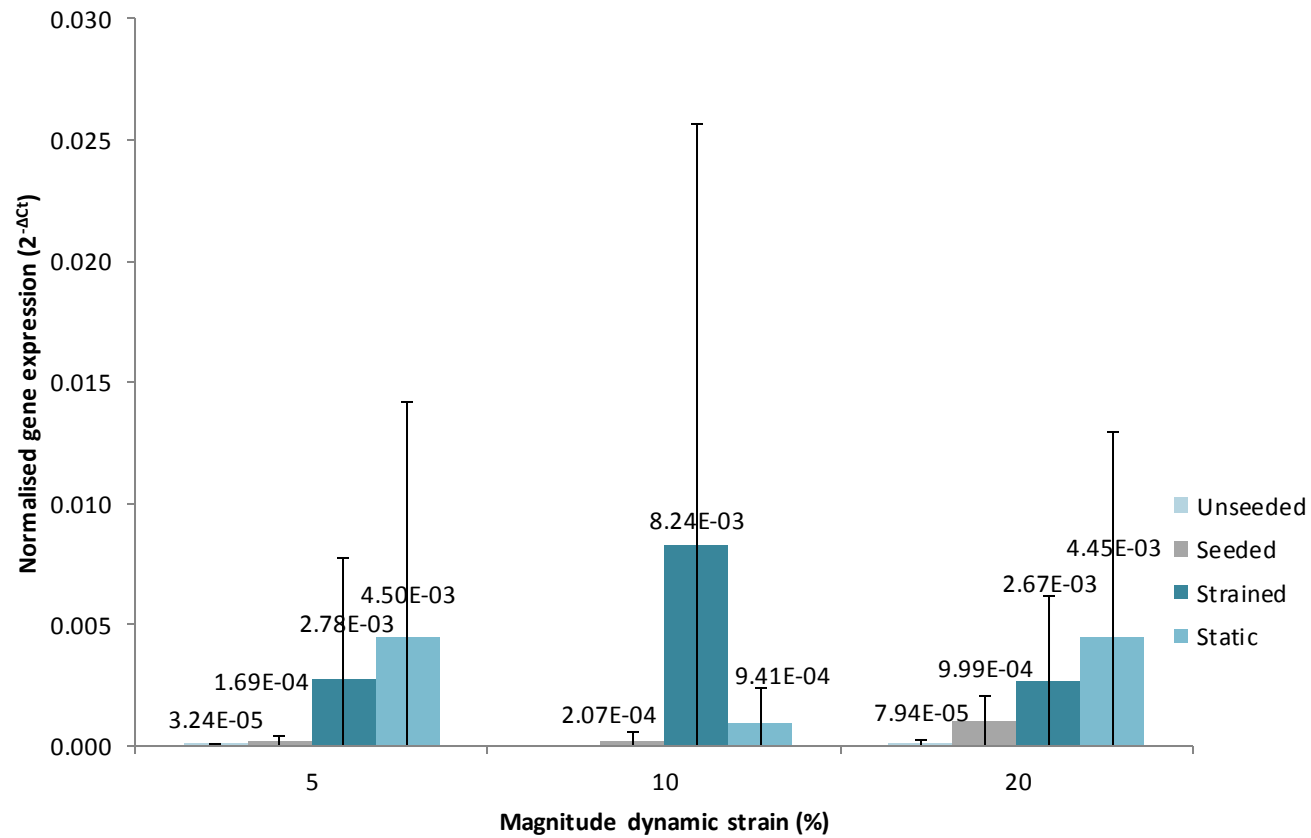
Fig. 7.14: Normalised SOX-9 expression of hMSC cultured in Tencell culture experiments. Strained samples were subjected to uniaxial strains of 5, 10 and 20%. There were no significant differences in gene expression between groups in any experiment (p=0.394, 0.388 and 0.335 respectively). Statistical analysis was done by ANOVA.

7.4.5.4 RUNX2

There were no significant differences in RUNX2 expression between sample types for all conditions examined (Fig. 7.15). Expression of RUNX2 was slightly downregulated in cells subjected to 5 and 20 % strain as compared to static controls, but was slightly upregulated by cells cultured under 10 % strain.
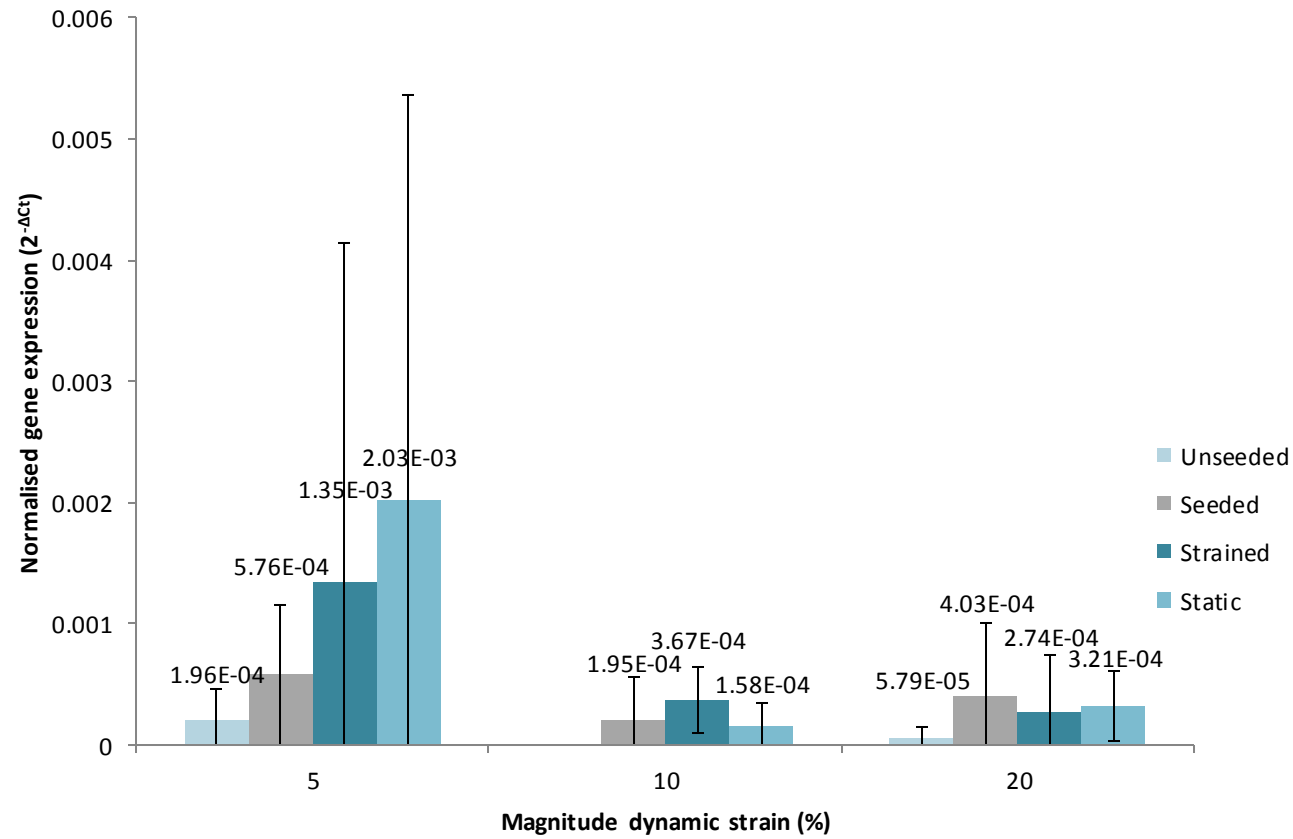
Fig. 7.15: Normalised RUNX2 expression of hMSC cultured in Tencell culture experiments. Strained samples were subjected to uniaxial strains of 5, 10 and 20%. There were no significant differences in gene expression between sample types in any experiment (p=0.395, 0.264 and 0.635 respectively). Statistical analysis was done by ANOVA.

7.4.5.5 Smooth muscle genes

Expression of smooth muscle 22α was downregulated in strained cells compared to statically cultured controls in the 5 and 20 % strain experiments. There were no significant differences in expression of smooth muscle 22α between sample types for any condition examined (Fig. 7.16). Expression of smooth muscle α-actin was unchanged by the application of strain; there were no significant differences in its expression in the 5 and 10% experiments, and differences in expression in the 20 % experiment were between the seeding suspension cells prior to application to the scaffold (unseeded) and seeded and strained samples (p=0.018) (Fig. 7.17). Calponin was undetectable in RNA isolated from all samples tested.
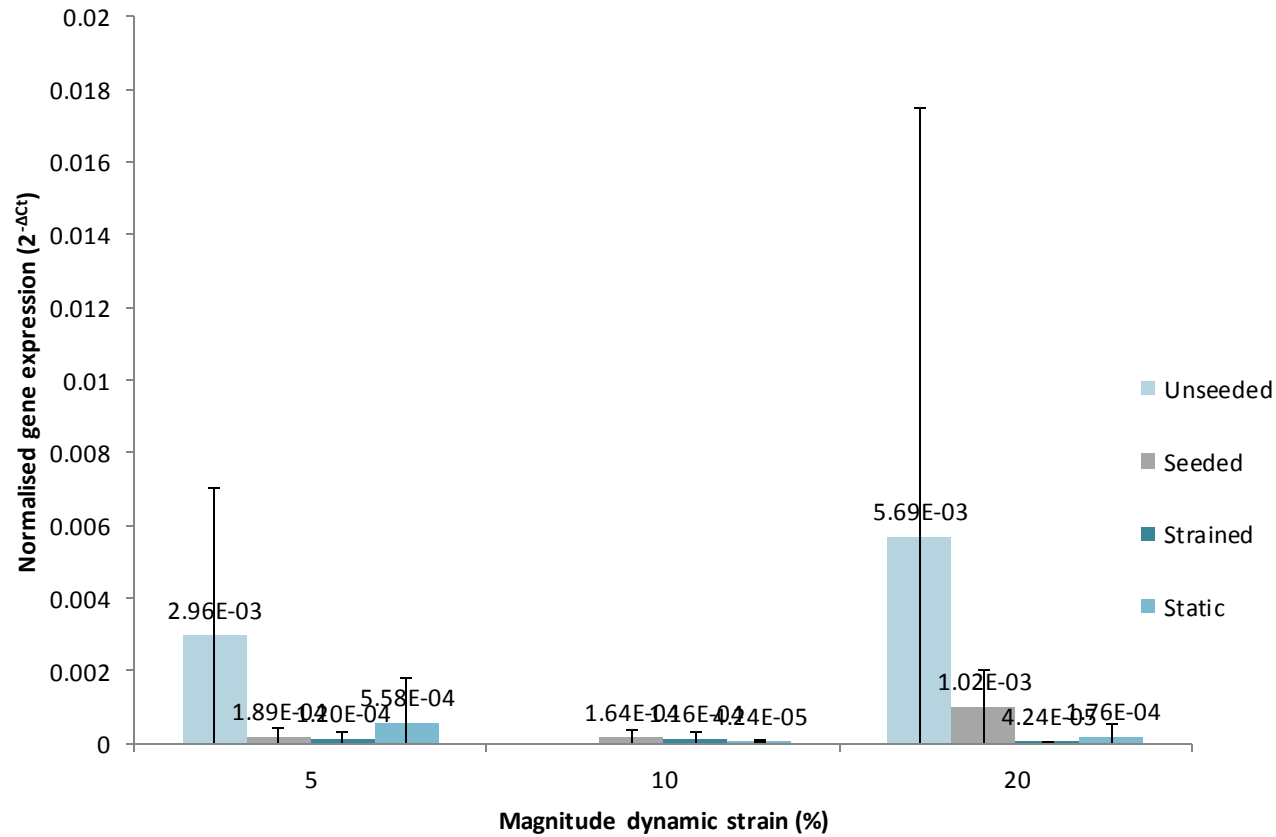
Fig. 7.16: Normalised smooth muscle 22α expression of hMSC cultured in Tencell culture experiments. Strained samples were subjected to uniaxial strains of 5, 10 and 20%. There were no significant differences in gene expression between groups in any experiment (p=0.071, 0.324 and 0.054 respectively). Statistical analysis was done by ANOVA.
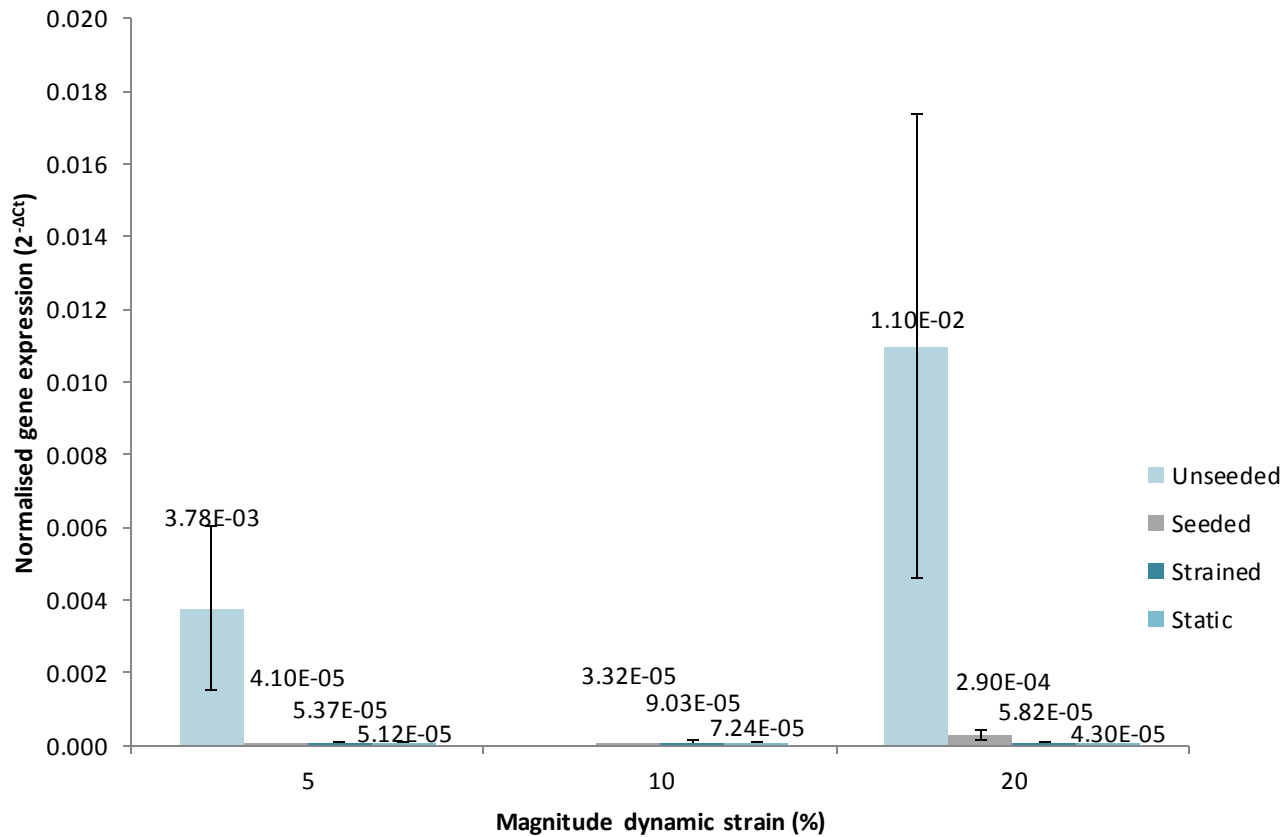
Fig. 7.17: Normalised smooth muscle α-actin expression of hMSC cultured in Tencell culture experiments. Strained samples were subjected to uniaxial strains of 5, 10 and 20%. There were no significant differences in gene expression between groups the 5 and 10% strain experiments (p=0.072 and 0.463 respectively). Seeding suspension hMSC cultured as part of the 20% strain experiment expressed significantly more smooth muscle α-actin than those cultured on strained and seeded samples (p=0.018). Statistical analysis done by ANOVA and Tukey's post-hoc test.

7.5 Discussion

The experiments presented in this chapter sought to validate a mechanostimulation regime for the application of uniaxial strain to hMSC-seeded pericardial matrices, and to perform gene expression analyses on RNA isolated from samples subjected to strains of 5, 10 and 20 %.

Strain has been shown to increase cell numbers within tissue engineered constructs (Mack *et al.*, 2013), but this is likely to be grossly dependent on the cell type used and the stimulation regime. In these studies, the luminescence counts of scaffolds cultured under 10% strain for 24 hours were considerably decreased as compared to controls, but were slightly higher when strain was applied for a 4 hour period for scaffolds cultured for the same total period. Previous publications reporting the survival of rat MSC following culture for 3-7 days at strains of 1-10% reported a loss of cell viability at strains of 10%, but good cell survival at strains ≤ 5% (McKayed *et al.*, 2016). It appears that a compromise between the need to apply relevant magnitudes of strain for as long as feasible, in order to detect differences in gene expression, and the need to maintain cell viability must be found. Strains of magnitude < 5% were not considered relevant to future tissue engineered applications, so the duration of cyclic strain was reduced. It is likely that strain periods of 24 hours induce cellular apoptosis, but strain periods of 4 hours are tolerated.

Scaffold histoarchitecture and the penetration of the scaffold by cells appears unchanged by sample type. Hence, any differences in gene expression by sample type in these experiments can be reliably attributed to he strain applied, and not changes in the immediate microenvironment of the cells. However, the seeded substrates examined may not have accurately represented three—dimensional conditions since hMSC grew as monolayers on the tissue surface. This may be addressed in future by validating an extended seeding period with respect to penetration of the scaffold.

The gene expression data obtained in these investigations was plotted as $2^{-\Delta CT}$ values, and not fold change vaues. It is strongly recommended in the literature that investigators wishing to plot qPCR data as individual data points for graphical presentation employ this approach (Schmittgen and Livak, 2008). Furthermore, it is only possible to calculate confidence limits for $2^{-\Delta CT}$ data from experimental replicates tested within the same experiment, as in this experimental design. To calculate confidence limits and significance levels for fold change data,

a minimum of three experiments for each different strain must be performed, which was not practical during this project.

Overall, the majority of the biggest differences in gene expression between strained and unstrained samples were detected in samples cultured at 10% strain. However, the only statistically significant differences in gene expression found were between the cell suspension used for scaffold seeding and other samples, between which the only common difference was the cell culture substrate.

Statistically significant differences in gene expression between seeding suspension cells and other samples were found for the tenogenic and smooth muscle lineages, and there were no significant differences by sample type in the differential potential of hMSC towards the chondrogenic, osteogenic and adipogenic lineages. Interestingly, although uniaxial strain has generally been found to augment hMSC differentiation towards a tenogenic lineage, as may be expected given the *in vivo* role of tendon tissue (Chen, 2008), some investigators have obtained mixed results and have hence concluded that substrate identity is critical in determining the impact of strain on gene expression in hMSC (Ngiam *et al.*, 2010). Similarly, although cyclic strain has been found to direct hMSC towards an osteoblastic lineage, the influence of substrate cues in these investigations was also recognised (Huang and Ogawa, 2010). The lack of significant differences in RUNX2 and SOX-9 expression for any condition may reflect the fact that the stimuli applied in this project do not resemble the cues experienced by cartilage and bone tissue *in vivo*. It is also possible that the use of more clinically relevant matrices, such as acellular blood vessels for smooth muscle tissue engineering, may generate statistically significant effects, and should be investigated in future.

Other investigators have previously reported that adipogenic differentiation of hMSC is ablated by uniaxial strain (Sen *et al.*, 2008; Khayat *et al.*, 2012). In contrast, no statistically significant effect on adipogenic gene expression was found for any sample or strain condition in this study. However, it is possible that adipogenic markers were virtually absent from hMSC derived from all sample types, explaining a lack of change in gene expression; although some mRNA for these genes did exist since the reaction kinetics of these assays differed significantly from controls in which only background noise was present. Similarly, there were no differences between the expression of smooth muscle genes in strained and unstrained samples despite prior reports to the contrary (Park *et al.*, 2004), and calponin was undetectable in every case. This is logical; calponin is expressed by fully differentiated smooth muscle cells only (NCBI, 2016c). Even if the applied stimulus induced differentiation towards

the smooth muscle lineage, the cells would not be likely to be specialised at the point of testing.

To summarise, the main trends apparent from gene expression analyses are the lack of statistically significant differences in gene expression between strained and unstrained samples, the presence of significant differences between unseeded and other sample types for some genes and the fact that the largest differences in gene expression between strained and unstrained samples (although not significant) were almost always observed in the 10% strain condition. In common with other investigators, it seems logical to conclude that in the experimental regime used the mechanostimuli applied may not have been sufficient to induce significant changes in gene expression. However, also in line with previous reports, it is possible that the substrate used exerted a strong effect on the differentiation potential of the hMSC, and that for these investigations this effect was far greater than that of the applied strain. It has been thoroughly established that substrate composition (Krishnamurithy *et al.*, 2016), stiffness (Engler *et al.*, 2006; Even-Ram *et al.*, 2006; Tse and Engler, 2011; Young *et al.*, 2013) and surface topography (Kuo *et al.*, 2012; Earls *et al.*, 2013; MacQueen *et al.*, 2013; Blumenthal *et al.*, 2014; Mohammadi *et al.*, 2014; Macri-Pellizzeri *et al.*, 2015) are considerable factors in the differentiation potential of hMSC. Despite not yielding any statistically significant differences, the fact that the largest differences in gene expression between unseeded and other samples usually occur in the 10% strain condition is suggestive that this magnitude of strain is the most physiologically relevant .

Additionally, natural variation in the pericardial matrix between individuals may contribute to differences in gene expression, and obfuscate effects imparted by applied strains. A further limitation to this study that should be addressed in any future, similar studies is the lack of control During tissue dissection, variation between individuals is apparent on the macroscale of this tissue. A further limitation to this study that should be addressed in any future, similar studies is the lack of control assays for differentiation markers; such controls would confirm the success of individual qPCR runs. However, the probably that primer pairs pre-validated with control, differentiated cell RNA will produce a false negative in assays conducted under the same conditions is remote.

Chapter 8:   Final discussion, conclusions and future work

In this work, investigations were conducted to devise a three-dimensional, uniaxial strain culture system for hMSC. In initial experiments, a stock of acellular porcine pericardium was produced for subsequent cell culture. Histological staining, DNA assay data and biocompatibility and sterility testing of this material confirmed the removal of cellular components, within widely accepted limits, and its suitability for use as a cell culture substrate. Seeding investigations were then conducted to discern an optimal seeding density and method for bioreactor culture investigations; with the methodology devised to ensure sufficient cell numbers for the assessment of cell viability by the ATPlite™, and sufficient RNA in cell lysate for extensive qPCR analyses. During this work, two seeding rings were tested, since the initial choice (the Tencell seeding rings) was found to be cytotoxic, and an hMSC seeding density of 1.26×10^5 cells cm^{-2} was found to correspond to the minimum point at which both RNA extract and viability assay criteria were satisfied (namely, sufficient RNA for accurate quantification and purity assessment by NanoDrop spectrophotometry, and sufficient luminescence counts for reliable detection). Primer design and validation investigations determined primer pairs and assay conditions for the relative quantification of markers of tenogenic, smooth muscle, adipogenic, osteogenic and chondrogenic differentiation. Re-engineering and validation of the Tencell bioreactor and cell culture protocol resolved temperature regulation, evaporation, pH maintenance, cell viability and displacement issues. Finally, the Tencell/substrate/hMSC system was trialled at uniaxial strains of 5, 10 and 20% for applicability in studies concerned with the impact of mechanotransduction on the differentiation potential of hMSC, assessed by the gene expression of markers of interest. No statistically significant differences in gene expression were found between strained and unstrained Tencell-cultured hMSC.

Multipotential mesenchymal stromal cells have potential for use in tissue engineered therapies targeting a wide range of tissues; they are able to differentiate into the mesenchymal lineages of fat, bone and cartilage and an ever-expanding repertoire of other cell types, including smooth muscle (Park *et al.*, 2004), tendon (Butler *et al.*, 2008; Benhardt and Cosgriff-Hernandez, 2009), hepatocytes (Petersen *et al.*, 1999) and neuronal phenotypes

(Yim *et al.*, 2007). The utility of MSC is not solely based on their differentiation potential, however; they also elicit milder immuoresponses than other transplanted allo-/xenogeneic cells, reducing the risk of complications in future clinical applications (Dazzi and Horwood, 2007; Ren *et al.*, 2008; Al Jumah and Abumaree, 2012; Gebler *et al.*, 2012; Soleymaninejadian *et al.*, 2012).

A large body of literature exists describing the differentiation of hMSC using soluble factors for potential applications in tissue engineering. Approaches for the chondrogenic (Mucsi *et al.*, 1996; Barry and Murphy, 2004; Csaki *et al.*, 2008), osteogenic (Hanada *et al.*, 1997; Liu *et al.*, 1999; Fujita *et al.*, 2001; Tuan *et al.*, 2003; Tae *et al.*, 2006; Lodish *et al.*, 2008), adipogenic (Pittenger *et al.*, 1999; Tuan *et al.*, 2003; Tae *et al.*, 2006) and smooth muscle (Gong *et al.*, 2009; Huang *et al.*, 2012) differentiation of hMSC predominantly using soluble factors have been documented, but the *in vivo* niche of hMSC also comprises cellular, ECM and physical stimuli that regulate their differentiation and homeostasis. Indeed, there is myriad evidence that mechanotransduction plays a role in the differentiation of hMSC (Altman *et al.*, 2002a; Discher, 2005; Engler *et al.*, 2006; Even-Ram *et al.*, 2006; Benhardt and Cosgriff-Hernandez, 2009; Chowdhury *et al.*, 2010; Lee *et al.*, 2011; Tse and Engler, 2011; Bukoreshtliev *et al.*, 2012; Holle *et al.*, 2013; MacQueen *et al.*, 2013; Shin *et al.*, 2013), but protocols to harness physical stimuli using carefully validated bioreactors are scant. Hence, although this study may be considered more fundamental than translational in nature, basic understanding of the role of mechanical stimuli in tissue engineering may prove crucial to the success of future therapies.

The broad aim of this project was to devise a validated three dimensional, uniaxial strain bioreactor and culture protocol for mechanotransduction studies in hMSC. Porcine pericardia (n=67) were utilised due to the limited availability of human tissue. Porcine tissue is routinely used to model human biology in tissue engineered investigations, and to date no evidence of significant morphological differences between human and porcine pericardium is forthcoming (Gilbert *et al.*, 2006; Mendoza-Novelo *et al.*, 2011). The pericardia used were shown to retain native histoarchitecture and penetration of such scaffolds by MSC was previously reported by coworkers (Morticelli, 2013). Additionally, seeded cells are able to make biologically-relevant adhesions with naturally-derived matrices (Steward *et al.*, 2014).

A number of proteins associated with cellular adhesions are known to act as mechanosensors in other cell types (Wang and Ingber, 1995; Wang *et al.*, 2001; Tuli *et al.*, 2003; Wang *et al.*, 2003; Tzima *et al.*, 2005; Wang and Suo, 2005; Vogel, 2006; Uda *et al.*, 2011; Sun *et al.*, 2012b; Tabdili *et al.*, 2012; Tsai *et al.*, 2015), and the collagenous histoarchitecture of pericardium was found to be unchanged following decellularisation in this study. A previously reported

decellularisation protocol was used to prepare the acellular substrates (Mirsadraee *et al.*, 2006a; Mirsadraee *et al.*, 2007; Mendoza-Novelo *et al.*, 2011; Morticelli, 2013), using many reagents in common with protocols reported elsewhere (Gilbert *et al.*, 2006). Although the decellularisation protocol for porcine pericardium is comparatively short (4 d), it is a labour intensive procedure with low scaffold output per run. Limitations on process scale-up include the dimensions of commercially-available laboratory shakers and inevitably high demands on incubator space in shared facilities. However, for more extensive studies of mechanotransduction or translational research with acellular pericardium, process scale-up should be investigated.

A loss of tissue surface GAGs was observed in acellular tissue as compared to native pericardia, as has been widely reported previously. This is probably a consequence of treatment with SDS, and is not expected to impact the differentiation potential of seeded hMSC (Lovekamp *et al.*, 2006; Mendoza-Novelo *et al.*, 2011). Confirmation of tissue biocompatibility and the absence of residual DNA was essential prior to its use as a tissue culture substrate; differences in gene expression observed must be attributable to the strains applied, and not toxicity or the presence of contaminating genomic DNA respectively (McPherson and Møller, 2006).

Although optimal cell seeding densities for hMSC on acellular pericardium were already known (Morticelli, 2013), the amount and purity of RNA isolated from the total number of cells to be applied to the scaffold for each prevalidated density was measured to develop a seeding strategy compatible with RNA quality checks. Poor quality RNA impacts the efficiency of PCR assays; if assay efficiency is not in the range 90-110%, the assumptions of the comparative C_T method of relative gene expression are not met and accurate data cannot be obtained. Accepted minimum guidelines to safeguard the quality of qPCR analyses state that investigators should confirm the quality of template material by nucleic acid spectrophotometry prior to use in assays (Bustin *et al.*, 2009). Absorbance ratio values are unreliable, and hence isolate purity cannot be determined, at RNA concentrations of < 15 ng.µL^{-1}, and lysates containing $\geq 1 \times 10^5$ cells satisfy this requirement.

The luminescence of seeded/cultured substrates when treated with the ATPlite™ assay was measured throughout this project to identify any losses in cell viability during method development. Although a calibration curve of the relationship between luminescence counts and the number of cells lysed during ATPlite™ assays was prepared during seeding investigations, the amount of ATP produced by cells is not constant throughout the cell cycle, nor independent of culture conditions, so attempts at cell enumeration had limited accuracy (Lundin *et al.*, 1986; Stanley, 1986). The difference between good and low cell viability is,

nevertheless, very apparent using the ATPlite™ assay, and it is suggested that this assay be used in a binary fashion to identify seeded substrates as viable or otherwise; luminescence counts of < 10000 A.U. can be assumed to indicate a lack of cell survival of hMSC seeded on acellular pericardium matrix. In investigations where the number of live cells present following a given procedure forms a vital metric, accurate cell numbers could be found from the RNA content of substrate isolate or by counting the number of dead cells present by medium volume.

Other, more sensitive assays that enable cell quantification through colorimetry are widely reported, such as the Alamar blue (Nakayama *et al.*, 1997), tetrazolium dye (Roehm *et al.*, 1991) and Neutral red (Repetto *et al.*, 2008) assays. One possible limitation to the use of these assays is that, unlike the ATPlite™ procedure in which cell are lysed, cells must be alive during analysis. This may be overcome by devising strategies to detach cells from tissue scaffolds, or aid penetration of the reagents into the construct. Achieving highly efficient cell detachment, particularly in thicker tissues and where cell penetration is extensive, is unlikely; hence validation of appropriate protocols of cells *in situ* is suggested. Although any new viability protocol must be carefully validated against established techniques, acellular pericardium is extremely thin (~100 – 200 μM) and is readily penetrated by reagents. Importantly, other investigators have already reported successful use of the 3-[4,5-dimethylthiazol-2-yl]-2,5-diphenyltertrazolium bromide (MTT) on seeded scaffolds; Zund *et al* seeded human aortic myofibroblasts on PGA scaffolds and validated calculated cell numbers by manual counting, with favourable results (Zund *et al.*, 1999).

During all phases of these investigations, it was essential to validate cell culture conditions to render any subsequent differences in gene expression attributable to mechanotransduction using the bioreactor and protocol validated. Optimal *in vitro* culture conditions have been thoroughly validated for standard cell culture incubators, but cannot be assumed to exist during the development of novel seeding procedures and bioreactor methodologies (Ham and Puck, 1962; Hayflick, 1965; Eagle, 1971). For example, the optimal medium seeding volume to be used with any new seeding/culture apparatus should be determined at the outset of use, to ensure adequate oxygen differentiation through the depth of culture medium. Changes in the partial pressure of oxygen in culture medium in two dimensional cell seeding/culture and in bioreactors is known to affect stem cell differentiation (Grayson *et al.*, 2006; Rafiq *et al.*, 2013).

Evaporation of culture medium was apparent during both seeding attempts and bioreactor culture during the course of this project. The osmolarity of culture medium is designed to be

isotonic to the cell cytoplasm, and increases in medium salt concentration induces osmosis to the external environment, causing loss of viability (Waymouth, 1970). Reduced cell viability was apparent in seeding investigations as a result of culture medium concentration, and likely contributed, amongst other factors, to the absence of viable cells in Tencell-cultured substrates prior to inclusion of chamber humidification measures. Similarly, there was a significant loss of cell viability in Tencell cultured hMSC prior to the use of HEPES to augment sodium bicarbonate medium buffering – this was probably caused by suboptimal partial pressures of carbon dioxide in the culture chamber, and reduced concentrations of carbonic acid in the medium as a result.

Despite successful cell culture of hMSC in Tencell during this project, it is suggested that the Tencell apparatus be fully redesigned in light of practical difficulties experienced. To the author's knowledge, there are no commercially available uniaxial strain bioreactors. No general consensus on in-house apparatus design has emerged; this proves problematic for data comparison between studies (Screen *et al.*, 2005; Jang *et al.*, 2011; Shi *et al.*, 2011; Rathbone *et al.*, 2012; Lei and Ferdous, 2016; McKayed *et al.*, 2016). However, most bioreactors comprise actuating/motion transforming systems, monitoring and control systems, sample culture chamber(s) and nutrition/waste exchange systems (Lei and Ferdous, 2016). The Tencell bioreactor utilises a linear actuator coupled to a motor driven clamp, temperature monitoring system and individual culture chambers, but has no nutrient/waste exchange system, necessitating manual medium changes. Critically, the apparatus is approximately 1.5 m in length and cannot be housed in a standard cell culture incubator; after initial flushing of the culture chamber, there is no capacity to monitor the gas composition during investigations (Fig. 6.1).

Other in-house manufactured uniaxial strain bioreactors reported in the literature may provide inspiration for future redesign efforts. In a seminal work, referenced extensively in this thesis, Park *et al* designed, validated and applied a custom-designed system to the study of gene expression in hMSC in response to uniaxial strain (Park *et al.*, 2004). Similarly, this apparatus comprised a motor driven clamp, but arm displacement and hence uniaxial strain was achieved via a cam-motor system. One major advantage of this design over the Tencell system is that culture wells featured individual lids; hence manipulations involving one sample did not compromise constructs in proximal wells. Tencell is set up for culture using a large number of screws and fixation posts, meaning that there is a large period of time (~ 5 hr) during which samples fitted first are exposed to ambient conditions whilst the lid is detached. Culture conditions, such as temperature and medium pH, which may be altered as a result of

extended exposure to ambient conditions, must be maintained to allow any changes in gene expression to be attributed to applied strains (Ham and Puck, 1962; Good *et al.*, 1966; Waymouth, 1970). Another study, examining the ultimate tensile strain and elastic modulus of reseeded acellular rabbit hindpaw tendons, also reported the use of a single chamber to house multiple replicates, but suffered from an additional caveat in that only four samples could be cultured simultaneously (Saber *et al.*, 2010). This does not allow the culture of sufficient strained and static experimental replicates in the same culture, possibly introducing batch-to-batch variability.

The displacement of the Tencell displacement arms was calibrated using a bespoke dial gauge, and the gradient and intercept of the resulting slopes were found to differ significantly. However, the amplifier knob used to select the magnitude of displacement is analogue and thus depends on human judgement in selecting the strain accurately. The accuracy of actual arm displacement with respect to that desired may be improved by incorporating a digital display into the displacement module, to allow strain to be selected consistently. Differences between displacement arms were considered minor when compared to the large degree of variation in tissue samples typically observed between individuals, but a proportion of the measured variation in arm displacement may be eliminated by measuring arm displacement simultaneously. Only one dial gauge was manufactured for displacement arm validation; arm displacements were manually selected anew for each arm tested, and the dial gauge moved following each validation. Should additional dial gauges be manufactured and calibrated, Tencell arm displacement may be found to be more consistent between experimental replicates.

Furthermore, arm displacement in Tencell was validated only in the absence of attached tissue substrates and online measurement of the actual strain applied to seeded cells was not possible. In contrast, Park *et al* were able to determine a region of scaffold that experienced uniform uniaxial strain, with minimal substrate compression in the perpendicular axis, by recording the motion of a printed grid under strain using high-speed photography (Park *et al.*, 2004). The substrate strained area is very small in Tencell ($\sim 1 \text{ cm}^2$), and cannot be adjusted, so it is suggested that any new design incorporate a larger seeded area and be validated with respect to strain uniformity across this region. Other methods of less invasive, online monitoring, such as laser-based micrometers should be incorporated to provide more accurate data (Salazar *et al.*, 2015; Lei and Ferdous, 2016). Such instruments may also provide an early indication of faults ofthe displacement components of bioreactors.

Indeed, the only online monitoring system present in Tencell is the temperature control module, and unlike contemporary cell culture incubators, the partial pressure of CO_2 is not monitored and adjusted in real time (Lei and Ferdous, 2016). Additionally, although culture medium evaporation was reduced to negligible levels during this project, and no Tencell culture samples tested positive for microbial contamination, the open wells inside the culture chamber present an inherent evaporation and contamination risk. It is anticipated that this risk could again be dramatically reduced by designing a basic individual well lid, with a space to accommodate arm displacement.

Caveats of the Tencell bioreactor, and solutions/criteria to be considered in the design of a newly designed uniaxial strain bioreactor, are summarised in Table 8.1.

Table 8.1: Caveats encountered during use of the Tencell bioreactor and solutions/criteria to be incorporated into the design into the design of an alternative uniaxial strain bioreactor

Issue	Solution	References
Single chamber lid, causing exposure of all samples fitted to ambient conditions and airborne bacteria	Individual chambers/lids for each sample	(Park et al., 2004)
Chamber lid not autoclavable, raising infection risk	Manufacture sample lids from autoclavable, transparent material such as polydimethylsiloxane (PDMS)	(Morita et al., 2014; Lei and Ferdous, 2016)
Apparatus dimensions not compatible with incubator culture	Reduce configuration to fit standard cell culture incubator	N/A
Small cell culture area, reducing total number cells cultured per sample	Design larger culture wells/smaller clamps for greater usable area	N/A
Analogue device displays, reliant on operator judgement	Utilise digital device displays	N/A
Lack of online gas monitoring	House bioreactor inside standard cell culture incubator, and design vented sample lids	N/A
Lack of online strain monitoring	Incorporate non-invasive strain monitoring instrumentation, such as laser-based micrometer	(Lei and Ferdous, 2016)

Genes indicative of differentiation towards the lineages of interest were selected based on those commonly studied in similar studies in the literature, and typical expression in the

human body, as determined by resources provided by the NCBI (Ncbi, 2012a; Ncbi, 2012b; NCBI, 2014; NCBI, 2016l; NCBI, 2016c; NCBI, 2016a; NCBI, 2016j; NCBI, 2016d; NCBI, 2016e; NCBI, 2016i; NCBI, 2016g; NCBI, 2016b; NCBI, 2016k; NCBI, 2016f; NCBI, 2016m; NCBI, 2016h). Primers were validated with respect to their specificity and efficiency to meet the key assumptions of the comparative C_T method of calculating relative gene expression data: briefly, that only one amplicon is generated and the quantity of amplicon doubles with each thermal cycle. Performing *in silico* validation prior to labour-intensive and expensive laboratory testing is highly recommended (NCBI, 2014; Sigma-Aldrich, 2014). Primer sequences sourced from publications must still be validated with the reagents to be used in gene expression analyses; primer activity may differ significantly between laboratories using different reaction mixtures, and the exact cycler profile used in qPCR is often not disclosed in publications (Banes *et al.*, 1999; Beck *et al.*, 2000; Chen *et al.*, 2001; Kim *et al.*, 2002; Arnoczky *et al.*, 2004; Bershadsky *et al.*, 2006; Chen *et al.*, 2008). For example, different qPCR mixtures may contain a variety of different concentrations of magnesium chloride. Magnesium ions forms complexes with nucleotides and altering their concentration affects polymerase and primer/template complex activities under otherwise identical conditions. Other ions released during buffer dissociation are also known to exert similar affects (McPherson and Møller, 2006).

Seeded pericardium matrices were cultured in the Tencell bioreactor under cyclic uniaxial strains of 5, 10 and 20%, but few statistically significant differences in gene expression were found, and where apparent, were between seeding cell suspension and other sample types. It was concluded that, for the protocol developed, the differences in gene expression between hMSC cultured on tissue culture plastic and acellular pericardium were far greater than any differences induced by strain.

In future, similar investigations using Tencell should allow for a minimum of three repeats experiments per strain regime tested, to allow fold change values, with associated confidence limits, to be quoted. The large error bars associated with $2^{-\Delta ct}$ data in this project may be due to the expected inhomogeneity of the natural substrate. Since any future tissue engineered therapies developed harnessing physical stimuli would be implanted *in vivo*, investigations of this nature should be conducted in biologically-relevant substrates to account for the influence of variation between individuals. Work conducted with artificial, unrealistically homogenous substrates may not accurately model hMSC behaviour *in vivo* (Engler et al., 2006; Park et al., 2012b). However, donor variation of pericardial tissue was apparent by eye. Consistent, reproducible three-dimensional matrices are needed for studies of

mechanotransduction, if the role of force- and substrate composition/topographical-mediated cues are to be decoupled. This may be achieved using genetically engineered animals, or perhaps less controversially, the development of ECM protein substrates comprised of more than one protein in a biomimetic structure.

Crucially, the actual applied strain across the scaffold was not measured. Analyses performed in this project were based on the assumption that physical stimuli are uniformly distributed across the scaffold surface, and that only one gene expression mechanoresponse could result. In fact, strain is often nonuniformly distributed across materials, and strained scaffolds may experience some compression in the orthogonal direction; a field of heterogeneous stimuli across the scaffold surface, and hence variety of mechanoresponses elicited, may explain the large error bars and lack of significant differences in gene expression data (Park *et al.*, 2004).

As discussed in Chapter 5, it is not realistic to determine a universal housekeeping gene for normalisation of relative gene expression data; most housekeeping genes display some variability in gene expression by sample type and conditions. Hence, the use of just one housekeeping gene in this work is a major limitation and may also account for the absence of significant differences in marker gene expression (Li *et al.*, 2015; Rauh *et al.*, 2015). A three-step qPCR assay validation approach should be adopted by investigators using this method of qPCR: primer pairs should be tested for specificity and reaction efficiency as described in Chapter 5, including a selection of potential housekeeping genes (>5) pre-screened by literature review, followed by housekeeping gene expression variability testing. It is suggested that, for simplicity, the coefficient of variation for gene be calculated for comparison (Rauh *et al.*, 2015).

Other factors that may obfuscate a potential impact of tensile strain on hMSC differentiation potential include donor variability, cell alignment responses and the degree of penetration of the scaffold by cells. The inclusion of cells from only one donor for each strain magnitude is a caveat of this study; large differences in the functional characteristics of hMSC between donors are widely reported in the literature, including differentiation capacity (Kern *et al.*, 2006; Bernardo *et al.*, 2007; Kota *et al.*, 2017; Sharma *et al.*, 2017). In future, a minimum of three different donors should be examined for each strain regime examined.

Visualisation of the histoarchitecture of seeded, statically-cultured and strained substrates revealed no penetration of the scaffold by hMSC in any instance. Although hMSC seeded on pericardium matrices in monolayer experience a culture environment more similar to the *in vivo* niche than those cultured on tissue culture plastic, the applied physical stimuli would be

more relevant to the biological environment if cellular adhesions were made in three dimensions within the scaffold (Chen, 2010; Sun *et al.*, 2012a).

Previous work by coworkers indicated that hMSC penetrate acellular pericardium scaffolds after seeding periods of 7-14 days (Morticelli, 2013). Future investigation concerning gene expression in hMSC cultured in this substrate could test the effect of uniaxial strain in a truly three-dimensional environment by employing longer seeding times. Additionally, the likelihood of significant changes in marker gene expression after just one four-hour period of cyclic strain are low. It is suggested that a culture period of 3d, with daily cyclic strain (4 hr), be trialled and changes in gene expression compared with that obtained after only one day of culture. The degree of penetration of the scaffold by hMSC can be assessed by haematoxylin and eosin staining of seeded tissue sections. Validation work by colleagues has indicated that culture periods of 3d are feasible in Tencell with an appropriate humidification and medium replenishment regime to maintain critical culture conditions (Normalina Sandora, personal communication).

Re-orientation of cells following uniaxial strain has been widely reported in the literature (Park *et al.*, 2004; Hoffman *et al.*, 2011; Khademolhosseini *et al.*, 2016). In fact, increases in marker gene expression of strained constructs have been observed to disappear following alignment responses (Park *et al.*, 2004). Alignment parallel to the direction of force application may reduce the detection of strain at force-mediated elements, such as focal adhesions, and ablate any intracellular signalling triggered by conformational changes at these sites. Analysis of cytoskeletal characterisation, by staining of F-actin with Phalloidin, is recommended for similar studies (Khademolhosseini *et al.*, 2016). In this work, this analysis could have been incorporated alongside gene expression, cell viability and histology tests of seeded, strained and unstrained samples, to elucidate any differences attributable to strain orientation. Directional analyses data may also be rendered quantitative, and hence allow the calculation of minimum significant differences between groups, surprisingly simply; Khademolhosseini *et al* produced a strain assessment tool from off-the-shelf components, and measured the coherency of actin filaments using the package OrientationJ (Sage, 2017).

There is evidence that gene expression of hMSC under different strain regimes are indeed distinct. For example, some investigators have suggested that the frequency at which physical stimuli are applied may affect the mechanoresponses elicited (Hoffman and Crocker, 2009; Hoffman *et al.*, 2011). It would be particularly interesting to determine if gene expression profiles of hMSC differ between frequencies of application of 0.5, 1.0 and 2.0 Hz. Further, the gene expression of hMSC cultured under different physical stimuli is likely to differ and

analyses of cells subjected to biaxial strain in pericardial matrices is suggested. However, since the Tencell bioreactor does not facilitate biaxial straining of substrates, a separate device would be required, which should be carefully validated to ensure that the environmental conditions maintained in the device are comparable with Tencell.

In this project, an existing, previously non-functional uniaxial strain bioreactor and hMSC culture protocol were re-engineered and validated for use in gene expression studies of hMSC. Expression of markers of differentiation towards the tenogenic, smooth muscle, osteogenic, adipogenic and chondrogenic lineages did not differ between strained and unstrained samples at applied strains of 5, 10 ad 20%, and the influence of uniaxial strain may be more effectively discerned with a redesigned bioreactor. A greater understanding of the role of uniaxial strain, as experienced by many tissues throughout the body, may lead to more efficacious differentiation of hMSC in future tissue-engineered therapies. Subsequent investigators in this field may wish to examine the role of the frequency of application of cydic strain, the type of strain applied, and the penetration of the scaffold used, to create a fuller understanding of the complex interplay between all factors of the hMSC microenvironment in determining their differentiation path.

Chapter 9:   References

AASEN, T., RAYA, A., BARRERO, M. J., GARRETA, E., CONSIGLIO, A., GONZALEZ, F., VASSENA, R., BILIĆ, J., PEKARIK, V., TISCORNIA, G., EDEL, M., BOUÉ, S. & IZPISÚA BELMONTE, J. C. 2008. Efficient and rapid generation of induced pluripotent stem cells from human keratinocytes. *Nature biotechnology,* 26**,** 1276-84.

ADAMS, M. D., KELLEY, J. M., GOCAYNE, J. D., DUBNICK, M., POLYMEROPOLOUS, M. H., XIAO, H., MERRIL, C. R., WU, A., OLDE, B., MORENO, R. F., KERLAVAGE, A. R., MCCOMBIE, W. R. & VENTER, J. C. 1991. Complementary DNA Sequencing: Expressed Sequence Tags and the Human Gneome Project *Science,* 252**,** 1651-1656.

AL JUMAH, M. A. & ABUMAREE, M. H. 2012. The Immunomodulatory and Neuroprotective Effects of Mesenchymal Stem Cells (MSCs) in Experimental Autoimmune Encephalomyelitis (EAE): A Model of Multiple Sclerosis (MS). *International journal of molecular sciences,* 13**,** 9298-331.

ALBERTS, B., JOHNSON, A., LEWIS, J., RAFF, M., ROBERTS, K. & WALTER, P. 2008. *Molecular Biology of the Cell,* New York, Taylor & Francis Group.

ALTMAN, G. H., HORAN, R. L., MARTIN, I., FARHADI, J., STARK, P. R. H., VOLLOCH, V., RICHMOND, J. C., VUNJAK-NOVAKOVIC, G. & KAPLAN, D. L. 2002a. Cell differentiation by mechanical stress. *FASEB journal : official publication of the Federation of American Societies for Experimental Biology,* 16**,** 270-2.

ALTMAN, G. H., LU, H. H., HORAN, R. L., CALABRO, T., RYDER, D., KAPLAN, D. L., STARK, P., MARTIN, I., RICHMOND, J. C. & VUNJAK-NOVAKOVIC, G. 2002b. Advanced Bioreactor with Controlled Application of Multi-Dimensional Strain For Tissue Engineering. *Journal of Biomechanical Engineering,* 124**,** 742-742.

ALTMAN, J. 1966. Autoradiographic and Histological Studies of Postnatal Neurogenesis II: A longitudinal investigation of the kinetics, migration and transformation of cells incorporating tritiated thymidine in infant rats, with special reference to postnatal neurogenesis. *J. Comparative Neurology,* 128**,** 431-431.

ALTMAN, J. 1969a. Autoradiographic and Histological Studies o f Postnatal Neurogenesis I: Dating the time of production and onset of differentiation of cerebellar microneurons in rats. *J. Comparative Neurology,* 136**,** 269-293.

ALTMAN, J. 1969b. Autoradiographic and Histological Studies of Postnatal Neurogenesis IV: Cell proliferation and migration in the anterior forebrain, with special reference to persisting neurogenesis in the olfactory bulb. *J. Comparative Neurology,* 136**,** 433-433.

ALTMAN, J. & DAS, G. D. 1965. Autoradiographic and histological evidence of postnatal hippocampal neurogenesis in rats. *The Journal of comparative neurology,* 124**,** 319-35.

ALTMAN, J. & DAS, G. D. 1967. Post natal neurogenesis in guinea pig. *Nature,* 214**,** 1098-1098.

ANDERSEN, C. L., JENSEN, J. L. & ØRNTOFT, T. F. 2004. Normalization of Real-Time Quantitative Reverse Transcription-PCR Data: A Model-Based Variance Estimation Approach to Identify Genes Suited for Normalization, Applied to Bladder and Colon Cancer Data Sets. *Cancer Res,* 64**,** 5245–5250,.

ANSALONI, L., CAMBRINI, P., CATENA, F., DI SAVERIO, S., GAGLIARDI, S., GAZZOTTI, F., HODDE, J. P., METZGER, D. W., D'ALESSANDRO, L. & PINNA, A. D. 2007. Immune response to small intestinal submucosa (surgisis) implant in humans: preliminary observations. *J Invest Surg,* 20**,** 237-41.

ARNOCZKY, S. P., TIAN, T., LAVAGNINO, M. & GARDNER, K. 2004. Ex vivo static tensile loading inhibits MMP-1 expression in rat tail tendon cells through a cytoskeletally based mechanotransduction mechanism. *Journal of orthopaedic research : official publication of the Orthopaedic Research Society,* 22**,** 328-33.

ATHAVALE, S. M., PHILLIPS, S., MANGUS, B., DATTA, J., SINARD, R. J., NETTERVILLE, J. L., BURKEY, B. B. & YARBROUGH, W. G. 2012. Complications of alloderm and dermamatrix for parotidectomy reconstruction. *Head & Neck,* 34**,** 88-93.

ATKINS, P. & DE PAULA, J. 2010. *Atkins' Physical Chemistry*, Oxford University Press.

BADYLAK, S. F., RECORD, R., LINDBERG, K., HODDE, J. & PARK, K. 1998. Small intestinal submucosa: a substrate for in vitro cell growth. *Journal of Biomaterials Science, Polymer Edition,* 9**,** 863-878.

BADYLAK, S. F., TAYLOR, D. & UYGUN, K. 2011. Whole-organ tissue engineering: decellularization and recellularization of three-dimensional matrix scaffolds. *Annu Rev Biomed Eng,* 13**,** 27-53.

BADYLAK, S. F., TULLIUS, R., KOKINI, K., SHELBOURNE, K. D., KLOOTWYK, T., VOYTIK, S. L., KRAINE, M. R. & SIMMONS, C. 1995. The use of xenogeneic small intestinal submucosa as a biomaterial for Achille's tendon repair in a dog model. *Journal of biomedical Materials Research,* 29**,** 977-985.

BAI, K., HUANG, Y., JIA, X., FAN, Y. & WANG, W. 2010. Endothelium oriented differentiation of bone marrow mesenchymal stem cells under chemical and mechanical stimulations. *Journal of biomechanics,* 43**,** 1176-81.

BAIGUERA, S., DEL GAUDIO, C., JAUS, M. O., POLIZZI, L., GONFIOTTI, A., COMIN, C. E., BIANCO, A., RIBATTI, D., TAYLOR, D. A. & MACCHIARINI, P. 2012. Long-term changes to in vitro preserved bioengineered human trachea and their implications for decellularized tissues. *Biomaterials,* 33**,** 3662-72.

BANES, A. J., HORESOVSKY, G., LARSON, C., TSUZAKI, M., JUDEX, S., ARCHAMBAULT, J., ZERNICKE, R., HERZOG, W., KELLEY, S. & MILLER, L. 1999. Mechanical load stimulates expression of novel genes in vivo and in vitro in avian flexor tendon cells. *Osteoarthritis and cartilage / OARS, Osteoarthritis Research Society,* 7**,** 141-53.

BAPTISTA, P. M., SIDDIQUI, M. M., LOZIER, G., RODRIGUEZ, S. R., ATALA, A. & SOKER, S. 2011. The use of whole organ decellularization for the generation of a vascularized liver organoid. *Hepatology,* 53**,** 604-17.

BARBER, F. A., MCGARRY, J. E., HERBERT, M. A. & ANDERSON, R. B. 2008. A biomechanical study of Achilles tendon repair augmentation using GraftJacket matrix. *Foot Ankle Int,* 29**,** 329-33.

BARRET, J. P., DZIEWULSKI, P., MCCAULEY, R. L., HERNDON, D. L. & DESAI, M. H. 1999. Dural reconstruction of a class IV calvarial burn with decellularized human dermis. *Burns,* 25**,** 459-462.

BARRY, F. P. & MURPHY, J. M. 2004. Mesenchymal stem cells: clinical applications and biological characterization. *The international journal of biochemistry & cell biology,* 36**,** 568-84.

BECK, G. R., ZERLER, B. & MORAN, E. 2000. Phosphate is a specific signal for induction of osteopontin gene expression. *Proceedings of the National Academy of Sciences of the United States of America,* 97**,** 8352-7.

BECKER, S., SAINT-CYR, M., WONG, C., DAUWE, P., NAGARKAR, P., THORNTON, J. F. & PENG, Y. 2009. AlloDerm versus DermaMatrix in immediate expander-based breast reconstruction: a preliminary comparison of complication profiles and material compliance. *Plast Reconstr Surg,* 123**,** 1-6; discussion 107-8.

BENHARDT, H. A. & COSGRIFF-HERNANDEZ, E. M. 2009. The role of mechanical loading in ligament tissue engineering. *Tissue engineering. Part B, Reviews,* 15**,** 467-75.

BERNARDO, M. E., ZAFFARONI, N., NOVARA, F., COMETA, A. M., AVANZINI, M. A., MORETTA, A., MONTAGNA, D., MACCARIO, R., VILLA, R., DAIDONE, M. G., ZUFFARDI, O. & LOCATELLI, F. 2007. Human bone marrow derived mesenchymal stem cells do not undergo transformation after long-term in vitro culture and do not exhibit telomere maintenance mechanisms. *Cancer Res,* 67**,** 9142-9.

BERSHADSKY, A. D., BALLESTREM, C., CARRAMUSA, L., ZILBERMAN, Y., GILQUIN, B., KHOCHBIN, S., ALEXANDROVA, A. Y., VERKHOVSKY, A. B., SHEMESH, T. & KOZLOV, M. M. 2006.

Assembly and mechanosensory function of focal adhesions: experiments and models. *European journal of cell biology,* 85**,** 165-73.

BIANCO, P. 2011. Bone and the hematopoietic niche: a tale of two stem cells. *Blood,* 117**,** 5281-8.

BLUMENTHAL, N. R., HERMANSON, O., HEIMRICH, B. & SHASTRI, V. P. 2014. Stochastic nanoroughness modulates neuron-astrocyte interactions and function via mechanosensing cation channels. *Proceedings of the National Academy of Sciences of the United States of America,* 111**,** 16124-16129.

BOND, J. L., DOPIRAK, R. M., HIGGINS, J., BURNS, J. & SNYDER, S. J. 2008. Arthroscopic replacement of massive, irreparable rotator cuff tears using a GraftJacket allograft: technique and preliminary results. *Arthroscopy,* 24**,** 403-409 e1.

BOOTH, C., KOROSSIS, S., WILCOX, H. E., WATTERSON, K. G., KEARNEY, J., FISHER, J. & INGHAM, E. 2002. Tissue Engineering of Cardiac Valve Prostheses I: Development and Characterization of an Acellular Porcine Scaffold *Journal of Heart and Valve Disease,* 11**,** 457-462.

BOSE. 2017. *Bose® 3DCulturePro™ Bioreactor* [Online]. Available: http://trends.directindustry.com/bose-electroforce-systems-group/project-50709-136298.html [Accessed 13.6.17.

BRAUDE, E. A., FAWCETT, J. S. & TIMMONS, C. J. 1950. Fluorescence and the Beer-Lambert Law: A note on the technique of absorption spectrophotometry. *Journal of the chemical society***,** 1019-1021.

BRONZINI, I., PATRUNO, M., IACOPETTI, I. & MARTINELLO, T. 2012. Influence of temperature, time and different media on mesenchymal stromal cells shipped for clinical application. *Vet J,* 194**,** 121-3.

BROOKE, S., MESA, J., ULUER, M., MICHELOTTI, B., MOYER, K., NEVES, R. I., MACKAY, D. & POTOCHNY, J. 2012. Complications in tissue expander breast reconstruction: a comparison of AlloDerm, DermaMatrix, and FlexHD acellular inferior pole dermal slings. *Ann Plast Surg,* 69**,** 347-9.

BROWN, A. L., SROKOWSKI, E. M., SHU, X. Z., PRESTWICH, G. D. & WOODHOUSE, K. A. 2006. Development of a model bladder extracellular matrix combining disulfide cross-linked hyaluronan with decellularized bladder tissue. *Macromol Biosci,* 6**,** 648-57.

BROWN, B. N., VALENTIN, J. E., STEWART-AKERS, A. M., MCCABE, G. P. & BADYLAK, S. F. 2009. Macrophage phenotype and remodeling outcomes in response to biologic scaffolds with and without a cellular component. *Biomaterials,* 30**,** 1482-1492.

BROWN, K. E., GUEST, S. S., SMALE, S. T., HAHM, K., MERKENSCHLAGER, M. & FISHER, A. G. 1997. Association of transcriptionally silent genes with Ikaros complexes at centromeric heterochromatin. *Cell,* 91**,** 845-54.

BROWN, K. S. 2004. Stem Cells and the future of regenerative medicine. *Oncology nursing forum,* 31**,** 138-138.

BRUDER, S. P., JAISWAL, N. & HAYNESWORTH, S. E. 1997. Growth kinetics, self-renewal, and the osteogenic potential of purified human mesenchymal stem cells during extensive subcultivation and following cryopreservation. *Journal of Cellular Biochemistry,* 64**,** 278-294.

BUKORESHTLIEV, N. V., HAASE, K. & PELLING, A. E. 2012. Mechanical cues in cellular signalling and communication. *Cell and Tissue Research,* 352**,** 77-94.

BUSTIN, A. 2000. Absolute quantification of mRNA using real-time reverse transcription polymerase chain reaction assays. *Journal of Molecular Biology,* 25**,** 169-193.

BUSTIN, S. A., BENES, V., GARSON, J. A., HELLEMANS, J., HUGGETT, J., KUBISTA, M., MUELLER, R., NOLAN, T., PFAFFL, M. W., SHIPLEY, G. L., VANDESOMPELE, J. & WITTWER, C. T. 2009. The MIQE guidelines: minimum information for publication of quantitative real-time PCR experiments. *Clin Chem,* 55**,** 611-22.

BUTLER, C. R., HYNDS, R. E., CROWLEY, C., GOWERS, K. H., PARTINGTON, L., HAMILTON, N. J., CARVALHO, C., PLATE, M., SAMUEL, E. R., BURNS, A. J., URBANI, L., BIRCHALL, M. A.,

LOWDELL, M. W., DE COPPI, P. & JANES, S. M. 2017. Vacuum-assisted decellularization: an accelerated protocol to generate tissue-engineered human tracheal scaffolds. *Biomaterials,* 124**,** 95-105.

BUTLER, D. L., JUNCOSA-MELVIN, N., BOIVIN, G. P., GALLOWAY, M. T., SHEARN, J. T., GOOCH, C. & AWAD, H. 2008. Functional Tissue Engineering for Tendon Repair : A Multidisciplinary Strategy Using Mesenchymal Stem Cells , Bioscaffolds , and Mechanical Stimulation. *Journal of Orhtopaedic research***,** 1-9.

BYFIELD, F. J., WEN, Q., LEVENTAL, I., NORDSTROM, K., ARRATIA, P. E., MILLER, R. T. & JANMEY, P. A. 2009. Absence of filamin A prevents cells from responding to stiffness gradients on gels coated with collagen but not fibronectin. *Biophysical journal,* 96**,** 5095-102.

CAO, D., LIU, W., WEI, X., XU, F., CUI, L. & CAO, Y. 2006. In vitro tendon engineering with avian tenocytes and polyglycolic acids: a preliminary report. *Tissue engineering,* 12**,** 1369-77.

CERNOMAZ, A. T., MACOVEI, II, PAVEL, I., GRIGORIU, C., MARINCA, M., BATY, F., PETER, S., ZONDA, R., BRUTSCHE, M. & GRIGORIU, B. 2016. Comparison of next generation sequencing, SNaPshot assay and real-time polymerase chain reaction for lung adenocarcinoma EGFR mutation assessment. *BMC Pulm Med,* 16**,** 88.

CHANG, C. W., PETRIE, T., CLARK, A., LIN, X., SONDERGAARD, C. S. & GRIFFITHS, L. G. 2016. Mesenchymal Stem Cell Seeding of Porcine Small Intestinal Submucosal Extracellular Matrix for Cardiovascular Applications. *PLoS One,* 11**,** e0153412.

CHANG, Y., LAI, P.-H., WEI, H.-J., LIN, W.-W., CHEN, C.-H., HWANG, S.-M., CHEN, S.-C. & SUNG, H.-W. 2007. Tissue regeneration observed in a basic fibroblast growth factor-loaded porous acellular bovine pericardium populated with mesenchymal stem cells. *The Journal of thoracic and cardiovascular surgery,* 134**,** 65-73, 73.e1-4.

CHAROENPANICH, A. 2012. Microarray analysis of human MSC in 3D collagen culture: 10% uniaxial cyclic tensile strain upregulates genes associated with musculoskeletal and cardiovascular development *Journal of Tissue Engineering and Regenerative Medicine,* 6**,** 343-344.

CHAUVIERE, M. V., SCHUTTER, R. J., STEIGELMAN, M. B., CLARK, B. Z., GRAYSON, J. K. & SAHAR, D. E. 2014. Comparison of AlloDerm and AlloMax tissue incorporation in rats. *Ann Plast Surg,* 73**,** 282-5.

CHEN, C. S. 2008. Mechanotransduction - a field pulling together? *Journal of cell science,* 121**,** 3285-92.

CHEN, C. S. & INGBER, D. E. 1999. Tensegrity and mechanoregulation: from skeleton to cytoskeleton. *Osteoarthritis and cartilage / OARS, Osteoarthritis Research Society,* 7**,** 81-94.

CHEN, F. H., ROUSCHE, K. T. & TUAN, R. S. 2006. Technology Insight: adult stem cells in cartilage regeneration and tissue engineering. *Nature clinical practice. Rheumatology,* 2**,** 373-82.

CHEN, J., FABRY, B., SCHIFFRIN, E. L. & WANG, N. 2001. Twisting integrin receptors increases endothelin-1 gene expression in endothelial cells. *American journal of physiology. Cell physiology,* 280**,** C1475-84.

CHEN, T. 2009. Effects of Low Temperature and Lactate on Osteogenic Differentiation of Human Amniotic Mesenchymal Stem Cells *Biotechnology and Bioprocess Engineering,* 14**,** 708-715.

CHEN, X.-D. 2010. Extracellular matrix provides an optimal niche for the maintenance and propagation of mesenchymal stem cells. *Birth defects research. Part C, Embryo today : reviews,* 90**,** 45-54.

CHEN, Y. J., HUANG, C. H., LEE, I. C., LEE, Y. T., CHEN, M. H. & YOUNG, T. H. 2008. Effects of cyclic mechanical stretching on the mRNA expression of tendon/ligament-related and osteoblast-specific genes in human mesenchymal stem cells. *Connective tissue research,* 49**,** 7-14.

CHOPRA, A., LIN, V., MCCOLLOUGH, A., ATZET, S., PRESTWICH, G. D., WECHSLER, A. S., MURRAY, M. E., OAKE, S. A., KRESH, J. Y. & JANMEY, P. A. 2012. Reprogramming

cardiomyocyte mechanosensing by crosstalk between integrins and hyaluronic acid receptors. *Journal of biomechanics,* 45**,** 824-31.

CHOUMERIANOU, D. M., DIMITRIOU, H. & KALMANTI, M. 2008. Stem cells: promises versus limitations. *Tissue engineering. Part B, Reviews,* 14**,** 53-60.

CHOWDHURY, F., NA, S., LI, D., POH, Y.-C., TANAKA, T. S., WANG, F. & WANG, N. 2010. Material properties of the cell dictate stress-induced spreading and differentiation in embryonic stem cells. *Nature materials,* 9**,** 82-8.

CRAPO, P. M., GILBERT, T. W. & BADYLAK, S. F. 2011. An overview of tissue and whole organ decellularization processes. *Biomaterials,* 32**,** 3233-43.

CROWLEY, C., DE SANTIS, M., URBANI, L., KHEDR, M., TEDESCHI, A., MERAN, L., LEE, S., CAMPINOTI, S., LI, V., BONFANTI, P., BURNS, A., EATON, S., BIRCHALL, M. A. & DE COPPI, P. 2017. 3D-culture of intestinal stem cells using an extracellular matrix hydrogel derived from decellularised intestinal tissue. *Cytotherapy,* 19**,** S25.

CSAKI, C., SCHNEIDER, P. R. A. & SHAKIBAEI, M. 2008. Mesenchymal stem cells as a potential pool for cartilage tissue engineering. *Annals of anatomy = Anatomischer Anzeiger : official organ of the Anatomische Gesellschaft,* 190**,** 395-412.

D'IPPOLITO, G., SCHILLER, P. C., RICORDI, C., ROOS, B. A. & HOWARD, G. A. 1999. Age-related osteogenic potential of mesenchymal stromal stem cells from human vertebral bone marrow. *Journal of bone and mineral research : the official journal of the American Society for Bone and Mineral Research,* 14**,** 1115-22.

DA SILVA MEIRELLES, L. 2006. Mesenchymal stem cells reside in virtually all post-natal organs and tissues. *Journal of Cell Science,* 119**,** 2204-2213.

DALOUS, J., LARGHERO, J. & BAUD, O. 2012. Transplantation of umbilical cord-derived mesenchymal stem cells as a novel strategy to protect the central nervous system: technical aspects, preclinical studies, and clinical perspectives. *Pediatric research,* 71**,** 482-90.

DAZZI, F. & HORWOOD, N. J. 2007. Potential of mesenchymal stem cell therapy. *Current opinion in oncology,* 19**,** 650-5.

DE BARI, C., DELL'ACCIO, F., TYLZANOWSKI, P. & LUYTEN, F. P. 2001. Multipotent mesenchymal stem cells from adult human synovial membrane. *Arthritis and rheumatism,* 44**,** 1928-42.

DEANS, R. J. & MOSELEY, A. B. 2000. Mesenchymal stem cells: biology and potential clinical uses. *Experimental hematology,* 28**,** 875-84.

DEASY, B. M., LI, Y. & HUARD, J. 2004. Tissue engineering with muscle-derived stem cells. *Current opinion in biotechnology,* 15**,** 419-23.

DEEKEN, C. R., WHITE, A. K., BACHMAN, S. L., RAMSHAW, B. J., CLEVELAND, D. S., LOY, T. S. & GRANT, S. A. 2011. Method of preparing a decellularized porcine tendon using tributyl phosphate. *J Biomed Mater Res B Appl Biomater,* 96**,** 199-206.

DEGAWA-YANAUCHI, M., MOSS, K. A., BOVENKERK, J. E., SHANKAR, S. S., MORRISON, C. L., LELLIOT, C. J., VIDAL-PUIG, A., JONES, R. & CONSIDINE, R. V. 2005. Regulation of Adiponectin Expression in Human Adipocytes: Effects of Adiposity, Glucocorticoids, and Tumor Necrosis Factor α. *Obesity research,* 13**,** 662-669.

DEGUCHI, S. & SATO, M. 2010. Nuclear Mechanics and Mechanotransduction. *In:* MOFRAD, M. R. K. & KAMM, R. D. (eds.). Cambridge: Cambridge University Press.

DELIDOW, B. C., PELUSO, J. J. & WHITE, B. A. 1989. Quantitative Measurement of mRNAs by Polymerase Chain Reaction. *Gene Analysis Techniques,* 6**,** 120-124.

DENG, W., OBROCKA, M., FISCHER, I. & PROCKOP, D. J. 2001. In vitro differentiation of human marrow stromal cells into early progenitors of neural cells by conditions that increase intracellular cyclic AMP. *Biochemical and biophysical research communications,* 282**,** 148-52.

DHANASEKARAN, M., INDUMATHI, S., RASHMI, M., RAJKUMAR, J. S. & SUDARSANAM, D. 2012. Unravelling the retention of proliferation and differentiation potency in extensive

culture of human subcutaneous fat-derived mesenchymal stem cells in different media. *Cell proliferation,* 45**,** 516-26.

DISCHER, D. E. 2005. Tissue Cells Feel and Respond to the Stiffness of Their Substrate. *Science,* 310**,** 1139-1143.

DOMINICI, M., LE BLANC, K., MUELLER, I., SLAPER-CORTENBACH, I., MARINI, F. C., KRAUSE, D. S., DEANS, R. J., KEATING, A., PROCKOP, D. J. & HORWITZ, E. M. 2006. Minimal criteria for defining multipotent mesenchymal stromal cells. The International Society for Cellular Therapy position statement. *Cytotherapy,* 8**,** 315-317.

DONG, J., LI, Y. & MO, X. 2013. The study of a new detergent (octyl-glucopyranoside) for decellularizing porcine pericardium as tissue engineering scaffold. *J Surg Res,* 183**,** 56-67.

DUCY, P. 2000. Cbfa1 : A Molecular Switch in Osteoblast Biology. *Developmental dynamics,* 471**,** 461-471.

DUCY, P., ZHANG, R., GEOFFROY, V., RIDALL, A. L. & KARSENTY, G. 1997. Osf2/Cbfa1: a transcriptional activator of osteoblast differentiation. *Cell,* 89**,** 747-54.

DÜNNWALD, J. & OTTO, A. 1989. An investigation of phase transitions in rust layers using raman spectroscopy. *Corrosion Science,* 29**,** 1167-1176.

DYTHAM, C. 2011. *Choosing and Using Statistics: A Biologist's guide,* Sussex, Wiley-Blackwell.

EAGLE, H. 1971. Buffer Combinations for Mammalian Cell Culture. *Science,* 174**,** 500-503.

EAKER, S., ABRAHAM, E., ALLICKSON, J., BRIEVA, T. A., BAKSH, D., HEATHMAN, T. R. J., MISTRY, B. & ZHANG, N. 2017. Bioreactors for cell therapies: Current status and future advances. *Cytotherapy,* 19**,** 9-18.

EARLS, J. K., JIN, S. & YE, K. 2013. Mechanobiology of human pluripotent stem cells. *Tissue Eng Part B Rev,* 19**,** 420-30.

EDELMAN, D. S. & SELESNICK, H. 2006. ''Sports'' hernia: treatment with biologic mesh (Surgisis). *Surgical Endoscopy and other interventional techniques,* 20**,** 971–973.

EDWARDS, K., LOGAN, J. & SAUNDERS, N. 2004. *Real time PCR: An essential guide,* Norfolk, Horizon bioscience.

EINSELE, A. & FIECHTER, A. 1969. Zum Entwurf von Bio-Reaktoren für die mikrobielle Oxydation von Kohlenwasserstoffen. *Pathologia et Microbiologia,* 34**,** 149-150.

ELDER, B. D., ELESWARAPU, S. V. & ATHANASIOU, K. A. 2009. Extraction techniques for the decellularization of tissue engineered articular cartilage constructs. *Biomaterials,* 30**,** 3749-56.

ELLIS, W. M., GEORGIOU, G. M., ROBERTON, R. M. & JOHNSON, G. R. 1984. The use of discontinuous gradients to separate populations of cells from human bone marrow and peripheral blood. *Journal of Immunological Methods,* 66**,** 9-16.

ENGLER, A. J., SEN, S., SWEENEY, H. L. & DISCHER, D. E. 2006. Matrix Elasticity Directs Stem Cell Lineage Specification. *Cell,* 126**,** 677-689.

ERICES, A., CONGET, P. & MINGUELL, J. J. 2000. Mesenchymal progenitor cells in human umbilical cord blood. *British journal of haematology,* 109**,** 235-242.

EVANS, M. J. & KAUFMAN, M. H. 1981. Establishment in culture of pluripotential cells from mouse embryos. *Nature,* 292**,** 154-156.

EVEN-RAM, S., ARTYM, V. & YAMADA, K. M. 2006. Matrix control of stem cell fate. *Cell,* 126**,** 645-7.

FABRE, A. L., COLOTTE, M., LUIS, A., TUFFET, S. & BONNET, J. 2014. An efficient method for long-term room temperature storage of RNA. *Eur J Hum Genet,* 22**,** 379-85.

FLYNN, L., PRESTWICH, G. D., SEMPLE, J. L. & WOODHOUSE, K. A. 2007. Adipose tissue engineering with naturally derived scaffolds and adipose-derived stem cells. *Biomaterials,* 28**,** 3834-42.

FRIEDENSTEIN, A. J., CHAILAKH, R. K. & LALYKINA, K. S. 1970. DEVELOPMENT OF FIBROBLAST COLONIES IN MONOLAYER CULTURES OF GUINEA-PIG BONE MARROW AND SPLEEN CELLS. *Cell and Tissue Kinetics,* 3**,** 393-393.

FRIEDENSTEIN, A. J., CHAILAKHAYAN, R. K. & GERASIMOV, U. V. 1987. BONE-MARROW OSTEOGENIC STEM-CELLS - INVITRO CULTIVATION AND TRANSPLANTATION IN DIFFUSION-CHAMBERS. *Cell and Tissue Kinetics,* 20**,** 263-272.

FRIEDENSTEIN, A. J., CHAILAKHYAN, R. K., V, L. N., PANASYUK, A. F. & KEILISS-BOROK, I. V. 1974. Stromal cells responsible for transferring the microenvironment of the hemopoeitic tissues. *Transplantation,* 17**,** 331-340.

FRIEDENSTEIN, A. J., PIATETZKY-SHAPIRO, I. I. & PETRAKOVA, K. V. 1966. Osteogenesis in transplants of bone marrow cells. *Journal of embryology and experimental morphology,* 16**,** 381-90.

FRIEDL, G., SCHMIDT, H., REHAK, I., KOSTNER, G., SCHAUENSTEIN, K. & WINDHAGER, R. 2007. Undifferentiated human mesenchymal stem cells (hMSCs) are highly sensitive to mechanical strain: transcriptionally controlled early osteo-chondrogenic response in vitro. *Osteoarthritis and cartilage,* 15**,** 1293-1300.

FUCHS, E., TUMBAR, T. & GUASCH, G. 2004. Socializing with the neighbors: stem cells and their niche. *Cell,* 116**,** 769-78.

FUJITA, T., IZUMO, N., FUKUYAMA, R., MEGURO, T., NAKAMUTA, H., KOHNO, T. & KOIDA, M. 2001. Phosphate provides an extracellular signal that drives nuclear export of Runx2/Cbfa1 in bone cells. *Biochemical and biophysical research communications,* 280**,** 348-52.

FURUKAWA, K., PICHORA, J., STEINMANN, S., FABER, K. J., JOHNSON, J. A. & KING, G. J. 2007. Efficacy of interference screw and double-docking methods using palmaris longus and GraftJacket for medial collateral ligament reconstruction of the elbow. *J Shoulder Elbow Surg,* 16**,** 449-53.

GALMICHE, M. C., KOTELIANSKY, V. E., BRIÈRE, J., HERVÉ, P. & CHARBORD, P. 1993. Stromal cells from human long-term marrow cultures are mesenchymal cells that differentiate following a vascular smooth muscle differentiation pathway. *Blood,* 82**,** 66-76.

GARDIN, C., RICCI, S., FERRONI, L., GUAZZO, R., SBRICOLI, L., DE BENEDICTIS, G., FINOTTI, L., ISOLA, M., BRESSAN, E. & ZAVAN, B. 2015. Decellularization and Delipidation Protocols of Bovine Bone and Pericardium for Bone Grafting and Guided Bone Regeneration Procedures. *PLoS One,* 10**,** e0132344.

GE. 2017. *Bioreactors for Cell Culture* [Online]. Available: http://www.gelifesciences.com/webapp/wcs/stores/servlet/catalog/en/GELifeScience s-uk/products/AlternativeProductStructure_24446/ [Accessed 13.06.2017.

GEBLER, A., ZABEL, O. & SELIGER, B. 2012. The immunomodulatory capacity of mesenchymal stem cells. *Trends in molecular medicine,* 18**,** 128-34.

GEIGER, B., SPATZ, J. P. & BERSHADSKY, A. D. 2009. Environmental sensing through focal adhesions. *Nature reviews. Molecular cell biology,* 10**,** 21-33.

GIENI, R. S. & HENDZEL, M. J. 2008. Mechanotransduction from the ECM to the genome: are the pieces now in place? *Journal of cellular biochemistry,* 104**,** 1964-87.

GILBERT, T. W., FREUND, J. M. & BADYLAK, S. F. 2009. Quantification of DNA in biologic scaffold materials. *The Journal of surgical research,* 152**,** 135-9.

GILBERT, T. W., SELLARO, T. L. & BADYLAK, S. F. 2006. Decellularization of tissues and organs. *Biomaterials,* 27**,** 3675-83.

GLASEL, J. A. 1995. Validity of nucleic acid purities monitored by 260/280 nm absorbency ratios. *Biotechniques,* 18**,** 62-63.

GODARA, P., NORDON, R. E. & MCFARLAND, C. D. 2008. Mesenchymal stem cells in tissue engineering. *Journal of Chemical Technology and Biotechnology,* 407**,** 397-407.

GOERKE, S. M., PLAHA, J., HAGER, S., STRASSBURG, S., PH, D., TORIO-PADRON, N. & BJO, G. 2012. Human Endothelial Progenitor Cells Induce Extracellular Signal-Regulated Kinase-Dependent Differentiation of Mesenchymal Stem Cells into Smooth Muscle Cells upon Cocultivation. *Tissue engineering@ Part A,* 18**,** 2395-2405.

GOMILLION, C. T. & BURG, K. J. L. 2006. Stem cells and adipose tissue engineering. *Biomaterials,* 27**,** 6052-63.

GONG, Z., KRAUSE, D., NIKLASON, L. E., CALKINS, G. & CHENG, E. 2009. Influence of Culture Medium on Smooth Muscle Cell Differentiation from Human Bone Marrow Derived Mesenchymal Stem Cells. *Tissue engineering: Part A,* 15**,** 319-330.

GONG, Z. & NIKLASON, L. E. 2008. Small-diameter human vessel wall engineered from bone marrow-derived mesenchymal stem cells (hMSCs). *FASEB journal : official publication of the Federation of American Societies for Experimental Biology,* 22**,** 1635-48.

GOOD, N. E., WINGET, D., WINTER, W., CONNOLLY, T. N., IZAWA, S. & SINGH, R. M. M. 1966. Hydrogen ion buffers for biological research. *Biochemistry,* 5**,** 467-477.

GOTTS, J. E. & MATTHAY, M. A. 2012. Mesenchymal stem cells and the stem cell niche: a new chapter. *American journal of physiology. Lung cellular and molecular physiology,* 302**,** L1147-9.

GRAD, S., GOLDHAHN, J., SALZMANN, G., LI, Z., ALINI, M., STODDART, M. J. & PLATZ, D. 2011. A combination of shear and dynamic compression leads to mechanically induced chondrogenesis of human mesenchymal stem cells. *European cells & materials,* 22**,** 214-225.

GRAYSON, W. L., ZHAO, F., IZADPANAH, R., BUNNELL, B. & MA, T. 2006. Effects of Hypoxia on Human Mesenchymal Stem Cell Expansion and Plasticity in 3D Constructs. 339**,** 331-339.

GRIMSEY, N. L., MOODLEY, K. S., GLASS, M. & GRAHAM, E. S. 2012. Sensitive and accurate quantification of human leukocyte migration using high-content Discovery-1 imaging system and ATPlite assay. *J Biomol Screen,* 17**,** 386-93.

GUTENBERG, J. 2012. Abstracts of the 3rd TERMIS (Tissue Engineering & Regenerative Medicine International Society) World Congress 2012. September 5-8, 2012. Vienna, Austria. *Journal of tissue engineering and regenerative medicine,* 6 Suppl 1**,** 1-465.

HAASE, K. & PELLING, A. E. 2015. Investigating cell mechanics with atomic force microscopy. *Journal of The Royal Society Interface,* 12**,** 20140970-20140970.

HAM, R. G. & PUCK, T. T. 1962. A Regulated Incubator CO_2 Concentration, Humidity and Temperature for Use in Animal Cell Culture. *Proceedings of the society for experimental biology and medicine,* 111**,** 67-70.

HANADA, K., DENNIS, J. E. & CAPLAN, A. I. 1997. Stimulatory Effects of Basic Fibroblast Growth Factor and Bone Morphogenetic Protein-2 on Osteogenic Mesenchymal Stem Cells. *Journal of bone and mineral research : the official journal of the American Society for Bone and Mineral Research,* 12**,** 1606-1614.

HANKEMEIER, S., HURSCHLER, C., ZEICHEN, J., VAN GRIENSVEN, M., MILLER, B., MELLER, R., EZECHIELI, M., KRETTEK, C. & JAGODZINSKI, M. 2009. Bone marrow stromal cells in a liquid fibrin matrix improve the healing process of patellar tendon window defects. *Tissue engineering. Part A,* 15**,** 1019-30.

HARA, K., YAMADA, Y., NAKAMURA, S., UMEMURA, E., ITO, K. & UEDA, M. 2011. Potential characteristics of stem cells from human exfoliated deciduous teeth compared with bone marrow-derived mesenchymal stem cells for mineralized tissue-forming cell biology. *Journal of endodontics,* 37**,** 1647-52.

HAYFLICK, L. 1965. The limited in vitro lifetime of human diploid cell strains. *Experimental Cell Research,* 37**,** 614-636.

HEATH, C. A. 2000. The Effects of Physical Forces on Cartilage Tissue Engineering. *Biotechnology and Genetic Engineering Reviews,* 17**,** 533-552.

HEATHMAN, T. R., STOLZING, A., FABIAN, C., RAFIQ, Q. A., COOPMAN, K., NIENOW, A. W., KARA, B. & HEWITT, C. J. 2016. Scalability and process transfer of mesenchymal stromal cell production from monolayer to microcarrier culture using human platelet lysate. *Cytotherapy,* 18**,** 523-35.

HEE-HOON, Y. 2015. Effect of Low Temperature on Schwann-Like Cell Differentiation of Bone Marrow Mesenchymal Stem Cells *Tissue Engineering and Regenerative Medicine,* 12**,** 259-267.

HO, F. C., ZHANG, W., LI, Y. Y. & CHAN, B. P. 2015. Mechanoresponsive, omni-directional and local matrix-degrading actin protrusions in human mesenchymal stem cells microencapsulated in a 3D collagen matrix. *Biomaterials,* 53**,** 392-405.

HOFFMAN, B. D. & CROCKER, J. C. 2009. Cell mechanics: dissecting the physical responses of cells to force. *Annual review of biomedical engineering,* 11**,** 259-88.

HOFFMAN, B. D., GRASHOFF, C. & SCHWARTZ, M. A. 2011. Dynamic molecular processes mediate cellular mechanotransduction. *Nature,* 475**,** 316-323.

HOGANSON, D. M., O'DOHERTY, E. M., OWENS, G. E., HARILAL, D. O., GOLDMAN, S. M., BOWLEY, C. M., NEVILLE, C. M., KRONENGOLD, R. T. & VACANTI, J. P. 2010a. The retention of extracellular matrix proteins and angiogenic and mitogenic cytokines in a decellularized porcine dermis. *Biomaterials,* 31**,** 6730-7.

HOGANSON, D. M., OWENS, G. E., O'DOHERTY, E. M., BOWLEY, C. M., GOLDMAN, S. M., HARILAL, D. O., NEVILLE, C. M., KRONENGOLD, R. T. & VACANTI, J. P. 2010b. Preserved extracellular matrix components and retained biological activity in decellularized porcine mesothelium. *Biomaterials,* 31**,** 6934-40.

HOGG, P., ROONEY, P., LEOW-DYKE, S., BROWN, C., INGHAM, E. & KEARNEY, J. N. 2015. Development of a terminally sterilised decellularised dermis. *Cell Tissue Bank,* 16**,** 351-9.

HOLLE, A. W., TANG, X., VIJAYRAGHAVAN, D., VINCENT, L. G., FUHRMANN, A., CHOI, Y. S., DEL ÁLAMO, J. C. & ENGLER, A. J. 2013. In situ mechanotransduction via vinculin regulates stem cell differentiation. *Stem cells (Dayton, Ohio),* 31**,** 2467-77.

HSU, S.-H. & HUANG, G.-S. 2013. Substrate-dependent Wnt signaling in MSC differentiation within biomaterial-derived 3D spheroids. *Biomaterials,* 34**,** 4725-38.

HU, C., ZHOU, N., LI, J., SHI, D., CAO, H., LI, J. & LI, L. 2016. Porcine Adipose-Derived Mesenchymal Stem Cells Retain Their Stem Cell Characteristics and Cell Activities While Enhancing the Expression of Liver-Specific Genes after Acute Liver Failure. *Int J Mol Sci,* 17.

HUANG, A. H., FARRELL, M. J. & MAUCK, R. L. 2010. Mechanics and mechanobiology of mesenchymal stem cell-based engineered cartilage. *J Biomech,* 43**,** 128-36.

HUANG, A. H., LEE, Y. U., CALLE, E. A., BOYLE, M., STARCHER, B. C., HUMPHREY, J. D. & NIKLASON, L. E. 2015. Design and Use of a Novel Bioreactor for Regeneration of Biaxially Stretched Tissue-Engineered Vessels. *Tissue Eng Part C Methods,* 21**,** 841-51.

HUANG, C. & OGAWA, R. 2010. Mechanotransduction in bone repair and regeneration. *The FASEB journal : official publication of the Federation of American Societies for Experimental Biology,* 24**,** 3625-32.

HUANG, C. H., CHEN, M. H., YOUNG, T. H., JENG, J. H. & CHEN, Y. J. 2009. Interactive effects of mechanical stretching and extracellular matrix proteins on initiating osteogenic differentiation of human mesenchymal stem cells. *Journal of cellular biochemistry,* 108**,** 1263-73.

HUANG, Y., ZHENG, L., GONG, X., JIA, X., SONG, W., LIU, M. & FAN, Y. 2012. Effect of cyclic strain on cardiomyogenic differentiation of rat bone marrow derived mesenchymal stem cells. *PloS one,* 7**,** e34960-e34960.

HUGGETT, J., DHEDA, K., BUSTIN, S. & ZUMLA, A. 2005. Real-time RT-PCR normalisation; strategies and considerations. *Genes Immun,* 6**,** 279-84.

HUI, J. H. P., LI, L. I., TEO, Y.-H., OUYANG, H.-W., PH, D. & LEE, E.-H. 2005. Comparative Study of the Ability of Mesenchymal Stem Cells Derived from Bone Marrow , Periosteum , and Adipose Tissue. *Tissue engineering,* 11**,** 904-913.

ISHIHARA, T., FERRANS, V. J., JONES, M., BOYCE, S. W., KAWANAMI, O. & ROBERTS, W. C. 1980. Histologic and ultrastructural features of normal human parietal pericardium. *The American journal of cardiology,* 46**,** 744-53.

ISLAM, S. & ALISON, M. R. 2009. Attributes of adult stem cells. *Journal of Pathology,* 217**,** 144-160.

JAIN, M., NIJHAWAN, A., TYAGI, A. K. & KHURANA, J. P. 2006. Validation of housekeeping genes as internal control for studying gene expression in rice by quantitative real-time PCR. *Biochem Biophys Res Commun,* 345**,** 646-51.

JANG, J.-Y., LEE, S. W., PARK, S. H., SHIN, J. W., MUN, C., KIM, S.-H., KIM, D. H. & SHIN, J.-W. 2011. Combined effects of surface morphology and mechanical straining magnitudes on the differentiation of mesenchymal stem cells without using biochemical reagents. *Journal of biomedicine & biotechnology,* 2011**,** 860652-860652.

JUNG, N., PARK, S., CHOI, Y., PARK, J. W., HONG, Y. B., PARK, H. H., YU, Y., KWAK, G., KIM, H. S., RYU, K. H., KIM, J. K., JO, I., CHOI, B. O. & JUNG, S. C. 2016. Tonsil-Derived Mesenchymal Stem Cells Differentiate into a Schwann Cell Phenotype and Promote Peripheral Nerve Regeneration. *Int J Mol Sci,* 17.

KARSAI, A., MÜLLER, S., PLATZ, S. & HAUSER, M. 2002. Evaluation of a Homemade SYBR® Green I Reaction Mixture for Real-Time PCR Quantification of Gene Expression. *Biotechniques,* 32**,** 790-796.

KATSUMI, A., NAOE, T., MATSUSHITA, T., KAIBUCHI, K. & SCHWARTZ, M. A. 2005. Integrin activation and matrix binding mediate cellular responses to mechanical stretch. *The Journal of biological chemistry,* 280**,** 16546-9.

KELLY, D. J. & JACOBS, C. R. 2010. The role of mechanical signals in regulating chondrogenesis and osteogenesis of mesenchymal stem cells. *Birth defects research. Part C, Embryo today : reviews,* 90**,** 75-85.

KERN, S., EICHLER, H., STOEVE, J., KLUTER, H. & BIEBACK, K. 2006. Comparative analysis of mesenchymal stem cells from bone marrow, umbilical cord blood, or adipose tissue. *Stem Cells,* 24**,** 1294-301.

KHADEMOLHOSSEINI, F., LIU, C. C., LIM, C. J. & CHIAO, M. 2016. A magnetically actuated cellular strain assessment tool for quantitative analysis of strain induced cellular reorientation and actin alignment. *Rev Sci Instrum,* 87**,** 085004.

KHAYAT, G., ROSENZWEIG, D. H. & QUINN, T. M. 2012. Low frequency mechanical stimulation inhibits adipogenic differentiation of C3H10T1/2 mesenchymal stem cells. *Differentiation; research in biological diversity,* 83**,** 179-84.

KIM, B. S., NIKOLOVSKI, J., BONADIO, J. & MOONEY, D. J. 1999. Cyclic mechanical strain regulates the development of engineered smooth muscle tissue. *Nature biotechnology,* 17**,** 979-83.

KIM, D. H., KIM, S.-H., HEO, S.-J., SHIN, J. W., LEE, S. W., PARK, S. A. & SHIN, J.-W. 2009. Enhanced differentiation of mesenchymal stem cells into NP-like cells via 3D co-culturing with mechanical stimulation. *Journal of bioscience and bioengineering,* 108**,** 63-7.

KIM, S. G., AKAIKE, T., SASAGAW, T., ATOMI, Y. & KUROSAWA, H. 2002. Gene expression of type I and type III collagen by mechanical stretch in anterior cruciate ligament cells. *Cell structure and function,* 27**,** 139-44.

KIM, Y. M., JEON, E. S., KIM, M. R., JHO, S. K., RYU, S. W. & KIM, J. H. 2008. Angiotensin II-induced differentiation of adipose tissue-derived mesenchymal stem cells to smooth muscle-like cells. *Int J Biochem Cell Biol,* 40**,** 2482-91.

KOLF, C. M., CHO, E. & TUAN, R. S. 2007. Mesenchymal stromal cells. Biology of adult mesenchymal stem cells: regulation of niche, self-renewal and differentiation. *Arthritis research & therapy,* 9**,** 204-204.

KOTA, D. J., PRABHAKARA, K. S., TOLEDANO-FURMAN, N., BHATTARAI, D., CHEN, Q., DICARLO, B., SMITH, P., TRIOLO, F., WENZEL, P. L., COX, C. S., JR. & OLSON, S. D. 2017. Prostaglandin E2 Indicates Therapeutic Efficacy of Mesenchymal Stem Cells in Experimental Traumatic Brain Injury. *Stem Cells,* 35**,** 1416-1430.

KREJA, L., LIEDERT, A., SCHLENKER, H., BRENNER, R. E., FIEDLER, J., FRIEMERT, B., DÜRSELEN, L. & IGNATIUS, A. 2012. Effects of mechanical strain on human mesenchymal stem cells and ligament fibroblasts in a textured poly(L-lactide) scaffold for ligament tissue engineering. *Journal of materials science. Materials in medicine,* 23**,** 2575-82.

KRISHNAMURITHY, G., YAHYA, N. A., MEHRALI, M., MEHRALI, M., MOHAN, S., MURALI, M. R., RAGHAVENDRAN, H. R. B. & KAMARUL, T. 2016. Effects of carbon doping on the microstructural, micro/nano-mechanical, and mesenchymal stromal cells biocompatibility and osteogenic differentiation properties of alumina. *Ceramics International,* 42**,** 18247-18256.

KU, C.-H., JOHNSON, P. H., BATTEN, P., SARATHCHANDRA, P., CHAMBERS, R. C., TAYLOR, P. M., YACOUB, M. H. & CHESTER, A. H. 2006. Collagen synthesis by mesenchymal stem cells and aortic valve interstitial cells in response to mechanical stretch. *Cardiovascular research,* 71**,** 548-56.

KUHN, N. Z. & TUAN, R. S. 2010. Regulation of stemness and stem cell niche of mesenchymal stem cells: implications in tumorigenesis and metastasis. *Journal of cellular physiology,* 222**,** 268-77.

KUO, C. K. & TUAN, R. K. 2008a. Mechanoactive tenogenic differentiation of human mesenchymal stem cells. *Tissue engineering. Part A,* 14**,** 1615-27.

KUO, C. K. & TUAN, R. S. 2008b. Mechanoactive tenogenic differentiation of human mesenchymal stem cells. *Tissue engineering. Part A,* 14**,** 1615-27.

KUO, S.-W., LIN, H.-I., HO, J. H.-C., SHIH, Y.-R. V., CHEN, H.-F., YEN, T.-J. & LEE, O. K. 2012. Regulation of the fate of human mesenchymal stem cells by mechanical and stereo-topographical cues provided by silicon nanowires. *Biomaterials,* 33**,** 5013-22.

KURPINSKI, K., CHU, J., HASHI, C. & LI, S. 2006. Anisotropic mechanosensing by mesenchymal stem cells. *Proceedings of the National Academy of Sciences of the United States of America,* 103**,** 16095-100.

LANGE, P., GRECO, K., PARTINGTON, L., CARVALHO, C., OLIANI, S., BIRCHALL, M. A., SIBBONS, P. D., LOWDELL, M. W. & ANSARI, T. 2017. Pilot study of a novel vacuum-assisted method for decellularization of tracheae for clinical tissue engineering applications. *J Tissue Eng Regen Med,* 11**,** 800-811.

LAPERLE, A., MASTERS, K. S. & PALECEK, S. P. 2015. Influence of substrate composition on human embryonic stem cell differentiation and extracellular matrix production in embryoid bodies. *Biotechnol Prog,* 31**,** 212-9.

LAVRENTIEVA, A., HATLAPATKA, T., NEUMANN, A., WEYAND, B. & KASPER, C. 2013. *Mesenchymal Stem Cells: Basics and Clinical Application I,* Berlin, Springer.

LEE, D. A., KNIGHT, M. M., CAMPBELL, J. J. & BADER, D. L. 2011. Stem cell mechanobiology. *J Cell Biochem,* 112**,** 1-9.

LEE, E. W., BERBOS, Z., ZALDIVAR, R. A., LEE, M. S. & HARRISON, A. R. 2010. Use of DermaMatrix graft in oculoplastic surgery. *Ophthal Plast Reconstr Surg,* 26**,** 153-4.

LEE, K. B., HUI, J. H., SONG, I. C., ARDANY, L. & LEE, E. H. 2007. Injectable mesenchymal stem cell therapy for large cartilage defects--a porcine model. *Stem Cells,* 25**,** 2964-71.

LEE, M. S. 2004. GraftJacket Augmentation of Achilles Tendon Rupture. *Orthopedics,* 27**,** S151-S153.

LEE, Y. P., JO, M., LUNA, M., CHIEN, B., LIEBERMAN, J. R. & WANG, J. C. 2005. The Efficacy of Different Commercially Available Demineralized Bone Matrix Substances in an Athymic Rat Model. *Journal of spinal disorders and techniques,* 18**,** 439-444.

LEHMANN, J. M., LENHARD, J. M., OLIVER, B. B., RINGOLD, G. M. & KLIEWER, S. A. 1997. Peroxisome proliferator-activated receptors alpha and gamma are activated by indomethacin and other non-steroidal anti-inflammatory drugs. *The Journal of biological chemistry,* 272**,** 3406-10.

LEI, Y. & FERDOUS, Z. 2016. Design considerations and challenges for mechanical stretch bioreactors in tissue engineering. *Biotechnol Prog,* 32**,** 543-53.

LI, X., YANG, Q., BAI, J., YANG, Y., ZHONG, L. & WANG, Y. 2015. Identification of optimal reference genes for quantitative PCR studies on human mesenchymal stem cells. *Mol Med Rep,* 11**,** 1304-11.

LIDEN, B. A. & SIMMONS, M. 2009. Histologic Evaluation of a 6-Month GraftJacket Matrix Biopsy Used for Achilles Tendon Augmentation. *Journal of the American Podiatric Medical Association,* 99**,** 104-107.

LIN, T. W. T. W., CARDENAS, L. & SOSLOWSKY, L. J. L. J. 2004. Biomechanics of tendon injury and repair. *Journal of biomechanics,* 37**,** 865-77.

LIU, P., OYAJOBI, B. O., RUSSELL, R. G. & SCUTT, A. 1999. Regulation of osteogenic differentiation of human bone marrow stromal cells: interaction between transforming growth factor-beta and 1,25(OH)(2) vitamin D(3) In vitro. *Calcified tissue international,* 65**,** 173-80.

LODISH, H., KAISER, C. A., BRETSCHER, A., AMON, A., BERK, A., KRIEGER, M., PLOEGH, H. & SCOTT, M. P. 2008. *Molecular Cell Biology,* New York, MacMillan Higher Education.

LOUIS-UGBOO, J., MURAKAMI, H., KIM, H. S., MINAMIDE, A. & BODEN, S. D. 2004. Evidence of osteoinduction by Grafton demineralized bone matrix in nonhuman primate spinal fusion. *Spine,* 29**,** 360-360.

LOVEKAMP, J. J., SIMIONESCU, D. T., MERCURI, J. J., ZUBIATE, B., SACKS, M. S. & VYAVAHARE, N. R. 2006. Stability and function of glycosaminoglycans in porcine bioprosthetic heart valves. *Biomaterials,* 27**,** 1507-18.

LUI, P. P. Y., RUI, Y. F., NI, M. & CHAN, K. M. 2011. Tenogenic differentiation of stem cells for tendon repair – what is the current evidence ?

LUNDIN, A., HASENSON, M., PERSSON, J. & POUSETTE, A. 1986. Estimation of Biomass in Growing Cell Lines by Adenosine Triphosphate Assay. *Methods in Enzymology,* 133**,** 14-22.

MACK, J. J., CORRIN, A. A., DOS SANTOS E LUCATO, S. L., DUNN, J. C., WU, B. W. & COX, B. N. 2013. Enhanced cell viability via strain stimulus and fluid flow in magnetically actuated scaffolds. *Biotechnol Bioeng,* 110**,** 936-46.

MACQUEEN, L., SUN, Y. & SIMMONS, C. A. 2013. Mesenchymal stem cell mechanobiology and emerging experimental platforms. *J R Soc Interface,* 10**,** 20130179.

MACRI-PELLIZZERI, L., PELACHO, B., SANCHO, A., IGLESIAS-GARCIA, O., SIMON-YARZA, A. M., SORIANO-NAVARRO, M., GONZALEZ-GRANERO, S., GARCIA-VERDUGO, J. M., DE-JUAN-PARDO, E. M. & PROSPER, F. 2015. Substrate stiffness and composition specifically direct differentiation of induced pluripotent stem cells. *Tissue Eng Part A,* 21**,** 1633-41.

MAIER, S., LUTZ, R., GELMAN, L., SARASA-RENEDO, A., SCHENK, S., GRASHOFF, C. & CHIQUET, M. 2008. Tenascin-C induction by cyclic strain requires integrin-linked kinase. *Biochimica et biophysica acta,* 1783**,** 1150-62.

MAKSIMOV, A. A. 2009. The lymphocyte as a stem cell, common to different blood elements in embryonic development and during the post-fetal life of mammals. *Cell therapy and transplantation,* 1**,** 14-18.

MARSANO, A., WENDT, D., RAITERI, R., GOTTARDI, R., STOLZ, M., WIRZ, D., DANIELS, A. U., SALTER, D., JAKOB, M., QUINN, T. M. & MARTIN, I. 2006. Use of hydrodynamic forces to engineer cartilaginous tissues resembling the non-uniform structure and function of meniscus. *Biomaterials,* 27**,** 5927-34.

MARTIN, G. R. 1981. Isolation of a pluripotent cell line from early mouse embryos cultured in medium conditioned by teratocarcinoma stem cells Developmental Biology. 78**,** 7634-7638.

MAUNEY, J. R., PH, D., VOLLOCH, V. & KAPLAN, D. L. 2005. Role of Adult Mesenchymal Stem Cells in Bone Tissue. *Tissue engineering,* 11**,** 787-798.

MCKAYED, K., PRENDERGAST, P. J. & CAMPBELL, V. A. 2016. Aging enhances the vulnerability of mesenchymal stromal cells to uniaxial tensile strain-induced apoptosis. *J Biomech,* 49**,** 458-62.

MCPHERSON, M. & MØLLER, S. 2006. *PCR,* Oxford, Taylor & Francis Group.

MEINEL, L., KARAGEORGIOU, V., FAJARDO, R., SNYDER, B., SHINDE-PATIL, V., ZICHNER, L., KAPLAN, D., LANGER, R. & VUNJAK-NOVAKOVIC, G. 2004. Bone tissue engineering

using human mesenchymal stem cells: effects of scaffold material and medium flow. *Annals of biomedical engineering,* 32**,** 112-22.

MENDOZA-NOVELO, B., AVILA, E. E., CAUICH-RODRÍGUEZ, J. V., JORGE-HERRERO, E., ROJO, F. J., GUINEA, G. V. & MATA-MATA, J. L. 2011. Decellularization of pericardial tissue and its impact on tensile viscoelasticity and glycosaminoglycan content. *Acta biomaterialia,* 7**,** 1241-8.

MIRSADRAEE, S., WILCOX, H. E., KOROSSIS, S. A. & INGHAM, E. 2006. Development and Characterization of an Acellular Human Pericardial Matrix for Tissue Engineering. *Tissue engineering,* 12**,** 763-773.

MIRSADRAEE, S., WILCOX, H. E., WATTERSON, K. G., KEARNEY, J. N., HUNT, J., FISHER, J. & INGHAM, E. 2007. Biocompatibility of acellular human pericardium. *The Journal of surgical research,* 143**,** 407-14.

MIURA, K., OKADA, Y., AOI, T., OKADA, A., TAKAHASHI, K., OKITA, K., NAKAGAWA, M., KOYANAGI, M., TANABE, K., OHNUKI, M., OGAWA, D., IKEDA, E., OKANO, H. & YAMANAKA, S. 2009. Variation in the safety of induced pluripotent stem cell lines. *Nat Biotechnol,* 27**,** 743-5.

MIYANISHI, K., TRINDADE, M. C. D., LINDSEY, D. P., BEAUPRÉ, G. S., CARTER, D. R., GOODMAN, S. B. & SHURM, D. J. 2006. Effects of Hydrostatic Pressure and Transforming Growth Factor-β3 on Adult Human Mesenchymal Stem Cell Chondrogenesis In Vitro. *Tissue Engineering,* 12**,** 1419-1428.

MIZUKAMI, A., FERNANDES-PLATZGUMMER, A., CARMELO, J. G., SWIECH, K., COVAS, D. T., CABRAL, J. M. & DA SILVA, C. L. 2016. Stirred tank bioreactor culture combined with serum-/xenogeneic-free culture medium enables an efficient expansion of umbilical cord-derived mesenchymal stem/stromal cells. *Biotechnol J,* 11**,** 1048-59.

MOHAMMADI, H., JANMEY, P. A. & MCCULLOCH, C. A. 2014. Lateral boundary mechanosensing by adherent cells in a collagen gel system. *Biomaterials,* 35**,** 1138-49.

MORITA, Y., SATO, T., WATANABE, S. & JU, Y. 2014. Determination of Precise Optimal Cyclic Strain for Tenogenic Differentiation of Mesenchymal Stem Cells Using a Non-uniform Deformation Field. *Experimental Mechanics,* 55**,** 635-640.

MORTICELLI, L. 2013. *Guided Functional Re-Engineering of the Mitral Valve Leaflet.* Doctor of Philosophy, University of Leeds.

MOSTOW, E. N., HARAWAY, G. D., DALSING, M., HODDE, J. P., KING, D. & GROUP, O. V. U. S. 2005. Effectiveness of an extracellular matrix graft (OASIS Wound Matrix) in the treatment of chronic leg ulcers: a randomized clinical trial. *J Vasc Surg,* 41**,** 837-43.

MUCSI, I., SKORECKI, K. L. & GOLDBERG, H. J. 1996. Extracellular Signal-regulated Kinase and the Small GTP-binding Protein, Rac, Contribute to the Effects of Transforming Growth Factor-b1 on Gene Expression. *The Journal of Biological Chemistry,* 271**,** 16567-16572.

MUIZNIEKS, L. D. & KEELEY, F. W. 2013. Molecular assembly and mechanical properties of the extracellular matrix: A fibrous protein perspective. *Biochimica et biophysica acta,* 1832**,** 866-75.

MULLIS, K., FALOONA, F., SCHARF, S., SAIKI, R., HORN, G. & ERLICH, H. 1986. Specific Enzymatic Amplification of DNA *in vitro*: The Polymerase Chain Reaction. *Cold Spring Harbor symposia in quantitative biology,* 51**,** 263-273.

MURATA, T., KATAGIRI, H., ISHIHARA, H., SHIBASAKI, Y., ASANO, T., TOYODA, Y., PEKINER, B., PEKINER, C., MIWA, I. & OKA, Y. 1997. Co-localization of glucokinase with actin filaments. *FEBS Letters,* 406**,** 109-113.

MURPHY, J. M., DIXON, K., BECK, S., FABIAN, D., FELDMAN, A. & BARRY, F. 2002. Reduced chondrogenic and adipogenic activity of mesenchymal stem cells from patients with advanced osteoarthritis. *Arthritis and rheumatism,* 46**,** 704-13.

MURPHY, J. M., FINK, D. J., HUNZIKER, E. B. & BARRY, F. P. 2003. Stem cell therapy in a caprine model of osteoarthritis. *Arthritis and rheumatism,* 48**,** 3464-74.

MURRAY, R. K., BENDER, D. A., BOTHAM, K. M., KENNELLY, P. J., RODWELL, V. W. & WEIL, P. A. 2009. *Harper's Illustrated Biochemistry*.

MURUGANANDAN, S., ROMAN, A. A. & SINAL, C. J. 2009. Adipocyte differentiation of bone marrow-derived mesenchymal stem cells: cross talk with the osteoblastogenic program. *Cellular and molecular life sciences : CMLS,* 66**,** 236-53.

NA, S., COLLIN, O., CHOWDHURY, F., TAY, B., OUYANG, M., WANG, Y. & WANG, N. 2008. Rapid signal transduction in living cells is a unique feature of mechanotransduction. *Proceedings of the National Academy of Sciences of the United States of America,* 105**,** 6626-31.

NAKAYAMA, G. R., CATON, M. C., NOVA, M. P. & PARANDOOSH, Z. 1997. Assessment of the Alamar Blue assay for cellular growth and viability in vitro. *Journal of Immunological Methods,* 204**,** 205–208.

NASSIF, L & EL SABBAN, M. 2011. Mesenchymal Stem Cells in Combination with Scaffolds for Bone Tissue Engineering. *Materials,* 4**,** 1793-1804.

NATH, K., SAROSY, J. W., HAHN, J. & DI COMO, C. J. 2000. Effects of ethidium bromide and SYBR Green I on different polymerase chain reaction systems. *Journal of biochemical and biophysical methods,* 42**,** 15-29.

NCBI. 2012a. *RE: http://www.ncbi.nlm.nih.gov/gene/914.*

NCBI. 2012b. *RE: http://www.ncbi.nlm.nih.gov/gene/968.*

NCBI. 2014. *Basic Local Alignment Search Tool* [Online]. Available: https://blast.ncbi.nlm.nih.gov/Blast.cgi.

NCBI. 2016a. *Description of ACTA2 (Homo sapiens)* [Online]. Available: https://www.ncbi.nlm.nih.gov/gene/59.

NCBI. 2016b. *Description of adiponectin (Homo sapiens)* [Online]. Available: https://www.ncbi.nlm.nih.gov/gene/9370.

NCBI. 2016c. *Description of Calponin 1 (Homo sapiens)* [Online]. Available: https://www.ncbi.nlm.nih.gov/gene/1264.

NCBI. 2016d. *Description of collagen type I alpha 1 chain* [Online]. Available: https://www.ncbi.nlm.nih.gov/gene/1277.

NCBI. 2016e. *Description of collagen type III alpha 1 chain (Homo sapiens)* [Online]. Available: https://www.ncbi.nlm.nih.gov/gene/1281.

NCBI. 2016f. *Description of glyceraldehyde-3-phosphate (Homo sapiens)* [Online]. Available: https://www.ncbi.nlm.nih.gov/gene/2597.

NCBI. 2016g. *Description of peroxisome proliferator activated gamma (Homo sapiens)* [Online]. Available: https://www.ncbi.nlm.nih.gov/gene/5468.

NCBI. 2016h. *Description of ribosomal protein S28* [Online]. Available: https://www.ncbi.nlm.nih.gov/gene/6234.

NCBI. 2016i. *Description of runt related transcription factor 2 (Homo sapiens)* [Online]. Available: https://www.ncbi.nlm.nih.gov/gene/860.

NCBI. 2016j. *Description of scleraxis transcription factor (Homo sapiens)* [Online]. Available: https://www.ncbi.nlm.nih.gov/gene/642658.

NCBI. 2016k. *Description of SRY-box 9 (Homo sapiens)* [Online]. Available: https://www.ncbi.nlm.nih.gov/gene/6662.

NCBI. 2016l. *Description of transgelin (Homo sapiens)* [Online]. Available: https://www.ncbi.nlm.nih.gov/gene/6876.

NCBI. 2016m. *Description of β-actin (Homo sapiens)* [Online]. Available: https://www.ncbi.nlm.nih.gov/gene/60.

NEETHLING, W. M., STRANGE, G., FIRTH, L. & SMIT, F. E. 2013. Evaluation of a tissue-engineered bovine pericardial patch in paediatric patients with congenital cardiac anomalies: initial experience with the ADAPT-treated CardioCel(R) patch. *Interact Cardiovasc Thorac Surg,* 17**,** 698-702.

NEWTON, C. R., KALSHEKER, N., GRAHAM, A., POWELL, S., GAMMACK, A., RILEY, J. & MARKHAM, A. F. 1988. Diagnosis of α_1-antitrypsin antibody by enzymatic amplification of human genomic DNA and direct sequencing of polymerase chain reaction products *Nucleic Acids Research,* 16**,** 8233-8243.

NGIAM, M., LIAO, S., ONG JUN JIE, T., RAMAKRISHNA, S. & CHAN, C. K. 2010. Effects of mechanical stimulation in osteogenic differentiation of bone marrow-derived mesenchymal stem cells on aligned nanofibrous scaffolds. *Journal of Bioactive and Compatible Polymers,* 26**,** 56-70.

OKANO, H., NAKAMURA, M., YOSHIDA, K., OKADA, Y., TSUJI, O., NORI, S., IKEDA, E., YAMANAKA, S. & MIURA, K. 2013. Steps toward safe cell therapy using induced pluripotent stem cells. *Circ Res,* 112**,** 523-33.

OLOFSSON, T., GÄRTNER, I. & OLSSON, I. 1980. Separation of human bone marrow cells in density gradients of polyvinylpyrrolidone coated silica gel (Percoll). *Scandinavian Journal of Haematology,* 24**,** 254-262.

OMAE, H., ZHAO, C., SUN, Y. L., AN, K.-N. & AMADIO, P. C. 2009. Multilayer tendon slices seeded with bone marrow stromal cells: a novel composite for tendon engineering. *Journal of orthopaedic research : official publication of the Orthopaedic Research Society,* 27**,** 937-42.

ORR, A. W., HELMKE, B. P., BLACKMAN, B. R. & SCHWARTZ, M. A. 2006. Mechanisms of Mechanotransduction. *Developmental Cell,* 10**,** 11-20.

OTT, H. C., MATTHIESEN, T. S., GOH, S. K., BLACK, L. D., KREN, S. M., NETOFF, T. I. & TAYLOR, D. A. 2008. Perfusion-decellularized matrix: using nature's platform to engineer a bioartificial heart. *Nat Med,* 14**,** 213-21.

PAJOOHESH, M., NADERI-MANESH, H. & SOLEIMANI, M. 2016. MicroRNA-145-based differentiation of human mesenchymal stem cells to smooth muscle cells. *Biotechnol Lett,* 38**,** 1975-1981.

PAL, R., HANWATE, M. & TOTEY, S. M. 2008. Effect of holding time, temperature and different parenteral solutions on viability and functionality of adult bone marrow-derived mesenchymal stem cells before transplantation. *J Tissue Eng Regen Med,* 2**,** 436-44.

PARK, J. S., CHU, J. S., TSOU, A. D., DIOP, R., TANG, Z., WANG, A. & LI, S. 2011. The effect of matrix stiffness on the differentiation of mesenchymal stem cells in response to TGF-β. *Biomaterials,* 32**,** 3921-30.

PARK, J. S., CHU, J. S. F., CHENG, C., CHEN, F., CHEN, D. & LI, S. 2004. Differential effects of equiaxial and uniaxial strain on mesenchymal stem cells. *Biotechnology and bioengineering,* 88**,** 359-68.

PARK, S.-H., SIM, W. Y., MIN, B.-H., YANG, S. S., KHADEMHOSSEINI, A. & KAPLAN, D. L. 2012. Chip-Based Comparison of the Osteogenesis of Human Bone Marrow- and Adipose Tissue-Derived Mesenchymal Stem Cells under Mechanical Stimulation. 7**,** 1-11.

PARMAKSIZ, M., DOGAN, A., ODABAS, S., ELCIN, A. E. & ELCIN, Y. M. 2016. Clinical applications of decellularized extracellular matrices for tissue engineering and regenerative medicine. *Biomed Mater,* 11**,** 022003.

PEACH, M. S., JAMES, R., TOTI, U. S., DENG, M., MOROZOWICH, N. L., ALLCOCK, H. R., LAURENCIN, C. T. & KUMBAR, S. G. 2012. Polyphosphazene functionalized polyester fiber matrices for tendon tissue engineering: in vitro evaluation with human mesenchymal stem cells. *Biomedical materials (Bristol, England),* 7**,** 045016-045016.

PETERSEN, A. B. E., BOWEN, W. C., PATRENE, K. D., MARS, W. M., SULLIVAN, A. K., MURASE, N., BOGGS, S. S., GREENBERGER, J. S. & GOFF, J. P. 1999. Bone Marrow as a Potential Source of Hepatic Oval Cells. *Science,* 284**,** 1168-1170.

PITTENGER, M. F., MACKAY, A. M., BECK, S. C., JAISWAL, R. K., MOSCA, J. D., MOORMAN, M. A., SIMONETTI, D. W., CRAIG, S. & DANIEL, R. 1999. Multilineage potential of adult Human Mesenchymal Stem Cells. *Science,* 284**,** 143-147.

POLLARD, T. D. & EARNSHAW, W. C. 2002. *Cell biology,* Philadelphia, Elsevier Science Publishers B.V.

PONGERS-WILLEMSE, W. J., VERHAGEN, O. J. H. M., TIBBE, G. J. M., WIJKHUIJS, A. J. M., DE HAAS, V., ROOVERS, E., VAN DER SCHOOT, C. E. & VAN DONGEN, J. J. M. 1998. Real-time quantitative PCR for the detection of minimal residual disease in acute

lymphoblastic leukemia using junctional region specific TaqMan probes. *Leukemia,* 12**,** 2006-2014.

PRASERTSUNG, I., KANOKPANONT, S., BUNAPRASERT, T., THANAKIT, V. & DAMRONGSAKKUL, S. 2008. Development of acellular dermis from porcine skin using periodic pressurized technique. *Journal of biomedical materials research. Part B, Applied biomaterials,* 85**,** 210-9.

PROFFEN, B. L., VAVKEN, P., HASLAUER, C. M., FLEMING, B. C., HARRIS, C. E., MACHAN, J. T. & MURRAY, M. M. 2015. Addition of autologous mesenchymal stem cells to whole blood for bioenhanced ACL repair has no benefit in the porcine model. *Am J Sports Med,* 43**,** 320-30.

QI, M. C., HU, J., ZOU, S. J., CHEN, H. Q., ZHOU, H. X. & HAN, L. C. 2008. Mechanical strain induces osteogenic differentiation: Cbfa1 and Ets-1 expression in stretched rat mesenchymal stem cells. *International journal of oral and maxillofacial surgery,* 37**,** 453-8.

QUINTAVALLA, J., UZIEL-FUSI, S., YIN, J., BOEHNLEIN, E., PASTOR, G., BLANCUZZI, V., SINGH, H. N., KRAUS, K. H., O'BYRNE, E. & PELLAS, T. C. 2002. Fluorescently labeled mesenchymal stem cells (MSCs) maintain multilineage potential and can be detected following implantation into articular cartilage defects. *Biomaterials,* 23**,** 109-19.

RADA, T., REIS, R. L. & GOMES, M. E. 2009. Adipose tissue-derived stem cells and their application in bone and cartilage tissue engineering. *Tissue engineering. Part B, Reviews,* 15**,** 113-25.

RAFIQ, Q. A., BROSNAN, K. M., COOPMAN, K., NIENOW, A. W. & HEWITT, C. J. 2013. Culture of human mesenchymal stem cells on microcarriers in a 5 l stirred-tank bioreactor. *Biotechnol Lett,* 35**,** 1233-45.

RATHBONE, S. R., GLOSSOP, J. R., GOUGH, J. E. & CARTMELL, S. H. 2012. Cyclic tensile strain upon human mesenchymal stem cells in 2D and 3D culture differentially influences CCNL2, WDR61 and BAHCC1 gene expression levels. *Journal of the mechanical behavior of biomedical materials,* 11**,** 82-91.

RAUH, J., JACOBI, A. & STIEHLER, M. 2015. Identification of stable reference genes for gene expression analysis of three-dimensional cultivated human bone marrow-derived mesenchymal stromal cells for bone tissue engineering. *Tissue Eng Part C Methods,* 21**,** 192-206.

REING, J. E., BROWN, B. N., DALY, K. A., FREUND, J. M., GILBERT, T. W., HSIONG, S. X., HUBER, A., KULLAS, K. E., TOTTEY, S., WOLF, M. T. & BADYLAK, S. F. 2010. The effects of processing methods upon mechanical and biologic properties of porcine dermal extracellular matrix scaffolds. *Biomaterials,* 31**,** 8626-33.

REISISS, Y., GARCÍA-GARETA, E. & KORDA, M. 2013. The effect of temperature on the viability of human mesenchymal stem cells. *Stem cell research and therapy,* 4**,** 1-11.

REMLINGER, N. T., CZAJKA, C. A., JUHAS, M. E., VORP, D. A., STOLZ, D. B., BADYLAK, S. F., GILBERT, S. & GILBERT, T. W. 2010. Hydrated xenogeneic decellularized tracheal matrix as a scaffold for tracheal reconstruction. *Biomaterials,* 31**,** 3520-6.

REN, G., ZHANG, L., ZHAO, X., XU, G., ZHANG, Y., ROBERTS, A. I., ZHAO, R. C. & SHI, Y. 2008. Mesenchymal stem cell-mediated immunosuppression occurs via concerted action of chemokines and nitric oxide. *Cell stem cell,* 2**,** 141-50.

REPETTO, G., DEL PESO, A. & ZURITA, J. L. 2008. Neutral red uptake assay for the estimation of cell viability/cytotoxicity. *Nat Protoc,* 3**,** 1125-31.

RIEDER, E., KASIMIR, M. T., SILBERHUMER, G., SEEBACHER, G., WOLNER, E., SIMON, P. & WEIGEL, G. 2004. Decellularization protocols of porcine heart valves differ importantly in efficiency of cell removal and susceptibility of the matrix to recellularization with human vascular cells. *J Thorac Cardiovasc Surg,* 127**,** 399-405.

RINGE, J., KAPS, C., SCHMITT, B., BUSCHER, K., BARTEL, J., SMOLIAN, H., SCHULTZ, O., BURMESTER, G. R., HAUPL, T. & SITTINGER, M. 2002. Porcine mesenchymal stem cells. Induction of distinct mesenchymal cell lineages. *Cell Tissue Res,* 307**,** 321-7.

ROBINSON, M. J. & COBB, M. H. 1997. Mitogen-activated protein kinase pathways. *Current opinion in cell biology,* 9**,** 180-6.

ROEHM, N. W., RODGERS, G. H., HATFIELD, S. M. & GLASEBROOK, A. L. 1991. An improved colorimetric assay for cell proliferation and viability utilizing the tetrazolium salt XTT. *Journal of Immunological Methods,* 142**,** 257-265.

ROSARIO, D. J., REILLY, G. C., SALAH, E. A., GLOVER, M., BULLLOCK, A. J. & MACNEIL, S. 2008. Decellularization and sterilization of porcine urinary bladder matrix for tissue engineering in the lower urinary tract. *Regenerative Medicine,* 3**,** 145-156.

ROSCA, A. M. & BURLACU, A. 2010. Isolation of a mouse bone marrow population enriched in stem and progenitor cells by centrifugation on a Percoll gradient. *Biotechnol Appl Biochem,* 55**,** 199-208.

ROTH, J. S., BRATHWAITE, C., HACKER, K., FISHER, K. & KING, J. 2015. Complex ventral hernia repair with a human acellular dermal matrix. *Hernia,* 19**,** 247-52.

ROUFOSSE, C. A., DIREKZE, N. C., OTTO, W. R. & WRIGHT, N. A. 2004. Circulating mesenchymal stem cells. *The international journal of biochemistry & cell biology,* 36**,** 585-97.

SABER, S., ZHANG, A. Y., KI, S. H., LINDSEY, D. P., SMITH, R. L., RIBOH, J., PHAM, H. & CHANG, J. 2010. Flexor Tendon Tissue Engineering: Bioreactor Cyclic Strain Increases Construct Strength. *Tissue Engineering,* 16**,** 2085-2090.

SAGE, D. 2017. *OrientationJ: ImageJ's plugin for directional analysis in images* [Online]. Available: http://bigwww.epfl.ch/demo/orientation/.

SALAZAR, B. H., CASHION, A. T., DENNIS, R. G. & BIRLA, R. K. 2015. Development of a Cyclic Strain Bioreactor for Mechanical Enhancement and Assessment of Bioengineered Myocardial Constructs. *Cardiovasc Eng Technol,* 6**,** 533-45.

SCHÄFFLER, A. & SCHÖLMERICH, J. 2010. Innate immunity and adipose tissue biology. *Trends in immunology,* 31**,** 228-35.

SCHANER, P. J., MARTIN, N. D., TULENKO, T. N., SHAPIRO, I. M., TAROLA, N. A., LEICHTER, R. F., CARABASI, R. A. & DIMUZIO, P. J. 2004. Decellularized vein as a potential scaffold for vascular tissue engineering. *J Vasc Surg,* 40**,** 146-53.

SCHMIDT, J. B. & TRANQUILLO, R. T. 2016. Cyclic Stretch and Perfusion Bioreactor for Conditioning Large Diameter Engineered Tissue Tubes. *Ann Biomed Eng,* 44**,** 1785-97.

SCHMITTGEN, T. D. & LIVAK, K. J. 2008. Analyzing real-time PCR data by the comparative CT method. *Nature Protocols,* 3**,** 1101-1108.

SCHMITTGEN, T. D. & ZAKRAJSEK, B. A. 2000. Effect of experimental treatment on housekeeping gene expression: validation by real-time, quantitative RT-PCR. *Journal of biochemical and biophysical methods,* 46**,** 69-81.

SCREEN, H. R. C., SHELTON, J. C., BADER, D. L. & LEE, D. A. 2005. Cyclic tensile strain upregulates collagen synthesis in isolated tendon fascicles. *Biochemical and biophysical research communications,* 336**,** 424-9.

SEGUIN, A., RADU, D., HOLDER-ESPINASSE, M., BRUNEVAL, P., FIALAIRE-LEGENDRE, A., DUTERQUE-COQUILLAUD, M., CARPENTIER, A. & MARTINOD, E. 2009. Tracheal replacement with cryopreserved, decellularized, or glutaraldehyde-treated aortic allografts. *Ann Thorac Surg,* 87**,** 861-7.

SEKIYA, I., LARSON, B. L., SMITH, B. R., POCHAMPALLY, R., CUI, J. G. & PROCKOP, D. J. 2002. Expansion of human adult stem cells from bone marrow stroma: conditions that maximize the yields of early progenitors and evaluate their quality. *Stem Cells,* 20**,** 530-541.

SEN, B., GUILLUY, C., XIE, Z., CASE, N., STYNER, M., THOMAS, J., OGUZ, I., RUBIN, C., BURRIDGE, K. & RUBIN, J. 2011. Mechanically induced focal adhesion assembly amplifies anti-adipogenic pathways in mesenchymal stem cells. *Stem cells,* 29**,** 1829-36.

SEN, B., STYNER, M., XIE, Z., CASE, N., RUBIN, C. T. & RUBIN, J. 2009. Mechanical loading regulates NFATc1 and beta-catenin signaling through a GSK3beta control node. *J Biol Chem,* 284**,** 34607-17.

SEN, B., XIE, Z., CASE, N., MA, M., RUBIN, C. & RUBIN, J. 2008. Mechanical strain inhibits adipogenesis in mesenchymal stem cells by stimulating a durable beta-catenin signal. *Endocrinology,* 149**,** 6065-75.

SHANG, Q., WANG, Z., LIU, W., SHI, Y., CUI, L. & CAO, Y. 2000. Tissue-engineered bone repair of sheep cranial defects with autologous bone marrow stromal cells. *Journal of Craniofacial Surgery,* 12**,** 586-593.

SHARMA, J., HAMPTON, J. M., VALIENTE, G. R., WADA, T., STEIGELMAN, H., YOUNG, M. C., SPURBECK, R. R., BLAZEK, A. D., BOSH, S., JARJOUR, W. N. & YOUNG, N. A. 2017. Therapeutic Development of Mesenchymal Stem Cells or Their Extracellular Vesides to Inhibit Autoimmune-Mediated Inflammatory Processes in Systemic Lupus Erythematosus. *Front Immunol,* 8**,** 526.

SHI, Y., LI, H., ZHANG, X., FU, Y., HUANG, Y., LUI, P. P. Y., TANG, T. & DAI, K. 2011. Continuous cyclic mechanical tension inhibited Runx2 expression in mesenchymal stem cells through RhoA-ERK1/2 pathway. *Journal of cellular physiology,* 226**,** 2159-69.

SHI, Y., SU, J., ROBERTS, A. I., SHOU, P., RABSON, A. B. & REN, G. 2012. How mesenchymal stem cells interact with tissue immune responses. *Trends in immunology,* 33**,** 136-43.

SHIH, Y.-R. V., TSENG, K.-F., LAI, H.-Y., LIN, C.-H. & LEE, O. K. 2011. Matrix stiffness regulation of integrin-mediated mechanotransduction during osteogenic differentiation of human mesenchymal stem cells. *Journal of bone and mineral research : the official journal of the American Society for Bone and Mineral Research,* 26**,** 730-8.

SHIN, J. W., SWIFT, J., IVANOVSKA, I., SPINLER, K. R., BUXBOIM, A. & DISCHER, D. E. 2013. Mechanobiology of bone marrow stem cells: from myosin-II forces to compliance of matrix and nucleus in cell forms and fates. *Differentiation,* 86**,** 77-86.

SIGMA-ALDRICH. 2014. *OligoEvaluator™* [Online]. Available: www.oligoevaluator.com.

SIMINOVITCH, L., MCCULLOCH, E. A. & TILL, J. E. 1963. Distribution of colony-forming cells among spleen colonies. *J. cellular and comparative biology,* 62**,** 327-327.

SIMMONS, A. D., WILLIAMS, C., 3RD, DEGOIX, A. & SIKAVITSAS, V. I. 2017. Sensing metabolites for the monitoring of tissue engineered construct cellularity in perfusion bioreactors. *Biosens Bioelectron,* 90**,** 443-449.

SITTICHOKECHAIWUT, A., EDWARDS, J. H., SCUTT, A. M., REILLY, G. C. & SCIENCES, B. 2010. Short bouts of mechanical loading are as effective as dexmethasone at inducing matrix production by human bone marrow mesenchymal stem cells. *European cells & materials,* 20**,** 45-57.

SNYDER, S. J., ARNOCZKY, S. P., BOND, J. L. & DOPIRAK, R. 2009. Histologic evaluation of a biopsy specimen obtained 3 months after rotator cuff augmentation with GraftJacket Matrix. *Arthroscopy,* 25**,** 329-33.

SNYDER, S. J. & BOND, J. L. 2007. Technique for Arthroscopic Replacement of Severely Damaged Rotator Cuff Using "GraftJacket" Allograft. *Operative Techniques in Sports Medicine,* 15**,** 86-94.

SOBIERAJ, M., CUDAK, E., MROWCZYNSKI, W., NALECZ, T. K., WESTERSKI, P. & WOJTALIK, M. 2016. Application of the CardioCel bovine pericardial patch - a preliminary report. *Kardiochir Torakochirurgia Pol,* 13**,** 210-212.

SOLEYMANINEJADIAN, E., PRAMANIK, K. & SAMADIAN, E. 2012. Immunomodulatory properties of mesenchymal stem cells: cytokines and factors. *American journal of reproductive immunology (New York, N.Y. : 1989),* 67**,** 1-8.

SONNAERT, M., PAPANTONIOU, I., BLOEMEN, V., KERCKHOFS, G., LUYTEN, F. P. & SCHROOTEN, J. 2017. Human periosteal-derived cell expansion in a perfusion bioreactor system: proliferation, differentiation and extracellular matrix formation. *J Tissue Eng Regen Med,* 11**,** 519-530.

SOTERIOU, D., ISKENDER, B., BYRON, A., HUMPHRIES, J. D., BORG-BARTOLO, S., HADDOCK, M. C., BAXTER, M. A., KNIGHT, D., HUMPHRIES, M. J. & KIMBER, S. J. 2013. Comparative proteomic analysis of supportive and unsupportive extracellular matrix substrates for human embryonic stem cell maintenance. *J Biol Chem,* 288**,** 18716-31.

STANLEY, P. E. 1986. Extraction of Adenosine Triphosphate from Microbial and Somatic Cells. *Methods in Enzymology,* 133**,** 14-22.

STEWARD, A. J., WAGNER, D. R. & KELLY, D. J. 2014. Exploring the roles of integrin binding and cytoskeletal reorganization during mesenchymal stem cell mechanotransduction in soft and stiff hydrogels subjected to dynamic compression. *J Mech Behav Biomed Mater,* 38**,** 174-82.

STIMPFEL, M., SKUTELLA, T., KUBISTA, M., MALICEV, E., CONRAD, S. & VIRANT-KLUN, I. 2012. Potential stemness of frozen-thawed testicular biopsies without sperm in infertile men induced into the in vitro fertilization programme. *Journal of biomedicine & biotechnology,* 2012**,** 291038-291038.

STRANGE, G., BRIZARD, C., KARL, T. R. & NEETHLING, L. 2015. An evaluation of Admedus' tissue engineering process-treated (ADAPT) bovine pericardium patch (CardioCel) for the repair of cardiac and vascular defects. *Expert Rev Med Devices,* 12**,** 135-41.

SUN, Y., CHEN, C. S. & FU, J. 2012a. Forcing Stem Cells to Behave: A Biophysical Perspective of the Cellular Microenvironment. *Annual review of biophysics,* 41**,** 519-542.

SUN, Y., CHEN, C. S. & FU, J. 2012b. Forcing stem cells to behave: a biophysical perspective of the cellular microenvironment. *Annual review of biophysics,* 41**,** 519-42.

TABDILI, H., LANGER, M., SHI, Q., POH, Y.-C., WANG, N. & LECKBAND, D. 2012. Cadherin-dependent mechanotransduction depends on ligand identity but not affinity. *Journal of cell science,* 125**,** 4362-71.

TAE, S.-K., LEE, S.-H., PARK, J.-S. & IM, G.-I. 2006. Mesenchymal stem cells for tissue engineering and regenerative medicine. *Biomedical materials (Bristol, England),* 1**,** 63-71.

TAKAHASHI, K. & YAMANAKA, S. 2006. Induction of Pluripotent Stem Cells from Mouse Embryonic and Adult Fibroblast Cultures by Defined Factors. *Cell,* 126**,** 663-676.

TAKIKAWA, S., BAUER, T. W., KAMBIC, H. & TOGAWA, H. 2003. Comparative evaluation of the osteoinductivity of two formulations of human demineralized bone matrix. *Journal of Biomedical materials Research Part A,* 65A**,** 37-42.

TAMAMA, K., SEN, C. K. & WELLS, A. 2008. Differentiation of bone marrow mesenchymal stem cells into the smooth muscle lineage by blocking ERK/MAPK signaling pathway. *Stem Cells Dev,* 17**,** 897-908.

TAMURA, H. 2008. The role of rusts in corrosion and corrosion protection of iron and steel. *Corrosion Science,* 50**,** 1872-1883.

TSAI, A. C., LIU, Y., YUAN, X. & MA, T. 2015. Compaction, fusion, and functional activation of three-dimensional human mesenchymal stem cell aggregate. *Tissue Eng Part A,* 21**,** 1705-19.

TSE, J. R. & ENGLER, A. J. 2011. Stiffness gradients mimicking in vivo tissue variation regulate mesenchymal stem cell fate. *PLoS One,* 6**,** e15978.

TSUDA, Y., YASUTAKE, H., ISHIJIMA, A. & YANAGIDA, T. 1996. Torsional rigidity of single actin filaments and actin–actin bond breaking force under torsion measured directly by in vitro micromanipulation. *PNAS,* 93**,** 12937–12942.

TUAN, R. S., BOLAND, G. & TULI, R. 2003. Adult mesenchymal stem cells and cell-based tissue engineering. *Arthritis research and therapy,* 5**,** 32-45.

TULI, R., TULI, S., NANDI, S., HUANG, X., MANNER, P. A., HOZACK, W. J., DANIELSON, K. G., HALL, D. J. & TUAN, R. S. 2003. Transforming growth factor-beta-mediated chondrogenesis of human mesenchymal progenitor cells involves N-cadherin and mitogen-activated protein kinase and Wnt signaling cross-talk. *The Journal of biological chemistry,* 278**,** 41227-36.

TURINETTO, V., VITALE, E. & GIACHINO, C. 2016. Senescence in Human Mesenchymal Stem Cells: Functional Changes and Implications in Stem Cell-Based Therapy. *Int J Mol Sci,* 17.

TZIMA, E., IRANI-TEHRANI, M., KIOSSES, W. B., DEJANA, E., SCHULTZ, D. A., ENGELHARDT, B., CAO, G., DELISSER, H. & SCHWARTZ, M. A. 2005. A mechanosensory complex that mediates the endothelial cell response to fluid shear stress. *Nature,* 437**,** 426-31.

UDA, Y., POH, Y.-C., CHOWDHURY, F., WU, D. C., TANAKA, T. S., SATO, M. & WANG, N. 2011. Force via integrins but not E-cadherin decreases Oct3/4 expression in embryonic stem cells. *Biochemical and biophysical research communications,* 415**,** 396-400.

UYGUN, B. E., SOTO-GUTIERREZ, A., YAGI, H., IZAMIS, M. L., GUZZARDI, M. A., SHULMAN, C., MILWID, J., KOBAYASHI, N., TILLES, A., BERTHIAUME, F., HERTL, M., NAHMIAS, Y., YARMUSH, M. L. & UYGUN, K. 2010. Organ reengineering through development of a transplantable recellularized liver graft using decellularized liver matrix. *Nat Med,* 16**,** 814-20.

VAN TUYN, J., KNAÄN-SHANZER, S., VAN DE WATERING, M. J. M., DE GRAAF, M., VAN DER LAARSE, A., SCHALIJ, M. J., VAN DER WALL, E. E., DE VRIES, A. A. F. & ATSMA, D. E. 2005. Activation of cardiac and smooth muscle-specific genes in primary human cells after forced expression of human myocardin. *Cardiovascular research,* 67**,** 245-55.

VANDESOMPELE, J., DE PRETER, K., PATTYN, F., POPPE, B., VAN ROY, N., DE PAEPE, A. & SPELEMAN, F. 2002. Accurate normalization of real-time quantitative RT-PCR data by geometric averaging of multiple internal control genes. *Genome Biology,* 3**,** 0034.1–0034.11.

VASHI, A. V., WHITE, J. F., MCLEAN, K. M., NEETHLING, W. M., RHODES, D. I., RAMSHAW, J. A. & WERKMEISTER, J. A. 2015. Evaluation of an established pericardium patch for delivery of mesenchymal stem cells to cardiac tissue. *J Biomed Mater Res A,* 103**,** 1999-2005.

VÉRTESSY, B. G., OROSZ, F., KOVÁCS, J. & OVÁDI, J. 1997. Alternative Binding of Two Sequential Glycolytic Enzymes to Microtubules. *Journal of Biological Chemistry,* 272**,** 25542–25546.

VINDAS BOLANOS, R. A., COKELAERE, S. M., ESTRADA MCDERMOTT, J. M., BENDERS, K. E., GBURECK, U., PLOMP, S. G., WEINANS, H., GROLL, J., VAN WEEREN, P. R. & MALDA, J. 2017. The use of a cartilage decellularized matrix scaffold for the repair of osteochondral defects: the importance of long-term studies in a large animal model. *Osteoarthritis Cartilage,* 25**,** 413-420.

VOGEL, V. 2006. Mechanotransduction involving multimodular proteins: converting force into biochemical signals. *Annual review of biophysics and biomolecular structure,* 35**,** 459-88.

WANG, J. C., ALANAY, A., MARK, D., KANIM, L. E., CAMPBELL, P. A., DAWSON, E. G. & LIEBERMAN, J. R. 2007. A comparison of commercially available demineralized bone matrix for spinal fusion. *Eur Spine J,* 16**,** 1233-40.

WANG, J. H. C., JIA, F., GILBERT, T. W. & WOO, S. L. Y. 2003. Cell orientation determines the alignment of cell-produced collagenous matrix. *Journal of biomechanics,* 36**,** 97-102.

WANG, N. & INGBER, D. E. 1995. Probing transmembrane mechanical coupling and cytomechanics using magnetic twisting cytometry. *Biochemistry and cell biology = Biochimie et biologie cellulaire,* 73**,** 327-35.

WANG, N., NARUSE, K., STAMENOVIĆ, D., FREDBERG, J. J., MIJAILOVICH, S. M., TOLIĆ-NØRRELYKKE, I. M., POLTE, T., MANNIX, R. & INGBER, D. E. 2001. Mechanical behavior in living cells consistent with the tensegrity model. *Proceedings of the National Academy of Sciences of the United States of America,* 98**,** 7765-70.

WANG, N. & SUO, Z. 2005. Long-distance propagation of forces in a cell. *Biochemical and biophysical research communications,* 328**,** 1133-8.

WANG, T., DANG, G., GUO, Z. & YANG, M. 2005. Evaluation of autologous bone marrow mesenchymal stem cell-calcium phosphate ceramic composite for lumbar fusion in rhesus monkey interbody fusion model. *Tissue engineering,* 11**,** 1159-67.

WAYMOUTH, C. 1970. Osmolality of mammalian blood and of media for culture of mammalian cells. *In vitro,* 6**,** 109-127.

WERNIG, M., MEISSNER, A., FOREMAN, R., BRAMBRINK, T., KU, M., HOCHEDLINGER, K., BERNSTEIN, B. E. & JAENISCH, R. 2007. In vitro reprogramming of fibroblasts into a pluripotent ES-cell-like state. *Nature,* 448**,** 318-24.

WILLIAMS, C., PH, D., XIE, A. W., EMANI, S., YAMATO, M., OKANO, T., EMANI, S. M. & WONG, J. Y. 2012. A Comparison of Human Smooth Muscle and Mesenchymal Stem Cells as Potential Cell Sources for Tissue-Engineered Vascular Patches. 18**,** 986-999.

WILMUT, I., SCHNIEKE, A. E., MCWHIR, J., KIND, A. J. & CAMPBELL, K. H. S. 1997. Viable offspring derived from fetal and adult mammalian cells. *Nature,* 385**,** 810-813.

WONG, M. L. & MEDRANO, J. F. 2005. Real-time PCR for mRNA quantitation. *Biotechniques,* 39**,** 75-85.

WU, K., LIU, Y. L., CUI, B. & HAN, Z. 2006. Application of stem cells for cardiovascular grafts tissue engineering. *Transplant immunology,* 16**,** 1-7.

WU, X., KANG, H., LIU, X., GAO, J., ZHAO, K. & MA, Z. 2016. Serum and xeno-free, chemically defined, no-plate-coating-based culture system for mesenchymal stromal cells from the umbilical cord. *Cell Prolif,* 49**,** 579-88.

XU, B., SONG, G., JU, Y., LI, X., SONG, Y. & WATANABE, S. 2012. RhoA/ROCK, cytoskeletal dynamics, and focal adhesion kinase are required for mechanical stretch-induced tenogenic differentiation of human mesenchymal stem cells. *Journal of cellular physiology,* 227**,** 2722-9.

XU, K., KUNTZ, L. A., FOEHR, P., KUEMPEL, K., WAGNER, A., TUEBEL, J., DEIMLING, C. V. & BURGKART, R. H. 2017. Efficient decellularization for tissue engineering of the tendon-bone interface with preservation of biomechanics. *PLoS One,* 12**,** e0171577.

XUE, J. L., SALEM, T. Z., TURNEY, C. M. & CHENG, X. W. 2010. Strategy of the use of 28S rRNA as a housekeeping gene in real-time quantitative PCR analysis of gene transcription in insect cells infected by viruses. *Strategy of the use of 28S rRNA as a housekeeping gene in real-time quantitative PCR analysis of gene transcription in insect cells infected by viruses,* 163**,** 210-215.

YANG, X. 2012a. Clinical need for stem cell therapy and tissue engineering.

YANG, X. 2012b. Lecture: 'Clinical Need for Stem Cell Therapy and Tissue Engineering'.

YE, X., ZHAO, Q., SUN, X. & LI, H. 2009. Enhancement of mesenchymal stem cell attachment to decellularized porcine aortic valve scaffold by in vitro coating with antibody against CD90: a preliminary study on antibody-modified tissue-engineered heart valve. *Tissue engineering. Part A,* 15**,** 1-11.

YEH, D. D., NAZARIAN, R. M., DEMETRI, L., MESAR, T., DIJKINK, S., LARENTZAKIS, A., VELMAHOS, G. & SADIK, K. W. 2017. Histopathological assessment of OASIS Ultra on critical-sized wound healing: a pilot study. *J Cutan Pathol,* 44**,** 523-529.

YIM, E. K., PANG, S. W. & LEONG, K. W. 2007. Synthetic nanostructures inducing differentiation of human mesenchymal stem cells into neuronal lineage. *Exp Cell Res,* 313**,** 1820-9.

YIN, T. & LI, L. 2006. The stem cell niches in bone. *The Journal of Clinical Investigatiob,* 116**,** 1195-1201.

YIN, Z., CHEN, X., ZHU, T., HU, J. J., SONG, H. X., SHEN, W. L., JIANG, L. Y., HENG, B. C., JI, J. F. & OUYANG, H. W. 2013. The effect of decellularized matrices on human tendon stem/progenitor cell differentiation and tendon repair. *Acta Biomater,* 9**,** 9317-29.

YOSHIMOTO, H., SHIN, Y. M., TERAI, H. & VACANTI, J. P. 2003. A biodegradable nanofiber scaffold by electrospinning and its potential for bone tissue engineering. *Biomaterials,* 24**,** 2077-2082.

YOUNG, D. A., CHOI, Y. S., ENGLER, A. J. & CHRISTMAN, K. L. 2013. Stimulation of adipogenesis of adult adipose-derived stem cells using substrates that mimic the stiffness of adipose tissue. *Biomaterials,* 34**,** 8581-8.

YU, H., TAY, C. Y., LEONG, W. S., TAN, S. C. W., LIAO, K. & TAN, L. P. 2010. Mechanical behavior of human mesenchymal stem cells during adipogenic and osteogenic differentiation. *Biochemical and biophysical research communications,* 393**,** 150-5.

ZANG, M., ZHANG, Q., CHANG, E. I., MATHUR, A. B. & YU, P. 2012. Decellularized tracheal matrix scaffold for tissue engineering. *Plast Reconstr Surg,* 130**,** 532-40.

ZHANG, W., WANG, S., YIN, H., CHEN, E., XUE, D., ZHENG, Q., GAO, X. & PAN, Z. 2016. Dihydromyricetin enhances the osteogenic differentiation of human bone marrow mesenchymal stem cells in vitro partially via the activation of Wnt/beta-catenin signaling pathway. *Fundam Clin Pharmacol,* 30**,** 596-606.

ZHAO, J., GRIFFIN, M., CAI, J., LI, S., BULTER, P. E. M. & KALASKAR, D. M. 2016. Bioreactors for tissue engineering: An update. *Biochemical Engineering Journal,* 109**,** 268-281.

ZHENG, B., WANG, C., HE, L., XU, X., QU, J., HU, J. & ZHANG, H. 2013. Neural differentiation of mesenchymal stem cells influences chemotactic responses to HGF. *Journal of cellular physiology,* 228**,** 149-62.

ZHOU, J. & NIKLASON, L. E. 2012. Microfluidic artificial "vessels" for dynamic mechanical stimulation of mesenchymal stem cells. *Integrative biology : quantitative biosciences from nano to macro,* 4**,** 1487-97.

ZIMMERMANN, S., VOSS, M., KAISER, S., KAPP, U., WALLER, C. F. & MARTENS, U. M. 2003. Lack of telomerase activity in human mesenchymal stem cells. *Leukemia,* 17**,** 1146-9.

ZUK, P. A., ZHU, M., ASHJIAN, P., UGARTE, D. A. D., HUANG, J. I., MIZUNO, H., ALFONSO, Z. C., FRASER, J. K., BENHAIM, P. & HEDRICK, M. H. 2002. Human Adipose Tissue Is a Source of Multipotent Stem Cells □. *Molecular Biology of the Cell,* 13**,** 4279-4295.

ZUND, G., YE, Q., HOERSTRUP, S. P., SCHOEBERLEIN, A., SCHMID, A. C., GRUNENFELDER, J., VOGT, P. & TURINA, M. 1999. Tissue engineering in cardiovascular surgery: MTT, a rapid and reliable quantitative method to assess the optimal human cell seeding on polymeric meshes. *European Journal of Cardio-thoracic Surgery,* 15**,** 519–524.

Appendix: Suppliers of Equipment, Glassware and Consumables

Item	Supplier
Application loop	Greiner bio-one
Cover slips	Menzel-Glasef
Bijous	VWR international
Bunsen burner	Flamefas
Cryovials	Sarsedt
Dissection kit	Sanco
DNeasy kit	Quiagen (UK)
Filter (disposable, 0.2µm)	Sarforius stedim biotech
Filter paper	Whatman (UK)
Fresh blood agar (FBA) plates	Sarsedt
Glass bottles (0.5, 1.0 & 2.0L)	Fisherbrand
Haemocytometer	Fuchs Rosenthal
Histocassettes	Simport
Nutrient agar (NA) plate	Sarsedt
Optiplate-96	PerkinElmer (UK)
Plastic tub (airtight)	Anaeropack
Polarized light filters	RealD® (from 3D cinema glasses)
Sabouraud plates	Sarsedt

Item	Supplier
Scalpel blade (disposable, size 10)	Swann-morton®
Scalpel blade (disposable, size 22)	Swann-morton®
Six well plates	Thermo scientific
Sterile pot	Sterilin
SuperFrost™ plus microscope slides	Thermo scientific
Syringe (disposable, 20mL)	Terumo
Tissue culture flask (size T75)	Nunc
Tissue culture flask (size T5)	Nunc
X-Clear PCR tube strips	Starlab (Germany)

Equipment	Supplier
Autoclave (PACS 2000)	Getinge (Sweden)
Bag sealer	Hulme Martin (UK)
Balance	Mettler (UK)
Balance (four fugure)	AND (UK)
Biological safety cabinet (class II)	Heraeus Instruments (Germany)
Camera (for microscope; U-CMAD3)	Olympus (UK)
Cell culture cabinet (Class II; Hera safe)	Heraeus instruments (Germany)
Centrifuge (Harrier 15/80; for cell culture)	Sanyo (Japan)
Centrifuge (MIKRO 2212; for molecular biology)	Hettich zentrifugen (Germany)
Critical point drier (Polaron E300)	Quorum Technologies (UK)
Eppendorf heater/shaker (Thermomixer comfort)	Eppendorf (Germany)

Equipment	Supplier
Forceps (heated)	European Bios (Italy)
Freeze-drier (Modalyod-230)	Thermo Scientific (USA)
Freezer (-20 °C)	Electrolux (Sweden)
Freezer (-80 °C)	Sanyo (Japan)
Fumehood	Safelab (UK)
Dial Gauge	University of Leeds (UK) (custom manufactured)
Quanta 200F FEGSEM	FEI (USA)
Heat-sealer (sealboy)	Audion AE electro (Netherlands)
Image capture software (cell^B)	Olympus (UK)
Incubator (37 °C; MCO-20AIC)	Sanyo (Japan)
Light box (KL003)	Kenro Ltd (UK)
Magnetic stirrer (heated)	Stuart (UK)
Microscope (inverted, IX71)	Olympus (UK)
Microscope (inverted; CK40)	Olympus (UK)
Microscope (upright, BX51)	Olympus (UK)
Microtome (Manual; RM2125RTF)	Leica (Germany)
Microtome (automatic; RM2155)	Leica (Germany)
Microwave (CD399)	Buffalo (USA)
Mobile phone	HTC (UK) (personal property)
Oven (for dry heat sterilisation)	Genlab (UK)
Paraffin mounting section bath	Electrothermal (UK)
pH meter (3510)	Jenway (USA)
Electronic pipette (Fastpette)	Labnet (USA)
Plate reader (multiskan spectrum)	Thermo electron (USA)
Refrigerator	Indesit (Italy)
Nanodrop spectrophotometer (ND-1000)	Thermo Scientific (USA)
Mx3000P™ Real-Time PCR system [Thermal cycler]	Agilent technologies (USA)

Equipment	Supplier
Shaker (PSU-10i)	Grant-bio (UK)
208HR high resolution sputter coater	Cressington (UK)
Temperature monitor (handheld)	
Temperature controller [for Tencell; EZ-zone PM]	Watlow (USA)
Tencell bioreactor	University of Leeds (UK) (custom manufactured)
Thermomixer (comfort)	Eppendorf (Germany)
Tissue processor (TP1020)	Leica (Germany)
Ultrasonic cleaner bath	VWR international (UK)
Vortex (whirlimixer)	Electrol Ltd (USA)
Water bath (JB1)	Grant Instruments (UK)
Wax dispenser (E66)	Lamb (UK)
Wax oven (GPWAX-50-HYD)	Jim engineering (UK)